PL-TR-94-2268

MEASUREMENT AND ANALYSIS RELATED TO INFRARED EMISSIONS

R. E. Murphy
M. H. Bruce
B. D. Green
G. A. Vanasse

Research Sciences corp
594 Marrett Road, Suite 13
Lexington, MA   02173

30 September 1994

19950417 202

Final Report
6 June 1991-30 September 1994
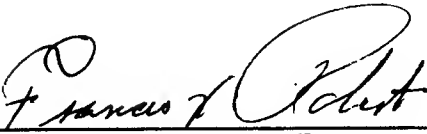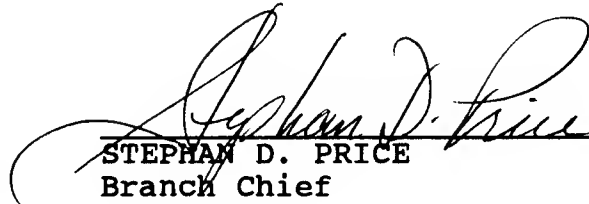
PHILLIPS LABORATORY
Directorate of Geophysics
AIR FORCE MATERIEL COMMAND
HANSCOM AIR FORCE BASE, MA 01731-3010

This technical report has been reviewed and is approved for publication

FRANCIS X. ROBERT
Contract Manager

STEPHAN D. PRICE
Branch Chief

ROGER VAN TASSEL
Division Director

This report has been reviewed by the ESC Public Affairs Office (PA) and is releasable to the National Technical Information Service (NTIS).

Qualified requestors may obtain additional copies from the Defense Technical Information Center. All others should apply to the National Technical Information Service.

If your address has changed, or if you wish to be removed from the mailing list, or if the addressee is no longer employed by your organization, please notify PL/TSI, Hanscom AFB, MA 01731-3010. This will assist us in maintaining a current mailing list.

Do not return copies of this report unless contractual obligations or notices on a specific document requires that it be returned.

REPORT DOCUMENTATION PAGE

Form Approved
OMB No. 0704-0188

1. AGENCY USE ONLY *(Leave blank)*	2. REPORT DATE 30 Sept 1994	3. REPORT TYPE AND DATES COVERED Final 6 June 91 - 30 Sept 94

4. TITLE AND SUBTITLE
MEASUREMENT AND ANALYSIS RELATED TO INFRARED EMISSIONS

5. FUNDING NUMBERS
Contract No.
F19628-91-C-0042

PE 63215C
PR S322 TA01 WU AI

6. AUTHOR(S)

R.E. Murphy, M.H. Bruce, B.D. Green* and G.A. Vanasse

7. PERFORMING ORGANIZATION NAME(S) AND ADDRESS(ES)
RESEARCH SCIENCES CORP
594 Marrett Rd., Suite 13
Lexington, MA 02173

8. PERFORMING ORGANIZATION REPORT NUMBER

9. SPONSORING/MONITORING AGENCY NAME(S) AND ADDRESS(ES)
PHILLIPS LABORATORY
29 RANDOLPH ROAD
HANSCOM AFB, MA 01731-3010
Contract Manager: Frank Robert/GPOB

10. SPONSORING/MONITORING AGENCY REPORT NUMBER
PL-TR-94-2268

11. SUPPLEMENTARY NOTES
*Physical Sciences Inc.
20 New England Business Center
Andover, MA 01810

12a. DISTRIBUTION/AVAILABILITY STATEMENT

Approved for public release; distribution unlimited.

12b. DISTRIBUTION CODE

13. ABSTRACT *(Maximum 200 words)*

PL/GPO field programs, CIRRIS-1A, EXCEDE III, FISTA and others have collected interferometer data i.e., interferograms, which were Fourier transformed to recover spectral information. Specific analysis has been performed to ascertain fundamental properties regarding the nature of the earth/atmosphere emissions. For the CIRRIS-1A nadir viewing interferometer data, fundamental relations regarding resolution limitations imposed by the finite character of the data are presented. Chromatic and achromatic sources are considered with conclusions on increasing spatial resolution. An extensive documentation on the earth/atmosphere ultraviolet radiation backgrounds is provided. Transformed EXCEDE III interferograms yielding high resolution spectra of electron (18 amp, 2.5 keV) irradiated air over 85 to 115 km are presented. The emission characteristics of many species are reveled including NO^+ ($\Delta v = 1$) with over 40 vibration-rotation lines isolated. Energy efficiency of NO^+ ($\Delta v = 1$) photon production is derived. A computer model of electron impacting air was generated to follow radiation history of NO^+. Detailed reaction rates have been derived for the nacient distribution of $N^+ + O_2 \rightarrow NO^+(v)$.

14. SUBJECT TERMS
Infrared   Radiation   Ultraviolet
Backgrounds Spectra   Atmospheric Chemistry

15. NUMBER OF PAGES
256

16. PRICE CODE

17. SECURITY CLASSIFICATION OF REPORT Unclassified	18. SECURITY CLASSIFICATION OF THIS PAGE Unclassified	19. SECURITY CLASSIFICATION OF ABSTRACT Unclassified	20. LIMITATION OF ABSTRACT SAR

TABLE OF CONTENTS

PART FOUR

LIST OF FIGURES

LIST OF FIGURES (Continued)

LIST OF FIGURES (Continued)

LIST OF FIGURES (Continued)

LIST OF TABLES

FORWARD

The Phillips Laboratory, Geophysics Directorate Optical Environment Division (PL/GPO) has conducted a number of field experiments designed to support the design of future space based surveillance systems. The objective of future DoD systems is to be able to collect information on sources of interest such as rocket launches, tracking, battle field movements, satellite deployments and a host of intelligence related activities. The radiation from the earth and its atmosphere competes with the signals generated by desired targets and acts as a source of clutter. Consequently, the ultimate goal of the field experiments and related theoretical efforts is to define the radiative nature of the earth and its atmosphere (usually from a space vantage point) in order to better compensate for the competing radiations the earth backgrounds will present to a system. The improvements in satellite capabilities and sensor improvements has made the missions of future systems ever increasing in complexity with the demand that weaker targets be observed and greater detail and resolution be obtained. The PL/GPO experiments and theoretical efforts are intended to provide critical information on the fundamental radiation processes emanating from the earths surface and within the atmosphere. This requires that background measurements be performed at different global locations, at different times of day and night and throughout the four seasons to provide a relevant data base and validate the new theoretical models. Three aspects of the radiation properties are of paramount importance. They are the spectral, spatial and temporal aspects of the hard earth and the atmosphere to altitudes of 300 km or so. Fortunately, the improved technology has also increased the ability of experimental scientists to measure the nature of the background radiation and keep pace with the system requirements. However, the advanced instrumentation usually requires much more sophisticated analysis to recover the essential information. The work presented in this final report is in support of the efforts at the Phillips Lab to increase knowledge of the earth and its atmosphere in terms of its radiative behavior.

The report is divided into four sections, each representing different areas of activity. The first section deals with the problem of attempting to improve the resolution of already collected data from the PL/GPO CIRRIS-1A shuttle measurements. CIRRIS-1A interferometer data of the nadir viewing earth was taken at about ten to one hundred times poorer spatial resolution than is now required. A theoretical development is presented on the techniques of improving the CIRRIS-1A resolution post flight.

Section Two provides an assessment of the ultraviolet backgrounds with regard to the basic knowledge available to define the earth background at shorter wavelengths. The UV advantage, so far as systems utilization is concerned, is tied to the high efficiency of photon counting devices and the short wavelength advantage for diffraction limited systems namely, a reduction of three or more in space telescope apertures. In this effort, the expert assistance of Dr. D.B. Green was acquired under Sub-contract F19628-91-C-0042-0001 with Physical Sciences Inc. of Andover, MA.

Section Three reports the results obtained in the analysis of the field data acquired by PL/GPO under the EXCEDE III experiment. In this work the interferometer spectra obtained by an electron irradiated portion of the atmosphere was analyzed. This particular experiment

relates to response of the atmosphere to electron bombardment with the culmination of infrared radiation.

The nature of the EXCEDE III experiment was such that fundamental processes which govern the infrared characteristics and intensity of radiation can be obtained through analysis of the spectral data. Many first time observations and results have been obtained. It is particularly satisfying that the detailed spectral information on a long-sought atmospheric infrared radiator i.e., NO^+ has finally been obtained. The individual vibration-rotation lines of $NO^+(v)$ have been measured, kinetics for its production determined, energy efficiency on an input/out basis determined and detailed reaction rates derived.

Finally in Section four, select high resolution spectra which were recovered by Fourier Transformation of interferograms recorded by the EXCEDE III interferometer-spectrometer are presented with the highest achievable resolution at the best signal-to-noise attainable. The spectra which were generated illustrate the emission characteristics, absolute intensities of numerous, identifiable, atmospheric radiating species and provide a general representation of the radiation background which was present under the conditions of the EXCEDE III electron irradiation. The spectra are of utility in predicting the infrared backgrounds which would be present in a high altitude nuclear detonation. The same information is also of use in understanding the mechanisms responsible for radiation produced in the aurora.

The work presented in this final report is all unclassified. Other results obtained under this contract in analysis of measurements by the PL/GPO FISTA aircraft have utilized the Scientific Report mechanism to present the analysis performed and may be obtained with the proper authorization through PL/GPO.

All special computer software developed during the course of the investigations under this contract have been made available to PL/GPO in convenient digital form. The Appendices at the end of this final report also provides a hard copy of the software programs which were developed.

ACKNOWLEDGEMENTS

PART ONE

TREATMENT OF INTERFEROGRAMS OF FLUCTUATING SPECTRA AND RESOLUTION ENHANCEMENT

INTRODUCTION

Fourier spectroscopy is a technique where a Michelson-type two-beam interferometer is used to obtain the autocorrelation function of the electromagnetic field entering the interferometer. The output of the interferometer is detected by a square law detector and recorded as a function of the optical path difference between the two interfering beams in the interferometer. The optical path difference is varied by displacing one or both of the mirrors of the interferometer. This displacement can be slow or rapid and either stepwise or continuous. The recorded output modulation is called an interferogram, $F(x)$ (with x being the optical path difference, OPD in the interferometer) and is the Fourier transform of the power spectral density $B(\sigma)$ of the incident radiation; σ being the wavenumber cm^{-1} of the radiation.

Most measurements in Fourier spectroscopy are made with the assumption that the spectral distribution of the source is constant throughout the duration of a scan which may be as long as several hours or as short as 1/20th of a second. The source radiance, the resolution $\delta\sigma$ required, and the desired signal to noise usually determine the scan time, i.e., the time required to obtain the full interferogram.

However, there are many instances in field measurements where a scan time is imposed by other considerations. The vehicle on which the interferometer spectrometer is borne may be traveling at high speed and the spectrometer field of view (FOV) accepting a temporally varying signal; i.e., like in the case of earthlimb measurements from rocket, shuttle or satellite. Such a case recently occurred on the CIRRIS-1A measurements from the shuttle Discovery.

EXTRACTING VALID SPECTRA

An attempt will be made to develop an algorithm which will allow extracting valid spectral data from a interferogram obtained while the source spectral distribution $B(\sigma)$ varied with time. There are two cases to be considered: the achromatic and the chromatic time-varying $B(\sigma)$. The former type will be considered first.

ACHROMATIC SPECTRAL VARIATIONS

Achromatic variation of the spectral distribution means that all the spectral elements vary in strength, or in intensity, at the same rate and direction. Source variations which are slow,

relative to the scan time, should not appreciably distort the spectral distribution obtained by transforming the interferogram if the source fluctuations can somehow be taken into account. One approach to accomplish this is to decimate the interferogram into segments within which the spectrum may be assumed not to vary. The average value of the interferogram within each segment yields a measure of the total energy of the spectrum during that segment. In essence, the assumption is that one-half the integral of the spectrum during each segment of the interferogram is represented by the average value of the interferogram within each segment. Normalizing the separate and individual segments' average values to the maximum average obtained during a scan will yield a multiplier which can then be used to massage the interferogram. For example, if one segment has an average value of half the maximum (this may be an extreme case) then the corresponding segment of the interferogram should have its amplitudes ($\pm$ swings around the average) doubled. Each segment is adjusted according to the plot of average value as a function of optical path difference and a corrected interferogram generated. Fourier transforming this latter interferogram should yield valid spectral data providing the assumption slowly varying for the spectrum is valid and the segments are chosen to be of appropriate lengths.

CHROMATIC SPECTRAL VARIATIONS

Chromatic variations in spectral distribution means that the individual spectral elements are not varying in unison but have differing rates of fluctuation. This can occur very easily during an earthlimb scan in elevation by the interferometer which takes place during one interferometer scan. This comes about because different molecular species are emitting from different atmospheric tangent heights. We will describe a procedure amenable to interferogram treatment for such measurement conditions and expected to yield valid spectral distributions.

Again, as in the achromatic case, we must assume something about the spectral variations. We assume it is possible to segment the interferogram into lengths L in OPD such that within each segment the spectral distribution is invariant both temporally and spectrally. We can imagine a scenario which requires that these segments be short; however, we still assume that each segment is very large compared to the interferogram sampling interval. The spectral distribution B (σ) is assumed to extend to Σ cm^{-1} and the corresponding sampling interval in the interferogram domain must be less than $\delta x = (1/2\Sigma)$; this leads to the condition that $L >> x$. The sampling interval in the spectral domain is given by $1/(2X)$ where X is the maximum value of the OPD.

The length L of each segment is assumed the same and available for Fourier transformation. Each segment is transformed to obtain what is assumed to be a valid B (σ) persisting throughout the corresponding segment. It should be noted that for a given optical path difference d, the interferometer transmission function in the spectral domain, is a cosine square function given by

$$Cos^2(\pi\sigma d) = \frac{1}{2} + \frac{1}{2}Cos(2\pi\sigma d) . \qquad (1)$$

2

Consequently, with the condition of large L or long segment, we are ensured that each segment gets to taste all the spectral elements a large number of times, which somehow lends credence to the segmenting process with the various spectral distributions having been obtained, it should now be possible to track the behavior in time of each spectral elements.

We propose a simulation by synthesizing an interferogram from given spectral distributions. That is, take a dozen or so B (σ)'s, $B_1(\sigma)$ to $B_{12}(\sigma)$, each one differing appreciably from the others. These distributions are then used to generate the separate segments of an interferogram to be joined together (avoiding discontinuities) to form the test interferogram. Actually, it probably would be easier to generate, say 12 interferograms and combine different segments into a test interferogram, instead of trying to keep track of the segments corresponding to the different spectral distributions. Once the test interferogram is generated it can be segmented and transformed; essentially just reversing the process of synthesizing. It also should be determined what effect varying the length of the segments has on the spectral distributions and how the distributions differ from that obtained from the whole test interferogram.

We would then take an actual interferogram, segment it as described above and obtain the corresponding spectra as a function of segment of the interferogram. The next step is to synthesize an interferogram from the varying spectral distributions and compare it with the actual interferogram. It is expected that by so doing it will be possible to verify whether or not the underlying assumptions are valid. Namely, are the segments too long or the time variations of the spectral more rapid than anticipated. An iteration can be done to improve the synthesized interferogram until a satisfactory fit to the actual interferogram is obtained. This forward and backward transformation should give a comfortable feeling about the validity of the results.

Finally, it would be possible to take existing interferograms from field experiments and attempt to extract valid spectral distributions even if the latter varied during the time of an interferometer scan.

SPECTRAL VARIATIONS

The previous Section discussed techniques for obtaining valid spectral distributions for achromatic and chromatic spectral variations of B(σ) which could occur during an interferometer scan. The techniques involved taking Fourier transforms and inverse transforms and performing iterations to arrive at a synthesized interferogram which was to be compared to an initial interferogram to judge its acceptability. An acceptable interferogram would confer confidence to the spectral distributions used in the interferogram synthesis. In this Section, we shall present an alternative approach, which involves convolution in the spectral domain, to arrive at the same results. It is imperative that we look at these so-called valid spectra.

The output signal from a Fourier Transform Spectrometer (FTS) as a function of path difference x is given by

$$D(x) = \int_0^{\Sigma} B(\sigma) \, d\sigma \, \cos^2 \pi \sigma x \qquad (2)$$

where $D(x)$ is the detector signal, $B(\sigma)$ is the power spectral density, and Σ is the maximum frequency of the spectrum in cm^{-1}. Eq (2) can be expanded and written as

$$D(x) = \int_0^{\Sigma} B(\sigma) \, d\sigma \, [\frac{1}{2} + \frac{1}{2} \cos(2\pi\sigma x)]$$

$$= \frac{1}{2} D(0) + \int_0^{\Sigma} B(\sigma) \cos(2\pi\sigma x) \, d\sigma \qquad (3)$$

We then define the interferogram function $F(x)$ (called the interferogram) as

$$F(x) = D(x) - \frac{1}{2}D(0) = \int_0^{\Sigma} B(\sigma) \cos(2\pi\sigma x) \, d\sigma \qquad (4)$$

The interferogram $F(x)$ is the modulation of $D(x)$ about the average value of the latter, i.e. the detector signal $D(x)$ which contained a DC part and an AC part. The average value, or the DC part, gives a measure of the total power in the spectrum while the AC part yields its spectral structure.

We let the maximum path difference for the interferogram be X and perform a cosine Fourier transform to obtain the spectral distribution;

$$B(\sigma) = \int_0^X F(x) \cos(2\pi\sigma x) \, dx \qquad (5)$$

4

With the same underlying assumptions and in the spirit introduced in the section, Extracting Valid Spectra, we shall decimate the interferogram in an attempt to obtain valid spectral distributions for achromatic or chromatic variations during an interferometer scan. This implies that during the change in path difference from 0 to x_1 we have $B_1(\sigma)$ given by

$$B_1(\sigma) = \int_0^{x_1} F(x) \, Cos(2\pi\sigma x) \, dx \approx \int_{-x_1}^{x_1} F(x) \, e^{-i2\pi\sigma x} dx, \tag{6}$$

and so on for $B_2(\sigma)$, $B_3(\sigma)$, ... etc, with each $B(\sigma)$ being constant (during the corresponding interval). For the second segment, we have

$$B_2(\sigma) \approx \int_{x_1}^{x_2} F(x) \, e^{-i2\pi\sigma x} dx \tag{7}$$

and we further make $0 \to x_1 = \Delta x = x_2 - x_1 = x_3 - x_2$ etc. In essence, we assume that the interferogram segment length L is short enough to be applicable to all the segments regardless of where they occur during the interferometer scan. It is also possible to vary L in accordance with a measurement scenario providing it can be established unambiguously how the field-of-view of the interferometer is changing during a scan; however, it does not appear that this approach would be worthwhile.

In passing, it should be noted that we assume the interferogram is an even function as well as the spectral distributions. (Although in reality $B(\sigma)$ extends from 0 to Σ cm^{-1}, in the process of Fourier transforming an even $F(x)$ we obtain the mirror image of $B(\sigma)$ as well extending from 0 to $-\Sigma$ cm^{-1}). It is because of the mathematical birth of the negative cm^{-1} spectra that the interferogram must be sampled at an interval δx less than $1/(2\Sigma)$. Actually for a spectrum extending from σ_1 to σ_2 cm^{-1} the sampling theorem states that

$$\delta x \leq \frac{1}{2\Delta\sigma} = \frac{1}{2(\sigma_2 - \sigma_1)} \tag{8}$$

in order to prevent spectral aliasing.

Let us consider one segment, say the third, and proceed to the extraction from it of a spectral distribution $B_3(\sigma)$ which is considered valid. We have, disregarding constants,

5

$$B_3(\sigma) = \int_{x_2}^{x_3} F(x) e^{-i2\pi\sigma x} dx,$$

(9)

which may be written as

$$B_3(\sigma) = \int_{-\infty}^{\infty} A(x) F(x) e^{-i2\pi\sigma x} dx$$

(10)

where

$$A(x) = 0 \quad for \ |x_3| < x < |x_2|$$

$$= 1 \ otherwise$$

Figure 1 illustrates the function A(x) which in essence selects the appropriate segment to be analyzed.
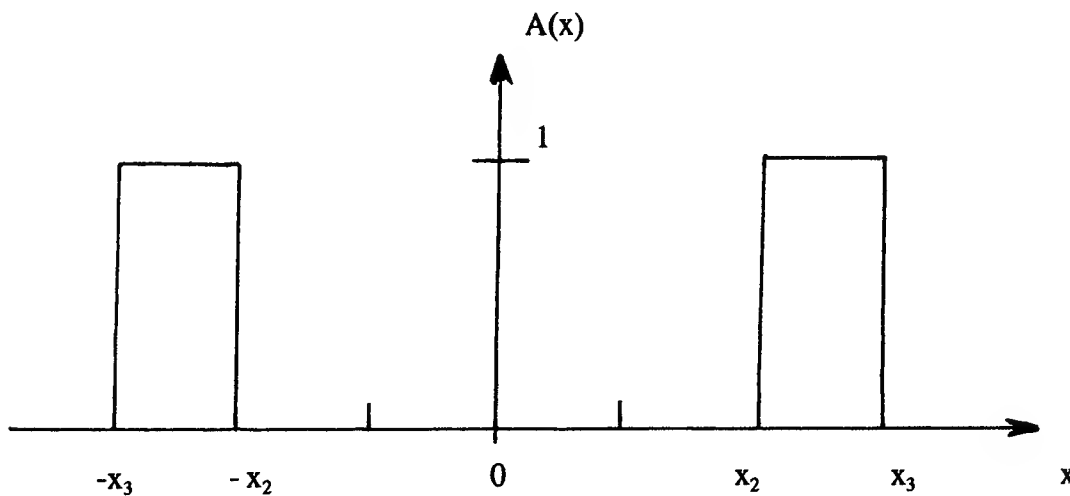
Figure 1. Graphic Representation of A(x).

It is fruitful to rewrite A(x) in terms of a convolution of a rect function R(x) with two delta functions; this is illustrated in Figure 11 below on a different scale.

(Convolution)

$$A(x) \qquad = \qquad R(x) \qquad * \qquad \delta [x \pm (x_2 + x_3)/2 = \Delta_3(x)$$

$$x_2 \qquad x_3 \qquad -\Delta x/2 \quad \Delta x/2 \qquad -[x_3 + x_2]/2 \qquad [x_3 + x_2]/2$$
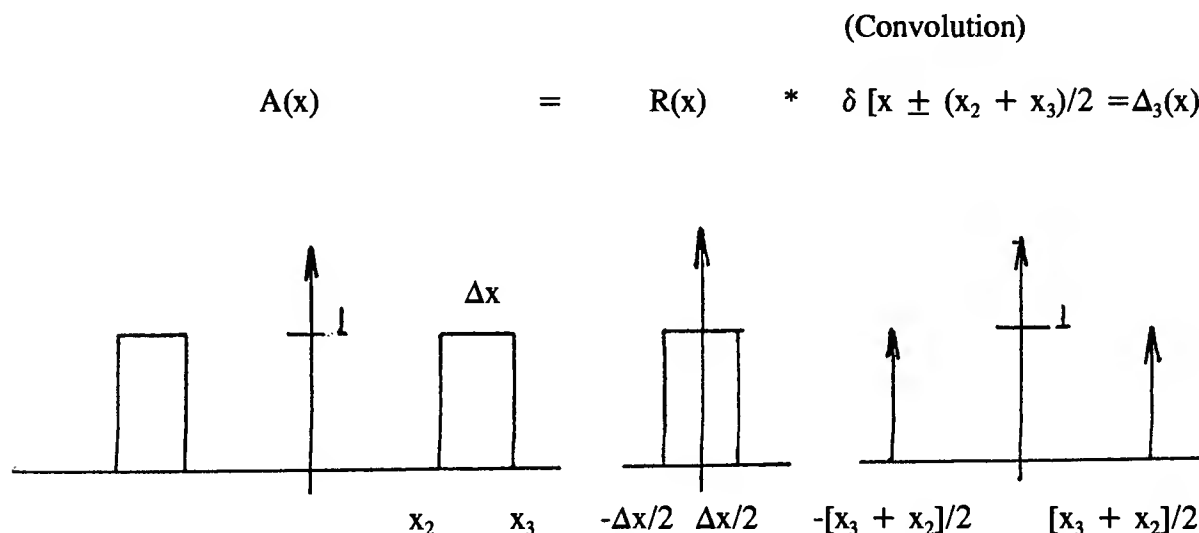
Figure 2. Illustration with the Use of Delta Functions.

We can now rewrite Eq (10) as follows,

$$B_3 (\sigma) = \int_{-\infty}^{\infty} [R(x) * \Delta_3 (x)] F(x)^{-i2\pi\sigma x} dx \tag{11}$$

It should be noted that R(x) has a fixed width regardless of the interferogram segment but that $\Delta(x)$ consists of two delta functions spaced farther apart as the segment number increases. At this juncture it is instructive to make a few observations. Interferogram segmenting is clearly legitimate since

$$\int [A(x) + B(x] e^{-i2\pi\sigma x} dx = \int A(x) e^{-i2\pi\sigma x} dx + \int B(x) e^{-i2\pi\sigma x}. \tag{12}$$

Furthermore, we may write the discrete Fourier transform in the following matri-type display,

7

$$B(0) = F(0) + F(\tfrac{1}{2\Sigma})\,Cos2\pi\cdot 0\cdot\tfrac{1}{2\Sigma} + \ldots\ldots\ldots$$

$$B(\tfrac{1}{2x}) = F(0) + F(\tfrac{1}{2\Sigma})\,Cos2\pi\cdot\tfrac{1}{2x}\cdot\tfrac{1}{2\Sigma} + F[\tfrac{2}{2\Sigma}]\,Cos2\pi\,\tfrac{1}{2x}\cdot\tfrac{2}{2\Sigma} + F(\tfrac{N_I}{2\Sigma})\,Cos2\pi\cdot\tfrac{1}{2x}\cdot\tfrac{N_I}{2\Sigma}$$

$$B(\tfrac{2}{2x}) = F(0) + F(\tfrac{1}{2\Sigma})\,Cos2\pi\cdot\tfrac{1}{2x}\cdot\tfrac{1}{2\Sigma} + F[\tfrac{2}{2\Sigma}]\,Cos2\pi\,\tfrac{2}{2x}\cdot\tfrac{2}{2\Sigma} + F(\tfrac{N_I}{2x})\,Cos2\pi\cdot\tfrac{2}{2x}\cdot\tfrac{N_I}{2\Sigma}$$

$$\vdots$$

$$\int$$

$$\vdots$$

$$B(\sigma) = B(\tfrac{N_s}{2x}) + F(0) + F(\tfrac{1}{2\Sigma})\,cos2\pi\,\tfrac{N_s}{2x}\cdot\tfrac{1}{2\Sigma}\ \ldots\ldots\ldots\ldots + F(\tfrac{N_I}{2\Sigma})\,Cos2\pi\cdot\tfrac{N_s}{2x}\cdot\tfrac{N_I}{2\Sigma}$$

In the above we have taken an interferogram sampling integral of $\delta x = 1/(2\Sigma)$ and a spectral interval $\delta\sigma = 1/(2X)$. The number of samples N_I of F(x) is $X/[1/(2\Sigma)] = 2\Sigma X$. and the number N_s of spectral samples (or elements) is $\Sigma/[1/(2X)] = 2\Sigma X$. We have then $N_I = 2\Sigma X = N_s$; the same number of samples in both domains. It is seen from the above presentation of $B(\sigma)$ and F(x) that the usual Fourier analysis calculates the value of a spectral element by using all the samples from the interferogram. For example, for the spectral element $2/(2X)$ cm^{-1}, $B[2/(2X)]$ is calculated by going along the row corresponding to $B[2/(2X)]$ and increasing the frequency of the cosine function multiplying F(x) as the sample position in x is increased. For each spectral element the whole interferogram must be used in order to get the best resolution $\delta\sigma = 1/X$.

It is interesting to note in passing that there is no reason whatsoever to restrict ourselves to calculation along rows. We can perform the calculation (or transformation) just as well by proceeding according to columns; this we call a synthesis of the spectrum. In other words we imagine the $B(\sigma)$ to be represented by a plot in the spectral domain and look upon it as an image. What the operation by columns does is to slowly build up $B(\sigma)$ with higher and higher spatial structure as each interferogram sample with its corresponding cosine function is added to the previous sum. As can be seen from the matrix array when the third interferogram sample $F[2(2\Sigma)]$ is used it contributes to all (in reality to half the spectral elements) the spectral elements from B(0) to $B[N_s/(2X)]$. That is, the spatial frequency in cm^{-1} space is fixed at $2/(2\Sigma)$ and the spectral components vary from 0 to $B(\Sigma)$; the amplitude of the corresponding cosine function is given by the value of the interferogram at that sample. For the last sample

8

$F[N_I/(2\Sigma)]$ we have a cosine function of amplitude $F[N_I/(2\Sigma)]$ and frequency in the cm^{-1} domain of $N_I/(2\Sigma)$. This last frequency is seen to be the N_I th harmonic of the fundamental $1/(2\Sigma)$.

Let us now go back and rewrite Eq (11);

$$B_3(\sigma) = \int_{-\infty}^{\infty} [R(x) * \Delta_3(x)] \; F(x) \, e^{-i2\pi\sigma x} dx$$

$$= \int_{-\infty}^{\infty} [A(x) \;\; . \;\; F(x) \, e^{-i2\pi\sigma x} dx, \tag{13}$$

where A(x) is a weighing function in the interferogram domain. Using the convolution theorem we may write

$$B_3(\sigma) = \widetilde{A(\sigma)} * B(\sigma), \tag{14}$$

with $B(\sigma) = \widetilde{F(\sigma)}$ being the Fourier transform of F(x), the tilda $\sim$ over a function indicating the Fourier transform of the function and the asterisk * indicating convolution. It is important to note that $B(\sigma)$ is the spectral distribution that would be obtained by transforming a complete interferogram with no variations in spectral distribution throughout the scan, i.e., disregarding the limits,

$$B(\sigma) = \int_{-\infty}^{\infty} F(x) \, e^{-i2\pi\sigma x} dx \tag{15}$$

On the other hand, $B_3(\sigma)$ corresponds to a representation, an estimate, of the spectral distribution that existed between interferogram path differences x_2 to x_3 only. We must determine whether it is legitimate to take an interferogram with a varying $B(\sigma)$, obtain its Fourier transform and perform a convolution of Eq (14) in the spectral domain, to obtain the estimate $B_3(\sigma)$. From Eq (12) above it would appear that this is indeed the case.

A simulation should be done by generating an interferogram from a given $B(\sigma)$, pulling the segment from x_2 to x_3 (which we'll call $F_3(x)$) and inserting it into another arbitrary

9

interferogram at the proper location in path difference. Again, it should be noted that the spectral estimate $B_3(\sigma)$ is the correct $B(\sigma)$ convolved with a scanning function and may not look at all like the original $B(\sigma)$ used in generating that segment of F(x). The next step would be to perform the convolution on $B(\sigma)$ and compare the result with the estimate $B_3(\sigma)$. This simulation would verify the legitimacy of the procedure as well as checking out the software for convolutions in the spectral domain.

To be more specific about the estimate $B_3(\sigma)$ (we shall use the "hat" symbol ^ over the function to indicate an estimate) we use the convolution theorem again to obtain

$$(16)$$

$$\hat{B}_3(\sigma) \approx [\frac{\Delta x \, \sin\pi(\Delta x)\sigma}{\pi(\Delta x)\sigma} \cdot 2\cos2\pi\frac{(x_2 + x_3)}{2}] * B_3(\sigma)$$

where again $B_3(\sigma)$ is the spectral distribution that is assumed to have persisted during x_2 to x_3 of the interferogram segment $F_3(x)$ and is really what we are interested in obtaining.

The scanning function $\tilde{A}(\sigma)$ in the square brackets of Eq (16) represents a sinc (σ) modulated cosine function whose frequency, in cm^{-1} space, is the midpoint of the segment of the interferogram $F_3(x)$, i.e., $(x_2+x_3)/2$. Figure 3 is a representation of the scanning function $\tilde{A}(\sigma)$ for arbitrary values of Δx and $(x_2+x_3)/2$.

$$\tilde{A}(\sigma)$$
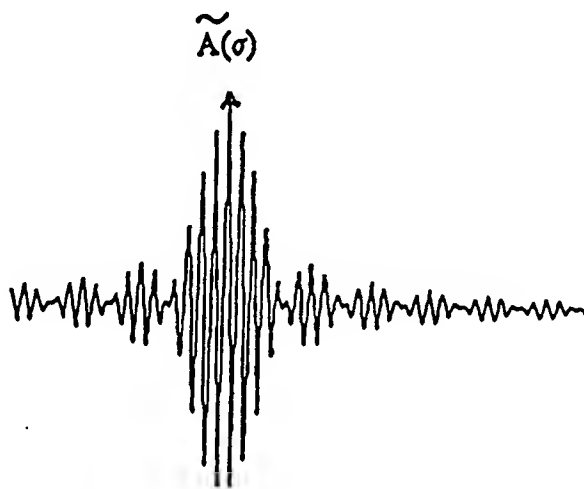
Figure 3. Graphic Representation of the Scanning Function A(σ).

In actual practice there would be many more cycles of the cosine function within the central lobe of the sinc function especially when considering the end of the interferogram or the last segment. To obtain an acceptable $B_3(\sigma)$ we must be able to perform a deconvolution or

a method of somehow extracting spectral information by jittering the window weighing function or interferogram segment a few, or several, sample points to more or less sweep the cosine peaks of $\widetilde{A}(\sigma)$ within the since function envelope. Even then it is not clear at present whether this is a fruitful approach. It is easy to obtain $\widehat{B}_3(\sigma)$ by performing the convolution; however, deconvolution is not so straightforward even when the scanning function is known.

TEST RESULTS AND CONCLUSION

This Section summarizes the technique and the results obtained in our attempt to obtain valid spectral distributions from an analysis of interferograms when the source spectral distribution $B(\sigma)$ varies during an interferometer scan. These variations may be due to a change of the field-of-view (FOV) of the interferometer or changing source emissions characteristics within a fixed FOV.

The output signal $D(x)$ from a Fourier Transform Spectrometer (FTS) as a function of path difference x amy be written as

$$D(x) = \frac{1}{2} D(0) + \int_0^\Sigma B(\sigma) \cos(2\sigma x) \, d\sigma, \tag{17}$$

with the corresponding interferogram $F(x)$ being

$$F(x) = D(x) - \frac{1}{2} D(0) + \int_0^\Sigma B(\sigma) \cos(2\sigma x) \, d\sigma. \tag{18}$$

From the Wiener-Khintchin theorem the spectral estimate $B(\sigma)$, of maximum wavenumber Σ, is obtained by taking the cosine Fourier transform of $F(x)$;

$$B(\sigma) = \int_{-\infty}^{\infty} F(x) \cos 2\pi\sigma x \, dx \tag{19}$$

where X is the maximum path difference for the interferometer scan. We assume we have a symmetric interferogram and rewrite the above expression as

11

$$B(\sigma) \approx \int_{-X}^{X} F(x) e^{-i2\pi\sigma x} dx . \tag{20}$$

As per the technique described in prior Sections, we decimated the interferogram into segments of length Δx which we assumed to be short enough that we could take $B(\sigma)$ to be constant during that time interval. The spectral distribution $B_j (\sigma)$ for the jth interferogram segment we represent by

$$B_j(\sigma) = \int_{-x_j}^{-x_{j-1}} + \int_{x_{j-1}}^{x_j} F(x) e^{-i2\pi\sigma x} dx . \tag{21}$$

Now if $B_j(\sigma)$ were constant from $x=0$ to $x=x_j$ we know that the proper estimate $\langle B_j(\sigma) \rangle$ would be given by

$$\langle B_j(\sigma) \rangle = \int_0^{x_j} F(x) Cos2\pi\sigma x dx = B_j(\sigma) * x_j \frac{sin2\pi\sigma x_j}{2\pi\sigma x_j} \tag{22}$$

with

$$S_j^o(\sigma) = \frac{sin2\pi\sigma x_j}{2\pi\sigma x_j} \tag{23}$$

In the above * stands for convolution and $S_j^o(\sigma)$ is called the scanning function. The scanning function $S_j^o(\sigma)$ has a width inversely proportional to x_j and would be obtained if the spectral distribution were delta functions $\delta(\sigma \pm \sigma_o)$ situated at $\pm \sigma_o$ in the spectral domain. The convolution of the real spectrum with a sinc function $S(\sigma)$ has always been considered an acceptable estimate.

We must now look at the spectral estimate obtained by analysis of a short segment of length Δx of the interferogram located at an arbitrary distance from the zero path difference (ZPD) of the interferogram. It is evident from the last equation that

12

$$B_j(\sigma) = \langle B_j(\sigma) \rangle - \langle B_{j-1}(\sigma) \rangle, \tag{24}$$

where the spectral distribution would be convolved with a scanning function consisting of the difference of two sinc functions. However, we find it more convenient to determine the scanning function via a different route to obtain a more easily visualized scanning function.

We may write $\hat{B}_j(\sigma)$ as

$$B_j(\sigma) \approx \int_{-\infty}^{\infty} W(x) \, F(x) \, e^{-i2\pi\sigma x} dx \tag{25}$$

where the weighing function $W(x)$ is as illustrated below;
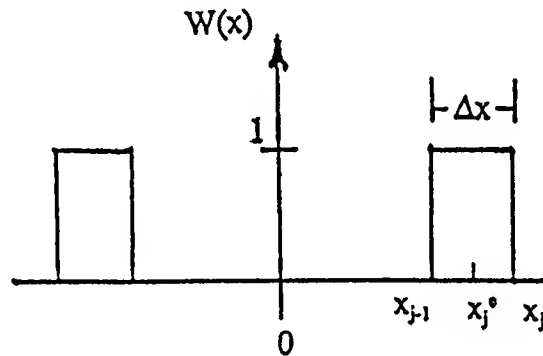
Figure 4. Weighing Function Consisting of Rec Functions.

We obtain, by the convolution theorem

$$B_j(\sigma) \approx W(\sigma) + B_j(\sigma) \tag{26}$$

13

where again B (σ) is taken as the real spectrum and the tilda ($\sim$) sign over W(σ) indicated Fourier transform. Now W(x) can be represented as the convolution of a rect function R(x) with the sum of two delta functions ↑__↑ (x), as illustrated below, with [↑__↑ (x)= $\delta(x-x_j^c)$ + $\delta(x+x_j^c)$].

R(x)

(Convolution)

*

−Δx/2   Δx/2

0   x_j^c
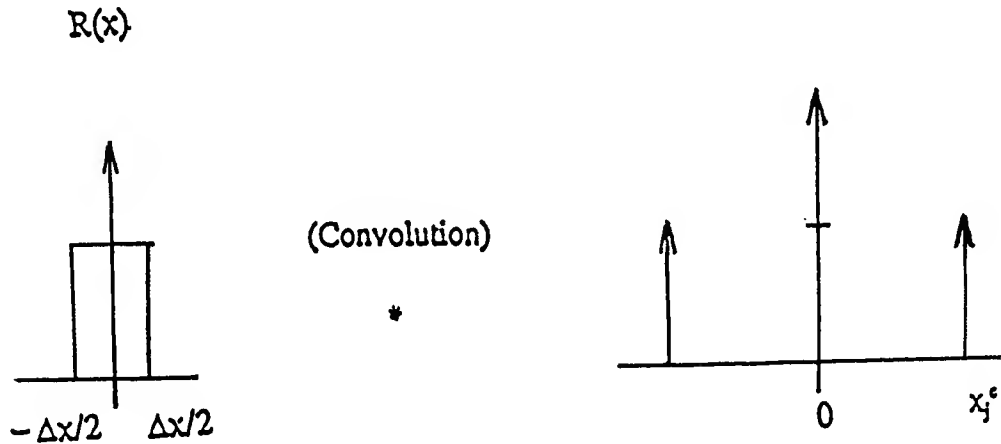
Figure 5.   Rectangular Function Convolved with Delta Functions.

From the above it is clear that

$$W(\sigma) = R(\sigma) . ↑ ↑(\sigma) ,$$

(27)

which yields as scanning function

$$S_j(\sigma) = W(\sigma) \approx [\frac{\Delta x \pi \sigma \Delta x}{\pi \sigma \Delta x}] [Cos 2\pi x_j^c \sigma] .$$

(28)

The scanning function is thus seen to be a sinc modulated cosine. The frequency of the cosine function corresponds to the center position of the jth segment and the sinc function has a width inversely proportional to the segment length Δx. The figure below illustrates the scanning function $S_j(\sigma)$; it was obtained by Fourier transforming a segment of an interferogram of monochromatic radiation. We clearly see the function S_j (σ) represented above, i.e., a constant frequency sine with amplitude varying as a sinc function.

14

$$S_j(\sigma).$$
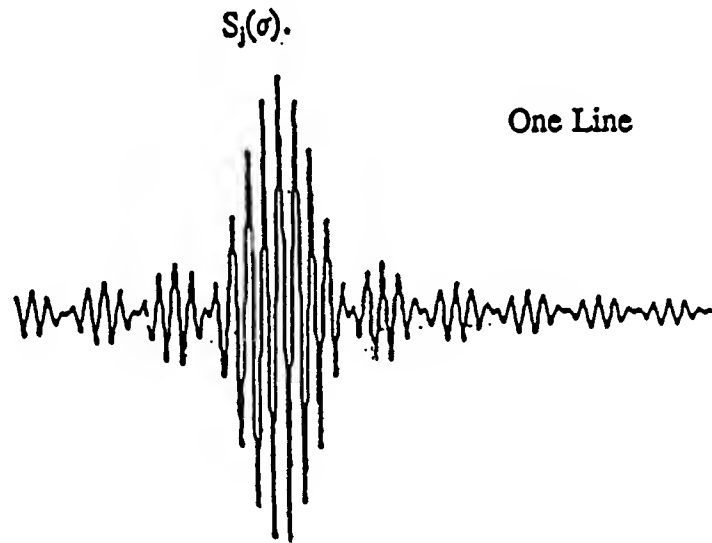
One Line

Figure 6. Graphical Representation of Function $S_j(\sigma)$, one line.

From the expression

$$B_j(\sigma) \approx \int_{-\infty}^{\infty} W(s) \, F(x) \, e^{-i2\pi\sigma x} dx \qquad (29)$$

we obtain the spectral estimate as

$$B_j(\sigma) \approx S_j(\sigma) * B_j(\sigma) \qquad (30)$$

The true spectrum $B_j(\sigma)$ is convolved with $S_j(\sigma)$ which, as we can see from Figure 7, is a more structured function than $S_j^o(\sigma)$ which is a simple sinc function.

The spectral estimates for dense and highly-structured spectra would clearly not be acceptable because of the scanning function $S_j(\sigma)$. It is indeed only in rare cases that a segmented interferogram will yield easily-interpreted spectral estimates. For example, if $B_j(\sigma)$ consists of a single spectral line of unknown frequency it is possible to determine this frequency by looking at the envelope of the spectral estimate; as is evident from Figure 6. From Figure 6 we can see that for widely-separated spectral lines of comparable strengths it is possible to

15

interpret the spectral estimate with respect to the line positions; however, the relative strengths of these lines would be questionable.

$$S_j(\sigma).$$
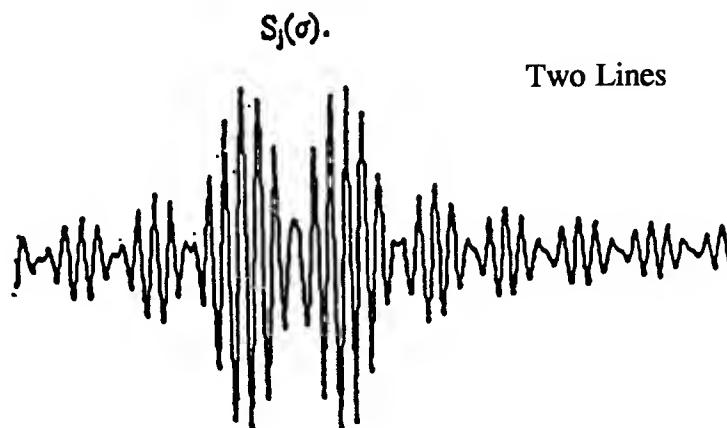
Two Lines

Figure 7.   Graphical Representation of $S_j(\sigma)$; two lines.

We have looked into the possibility of extracting useful spectra from segmented interferograms by converting the spectra to absolute values and looking at the envelope. That is, for the case of two lines as in Figure 7 we rectified the cosine function to end up with all positive amplitude and drew an envelope curve. Since the lines are separated by an interval greater than the width of the base of the sinc function in the scanning function $S_j(\sigma)$, a reasonable spectral estimate could be obtained. However, for closely-spaced lines the cosine functions, in $S_j(\sigma)$, interfere with each other either constructively or destructively depending on the wavenumbers of the lines and yield a highly-distorted spectral estimate.

From the above it was concluded that, except for sparse spectra consisting of a series of appreciably-separated lines, the technique of rectifying and analyzing envelopes of the scanning function obtained from decimated interferograms is not acceptable.

RESOLUTION ENHANCEMENT BY PHASE SHIFTING INTERFEROGRAMS

INTRODUCTION

Background material will now be presented which will lead to two conclusions that are contradictory; one comes from a theoretical treatment of ideal interferograms and the second from the physical properties of a Michelson interferometer treated as a transmission filter.

MONOCHROMATIC CASE

Let's assume we have monochromatic radiation of wavenumber σ_0 and of unit strength with the corresponding interferogram given by

16

$$F(x) = Cos2\pi\sigma_0 x \qquad (31)$$

The interferogram is a cosine function with a peak at ZPD and extending before and after ZPD. We assume that we have and error E in the determination of ZPD and perform the cosine Fourier transform as represented by

$$B(\sigma_0) = \int_0^X Cos2\pi\sigma_0(x + E) \, Cos2\pi\sigma x dx \qquad (32)$$

We can expand Eq 32 as follows

$$B(\sigma_0) = \int_0^X [Cos2\pi\sigma_0 x Cos2\pi\sigma_0 E - Sin2\pi x\sigma_0 Sin2\pi\sigma_0$$

$$= Cos2\pi\sigma_0\epsilon \int_0^X Cos2\pi\sigma_0 x Cos2\pi\sigma x dx$$

$$- Sin2\pi\sigma_0\epsilon \int_0^X Sin2\pi\sigma_0 x Cos2\pi\sigma x dx \qquad (33)$$

From Eq 33 we see that if $\epsilon = 0$, or $k\lambda_0 = k/\sigma_0$

$$B(\sigma_0) = \int_0^X Cos2\pi\sigma_0 x Cos2\pi\sigma x dx$$

which yields the correct scanning function, i.e.,

17

$$B(\sigma_0) \approx \int_0^x [Cos2\pi (\sigma - \sigma_0) x + Cos2\pi (\sigma + \sigma_0) x] \, dx \qquad (34)$$

$$= x [\frac{Sin2\pi (\sigma - \sigma_0) x}{2\pi (\sigma - \sigma_0) x} + \frac{Sin2\pi (\sigma + \sigma_0) x}{2\pi (\sigma + \sigma_0)) x}] \qquad (35)$$

Looking at only the positive frequency spectrum, namely

$$x \frac{Sin2\pi (\sigma - \sigma_0) x}{2\pi (\sigma - \sigma_0) x} \qquad (36)$$

we have a sinc function with full width at the base (at the first zeros) given by 2/x.

Returning to Eq 33 if $\epsilon = \lambda_0/4$ or $1/(4\sigma_0)$ then we retain only the 2nd integral which is an antisymmetrical profile being zero at $\sigma = \sigma_0$, i.e.,

$$\int_0^x Sin2\pi\sigma_0 x Cos2\pi\sigma x \, dx =$$

$$\frac{1}{2} \frac{1}{2\pi (\sigma - \sigma_0)} [1 - Cos2\pi (\sigma - \sigma_0) x] + \ldots \ldots \qquad (37)$$

where only the positive frequency term is shown in Eq 37.

We may conclude from the above that for monochromatic radiation, corresponding to a cosine function interferogram, the correct scanning function (in this case the spectrum estimate) is obtained if the cosine FT is taken starting at any peak of the interferogram; the point of ZPD is not unique in this case. If the spectrum consists of many emission lines separated enough to allow examination of the line shapes, it is possible to determine the error ϵ by placing $\epsilon = k/\sigma_c$

18

for the line shape which is a sinc function at the frequency σ_c wavenumber.

EQUALLY-SPACED LINES

This brings up an interesting observation. The interferogram corresponding to a spectrum of equally-spaced lines displays a central peak at ZPD plus signatures at intervals of path difference x/Δ where Δ is the separation of the spectral lines in cm^{-1}; that is for $x_1 = 1/\Delta$, $x_2 = 2/\Delta$, etc. These signatures occur on both sides of ZPD. These interferograms points x_1, x_2, etc correspond to path differences where all the spectral elements are in phase, or all the cosine functions peak simultaneously as they did at ZPD. If we were to take the FT starting at the path difference $-x_2$ would the spectrum display enhanced resolution when compared with the FT starting at ZPD? Intuition suggests this is true!

SYMMETRIZING THE INTERFEROGRAM

To continue along the same line, if the spectral lines are not strictly equally spaced the signatures will not be so distinct and will be somewhat broadened. Is it possible to symmetrize the interferogram around a signature, say $-x_1$ or $-x_2$, by taking the peak value of the signature as ZPD, perform the usual symmetrizing operation and then taking the FT starting from the peak value of the symmetrized signature? Again, intuitively one would say definitely yes!

INTERFEROMETER PHYSICAL PROPERTIES/TRANSMISSION FILTER

The above conclusion appears to contradict the prior conclusion that the negative portion of the interferogram, from $-X$ to 0, contains the same information as the positive part, from 0 to X, of the interferogram, and from the symmetry of the measurement this is apparently true. The incoming electromagnetic wave to the interferometer can be represented as a wavetrain $F(t)$ given by

$$F(t) = \int_{f_1}^{f_2} A(f) e^{i2\pi ft} df \tag{38}$$

where f is frequency and $A(f)$ represents the amplitude of the EMF for the frequency f; with f_1 and f_2 being the cutoff frequencies. An ideal interferometer of the Michelson type divides the amplitude of the incoming wave in two equal parts $F_1(t)$ and $F_2(t)$ where $F(t) = F_1(t) + F_2(t)$. The displacement of one mirror of the interferometer introduces a time delay τ in one of the divided wavetrains; the two wavetrains are then recombined. Mathematically this is represented by

19

$$I(\tau) \;=\; \int_0^T F_1(t)\,F_2(t\pm\tau)\,dt \qquad\qquad (39)$$

with the intensity at ZPD occurring when $\tau = 0$, I(0). Since $F_1(t) = F_2(t)$ it is immaterial which wavetrain is delayed with respect to the other regardless of the shape of the input wavetrain; i.e., it can be symmetric or asymmetric about a center portion. From the above it seems clear that no added information is obtained by going to negative lags as well as positive lags, and appears to contradict the conclusions arrived at for interferograms with obvious distinct signatures!

This latter conclusion can be reinforced (or supported) by considering the interferometer as a transmission filter. For a given optical path difference the transmission of the interferometer is a $\cos^2$ function of wavenumber (cm^{-1}); which may be written as a DC component plus a cosine function. The period in cm^{-1}s of this cosine transmission function is inversely proportional to the OPD in the interferometer. The maximum OPD, X, determines the finest structure which can be separated out of the spectrum; namely, the resolution is given by $\delta(\sigma) = 1/X$. Since it makes no difference to the electromagnetic field which mirror of the interferometer is displaced, or equivalently which wavetrain is delayed with respect to the other, going to the same OPD of X with the other interferometer mirror yields the same frequency.

FINAL ANALYSIS

Returning to Section "Symmetrizing the Interferogram" we find that intuition would support enhanced resolution. However results in the previous Section Interferometer Physical Properties/Transmission Filter" indicate that shifting ZPD to another optical path difference Δ introduced a phase factor given by $2\pi\sigma\Delta$. It was also shown that such shifting of ZPD is equivalent to shifting the central peak of the interferogram to the path difference Δ. Now the technique of symmetrizing an interferogram is as follows: 1) a short segment of the interferogram centered around ZPD is Fourier transformed; 2) the phase function $\phi(\sigma)$ for the spectrum is obtained; 3) the original interferogram is convolved with $\phi(x)$ the Fourier transform of $e^{-i\phi(\sigma)}$ to symmetrize the interferogram.

It should be noted that the same function $\phi(x)$ is used throughout the interferogram and consequently does a phase shifting at portions of the interferogram away from ZPD; including in the region of signatures. However, in order to symmetrize the interferogram about a signature at an OPD of Δ the phase factor $2\pi\sigma\Delta$ mentioned above would have to be added to $\phi(\sigma)$. The resultant phase function $\psi(\sigma) = \phi(\sigma) + 2\pi\sigma\Delta$ is a rapidly varying function and the symmetrizing operation would not work since the technique of Forman, Steel and Vanasse (FSV) assumes that the phase function is slowly varying.

Were it possible to symmetrize the interferogram about a signature, we would find that

20

we have essentially shifted the whole interferogram by an amount equal to the position of the signature. This is due to the fact that passing a function, i.e. the interferogram, through a linear phase shift filter does not distort the function but advances or delays it an amount equal to Δ. However, attempting to determine the proper phase function at a signature would require extremely high resolution because of the rapidly varying nature of this phase function; the result obtained using realistic data would yield a near-random distribution of phases across the spectrum.

CONCLUSION

In this report we have shown that it is not possible to treat an interferogram as an ordinary time function. The interferogram is an auto-correlation function and has the unique property of having its maximum value at the zero path difference, or a zero lag. The phases of the component sinusoid which make up the electromagnetic field function are lost. The individual sinusoid are shifted in phase by the interferometer so that they all interfere constructively at the zero path difference position in the interferogram. The amplitudes of these sinusoids are not obtained directly; it is their power spectral values that are determined by a Fourier transformation of the interferogram.

Spectral variations which may occur during an interferometer scan were classified as achromatic or chromatic. It was shown that in the achromatic case, when all the spectral components vary in unison, it is possible to correct for the temporal fluctuations before Fourier transformation to obtain valid spectral data. It was emphasized that in some case it is critical to correct for temporal fluctuations before symmetrizing an interferogram.

The chromatic case for spectral variations would require a deconvolution technique if one were to be studying a complex spectrum of arbitrary structure. This requirement is due to the complex nature of the scanning function resulting from decimating the interferogram into sections during which time the spectral distributions are stationary.

Finally, it was concluded that resolution enhancement by symmetrization of the interferogram would not yield hoped-for results. The physical experiment performed by the interferometer makes it abundantly clear that negative lags yield information redundant with that of positive lags. The bottom line is that the interferogram is not an ordinary time series.

21

BLANK

PART TWO

ULTRAVIOLET BACKGROUNDS

CHAPTER 1. INTRODUCTION

The atmospheric background radiances in the ultraviolet spectral region result from entirely different classes of processes than infrared backgrounds. Atomic and molecular electronic transitions determine the observed spectral distributions. Consequently, in Chapter 2 a brief overview of the concepts and terminology for predicting emissions and atmospheric transmission in this spectral region is provided. Scattered sunlight is a major contributor for illuminated conditions and a driver for the chemiluminescence reactions that dominate the nightglow. The solar interactions are described in Chapter 3. The atmospheric emission features present in the nightglow, dayglow, and aurorae are discussed in Chapter 4. Production mechanisms and characteristic intensities are given. Atmospheric solar scattering processes and predictive codes are outlined in Chapter 5. Substantial progress has been made during the last decade in our understanding of the atmospheric UV backgrounds, much of it under BMDO sponsorship. In particular, imaging arrays have permitted spatial distributions of the background radiances, and simultaneous spatial/spectral information about these backgrounds to be obtained. These recent advances in our knowledge of the airglow and auroral backgrounds and structure are reviewed in Chapter 6. A summary, a discussion of remaining unknowns, and a brief description of some near-term missions are presented in Chapter 7 relative to backgrounds due to ultraviolet radiation.

The ultraviolet (UV) portion of the spectrum is generally defined to encompass the spectral region between 100 and 4000Å (10 and 400 nm). The material presented will largely be limited to wavelengths above 1000Å although limited observations concerning shorter wavelengths, the so-called Extreme Ultraviolet (EUV), will be presented. For descriptive purposes the remainder of the UV spectrum is typically divided into three regions, each 1000Å (100 nm) wide. These are: the Far Ultraviolet (FUV), 1000 to 2000Å (100 to 200 nm); the Middle Ultraviolet (MUV), 2000 to 3000Å (200 to 300 nm); and the Near Ultraviolet (NUV), 3000 to 4000Å (300 to 400 nm).

There are two other descriptive terms of common usage in the atmospheric optics community. The first is the vacuum ultraviolet (VUV) corresponding to wavelengths below 2000Å (200 nm). This term arises because of the fact that laboratory observations at these wavelengths generally require the use of vacuum optical systems because of the severity of O_2 absorption (see Chapter 3). The other term is the so-called solar-blind region referring to wavelengths between 1000 and 3000Å (100 to 300 nm). This terminology is generally used to describe detectors which do not respond to longer wavelength light and thus can be used in sunlight without concern for saturation.

CHAPTER 2. RADIATION PHYSICS

INTRODUCTION

The purpose of this chapter is to provide a brief overview of the basic concepts, equations, and terminology used in both predicting atomic/molecular emissions and calculating their transfer through the atmosphere. Emphasis will be on electronic state transitions of species, these being most appropriate for the generation of UV emissions. Where possible references are provided for more detailed discussions on the subject, appropriate data bases and useful computer codes.

MOLECULAR EMISSION

Molecular radiation in the ultraviolet generally occurs in transitions between vibrational and rotational states of differing electronic states of the molecule. These individual transitions provide radiation over spectrally isolated regions according to selection rules to be discussed later. The accumulation of all such transitions between two electronic states is called a band spectrum with historical symbolic designations specifying the specific states of interaction. These designations are fairly straightforward for diatomic molecules and are covered in classic texts such as Pearse and Gaydon [1] and Herzberg [2]. The prediction of polyatomic molecule electronic states is considerably more complex, but still tractable. The work by Herzberg [3] remains a standard text in this latter area. There are many more modern texts which cover this whole area, for example Steinfeld [4], however, the earlier texts are still sound. Our emphasis will be on atoms and diatomic molecules, these providing the dominant UV atmospheric emissions. The specific terminology used to describe the radiation transfer of atomic/molecular emissions is summarized in Table 1 and described below.

The general relationship for the total emission from a given transition between two electronic states (radiant power per unit volume) is

$$j_{\nu'\nu''} = A_{\nu'\nu''} \, N_{\nu'} \qquad (2\text{-}1)$$

where ν' and ν'' are the upper and lower states respectively, $A_{\nu'\nu''}$ is the transition probability (Einstein coefficient) in units of s^{-1}, and $N_{\nu'}$ is the population of the upper state in units of molecules/cm^3. The units of j are thus photons/cm^3-s. Conversion from photons to watts is achieved by multiplying by $h\nu$, the energy of the transition involved, specified in joules. Conversion of the radiation density to sr^{-1} units is achieved by dividing by 4π. The intensity, specified in W/cm^2, is obtained through an integration of the radiation density over the line of sight, through use of the equation of radiative transfer, see the next Subsection.

Table 1. Terminology of Radiative Transfer of Molecular Emission

$j_{v',v''}$	Radiant power per unit density, W/cm^3
$I_{v',v''}$	Radiant intensity, W/cm^2 *
$A_{v',v''}$	Einstein coefficient, s^{-1} *
$\tau_{v'}$	Radiative lifetime of state v', s
$q_{v',v''}$	Franck-Condon factor, dimensionless
$|Re(r)|^2$	Electronic transition probability, (stat-coulomb-cm)^2
v	Frequency, cm^{-1}
F_{ik}	Oscillator strength for atomic transition from state i to k, dimensionless
g_i	Degeneracy for state i, dimensionless
kv	Absorption coefficient at frequency v, cm^{-1}
Δv_D	Doppler line width, cm^{-1}
S	Transition line strength, amagat^{-1} x cm^{-2}
*Quantities refer to transitions from state v' to v''	

The Einstein coefficients can be defined by more elemental quantities:

$$A_{v',v''} = \frac{64\pi^4 \, v^3}{3h} \, | \, \langle v' \, | \, Re(r) \, | \, v'' \rangle \, |^2 \tag{2-2}$$

where the bracketed term represents the integral of the state wave functions over the electric dipole-moment operator and h is Planck's constant. This former quantity is normally described as the product of two parts: (1) the Franck-Condon factor, which describes the overlap between the two states

$$q_{v',v''} = | \, \langle v' | v'' \rangle \, |^2 \tag{2-3}$$

and (2) the electronic transition probability $| \, R_e \, (r) \, |^2$. Note that the magnitude of R_e does vary somewhat with internuclear distance r. The assumption of the Franck-Condon approximation is that this variation is slow and that R_e may be replaced with an average value. (*See Fraser [5] on the R centroid method for evaluating the variation of R_e with internuclear separation.*)

Radiative calculations are often performed using lifetimes instead of Einstein coefficients. The total lifetime of a state designated by v' is given by

$$\frac{1}{\tau_{\nu'}} = \sum_{\nu''} A_{\nu',\nu''} \quad . \tag{2-4}$$

Knowledge of this terminology is sufficient to allow use of the literature to specify band and line intensities. Of course, not all transitions between upper and lower states are allowed. Allowed transitions are defined by a set of selection rules which are governed by such quantities as the spin and angular momentum of the electronic molecular states. These selection rules are well developed, although quite complex for some molecules. An excellent overview of selection rules for diatomic molecules is provided in Herzberg [2].

The Franck-Condon factors and electron transition moments (or r-centroids) for diatomic species has received significant attention and several surveys of these for air species such as O_2, N_2, O_2^+, N_2^+ are available. The most recent of these is by Gilmore et al. [6]. Other useful reviews have been provided by Krupenie [7], Lofthus and Krupenie [8], Slanger [9], and Hsu and Smith [10].

The last quantity required in the evaluation of Eq. (2-1) is the state population. Under equilibrium or at least Boltzmann conditions there are simple relations which allow evaluation of a specific state population, designated by quantum numbers for electronic state, spin, vibration and rotation, in terms of translational, rotational, vibrational and electronic temperatures (see, for example, Herzberg [2]). In general, however, the emission states of interest will be populated in non-equilibrium and often non-Boltzmann distributions, with population mechanisms involving electron or photon excitation, and chemical reaction. The details of these excitation mechanisms will be provided in Chapter 4.

The discussion so far has emphasized diatomic molecules. There are also a number of atomic transitions of relevance in atmospheric UV emissions. Equation (2-1) still pertains for atomic transitions, however, the expression for the Einstein coefficient simplifies. The atomic Einstein transition between states k and i with wavelength λ_j cm (note $\lambda = \nu^{-1}$) is

$$A_{ki} = \frac{6.67 \times 10^{27}}{\lambda^2} \frac{g_i}{g_k} f_{ik} \tag{2-5}$$

where g_i and g_k are the statistical weights of the lower and upper states and f_{ij} is the dimensionless absorption oscillator strength.* Tabulation of these quantities for relevant atmospheric transitions may be found in Weise et al. [11, 12].

RADIATIVE TRANSFER

As radiation from a specific species traverses the atmosphere, it can be absorbed and scattered. The absorption can be self-absorption, i.e., the inverse of the emission process, or

---

*Note that the emission oscillator strength $f_{ki} = g_i/g_k\ f_{ik}$.

co-incidental by other species and band systems. Scattering can be either by molecular or aerosol means with aerosols becoming more important at lower altitude, see Chapter 5.

The specification of transmitted radiation requires evaluation of the radiative transfer equation which involves use of several other radiometric quantities: absorption coefficient, line strength, and line shape. Although a discussion of the full radiative transfer equation is beyond the scope of this text, definitions of these quantities are provided below.

The basic quantity of the radiative transfer equation is the absorption coefficient k_ν, cm^{-1}. The quantity k_ν is a measure of the absorption of intensity I_ν at frequency ν per unit length, i.e.,

$$dI_\nu/dx \big|_{absorpt.} = -k_\nu I_\nu \quad . \tag{2-6}$$

In Eq. (2-6), the quantity k_ν includes the density of the absorbing state(s), although it is often expressed in terms of per unit density. Although at a given frequency the absorption may be due to just one transition in general, the quantity k_ν can be composed of contributions from a number of discrete and continuum absorbers. Here the discussion will be limited to a single absorbing transition.

A discrete optical transition actually radiates over a finite, rather than single, frequency range as determined by its line shape function. The line shape is generally written in terms of the absorption coefficient, k_ν, which is a measure of the absorption per unit length per unit density at frequency ν. The simplest line shape for a stable transition is the Doppler line shape which results from the Maxwellian velocity distribution of the molecule. This is specified as:

$$k_{\nu,0} = \frac{S}{\Delta\nu_D} \left[\frac{\ell n 2}{\pi} \right]^{1/2} e^{-\ell n 2 \left((\nu-\nu_o)/\Delta\nu_D \right)^2} \tag{2-7}$$

where ν_o is the central frequency of the transition and $\Delta\nu_D$ is the doppler line width in cm^{-1}:

$$\Delta\nu_D = \frac{\nu_o}{c} \left(2 \, k \, \ell n 2 \, T/M \right)^{1/2} \tag{2-8}$$

where c is the speed of light, k is Boltzmann's constant, T is translational temperature, and M is molecular weight in grams/mole.

The quantity S is the line strength, which is the integral of the absorption coefficient over frequency space

$$S = \int_0^\infty k_\nu \, d\nu \tag{2-9}$$

and is related to the Einstein coefficient defined earlier by the relationship

27

$$S_{\ell u} = \frac{1}{8\pi c \nu^2} \ N_\ell \ A_{u-\ell} \ \frac{g_u}{g_\ell} \left(1 - e^{-hc\nu_n/kT}\right) \tag{2-10}$$

where N is in molecules or atoms cm^{-3} and we have once again introduced the notation of lower and upper states as a reminder that all terms are specific to a given transition. Again, the band strength is often quoted in units of density at STP, i.e., with N_ℓ defined as 2.67×10^{19} mol/cm^3. This latter unit is designated by the term amagat.

These quantities are described in more detail in many standard texts, for instance, Mitchell and Zemansky [13] and Penner [14]. In particular, expansions on both line shape theory, including collisional effects, and radiative transfer may be found therein. Generally, atmospheric transmission for UV radiation can be adequately handled using the Doppler line shape formalism.

Radiative transfer involving only molecular absorption and fluorescence can be handled adequately with modest computer models in terms of the quantities defined above (see Mitchell and Zemansky [13] and Penner [14]). The inclusion of scattering effects significantly complicates the radiative transfer problem. Since the scattering process changes the photon direction, the prediction of radiative signal is no longer a straightforward line-of-sight calculation, but must include contributions from sources scattered into or out of the field of view. This subject is beyond the scope of this text but detailed elaborations may be found in Chandrasekhar [15], Van de Hulst [16], LaRocca [17], and Brasseur and Solomon [18] among others. Extant computer models for the prediction of atmospheric UV radiative transfer are reviewed in Chapter 5.

CHAPTER 2 REFERENCES

1   Pearse, R.W.B. and Gaydon, A.G., *The Identification of Molecular Spectra*, 3rd Edition, London, Chapman & Hill Ltd., 1963.

2   Herzberg, G., *Molecular Spectra and Molecular Structure, I. Spectra of Diatomic Molecules*, D. Van Nostrand Co., Princeton, 1950.

3   Herzberg, G., *Molecular Spectra and Molecular Structure, III. Electronic Spectra and Electronic Structure of Polyatomic Molecules*, Van Nostrand Reinhold Co., New York, 1966.

4   Steinfeld, J.F., *Molecules and Radiation, An Introduction to Modern Molecular Spectroscopy*, MIT Press, Cambridge, 1978.

5   Fraser, P.A., *A Method of Determining The Electronic Transition Moment for Diatomics Molecules*, Can. J. Phys. **32**, 515, 1954.

6   Gilmore, F.R., Laher, R.R., and Espy, P.J., *"Franck-Condon Factors, r-Centroids, Electronic Transition Moments and Einstein Coefficients for Many Nitrogen and Oxygen Band Systems,"* J. Phys. Chem. Res. Data **21**, 1005, 1992.

7   Krupenie, P.H., *"The Spectrum of Molecular Oxygen,"* J. Phys. Chem. Res. Data **1**, 423, 1972.

8   Lofthus, A. and Krupenie, P.H., *"The Spectrum of Molecular Nitrogen,"* J. Phys. Chem. Res. Data **6**, 113, 1977.

9   Slanger, T.G., *Auroral $N_2 (c'^1_4\Sigma_u^+\rightarrow a^1\pi_g)$ Emission, II,* Planet. Space Sci. **34**, 399, 1986.

10   Hsu, D.K. and Smith, W.H., *"Visible and Ultraviolet Region for Diatomic Molecules on Astrophysical Interest,"* Spectrosc. Lett. **10**, 181, 1977.

11   Weise, W.L., Smith, M.W., and Glennon, B.M., *"Atomic Transition Probabilities. Vol. II, Sodium Through Calcium,"* NSRDS-NBS22, 1969, U.S. Government Printing Office.

12   Weise, W.L., Smith, M.W., and Glennon, B.M., *"Atomic Transition Probabilities,"* Vol. I, Hydrogen Through Neon," NSRDS-NBS4, 1966, U.S. Government Printing Office.

13   Mitchell, A.C.G. and Zemansky, M.W., *Resonance Radiation and Excited Atoms,* Cambridge at the University Press, 1961.

14   Penner, S.S., *Quantitative Molecular Spectroscopy and Gas Emissivities,* Addison-Wesley Publishing Co., Reading, MA, 1959.

15   Chandrasekhar, S., *Radiative Transfer,* Dover Publications, NY, 1960.

16   Van de Hulst, H.C., *Light Scattering by Small Particles,* Wiley, Dover Publications, New York, 1957.

17   LaRocca, A.J. and Turner, R.E., *"Atmospheric Transmittance and Radiance: Methods of Calculation,"* IRIA Report 107600-10-T, Environmental Research Institute of Michigan, 1975.

18   Brasseur, G. and Solomon, S., *Aeronomy of the Middle Atmosphere,* Reidel, Dordrecht, 1984.

CHAPTER 3

THE SOLAR FLUX AND ITS INTERACTION WITH THE ATMOSPHERE

The properties of the solar flux and its interaction with the atmosphere are described in numerous standard texts. The information collected below is largely taken from several recent publications including Hall et al. [1], Rees [2], Meier [3], and Huffman [4].

THE SOLAR SPECTRUM

A representative solar spectrum for wavelengths above 3000Å as taken from Hall et al. [1] is shown in Figure 1. To first order this spectrum looks much like that of a blackbody with a characteristic temperature of ~6000 K. The total solar insolation at the top of the atmosphere, i.e., the integral of this spectrum over wavelength, is approximately 1.37 kW/m^2 and varies only slightly.

The UV portion of the solar flux is quite distinct from the visible in that it is spectrally structured and its intensity, below 1800Å, is highly variable depending strongly on solar
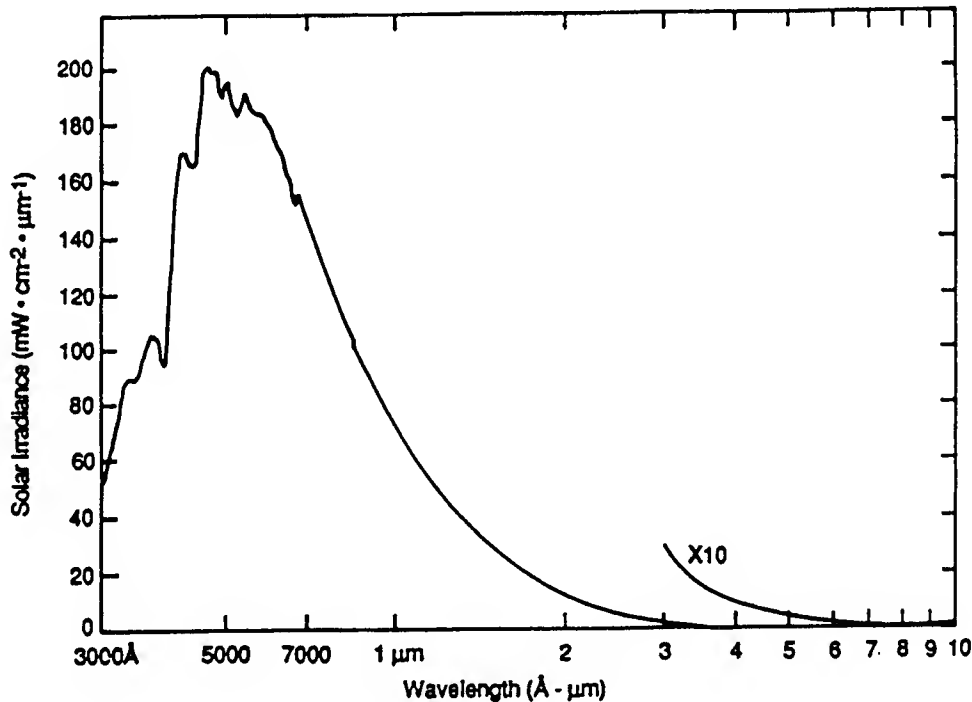
Figure 1.   The Solar Spectral Irradiance for Wavelengths Longer than 3000Å. The data between 3000Å and 3 μm are from Labs and Nickel and from Thekaekara above 3 μm. These data are from a summary given by Pierce and Allen [5]. (Excerpted from Hall et al. [1]).

activity. An example of this variability is shown in Figure 2, taken from Hall et al. [1] which shows observed UV intensity ratios between January 1979 solar maximum to the July 1976 solar minimum. This ratio approaches unity at wavelengths longer than ≈2300Å. Nicolet [7] has recently published a useful retrospective on the uncertainty and variability of reported measurements of solar UV emissions.

The spectral structure in the solar spectrum below 4000Å is shown in the composite solar spectral irradiance for solar minimum conditions as developed by Meier [3] which is presented in Figure 3. As can be seen, the solar spectrum below ~1300Å is dominated by isolated spectral lines of atomic/ionic species. The striking feature seen at 1216Å is the hydrogen Lyman α line. Hall et al. [1] provide a useful tabulation of the UV solar flux intensity at the top of the earth's atmosphere in 10Å intervals. A shortened version of that tabulation is provided in Table 3-1 for the wavelength range of 1000 to 3180Å. These values are appropriate to solar minimum.
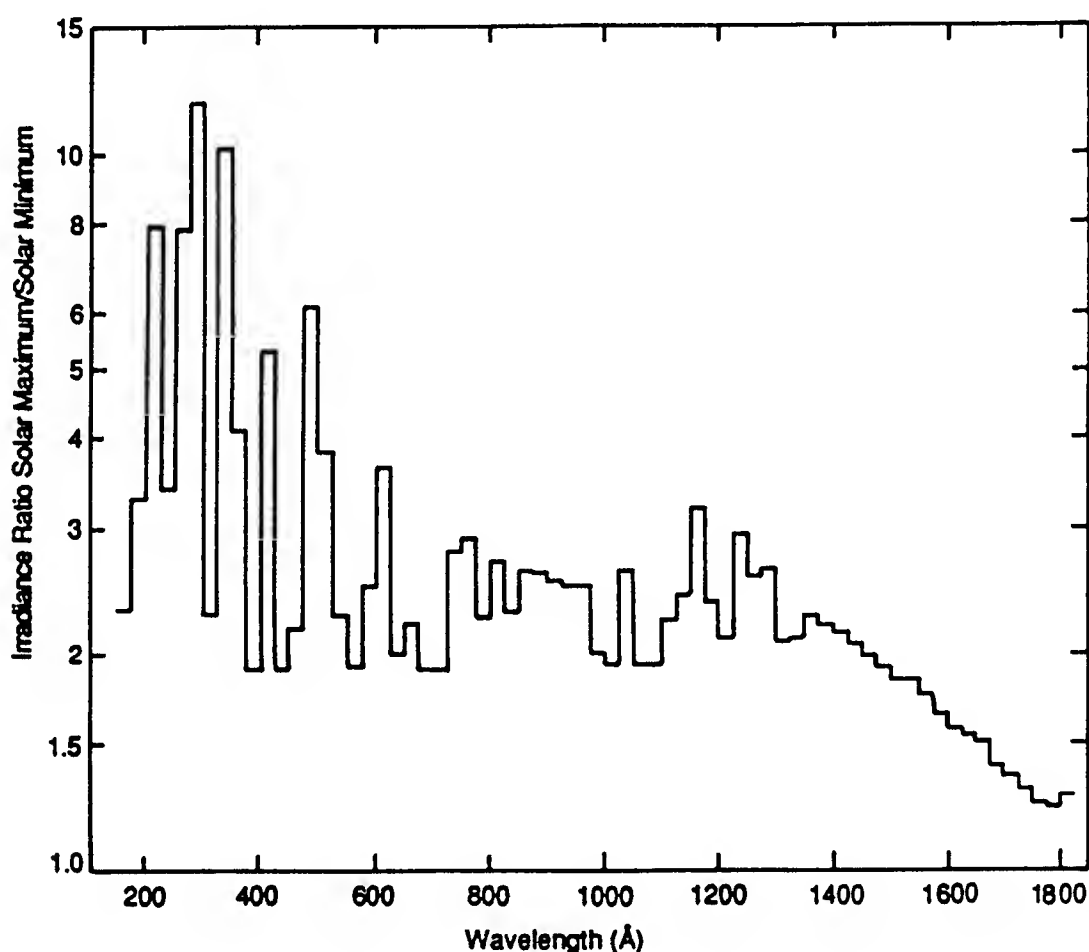
Figure 2.   The Ratio of the Solar Spectral Irradiance Near Solar Maximum During January 1979 to the Irradiance Near Solar Minimum During July 1976 for Solar Cycle 21. The ratios are plotted for 25Å intervals of wavelength [6]. (Excerpted from Hall et al. [1].)

31
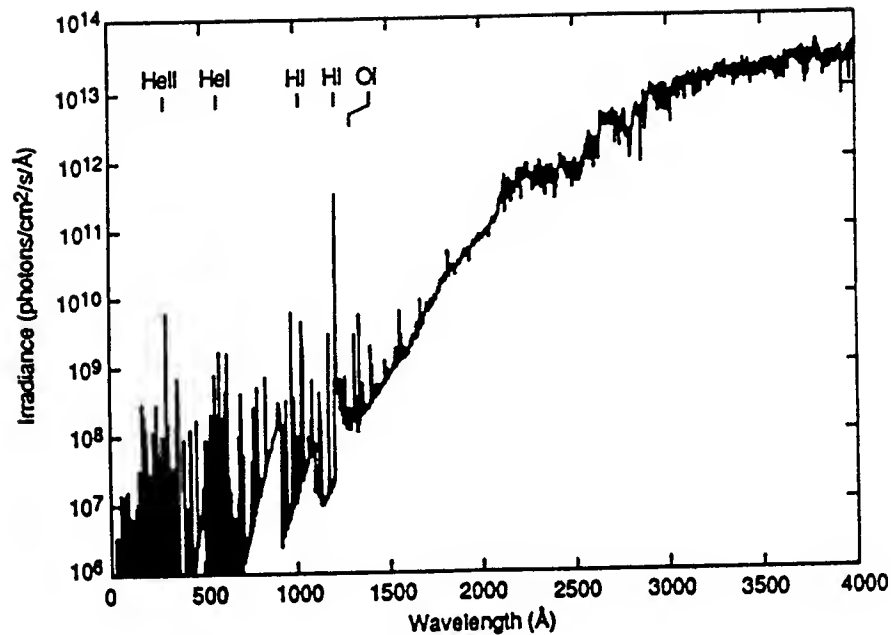
Figure 3.   Composite Solar Spectral Irradiance for Solar Minimum Conditions. SUSIM data
at 1.5Å resolution [8] are used from 1207 to 4000Å. These data were obtained
during the Spacelab 2 mission in July 1985. From 18 to 1100Å, the Hinteregger
et al. [9] quiet-Sun reference spectrum (SC No. 21REF) appropriate to July 1976
is used after binning into 1Å intervals. The Donnelly and Pope [10]
representation of weak lines, superimposed on strong lines from the SC No.
21REF tabulation is used to fill the gap between 1100 and 1207Å. (Excerpted
from Meier [3].)

As is well understood the visible portion of the solar spectrum will transmit through the
earth's atmosphere (although undergoing scattering) ultimately striking the surface and being
partially absorbed and partially reflected back to space. On the other hand the solar light
corresponding to the wavelengths of Table 1 and lower will be absorbed within the atmosphere.
In many instances this absorption will result in the creation of excited or reactive states which
can produce new emissions, see Chapter 4, discussing the airglow. In the following pages we
will provide a brief definition of the atmosphere and its composition and then characterize the
atmospheric absorption of solar UV emissions.

THE ATMOSPHERE

The properties of the atmosphere vary with geographical location, solar activity and
season. They are most easily discussed in terms of the U.S. Standard Atmosphere 1976, which
is a static atmosphere corresponding to mean annual conditions for moderate solar activities at
45°N. This atmosphere is described in detail in COESA [11]. The U.S. Air Force has also
established a set of standard atmospheres [12] specifying seasonal and geographical variability.
A useful summary of these standard atmospheres is provided by Champion et al. [13].

32

Table 2. Solar Irradiance for Quiet Sun at the Top of the Earth's Atmosphere (integrated over 10Å intervals). From Hall et al. [1]

Wavelength Interval Å	$\Phi_{\Delta\lambda}$ (10⁹ photons cm⁻² s⁻¹)	Wavelength Interval Å	$\Phi_{\Delta\lambda}$ (10⁹ photons cm⁻² s⁻¹)
1000 - 1010	0.119	1250 - 1260	1.080
1010 - 1020	0.222	1260 - 1270	0.930
1020 - 1030	3.671	1270 - 1280	0.750
1030 - 1040	3.794	1280 - 1290	0.500
1040 - 1050	0.244	1290 - 1300	0.860
1000 - 1050	8.05	1250 - 1300	4.12
1050 - 1060	0.292	1300 - 1310	4.585
1060 - 1070	0.405	1310 - 1320	0.780
1070 - 1080	0.528	1320 - 1330	0.780
1080 - 1090	1.021	1330 - 1340	5.300
1090 - 1100	0.599	1340 - 1350	0.920
1050 - 1100	2.85	1300 - 1350	12.37
1100 - 1110	0.083	1350 - 1360	1.47
1110 - 1120	0.022	1360 - 1370	1.05
1120 - 1130	0.679	1370 - 1380	1.13
1130 - 1140	0.045	1380 - 1390	1.04
1140 - 1150	0.077	1390 - 1400	2.70
1100 - 1150	0.906	1350 - 1400	7.39
1150 - 1160	0.129	1400 - 1410	2.70
1160 - 1170	0.219	1410 - 1420	1.59
1170 - 1180	2.872	1420 - 1430	1.90
1180 - 1190	0.493	1430 - 1440	2.10
1190 - 1200	0.675	1440 - 1450	2.10
1150 - 1200	4.39	1400 - 1450	10.39
1200 - 1210	4.855	1450 - 1460	2.30
1210 - 1220	251.774	1460 - 1470	3.00
1220 - 1230	0.636	1470 - 1480	3.80
1230 - 1240	1.480	1480 - 1490	3.70
1240 - 1250	0.640	1490 - 1500	3.40
1200 - 1250	259.39	1450 - 1500	16.20

Table 2. Solar Irradiance for Quiet Sun at the Top of the Earth's Atmosphere (integrated over 10Å intervals). From Hall et al. [1] (Continued)

Wavelength Interval Å	$\Phi_{\Delta\lambda}$ (10^9 photons cm^{-2} s^{-1})	Wavelength Interval Å	$\Phi_{\Delta\lambda}$ (10^9 photons cm^{-2} s^{-1})
1500 - 1510	3.90	1750 - 1760	56.99
1510 - 1520	4.50	1760 - 1770	61.97
1520 - 1530	5.50	1770 - 1780	74.02
1530 - 1540	5.90	1780 - 1790	80.99
1540 - 1550	9.50	1790 - 1800	82.96
1500 - 1550	29.30	1750 - 1800	356.93
1550 - 1560	8.80	1800 - 1810	103.00
1560 - 1570	9.00	1810 - 1820	126.00
1570 - 1580	7.70	1820 - 1830	132.02
1580 - 1590	7.10	1830 - 1840	131.96
1590 - 1600	7.20	1840 - 1850	110.95
1550 - 1600	39.80	1800 - 1850	603.93
1600 - 1610	7.90	1850 - 1860	190.51
1610 - 1620	9.40	1860 - 1870	237.55
1620 - 1630	11.10	1870 - 1880	265.25
1630 - 1640	12.00	1880 - 1890	279.95
1640 - 1650	15.30	1890 - 1900	293.84
1600 - 1650	55.70	1850 - 1900	1267.10
1650 - 1660	25.00	1900 - 1910	293.48
1660 - 1670	18.40	1910 - 1920	332.62
1670 - 1680	23.00	1920 - 1930	347.92
1680 - 1690	26.99	1930 - 1940	254.26
1690 - 1700	37.02	1940 - 1950	446.52
1650 - 1700	130.41	1900 - 1950	1674.80
1700 - 1710	43.00	1950 - 1960	427.16
1710 - 1720	43.99	1960 - 1970	485.73
1720 - 1730	45.98	1970 - 1980	487.21
1730 - 1740	41.99	1980 - 1990	492.68
1740 - 1750	50.02	1990 - 2000	552.41
1700 - 1750	224.98	1950 - 2000	2445.19

Table 2. Solar Irradiance for Quiet Sun at the Top of the Earth's Atmosphere (integrated over 10Å intervals). From Hall et al. [1] (Continued)

Wavelength Interval Å	$\Phi_{\Delta\lambda}$ (10^9 photons cm^{-2} s^{-1})	Wavelength Interval Å	$\Phi_{\Delta\lambda}$ (10^9 photons cm^{-2} s^{-1})
2000 - 2010	624.83	2250 - 2260	6.95 X 10^3
2010 - 2020	629.98	2260 - 2270	5.34
2020 - 2030	642.27	2270 - 2280	5.50
2030 - 2040	763.27	2280 - 2290	8.88
2040 - 2050	895.71	2290 - 2300	7.18
2000 - 2050	3556.06	2250 - 2300	33.85 X 10^3
2050 - 2060	909.75	2300 - 2310	6.88 X 10^3
2060 - 2070	964.77	2310 - 2320	5.94
2070 - 2080	1128.23	2320 - 2330	6.54
2080 - 2090	1270.13	2330 - 2340	5.42
2090 - 2100	2562.98	2340 - 2350	4.87
2050 - 2100	6845.86	2300 - 2350	29.65 X 10^3
2100 - 2110	2.72 X 10^{+3}	2350 - 2360	6.78 x 10^3
2110 - 2120	3.52	2360 - 2370	6.18
2120 - 2130	2.92	2370 - 2380	6.15
2130 - 2140	3.81	2380 - 2390	5.36
2140 - 2150	4.81	2390 - 2400	5.85
2100 - 2150	17.78 X 10^{+3}	2350 - 2400	30.32 x 10^3
2150 - 2160	3.74 X 10^{+3}	2400 - 2410	5.10 x 10^3
2160 - 2170	3.48	2410 - 2420	7.00
2170 - 2180	3.72	2420 - 2430	9.39
2180 - 2190	5.07	2430 - 2440	8.49
2190 - 2200	5.60	2440 - 2450	7.73
2150 - 2200	21.61 X 10^3	2400 - 2450	37.71 x 10^3
2200 - 2210	5.42 X 10^3	2450 - 2460	6.46 x 10^3
2210 - 2220	4.19	2460 - 2470	6.79
2220 - 2230	5.80	2470 - 2480	7.50
2230 - 2240	7.96	2480 - 2490	5.43
2240 - 2250	7.17	2490 - 2500	8.18
2200 - 2250	30.54 X 10^3	2450 - 2500	34.36 x 10^3

Table 2. Solar Irradiance for Quiet Sun at the Top of the Earth's Atmosphere (integrated over 10Å intervals). From Hall et al. [1] (Continued)

Wavelength Interval Å	$\Phi_{\Delta\lambda}$ (10^9 photons cm^{-2} s^{-1})	Wavelength Interval Å	$\Phi_{\Delta\lambda}$ (10^9 photons cm^{-2} s^{-1})
2500 - 2510	7.66 x 10^3	2750 - 2760	21.2 x 10^3
2510 - 2520	5.69	2760 - 2770	32.1
2520 - 2530	5.55	2770 - 2780	34.6
2530 - 2540	7.16	2780 - 2790	24.9
2540 - 2550	8.17	2790 - 2800	13.3
2500 - 2550	34.23 x 10^3	2750 - 2800	126.0 x 10^3
2550 - 2560	11.2 x 10^3	2800 - 2810	13.1 x 10^3
2560 - 2570	14.6	2810 - 2820	28.9
2570 - 2580	16.9	2820 - 2830	40.1
2580 - 2590	16.1	2830 - 2840	44.0
2590 - 2600	12.0	2840 - 2850	33.9
2550 - 2600	70.8 x 10^3	2800 - 2850	160.0 x 10^3
2600 - 2610	11.9 x 10^3	2850 - 2860	22.6 x 10^3
2610 - 2620	12.9	2860 - 2870	46.9
2620 - 2630	13.5	2870 - 2880	45.7
2630 - 2640	25.1	2880 - 2890	44.4
2640 - 2650	32.4	2890 - 2900	63.9
2600 - 2650	95.8 x 10^3	2850 - 2900	224.0 x 10^3
2650 - 2660	34.2 x 10^3	2900 - 2910	81.6 x 10^3
2660 - 2670	31.7	2910 - 2920	77.1
2670 - 2680	33.0	2920 - 2930	68.3
2680 - 2690	31.8	2930 - 2940	73.9
2690 - 2700	32.4	2940 - 2950	69.2
2650 - 2700	163.0 x 10^3	2900 - 2950	370.0 x 10^3
2700 - 2710	35.7 x 10^3	2950 - 2960	68.1 x 10^3
2710 - 2720	29.3	2960 - 2970	73.6
2720 - 2730	26.0	2970 - 2980	61.1
2730 - 2740	28.6	2980 - 2990	64.0
2740 - 2750	18.2	2990 - 3000	64.4
2700 - 2750	138.0 x 10^3	2950 - 3000	331.0 x 10^3

Table 2. Solar Irradiance for Quiet Sun at the Top of the Earth's Atmosphere (integrated over 10Å intervals). From Hall et al. [1] (Continued)

Wavelength Interval Å	$\Phi_{\Delta\lambda}$ (10^9 photons cm^{-2} s^{-1})	Wavelength Interval Å	$\Phi_{\Delta\lambda}$ (10^9 photons cm^{-2} s^{-1})
3000 - 3010	50.8 x 10³	3100 - 3110	78.5 x 10³
3010 - 3020	59.3	3110 - 3120	87.9
3020 - 3030	63.5	3120 - 3130	78.9
3030 - 3040	77.7	3130 - 3140	85.3
3040 - 3050	74.9	3140 - 3150	74.6
3000 - 3050	326.0 x 10³	3100 - 3150	405.2 x 10³
3050 - 3060	73.5 x 10³	3150 - 3160	66.5 x 10³
3060 - 3070	71.9	3160 - 3170	77.8
3070 - 3080	79.0	3170 - 3180	105.0
3080 - 3090	76.4		
3090 - 3100	58.5		
3050 - 3100	359.0 x 10³		

The atmosphere is most usefully defined in terms of its temperature-height profile which as shown in Figure 4a and b. The various characteristic thermal regions of the atmosphere, defined from the surface to 1000 km are delineated on these figures. Note that in the absence of interactions between the solar flux and the atmosphere the atmospheric temperature would decrease uniformly with increasing altitude. Thus, regions of increasing temperature clearly demarcate important solar absorptions. As discussed below solar UV absorption by O_3 dominates in the stratosphere and photo-dissociation of O_2 and photo-ionization by VUV photons dominate in the thermosphere. We note further that the exospheric temperature is strongly dependent on the intensity of VUV emissions, and thus on solar activity, and can vary between ~600 to 1900 K.

The atmosphere is often also denoted by species concentration rather than temperature variations. The region up to the mesopause, ~86 km, corresponds to a uniform mix of the major constituents O_2 and N_2 and is denoted as the homosphere. At higher altitudes oxygen atoms become a significant species and ultimately dominate the O_2 and N_2 concentrations. Generic species profile behavior for the U.S. Standard Atmosphere, 1976 are shown in Figure 5. The ionosphere, the region of the atmosphere containing significant electron/ion concentrations, begins at about 70 km. Again photo-ionization becomes important at wavelengths below about 1338Å (NO) and thus the atmospheric electron density will be variable with solar activity. Figure 6, taken from Huffman [4], exemplifies extreme day/night variations in electron densities and also delineates the various regions of the ionosphere.
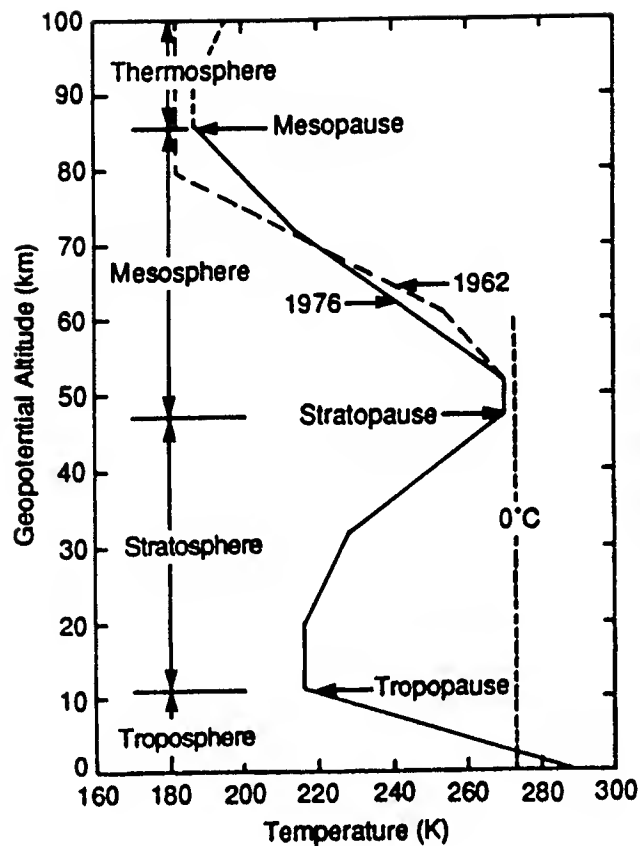
Figure 4a. Temperature-height profile for
  U.S. Standard Atmosphere, 1976. 0-86 km.
  (Excerpted from Champion et al. [13].)
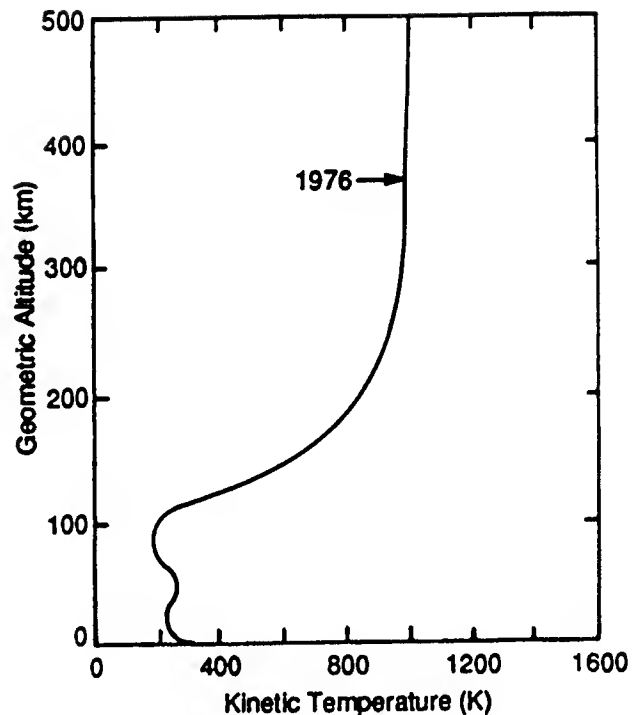
Figure 4b. Kinetic temperature as
  a function of geometric altitude.
  U.S. Standard Atmosphere, 1976.

Detailed empirical models of the thermosphere have been developed through collation of satellite, rocket and radar data. The most current thermospheric model is MSIS-90 [14-16] which allows specification of thermospheric species concentrations and temperatures as a function of solar and magnetic activity, local time and geographical location. A useful compilation of thermospheric variability as predicted from the MSIS-86 model is tabulated in Rees [2]. (Another model that has been widely used in the past is that of Jacchia [17]. Its use has largely been supplanted by the availability of MSIS-86 and MSIS-90).

A variety of three dimension global atmospheric models has been under development for a number of years although they are in general only accessible to specialists. Rees [2] provides a useful review of the state-of-the-art of thermospheric general circulation models. Descriptions of circulation models for the lower atmosphere may be found in standard texts, e.g., Brasseur and Solomon [18] and Chamberlain and Hunten [19].

38
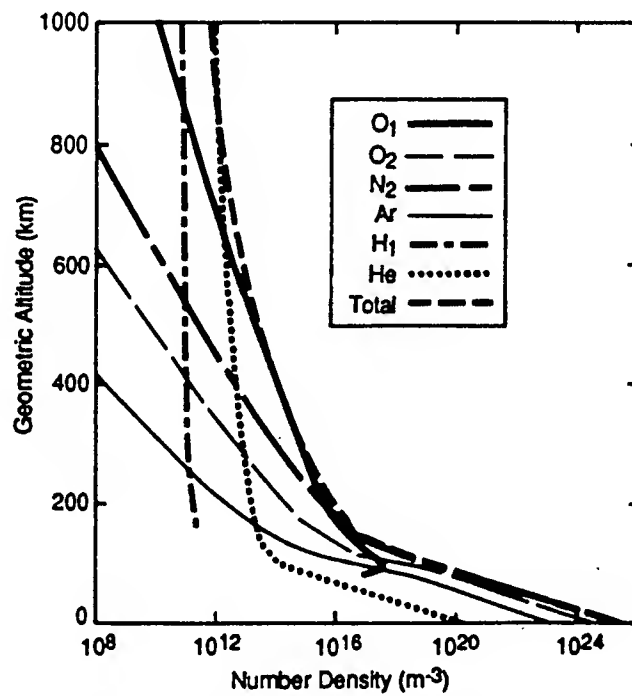
Figure 5.   Number Density of Individual Species and Total Number Density as a Function of Geometric Altitude. Excerpted from U.S. Standard Atmosphere, 1976.
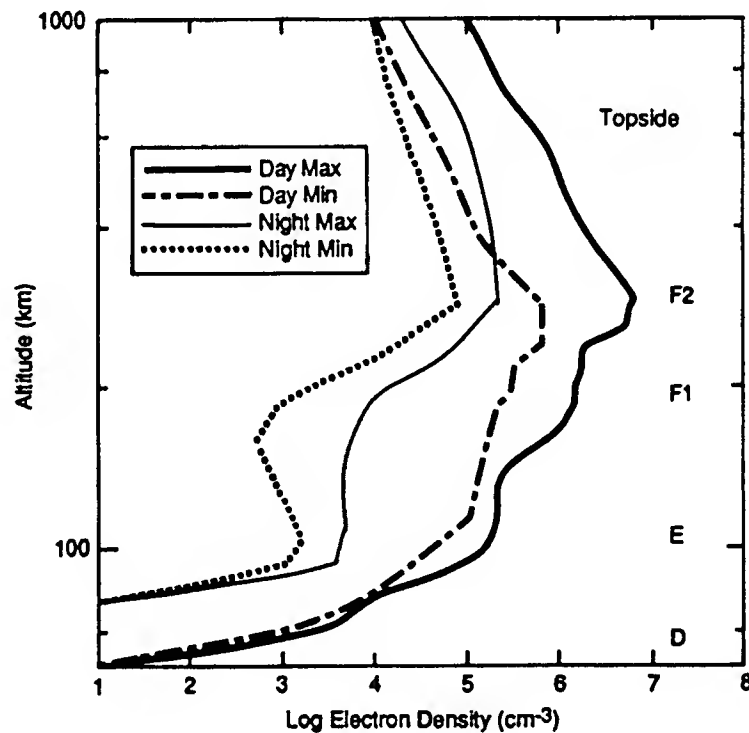
Figure 6.   Electron Density Profiles in the Ionosphere (based on data in the *Handbook of Geophysics and the Space Environment).* (Excerpted from Huffman [4].)

ATMOSPHERIC ABSORPTION OF SOLAR FLUX

It is clear that both the static and dynamic properties of the atmosphere are largely defined by the interaction of the solar flux with atmospheric species. The complex variation in temperature with altitude, the transition of the homosphere into the thermosphere, and the formation of the ionosphere are all primarily the result of atmospheric species absorption of ultraviolet solar emissions. The UV absorption occurs through a number of important interactions as discussed below.

One useful perspective for overviewing these interactions is to examine the altitude penetration depth of the solar UV flux as a function of wavelength. This type of presentation has been frequently provided in terms of the altitude for unit optical depth as a function of wavelength (unit optical depth is defined as the point where the intensity is attenuated to e^{-1} of its initial value). A representation of the altitude of unit optical depth versus wavelength for vertically incident UV radiation is shown in Figure 7, as excerpted from Meier [3]. As can
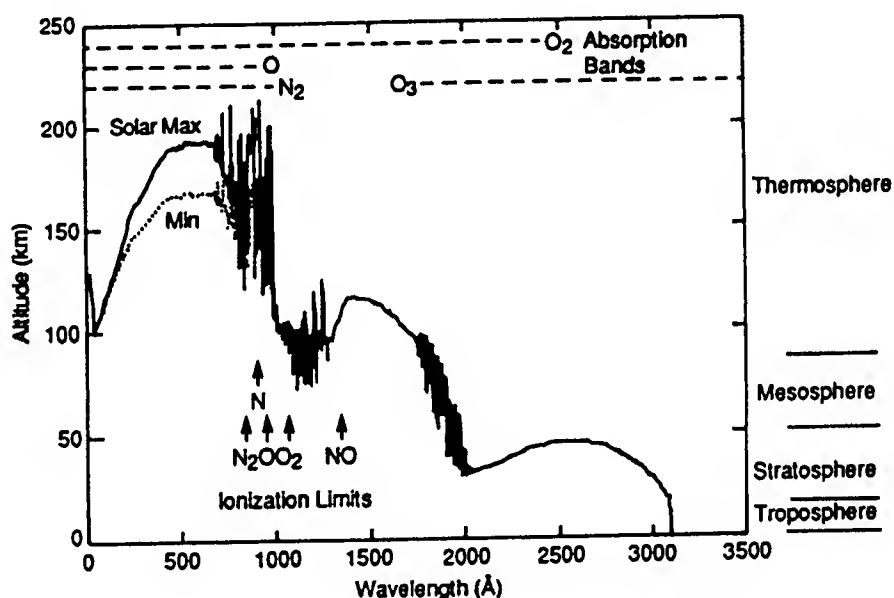
Figure 7. Altitude at Which Vertically Incident UV Radiation is Attenuated by e^{-1}. Dashed lines at top identify spectral regions where extinction by the indicated species is significant. Arrows give the ionization thresholds of important atmospheric species. Atmospheric regions are given on the right. Altitudes for solar max and min were obtained using the MSIS-86 model (see Chapter 2) above 90 km; below 90 km, the US standard atmosphere was used. Absorption cross sections were taken from Conway [20] for N_2, O_2, O in EUV, from Watanabe [21], Blake et al. [22], Yoshino et al. [23], and Nicolet and Kennes [24] for O_2 in the FUV and MUV, and from Molina and Molina [25] for O_3. Earlier versions of these curves appeared in Lean [26] and Chamberlain and Hunten [19]. (Excerpted from Meier [3].)

be seen Figure 7 also delineates the spectral regions over which various absorption features dominate. As mentioned earlier photoionization begins to play a role at wavelengths below 1338Å but does not become an important UV loss process until wavelengths below 1028Å. Oxygen photodissociation becomes important at wavelengths roughly below 1900Å and O_3 photo-dissociation in the stratosphere dominates at longer wavelengths. A convenient tabulation delineating the energetic onset of the various dissociation and ionization processes important in the atmosphere is provided in Table 3.

Table 3. Important Atmospheric Energy Thresholds (from ground states).
(Excerpted from Huffman [4].)

Transition	λ (Å)	E (eV)	Comment
$O_3(X^1A_1) \rightarrow O_2(X^3\Sigma_g^-) + O(^3P)$	11920.0	1.04	Dissociation
$O_3(X^1A_1) \rightarrow O_2(a^1\Delta) + O(^1D)$	3110.0	3.99	Hartley continuum
$O_2(X^3\Sigma_g^-) \rightarrow O(^3P) + O(^3P)$	2424.0	5.115	Herzberg continuum
$O_2(X^3\Sigma_g^-) \rightarrow O(^1D) + O(^3P)$	1751.0	7.081	S-R continuum
$O_2(X^3\Sigma_g^-) \rightarrow O_2^+ (X^2\Pi_g) + e$	1028.0	12.06	Photoion. continuum
$N_2(X^1\Sigma_g^+) \rightarrow N(^4S) + N(^4S)$	1270.0	9.759	Dissociation
$N_2(X^1\Sigma_g^+) \rightarrow N_2^+(X^2\Sigma_g^+) + e$	795.8	15.580	Photoion. continuum
$O(^3P) \rightarrow O^+(^4S) + e$	910.4	13.618	Photoion. continuum
$NO(X^2\Pi) \rightarrow NO^+(X) + e$	133.8	9.267	Photoion. continuum

Detailed cross sections for individual processes may be found in a number of standard references, e.g., Rees [2] and Huffman [4,27]. In this text we briefly discuss absorptive phenomenology associated with O_2 and O_3, the dominant species for atmospheric UV absorption above 1000Å.

An overview of the UV photo-absorption characteristics of O_2 is presented in Figure 8. Note that the figure scans almost eight orders of magnitude in absorption cross section, σ. The absorption cross section can be related to the altitude of unit optical depth presented in Figure 7 through the relationship

$$\int_H^\infty \sigma_x \, n_x \, dh = 1 \qquad (2\text{-}11)$$

where the subscript x denotes the species of interest, n_x is the species density, H is the altitude of unit optical depth, and the integral is over altitude h. Even very low O_2 absorptive cross

41
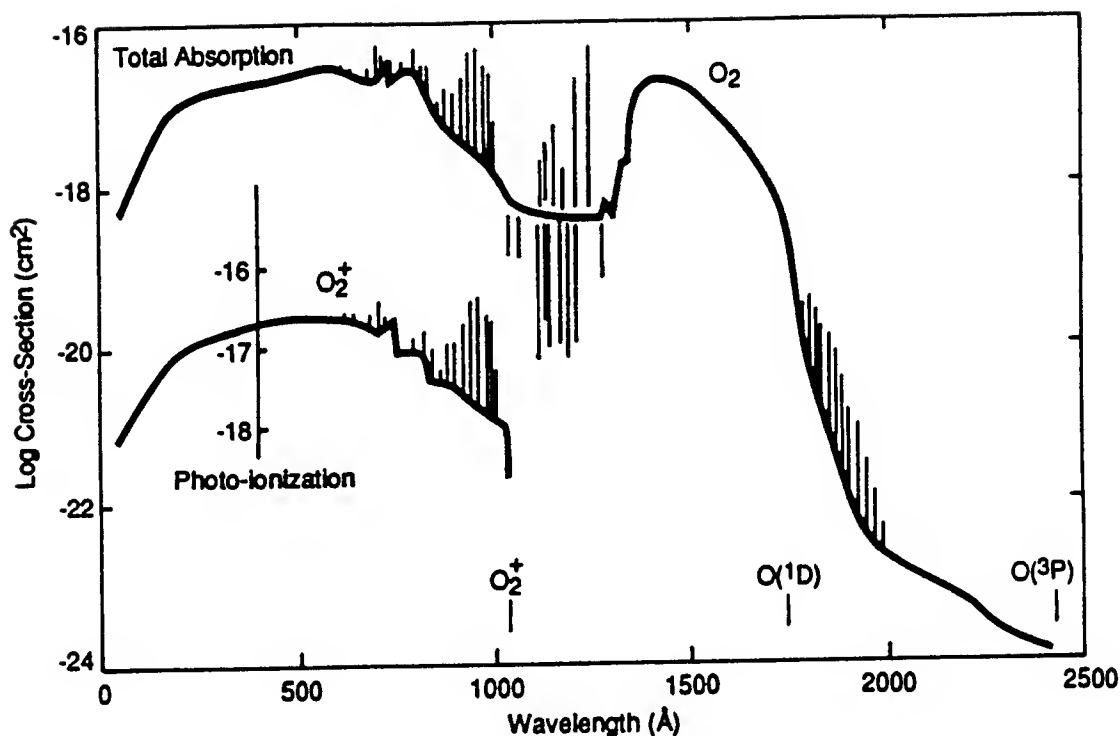
Figure 8. Absorption Cross Sections for Molecular Oxygen. (Excerpted from Huffman [4].)

sections can be important given the exponential increase in O_2 density with decreasing altitude, Figure 5.

The feature above 2000Å shown in Figure 8 corresponds to an absorption from the ground state into dissociative levels of the A electronic state, the weak forbidden Herzberg continuum ($X^3\Sigma_g \rightarrow A^3\Sigma_u^+$). A very detailed review of this continuum absorption is provided in Nicolet and Kennes [28]. There are additional weak Herzberg band absorptions to the right of the absorption cutoff shown in Figure 8. These are of marginal importance as discussed in Trakhovsky et al. [29].

The Schumman-Runge band system ($X^3\Sigma_g^- - B^3\Sigma_u^-$), absorption form the ground state into the B electronic state, begins to dominate at wavelengths below ~2050 Å. This band system corresponds to a large number of discrete transitions from and to differing vibrational and rotational states of O_2, the major transitions of which are delineated in Figure 8. Their proper specification provides perhaps the most challenging problem in the evaluation of atmospheric UV transmission. The state of the art of our understanding in this area has recently been addressed in a series of seminal articles by Nicolet and Kennes [24,30,31] and Nicolet et al. [32,33]. Readers requiring a detailed understanding of these band systems are referred to these articles.

The Schumman-Runge continuum continues down to ~1300 Å. Between the termination of that system and the onset of photo-ionization at ~1026 Å there are a series of absorption bands which allow some leakage of UV emissions. These leakage regions are called atmospheric windows, spectral regions where UV radiation can penetrate to lower altitudes. The effects of

42

these window regions are reflected in the structured UV penetration altitudes shown in Figure 7 between 1000 and 1300Å.

Absorption cross sections for ozone are presented in Figure 9a, b and c, as excerpted from Molina and Molina [25]. These are much simpler than those for O_2. The important photodissociative process in O_3 is in the Hartley bands which occur at wavelengths below 3100Å and result in production of electronically excited products, see Table 3. Ozone photodissociation at longer wavelengths proceeds through the Huggins bands which produce ground state products, Table 3. The UV cross sections for these bands are provided in Figure 9a-c. The Huggins bands are sufficiently weak to allow light of wavelength >3100Å to penetrate to the earth's surface, Figure 7, but they have been used to monitor the atmospheric ozone concentration.

As can be seen (Table 3) most of the ultraviolet ionization processes occur at wavelengths $\lesssim$1000Å, beyond the scope of this text. The one exception is NO. Interestingly, NO ionization by window region UV radiation is largely responsible for formation of the D region of the ionosphere, Figure 6.

There are of course other discrete absorptions, such as in the NO γ and δ bands, which although unimportant as UV loss mechanisms, do produce atmospheric fluorescence. They will be discussed in the following chapter on atmospheric emission.
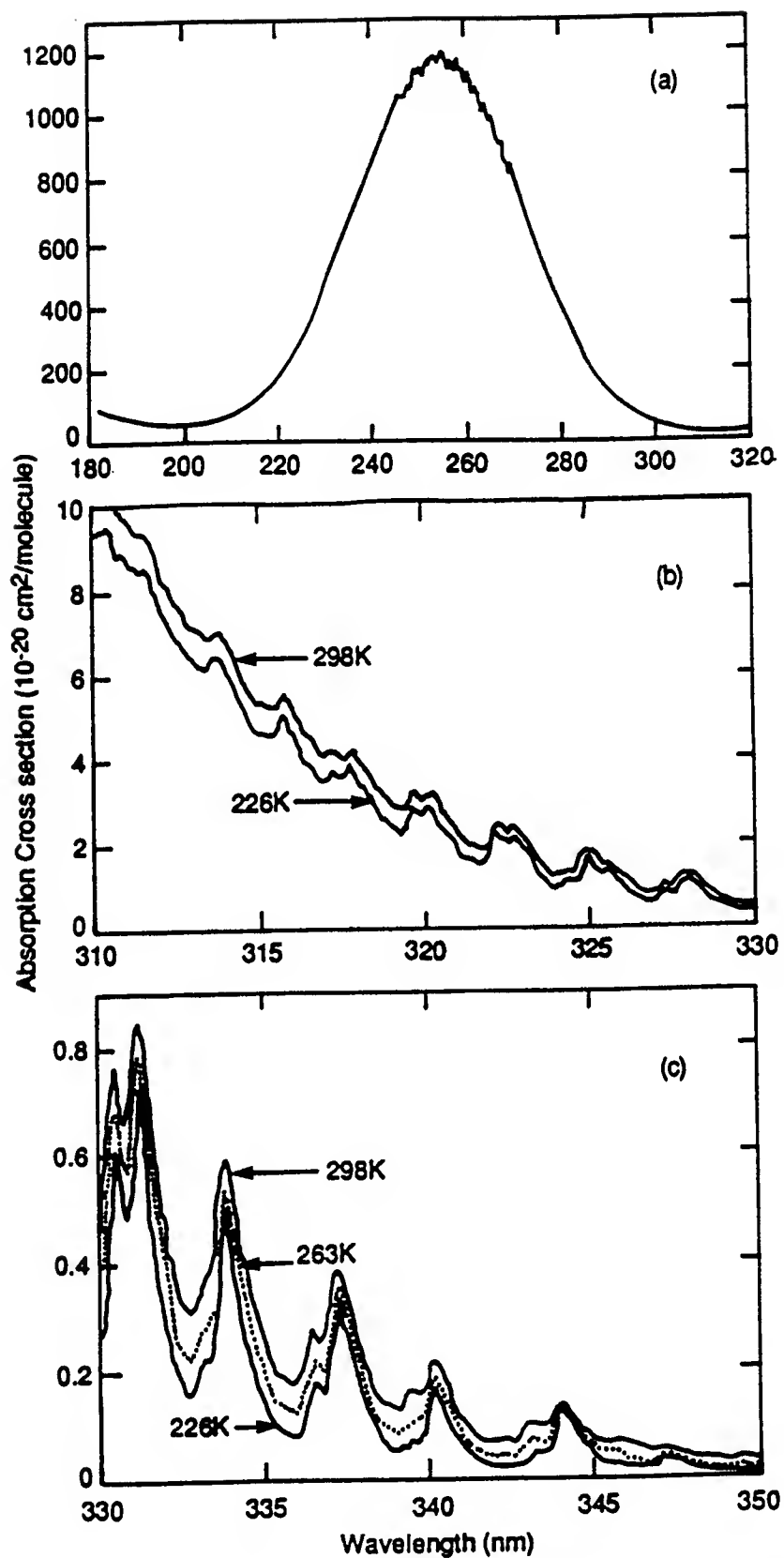
Figure 9.   Absorption cross sections of ozone: a) at 298 K in the region 180 to 320 nm; b) in the region 310-330 nm; c) in the region 330 to 350 nm.

44

CHAPTER 3 REFERENCES

1   Hall, L.A., Heroux, L.J. and Hinteregger, H.E., "Solar Ultraviolet Irradiance," Chapter 2 in *Handbook of Geophysics and The Space Environment*, ed. A.S. Jursa, Air Force Geophysics Laboratory, 1985.

2   Rees, M.H., *Physics and Chemistry of the Upper Atmosphere*, Cambridge University Press, Cambridge, 1989.

3   Meier, R.R., "Ultraviolet Spectroscopy and Remote Sensing of the Upper Atmosphere", *Space Science Reviews* **58**, 1991.

4   Huffman, R.E., "Atmospheric Ultraviolet Remote Sensing", Vol. 52 in the International Geophysics Series, Academic Press, Boston, 1992.

5   Pierce, A.K. and Allen, R.G., "The Solar Spectrum Between 0.3 and 10 μm," in *The Solar Output and Its Variation*, edited by O.R.White, Colorado Associated University Press, Boulder, 1977.

6   Hinteregger, H.E., "Representations of Solar EUV Fluxes for Aeronomical Applications," *Adv. Space Res.*, 1:39, COSPAR, 1981.

7   Nicolet, M., "Solar Spectral Irradiances with their Diversity between 120 and 900 nm," *Planet. Space Sci.* **37**, 1249, 1989.

8   Brueckner, G.E. and VanHoosier, M.E., "The Ultraviolet Solar Spectrum 120 to 400 nm Results from the SUSIM Experiment Onboard Spacelab-2," unpublished results, 1991.

9   Hinteregger, H.E., Fukui, K., and Gilson, B.R., "Observational, Reference and Model Data on Solar EUV from Measurements on AE-E," *Geophys. Res. Letters* **8**, 1147, 1981.

10   Donnelly, R.F. and Pope, J.H., *The 1-3000 Å Solar Flux for a Moderate Level of Solar Activity for Use in Modeling the Ionosphere and Upper Atmosphere*, NAOO Tech. Rpt. ERL 276-SEL 25, 1973.

11   COESA, *U.S. Standard Atmosphere, 1976*, U.S. Government Printing Office, Washington, DC, 1976.

12   Cole, A.E. and Kantor, A.J., "Air Force Reference Atmospheres," GL-TR-78-0051, 1978, ADA058505.

13   Champion, K.S., Cole, A.E., and Kantor, A.J., "Standard and Reference Atmospheres," Chapter 14 in *Handbook of Geophysics and The Space Environment*, ed. A.S. Jursa, 1985, AFGL-TR-85-0315, ADA16700.

14   Hedin, A.E., "A Revised Thermospheric Model Based on Mass Spectrometer and Incoherent Scatter Data: MSIS-83," *J. Geophys. Res.* **88**, 10, 170, 1983.

15   Hedin, A.E., "MSIS-86 Thermospheric Model," *J. Geophys. Res.* **92**, 2545-2657, 1987.

16   Hedin, A.E., "Extension of the MSIS Thermospheric Model into the Middle and Lower Atmosphere," *J. Geophys. Res.* **96**, 1159-1172, 1991.

17   Jacchia, L.G., "Revised Static Models of the Thermosphere and Exosphere with Empirical Temperature Profiles," *Special Report 332, Smithsonian Astrophysical Observatory*, Cambridge, Mass., 1971.

18   Brasseur, G. and Solomon, S., *Aeronomy of the Middle Atmosphere*, Reidel, Dordrecht, 1984.

19   Chamberlain, J.W. and Hunten, D.M., "Theory of Planetary Atmospheres," *International Geophysics Series*, Vol. 36, Academic Press, Orlando, 1987.

20   Conway, R.R., "Photoabsorption and Photoionization Cross Sections of O, O_2, and N_2 for Photoelectron Production Calculations: A Compilation of Recent Laboratory Measurements," *NRL Memo. Rept. 6155*, 1988.

21   Watanabe, K., in H.E. Landsberg and J. van Mieghem (eds.) "Ultraviolet Absorption Processes in Upper Atmosphere," *Advances in Geophysics*, Academic Press, New York, 1958.

22   Blake, A.A., Carver, J.H. and Haddad, G.N., "Photo-Absorption Cross Sections of Molecular Oxygen between 1250 and 2350 Å," *J. Quant. Spectr. Rad. Trans.* **6**, 451, 1966.

23   Yoshino, K., Freeman, D.E., Esmond, J.R., and Parkinson, W.H., "High Resolution Absorption Cross Section Measurements and Band Oscillator Strengths of the (1,0)-(12,0) Schumann-Runge Bands of O_2," *Planetary Space Sci.* **31**, 339, 1983.

24   Nicolet, M. and Kennes, R., "Aeronomic Problems of Molecular Oxygen Photodissociation - IV. The Various Parameters for the Herzberg Continuum," *Planet. Space Sci.* **36**:10, 1069-1076, 1988b.

25   Molina, L.T. and Molina, M.J., "Absolute Absorption Cross Sections of Ozone in the 185- to 350-nm Wavelength Range," *J. Geophys. Res.* **91**, 14501, 1986.

26   Lean, J., "Solar Ultraviolet Irradiance Variations: A Review," *J. Geophys. Res.* **92**, 839, 1987.

27   Huffman, R.E., Chapter 22, Atmospheric Emission and Absorption of Ultraviolet Radiation, in *Handbook of Geophysics and the Space Environment*, A. Jursa, scientific editor, 1985, AFGL-TR-85-0315, ADA167000.

28   Nicolet, M. and Kennes, R., "Aeronomic Problems of Molecular Oxygen Photodissociation - I. The O_2 Herzberg Continuum," *Planet. Space Sci.* **34**:11, 1043-1059, 1986.

29   Trakhovsky, E., Ben-Shalom, A., Oppenheim, U.P., Devir, A.D., Balfour, L.S., and Engel, M., "Contribution of Oxygen to Attenuation in the Solar Blind UV Spectral Region," *Appl. Opt.* **28**, 1588-1591, 1989.

30   Nicolet, M. and Kennes, R., "Aeronomic Problems of Molecular Oxygen Photodissociation - III. Solar Spectral Irradiances in the Region of the O_2 Herzberg Continuum, Schumann-Runge Bands and Continuum," *Planet. Space. Sci.* **36**:10, 1059-1068, 1988a.

31   Nicolet, M. and Kennes, R., "Aeronomic Problems of Molecular Oxygen Photodissociation - VI. Photodissociation Frequency and Transmittance in the Spectral Range of the Schumann-Runge Bands," *Planet. Space Sci.* **37**:4, 459-491, 1989.

32   Nicolet, M., Cieslik, S. and Kennes, R., "Aeronomic Problems of Molecular Oxygen Photodissociation - II. Theoretical Absorption Cross-Sections of the Schumann-Runge Bands at 79 K," *Planet. Space Sci.* **36**:10, 1039-1058, 1988.

33   Nicolet, M., Cieslik, S., and Kennes, R., "Aeronomic Problems of Molecular Oxygen Photodissociation - V. Predissociation in the Schumann-Runge Bands of Oxygen," *Planet. Space Sci.* **37**:4, 427-458, 1989.

CHAPTER 4. ATMOSPHERIC EMISSION PHENOMENOLOGY

INTRODUCTION

This chapter reviews the characteristics of background UV signatures in the atmosphere. Atmospheric emissions arise from the interaction of ambient gases with photons, electrons and protons as well as through chemical reaction among both neutral and ionic species. As such the intensity of emission, and indeed the emitting species themselves, will vary with time of day, solar cycle, geomagnetic activity and geographical location. Furthermore, the scattering of solar emissions can play a key role in the atmospheric UV signature depending on the viewing geometry of observer. This topic has been discussed in an earlier chapter and only the resulting scattered emission will be mentioned here.

There are numerous texts available which discuss UV atmospheric emissions in some detail, for example those of Huffman [1] and Rees [2], as well as an excellent recent review of atmospheric UV spectroscopy by Meier [3]. These sources have been used liberally in developing the present text and the reader is referred to those references for more detailed information.

In this chapter we will review UV emissions in the nightglow, dayglow and aurora detailing both emission production mechanisms and generic intensities. Background intensities will be expressed in Rayleighs. A Rayleigh corresponds to 10^6 photons/cm^2-s. Rayleigh units may be converted to W/cm^2 by multiplying by 10^{-6} times the photon energy in joules. Division by 4π provides emission intensities in units of sr^{-1}.

THE NIGHTGLOW

The nightglow is the most straightforward of atmospheric emissions in that, with the exception of the Lyman α transitions, the emissions are not directly related to solar illumination but rather produced solely by chemical reaction. The concentrations of reacting species are however directly related to the insolation history in that these species are formed through photodissociation and photo-ionization processes. Thus, the nightglow emissions will not only vary spatially and temporally but will also vary strongly with solar activity.

A generic UV nightglow spectrum, for nadir viewing from 600 km is shown in Figure 10, as excerpted from Meier [3]. As denoted in the caption, the figure is a composite from several sources and is *"representative of moderately active conditions in March 1978 and April 1979 near the equator at midnight"* [3]. The emission rates and band systems corresponding to Figure 10 are provided in Table 4. Again these intensities are highly variable.
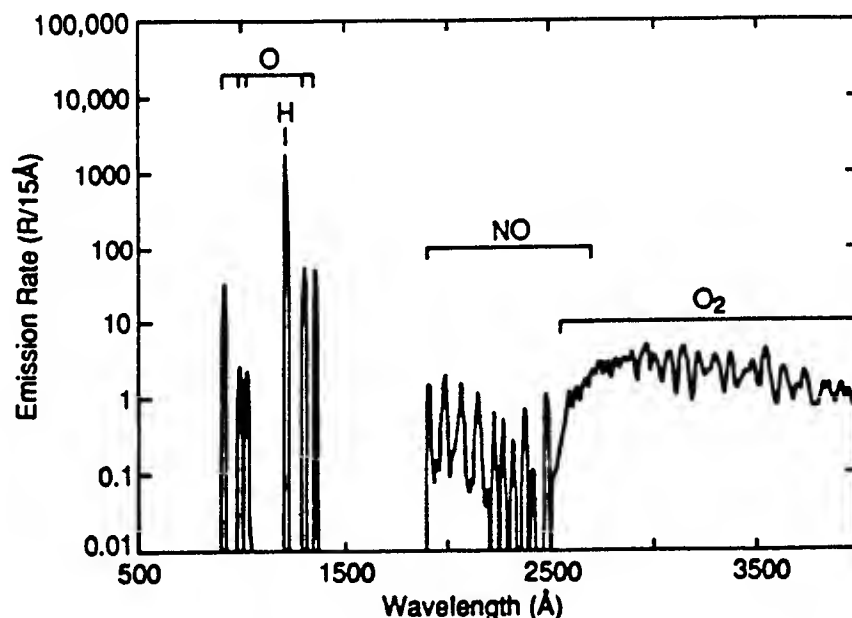
Figure 10.   Composite UV Nightglow Spectrum Adjusted to Nadir Viewing from 600 km in Equatorial Region. All spectral features have been smoothed to 15 Å resolution. The O_2 and NO molecular, the H geocoronal resonant scattering, and the O^+ + e → O recombination emissions are indicated. The O_2 spectrum was taken from the Hennes [4] rocket experiment, the NO spectrum from the Sharp and Rusch [5] rocket data, and the O I and H I lines from the STP 78-I satellite data of Chakrabarti et al. [6] The absolute values of the O_2 and NO bands were obtained by normalizing to the Huffman et al. [7] S3-4 equatorial spectrum (after converting the S3-4 data to absolute units). (Excerpted from Meier [3]).

As can be seen the UV nightglow spectrum is quite sparse consisting largely of neutral oxygen transitions, the NO α and δ bands and the O_2 Herzberg band. The atomic transitions result from radiative recombination of O^+, i.e.,

$$O^+ + e \rightarrow O^* + h\nu \qquad (4\text{-}1)$$

where the excited neutral atom subsequently radiates to lower states in the transitions noted in Table 4.

The NO emissions result from pre-association of N and O atoms presumably through the pathway

$$N(^4S) + O(^3P) \rightleftharpoons NO(a^4\pi) \rightleftharpoons NO(C^2\pi) \qquad (4\text{-}2)$$

followed by either emission of $NO(C^2\pi)$ to the ground state, the δ bands, or radiative cascade to the $A^2\Sigma^+$ state with subsequent emission to the NO ground state, the γ bands. These emissions depend upon the product of the concentration of two atomic species and thus do not

49

Table 4. UV Nightglow in Nadir from 600 km. (Excerpted from Meier [4-3].)

Species	Wavelength (Å)	Transition	Column Emission rate (R)
O_2	Total	$A^3\Sigma_u^+ - X^3\Sigma_g$ (Herzberg I)	225
O I	2972	$2p^4\,^1S - 2p^4\,^3P$	9
NO	1900	$C^2\Pi - X^2\Pi$ (δ band) (0,0)	5.5
NO	1980	$C^2\Pi - X^2\Pi$ (δ band) (0,1)	7.9
NO	2055	$C^2\Pi - X^2\Pi$ (δ band) (0,2)	6.5
NO	2134	$C^2\Pi - X^2\Pi$ (δ band) (0,3)	4.0
NO	2219	$C^2\Pi - X^2\Pi$ (δ band) (0,4)	2.1
NO	2310	$C^2\Pi - X^2\Pi$ (δ band) (0,5)	0.93
NO	2406	$C^2\Pi - X^2\Pi$ (δ band) (0,6)	0.38
NO	2509	$C^2\Pi - X^2\Pi$ (δ band) (0,7)	0.16
NO	2620	$C^2\Pi - X^2\Pi$ (δ band) (0,8)	0.06
NO	2262	$A^2\Sigma^+ - X^2\Pi$ (γ band) (0,0)	1.8
NO	2363	$A^2\Sigma^+ - X^2\Pi$ (γ band) (0,1)	2.4
NO	2471	$A^2\Sigma^+ - X^2\Pi$ (γ band) (0,2)	3.8
NO	2587	$A^2\Sigma^+ - X^2\Pi$ (γ band) (0,3)	1.5
NO	2713	$A^2\Sigma^+ - X^2\Pi$ (γ band) (0,4)	0.5
O I	1356	$2p^4\,^3P - 2s^5S^0$	52
O I	1304	$2p^4\,^3P - 3s^3S^0$	54
H I	1216	$1s^2S - 2p^2P$	1712
H I,O I	1026	$1s^2S - 2p^2P^0$, $2p^4\,^3P - 3d^3D^0$	2.3
O I	989	$2p^4\,^3P - 3s'\,^3D^0$	2.6
O I	911	$2p^4\,^3P - \infty$	34.5
HE II	304	$1s^2S - 2p^2P^0$	0.1-5

appear at altitudes below ~ 90 km but will radiate significantly over an altitude range larger than 100 km, see discussion in Strobel et al. [8]. A more spectrally detailed observation of nightglow NO band emissions as observed from the S3-4 satellite is shown in Figure 11.

The O_2 Herzberg emissions arise from the three body recombination of oxygen atoms

$$O + O + M \rightarrow O_2(A^3\Sigma_u^+) + M$$
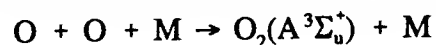
followed by radiation from the $A^3\Sigma_u^+$ state to the ground state, the Herzberg bands. Since the production rate for the $A^3\Sigma_u^+$ state depends not only on the square of oxygen atom concentration but also on the total density, this emission feature is more localized, peaking in a narrow altitude band around 95 km. A portion of the Herzberg band is also shown in more spectral detail in Figure 11. We note that other electronic states can be created in the recombination process and that there will also be contributions in the 3400 to 4000Å regions from the O_2 Chamberlain system, $A'^3\Delta_u \rightarrow a^1\Delta g$.
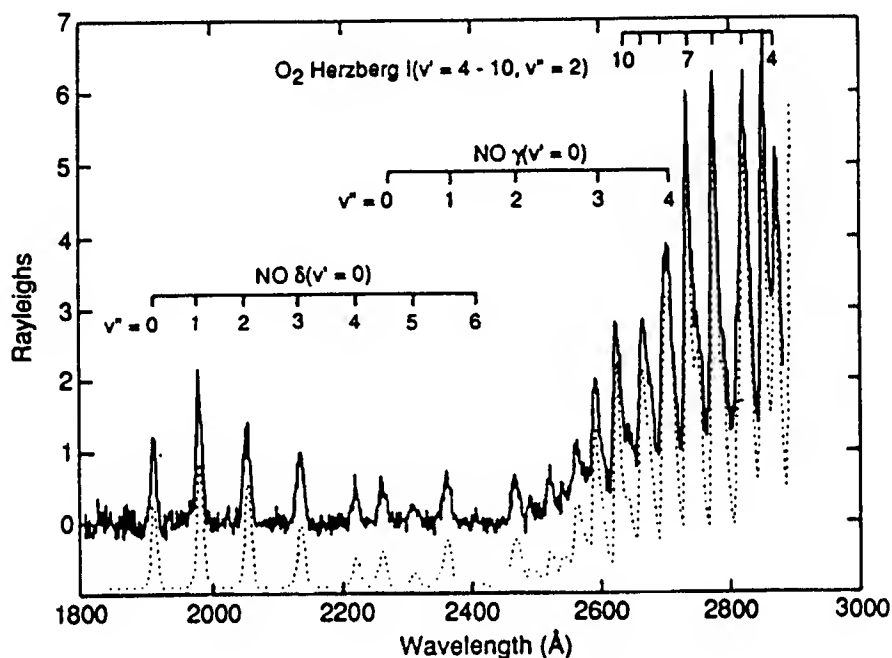
Figure 11.   Night Airglow Spectrum from the S3-4 Satellite (Exerpted from Eastes et al. [9].)

THE DAYGLOW

As would be expected, the dayglow is considerably richer than the nightglow. Of course, the nightglow emission mechanisms are also operative during the day, although their intensities are necessarily impacted by diurnal variations in species concentrations. During the day these latter mechanisms are supplemented by photo-ionization, photoelectron impact and resonant photo-excitation processes as well as by scattered and reflected solar radiation.

A generic nadir view of the earth ultraviolet midmorning dayglow from a viewing altitude of 200 km is shown in Figure 11, as excerpted from Meier [3]. This is a composite of several disparate measurements and should be viewed as accurate within a factor of two for moderate solar activity. The corresponding transition identification and representative intensities are provided in Table 5.

51
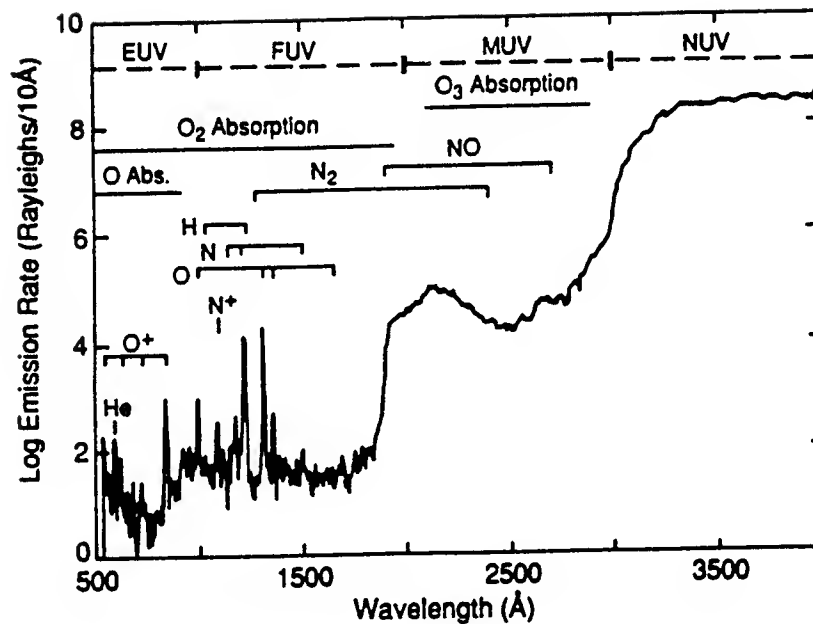
Figure 12.   Complete Earth dayglow spectrum, adjusted to nadir viewing from 200 km at
              midmorning. The various spectral bands defined at the top of the figure are
              the extreme, far, middle, and near-ultraviolet. Regions of absorption by
              oxygen species are indicated by thick horizontal lines; emission bands intervals
              are shown for N_2 and NO, and the stronger emission lines of atomic and ionic
              species are shown. The NUV emission rate was calculated assuming an Earth
              Albedo of 0.3 and a smoothed solar irradiance, the MUV was taken from
              Barth [10], the FUV from Huffman et al. [7] and the EUV from Gentieu et al.
              [11]. (Exerpted from Meier [3].)

Note the strong dominance of scattered solar light above ~1800Å in Figure 12. The top
of the figure delineates the spectral regions of absorption of solar emissions by O_3 and O_2 (see
Chapter 3). It is these absorption features which produce the step-like structure with increasing
wavelength. Solar light above ~3100Å will reach the surface and thus the intensity at those
wavelengths are affected by the surface albedo. Solar irradiation between 2000 and 3100Å is
absorbed by O_3, largely in the stratosphere, while solar UV emission is fully absorbed in the
mesosphere by oxygen molecules.

There are of course a number of molecular emission features which underlie the scattered
solar radiation seen in this nadir view. High altitude side- or up-viewing systems which
discriminate against solar scattered emissions would see these underlying emissions.

An example of this is provided in Figure 13, corresponding to a horizontal view of the
airglow at 150 km. (This figure excerpted from McEwan and Phillips [12] presents unpublished
data of C. Barth which are commonly referenced, e.g., Meier [3] and Rees [2].) As can be seen
a number of molecular band systems become apparent as well as a few atomic line transitions.
Differing excitation mechanisms are operative in producing these emissions.

Table 5. UV Dayglow in Nadir from 600 km. (Excerpted from Meier [3].)

Species	Wavelength (Å)	Transition	Column Emission rate (R)
N_2^+	3914	$B^2\Sigma_u^+ - X^2\Sigma_g^+$	6700
O_2	2500-2900	Herzberg bands	-
N II	2143	$2s\,2p^3\,^5S - 2s^22p^2\,^3P$	300
NO	2363	$A^2\Sigma^+ + X^2\Pi$ (γ band) (0, 1)	369
NO	2262	$A^2\Sigma^+ + X^2\Pi$ (γ band) (0, 0)	265
NO	2239	$A^2\Sigma^+ + X^2\Pi$ (γ band) (1, 1)	206
NO	2216	$A^2\Sigma^+ + X^2\Pi$ (γ band) (2, 2)	82
NO	2149	$A^2\Sigma^+ + X^2\Pi$ (γ band) (1, 0)	752
NO	2047	$A^2\Sigma^+ + X^2\Pi$ (γ band) (2, 0)	197
NO	2030	$A^2\Sigma^+ + X^2\Pi$ (γ band) (3, 1)	29
NO	2000-2700	Gamma bands	
N_2	Total	$A^3\Sigma_g^+ - X^1\Sigma_g^+$ (VK)	6820 (excitation only)
N_2	Total	$a^1\Pi_g - X^1\Sigma_g^+$ (LBH)	4560
N_2	2000-2400	Subtotal (LBH)	273
N_2	1947	$a^1\Pi_g - X^1\Sigma_g^+$ (4, 11)	70
N_2	1930	$a^1\Pi_g - X^1\Sigma_g^+$ (3, 10)	71
N_2	1856	$a^1\Pi_g - X^1\Sigma_g^+$ (3, 9)	95
N_2	1839	$a^1\Pi_g - X^1\Sigma_g^+$ (2, 8), (6, 11)	100
N_2	1771	$a^1\Pi_g - X^1\Sigma_g^+$ (2, 7), (6, 10)	127
N_2	1754	$a^1\Pi_g - X^1\Sigma_g^+$ (1, 6), (5, 9)	113
N_2	1690	$a^1\Pi_g - X^1\Sigma_g^+$ (1, 5), (5, 8)	116
N_2	1675	$a^1\Pi_g - X^1\Sigma_g^+$ (4, 7), (0, 4)	98
O I	1641	$2p^4\,^1D - 2p^3\,3s^3S^0$	50
N_2	1602	$a^1\Pi_g - X^1\Sigma_g^+$ (3, 5)	87
N_2	1586	$a^1\Pi_g - X^1\Sigma_g^+$ (2, 4)	73
N_2	1558	$a^1\Pi_g - X^1\Sigma_g^+$ (0, 2), (4, 5)	87
N_2	1531	$a^1\Pi_g - X^1\Sigma_g^+$ (2, 3)	104
N_2	1511	$a^1\Pi_g - X^1\Sigma_g^+$ (4, 4), (1, 2)	127
N_2	1495	$a^1\Pi_g - X^1\Sigma_g^+$ (3, 3), (6, 5)	109

Table 5. UV Dayglow in Nadir from 600 km. (Excerpted from Meier [3].) (Continued)

Species	Wavelength (Å)	Transition	Column Emission rate (R)
NI	1493	$2p^3\,^2D^0 - 3s^2P$	91 (e + N_2)
N_2	1465	$a^1\Pi_g - X^1\Sigma_g^+$ (1, 1)	144
N_2	1446	$a^1\Pi_g - X^1\Sigma_g^+$ (3, 2)	93
N_2	1431	$a^1\Pi_g - X^1\Sigma_g^+$ (2, 1), (5, 3)	144
N_2	1416	$a^1\Pi_g - X^1\Sigma_g^+$ (4, 2), (1, 0)	207
N_2	1398	$a^1\Pi_g - X^1\Sigma_g^+$ (6, 3), (3, 1)	62
N_2	1384	$a^1\Pi_g - X^1\Sigma_g^+$ (2, 0), (5, 2)	267
O I	1356	$2p^4\,^3P - 2p^33s^5S^0$	1068
N_2	1354	$a^1\Pi_g - X^1\Sigma_g^+$ (4, 11)	222
N_2	1325	$a^1\Pi_g - X^1\Sigma_g^+$ (4, 11)	200
O I	1304	$2p^4\,^3P - {}^2P^33s^3S^0$	10498
N_2	1298	$a^1\Pi_g - X^1\Sigma_g^+$ (5, 0)	(111)
N_2	1273	$a^1\Pi_g - X^1\Sigma_g^+$ (6, 0)	<70
N_2	1259	$b^1\Pi_g - X^1\Sigma_g^+$ (1, 10) (BH)	<30
N I	1243	$2p^3\,^2D^0 - 2p^23s'\,^2D$	150
H I	1216	$1s^2S - 2p^2P^0$	35000
N I	1200	$2p^3\,^4S^0 - 2p^23s^4P$	1500
O I	1173	$2p^4\,^1D_2 - 3s'\,^3D^0$	
N I	1176-1177	$2p^3\,^2D^0 - 2p^2(^3P)4s\,^2P$	<160
N I	1168	$2p^3\,^2D^0 - 2p^23d^4P$	170
O I	1152	$2p^4\,^1D - 3s'\,^1D^0$	150
N I	1143	$3p^3\,^2P^0 - 2p^23s^2S$	<45
N I	1134	$2s^22p^3\,^4S - 2s\,2p^4\,^4P$	400
N_2	1110	$b^1\Pi_u - X^1\Sigma_g^+$ (1,5)	<50
N I	1100	$2p^3\,^2D^0 - 2p^2(^3P)5s\,^2P$	55
N I	1097-1099	$2p^3\,^2D^0 - 2p^2(^3P)4d(^2P\ and\ ^4F)$	55
N II	1085	$2s^2\,2p^2\,^3P - 2s\,2p^3\,^3D^0$	500
N I	1067-1068	$2p^3\,^2D^0 - 2p^2(^3P)5d(^{2,4}D\ and\ ^{2,4}F)$	<120
N_2	1058	$b^1\Pi_u - X^1\Sigma_g^+$ (1, 3)	<120

Table 5. UV Dayglow in Nadir from 600 km. (Excerpted from Meier [3].) (Continued)

Species	Wavelength (Å)	Transition	Column Emission rate (R)
O I	1040	$2p^4\ ^3P - 2p^34s^3S^0$	60
N$_2$	1033	$b^1\Pi_u - X^1\Sigma_g^+$	(149)
O I	1027	$2p^4\ ^3P - 3d^3D^0$	340
H I	1026	$1s^2S - 3p^2P^0$	
N$_2$	1009	$b^1\Pi_u - X^1\Sigma_g^+\ (1, 1)$	150
O I	989	$2p^4\ ^3P - 2p^3(^2D^0)3s'^3D^0$	850
N$_2$	985	$b^1\Pi_u - X^1\Sigma_g^+\ (1, 0)$	95
H I	973	$1s^2S - 4p^2P^0$	14
N I	964-965	$2p^3\ ^4S^0 - 2p^2(^3P)4s^4P$	80
N I	953	$2p^3\ ^4S^0 - 2p^2(^3P)3d^4P$	125
N II	916	$2s^2\ 2p^2\ ^3P - 2s\ 2p^3\ ^3P^0$	185
N I	910	$2p^3\ ^4S^0 - 2p^2(^3P)5s\ ^4P$	90
N I	907	$2p^3\ ^4S - 2p^2(^3P)4d^2P^4P^4F$	< 80
N I	887	$2p^3\ ^4S - 2p^2(^3P)6s^4P^2P$	< 40
N I	875	$2p^3\ ^4S - 2p^2(^3P)6d^4P^2P$	< 35
N I	862	$2p^3\ ^4S - 2p^2(^3P)9d^4P^2P$	< 35
N I	859	$2p^3\ ^4S - 2p^2(^3P)11d^4P^2P$	< 35
O II	834	$2s^2\ 2p^3\ ^4S^0 - 2s\ 2p^4\ ^4P$	580
N II	776	$2s^2\ 2p^2\ ^1D - 2s\ 2p^3\ ^1D^0$	< 5
N II	747	$2p^2\ ^1D - 2p\ 3s\ ^1P^0$	< 4
O II	718	$2s^2\ 2p^3\ ^2D^0 - 2s\ 2p^4\ ^2D$	17
O II	673	$2p^3\ ^2P^0 - 2p^2(^3P)3s^2P$	6.5
N II	671	$2p^2\ ^3P - 2p\ 3s\ ^3P^0$	
N II	645	$2s^2\ 2p^2\ ^3P - 2s\ 2p^3\ ^3S^0$	7
O II	644	$2s^2\ 2p^3\ ^2P^0 - 2s\ 2p^4\ ^2S$	
N II	629	$2s\ 2p^3\ ^5S^0 - 2s\ 2p^2(^4P)3s^5P$	3
O II	617	$2p^3\ ^2D^0 - 2p^2(^3P)3s^2P$	60
O II	601	$2p^3\ ^2P^0 - 3s'\ ^2D$	9
He I	584	$1s^2\ ^1S - 1s2p^1P^0$	330

Table 5. UV Dayglow in Nadir from 600 km. (Excerpted from Meier [3].) (Continued)

Species	Wavelength (Å)	Transition	Column Emission rate (R)
O II	581	$2s^2\,2p^3\,^2P^0$ - $2s\,2p^4\,^2P$	< 20
O II	555	$2p^3\,^2D^0$ - $3s'\,^2D$	15
O II	539	$2p^3\,^4S^0$ - $3s\,^4P$	115
O II	538	$2s^2\,2p^3\,^2D^0$ - $2s\,2p^4\,^2P$	
He I	537	$1s^2\,^1S$ - $1s3p\,^1P^0$	
He I	522	$1s^2\,^1S$ - $1s4p\,^1P^0$	8.5
O II	515	$2p^3\,^2D$ - $2p^2(^3P)3d^2P^0$	
O II	482	$2p^3\,^2D^0$ - $2p^2(^3P)3d^2D$	8
O II	470	$2p^3\,^2P^0$ - $2p^2(^1D)3d'^2D$	< 8
O II	442	$2p^3\,^2D^0$ - $2p^2(^1D)3d'^2D$	12
O II	430	$2p^3\,^4S^0$ - $2p^2(^3P)3d^4P$	12
He II	304	$1s^2S$ - $2p^2P^0$	5 (Zenith)
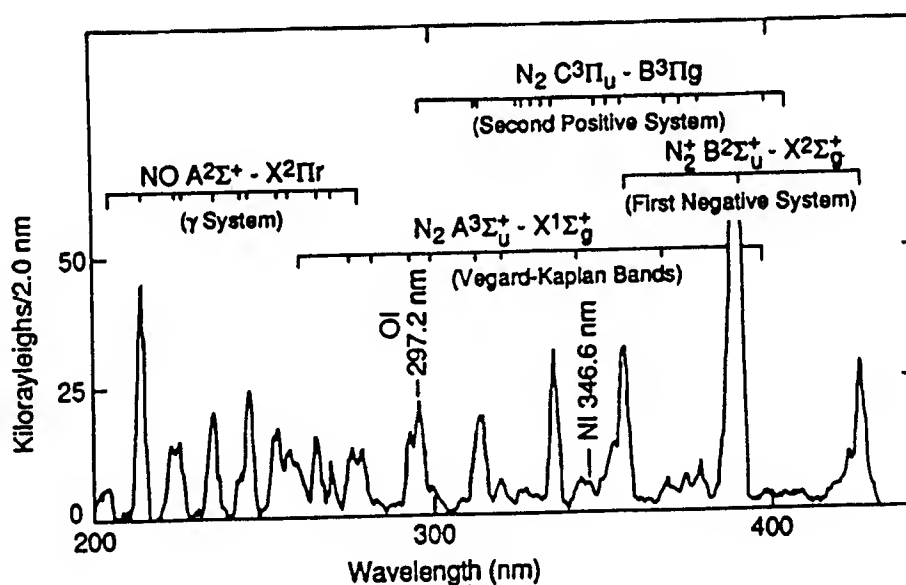
Figure 13. Spectrum of the Ultraviolet Dayglow Between 190 to 430 km as Observed from a Payload Viewing Horizontally at an Altitude of 150 km. This is unpublished data of C. Barth taken during a rocket experiment launched from White Sands, NM on June 1969.

For example, the NO γ ($A^2\Sigma^+ \rightarrow X^2\pi_u$) and N_2^+ first negative ($B^2\Sigma_u^+ \rightarrow X^2\Sigma_g^+$) bands result from resonant photo-excitation. On the other hand transitions between the nitrogen molecule ground state and the triplet states are optically forbidden and thus the N_2 Vegard-Kaplan ($A^3\Sigma_u^+ - X^1\Sigma_g^+$) and second positive ($C^3\pi_u \rightarrow B^3\pi_g$) emissions are produced by photo-electron excitation.

An expansion of the spectral features of dayglow emission in the 1100 to 1900Å region as reported by Huffman et al. [7] is shown in Figure 14. The dominant molecular emission seen between approximately 1250 and 1700Å is the N_2 Lyman-Birge-Hopfield ($2^1\pi_g - X^1\Sigma_g^+$) system. This system is also optically forbidden and is produced through photoelectron excitation.
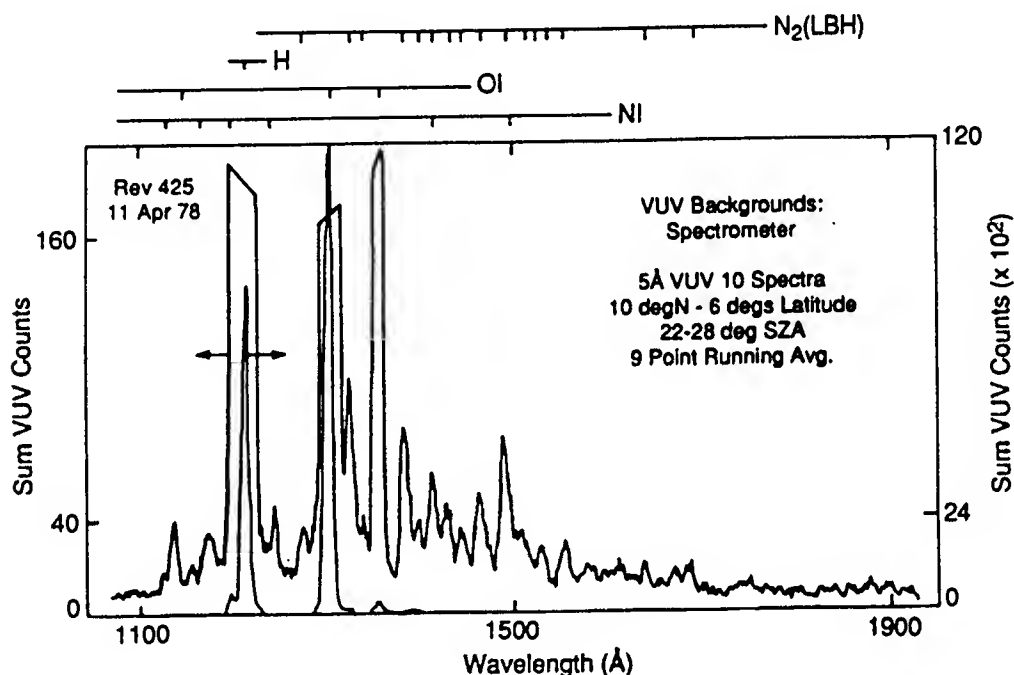
Figure 14.   S3-4 Satellite Nadir Observation. 5Å data in VUV near midday (Exerpted from Huffman et al. [7].)

Note that there are also a large number of transitions of neutral and ionized oxygen and nitrogen atoms observed throughout the ultraviolet. These emitting states may be created both by resonant photo-excitation and by photo-electron excitation. The hydrogen Lyman α emission is produced solely by resonant solar scattering.

As stated in the discussion on nightglow, the altitude dependence of these various emissions will be determined by a convolution of concentration profiles, solar flux and absorption depths. Thus in an uplooking scenario the relative intensities of different band systems will vary with platform altitude and viewing angle. All scattered solar radiation arises from altitudes below 100 km.

Again, both the dayglow intensities and their spectral variation will vary with solar activity, local time and geographic position. Twilight for example is a special case where solar illumination does not extend to the highly-scattering lower atmosphere although the thermosphere remains fully irradiated. The net effect is that sky radiances drop dramatically at twilight although all the basic emission features produced by photon or photo-electron excitation remain.

An interesting geographical anomaly is the so called tropical UV airglow [13,14] which corresponds to enhanced UV emission observed in near equatorial regions in early evenings. This emission is believed to result from radiative recombination of O^+ in the F region (see discussion in Huffman [1]).

A detailed review of the variability in the airglow is beyond the scope of this handbook. A recent review is provided by Meier [3].

THE AURORA

Auroral emissions result from energetic electron and proton bombardment of the atmosphere. These emissions occur at both poles within the auroral ovals delineated approximately by latitudes above 70 deg. This bombardment results from the precipitation of electrons and protons from the magnetosphere into the atmosphere and thus there is a strong, although not well defined, coupling between geomagnetic and auroral activity. (Auroral observations are typically coupled to the current magnetic index Kp).

Auroral precipitation phenomenology, variability and observations are well covered in classic texts such as Chamberlain [15] and Vallance Jones [16] and an excellent overview may be found in the article by Whalen et al. in the Handbook of Geophysics and the Space Environment [17]. In this chapter we will briefly discuss auroral UV emission levels and radiators.

Auroral precipitation is characterized both by the energy of the bombarding species and their power. The latter quantity is directly proportional to the auroral emission intensities, a fact which has led to the quantification of auroral powers in terms of an International Brightness Coefficient (IBC). This unit is logarithmic in terms of the column intensity of the $O(^1S \rightarrow {}^1D)$ transition at 5577Å, with an IBC I aurora corresponding to 1 kR emission from that source, an IBC II aurora corresponding to 10 kR, etc. Auroral activity does track the solar cycle and these emission levels will track solar activity. IBC III or greater auroras are significant events and are relatively uncommon. (An interesting review on great auroras, i.e., those that are particularly intense or extend to lower latitudes has recently been provided by Vallance Jones [18].

The energy of the bombarding electrons/protons determine their penetration depth into the atmosphere. Since the atmospheric species concentration is variable with altitude, this difference in energetics can produce different emissive band systems ratios. In any event, auroras rarely penetrate to altitudes below ~95 km.

The emitting species in an aurora are the same as those observed in the airglow although the relative band intensities may vary. Huffman [1] has provided a useful tabulation of representative UV auroral emissions which are reproduced in Tables 6 and 7. The data in Table 6 are taken from Vallance Jones [16] and are representative of rocket measurements scaled to an IBC III aurora. The data of Table 7 are for nadir satellite measurements from altitudes of 250 to 200 km, and are representative of measurements made during April to September 1978.

Auroral emissions are highly structured in comparison to the dayglow/nightglow and thus can present more of a challenge to systems designs. At high latitudes auroral UV backgrounds will far exceed the nightglow and be similar in intensity level to the airglow for nadir viewing.

The information provided above should provide the system designer a general overview of the terminology of UV atmosphere backgrounds, with typical average intensities, spectral distributions and variability. Detailed scenarios for specific systems are best defined through use of computer simulations. An overview of atmospheric UV models is presented in Chapter 5.

Table 6. NUV auroral intensities. (Excerpted from Huffman [1].)

Transition	λ(nm)	B(kR)	Comment
N_2^+ 1N (0,0)	391.4	60	1N: $B^2\Sigma_u^+ - X^2\Sigma_g^+$
N_2^+ 1N (1,1)	388.4	5	
N_2 2P (0,2)	380.5	20	2P: $C^3\Pi_u - B^3\Pi_g$
N_2 2P (1,3)	375.5	15	
N_2 2P (0,1)	357.7	30	
N_2 2P (1,2)	353.7	15	
N_2 2P (0,0)	337.1	20	
N_2 2P (1,0)	315.9	3	
N_2 2P (2,0)	297.0		blend w/O I
O I	297.2	2	$2p^4\ ^3P - 2p^4\ ^1S$

Table 7. MUV and FUV auroral intensities. (Excerpted from Huffman [1].)

Transition	λ(nm)	B(kR)	Comment
N_2 VK (0,6)	276.1	0.4	VK: $A^3\Sigma_u^+$ - $X^1\Sigma_g^+$
N_2 VK (0,5)	260.4	0.2	
N_2 VK (0,4)	246.2	0.2	
N_2 VK (1,4)	237.8	0.1	
N_2 VK (0,3)	233.3	0.1	
N_2 VK (1,3)	225.8	0.9	
N II	214.3	0.2	$2s^22p^2\ ^3P$ - $2s2p^3\ ^5S^\circ$
N_2 LBH $\Delta v = 8$	205.-	0.1	LBH: $a^1\Pi_g$ - $X^1\Sigma_g^+$
N_2 LBH $\Delta v = 7$	195.-	0.2	
N_2 LBH $\Delta v = 6$	184.-	0.2	
N_2 LBH $\Delta v = 5$	176.-	0.4	
N_2 LBH $\Delta v = 4$	167.-	0.3	
N_2 LBH $\Delta v = 3$	160.-	0.2	
N I	149.3	0.4	$2p^3\ ^2D^\circ$ - $3s\ ^2P$
N_2 LBH (1,1)	146.4	0.05	
N_2 LBH (2,1)	143.0	0.03	
N_2 LBH (1,0)	141.6	0.07	also LBH (4,2)
N_2 LBH (2,0)	138.4	0.08	also LBH (5,2)
O I	135.6	0.6	$2p^4\ ^3P^\circ$ - $3s\ ^3S$
N_2 LBH (3,0)	135.4	0.08	est., blend O I
N_2 LBH (4,0)	132.5	0.14	
O I	130.4	15.	$2p^4\ ^3P^\circ$ - $3s\ ^3S$
N_2 LBH (5,0)	129.8		blend O I
N_2 LBH (6,0)	127.3	0.08	
H Lyman α	121.6	3.	$1s\ ^2S^\circ$ - $2p\ ^2P$
N I	120.0	0.5	$2p^3\ ^4S^\circ$ - $3s\ ^4P$
N I	116.8	0.1	$2p^2\ ^2D^\circ$ - $3d\ ^2F$
O I	115.2	0.01	$2p^4\ ^1D$ - $3s'\ ^1D^\circ$
N I	113.4	0.09	$2p^3\ ^4S^\circ$ - $2p^4\ ^4P$

CHAPTER 4 REFERENCES

1   Huffman, R.E., "Atmospheric Ultraviolet Remote Sensing", Vol. 52 in the International Geophysics Series, Academic Press, Boston, 1992.

2   Rees, M.H., *Physics and Chemistry of the Upper Atmosphere*, Cambridge University Press, Cambridge, 1989.

3   Meier, R.R., "Ultraviolet Spectroscopy and Remote Sensing of the Upper Atmosphere", *Space Science Reviews* **58**, 1991.

4   Hennes, J.P., "Measurement of the Ultraviolet Nightglow Spectrum," *J. Geophys. Res.* **71**, 763, 1966.

5   Sharp, W.E. and D.W. Rusch, "Chemiluminescence of Nitric Oxide: The NO ($C^2\Pi$ - $A^2\Sigma^+$) Rate Constant", *J. Quant. Spectr. Rad. Trans.*, **25**, 413, 1981.

6   Chakrabarti, S., R. Kimble and S. Bowyer, "Spectroscopy of the EUV (350-1400Å) Nightglow", *J. Geophys. Res.*, **89**, 5660, 1984.

7   Huffman, R.E., LeBlanc, F.J., Larrabee, J.C., and Paulsen, D.E., "Satellite Vacuum Ultraviolet Airglow and Auroral Observations," *J. Geophys. Res.* **85**, 2201-2215, 1980.

8   Strobel, D.F., E.S. Oran and P.D. Feldman, "The Aeronomy of Odd Nitrogen in the Thermospheric Twilight Emissions", *J. Geophys. Res.*, **81**, 3745, 1976.

9   Eastes, R.W., R.E. Huffman, and F.J. LeBlanc, "NO and O_2 Ultraviolet Nightglow and Spacecraft Glow from the S3-4 Satellite", *Planet. Spa. Sci.*, **40**, 481-493, 1992.

10   Barth, C.A., "Ultraviolet Spectroscopy of Planets", Jet Propulsion Laboratory Tech. Rept. 32-822, Pasadena, CA, 1965.

11   Gentieu, E.P., P.D. Feldman and R.R. Meier, "Spectroscopy of the Extreme Ultraviolet Dayglow at 6.5Å Resolution: Atomic and Ionic Emissions Between 530 and 1240Å", *Geophys. Res. Letters*, **6**, 325, 1979.

12   McEwan, M.J. and L.F. Phillips, *Chemistry of the Atmosphere*, John Wiley and Sons, NY, 1975.

13   Barth, C.A. and S. Schaffner, "OGO-4 spectrometer measurements of the tropical ultraviolet airglow," *J. Geophys. Res.*, **75**, 4299-4306, 1970.

14   Hicks, G.T. and T.A. Chubb, "Equatorial aurora/airglow in the far ultraviolet," *J. Geophys. Res.*, **75**, 6233-6248, 1970.

15   Chamberlain, J.W., *Physics of the Aurora and Airglow*, Academic Press, 1961.

16   Vallance Jones, A., *Aurora*, D. Reidel, 1974.

17   Whalen, J.A., R.R. O'Neil and R.H. Picard, "The Aurora," in *Handbook of Geophysics and the Space Environment*, ed. A.S. Jursa, Air Force Geophysics Laboratory, 1985.

18   Vallance Jones, A., "Historical Review of Great Auroras," *Can. J. Phys.*, **70**, 479 (1992).

CHAPTER 5. ATMOSPHERIC SCATTERING OF SOLAR UV RADIATION

INTRODUCTION

As the solar UV radiation traverses the atmosphere it will not only be absorbed, as discussed in Chapter 3, but also scattered by atmospheric atoms, molecules and aerosols. The scattering process produces a change in direction of a light ray, thus providing both loss and source terms to the equation of radiative transfer. Multiple scattering can be an important effect during light transmission through the atmosphere. Because of this, computer models involving two- and three-dimensional solutions of the radiative transfer equation are generally required to specify the scattered solar light distribution.

This chapter will first review the various forms of atmospheric scattering of UV light and then discuss the computer models available for the specification of atmospheric ultraviolet backgrounds. No discussion of the radiative transfer equation and its solution techniques will be presented. Information on this subject can be found in many standard texts, e.g., Chandrasekhar [1], Kondratyev [2], Brasseur and Solomon [3], and Fenn et al. [4].

ATMOSPHERIC SCATTERING PROCESSES

Atmospheric scattering of solar ultraviolet light occurs through several distinct processes. Atmospheric molecular species absorption followed by subsequent re-emission, as discussed in Chapter 4, is a form of "non-resonant" scattering. Here, in the absence of collisional quenching, the absorbed light at wavelength λ is re-emitted isotropically at a series of wavelengths $\lambda + \Delta\lambda_i$, as determined by the details of the radiating band system, Chapter 2. Huffman [5] has provided a brief review of important molecular band systems providing non-resonant scattering, the majority of which are described in Chapter 4. In the UV these include the N_2^+ first negative system, the OH(A-X) transitions and the NO γ bands.

In the case of solar UV absorption by atomic species, the number of radiative transitions will be small, limited to allowed transitions among the multiplets of the upper and lower states. To first order the wavelength is preserved and these processes may be termed "resonant" scattering. (Note we exclude absorptions which can lead to excited state-excited state emission from this discussion.) In this instance the transition absorption strengths can be so high that multiple scattering will be important even at the high altitudes where atomic species are present. The techniques used to analyze high altitude resonant scattering radiative transfer are discussed by Meier [6]. Dominant UV resonant scattering occurs in the oxygen triplet at 130.4 nm and the hydrogen Lyman α transition at 121.6 nm. Both of these systems can produce scattered radiation levels of 10 to 20 kR [5]. Note the hydrogen Lyman α absorption dominantly occurs at high altitudes, producing the earth's hydrogen geocorona (see photos in Meier [6]). The combination of high altitude absorption and multiple scattering allows the solar Lyman α emissions to penetrate the earth's nightside, as mentioned in Chapter 4.

There are also weaker atomic absorptions which can provide scattered radiation in the

63

ultraviolet. These include for example, the oxygen 135.6 nm doublet and the hydrogen Lyman β transition at 102.5 nm. Of course these more weakly absorbing features can be dominated by other excitation mechanisms such as photo-electron excitation. This effect is graphically demonstrated in Figure 15 which shows the limb measurements of three UV spectral features versus altitude for a near overhead sun. The 130.4 nm feature is more representative of the local O-atom density profile (see discussion in Meier [6], however) than the 135.6 nm feature whose interpretation is complicated by multiple scattering [6,7].
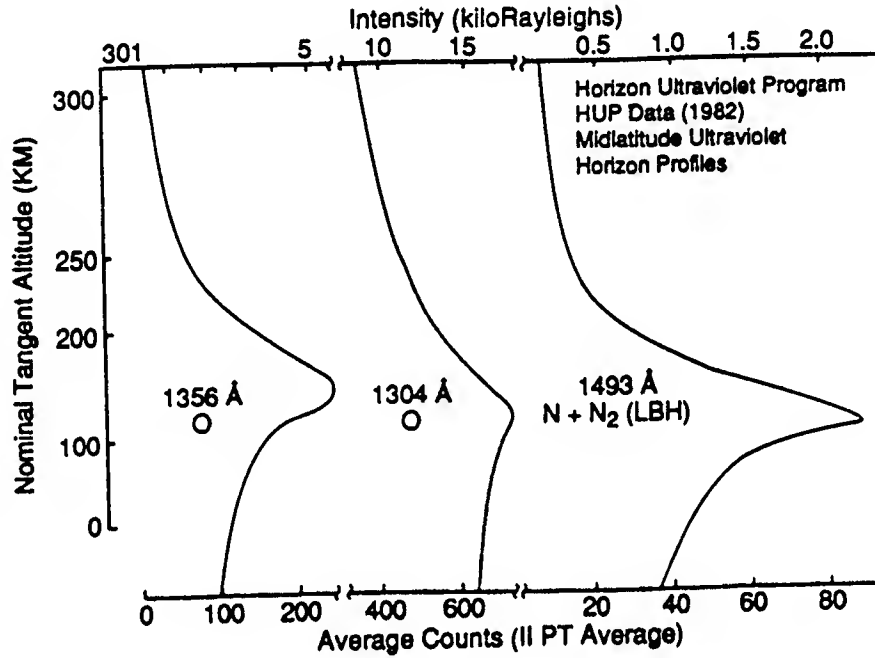
Figure 15.   Limb Profiles for OI 130.4 nm, OI 135.6 nm and NI/LBH 149.3 nm from HUP Shuttle Flight (day, midlatitude, near overhead sun). (Exerpted from Huffman [5].)

A more classical form of scattering, molecular Rayleigh scattering, becomes important at lower altitudes. This scattering results from the electromagnetic interaction of the light with air molecules. The cross section for molecular Rayleigh scattering is given by:

$$\sigma_s = \frac{24\pi^3}{N^2\lambda^4}\left[\frac{m^2-1}{m^2+2}\right]^2 D \qquad (5\text{-}1)$$

where N is the local number density, λ is the wavelength, D is the depolarization factor (typically 1.06 for air) [3,4] and m is the index of refraction of air, given approximately as:

$$m = 1 + \alpha(N/N_o) \qquad (5\text{-}2)$$

where α is the Dale Gladstone coefficient (which has a slight wavelength dependence) and N_o

is Loschmidt's number.

Note that molecular Rayleigh scattering strongly favors shorter wavelengths. Indeed this process produces the blue sky background. For point of reference the cross section at 250 nm is 1.24×10^{-25} cm^2, a small value in comparison to those for allowed optical absorptions. Nonetheless, molecular Rayleigh scattering in the stratosphere and above is the dominant source of radiance scattered to space in the wavelength region of approximately 200 nm to 320 nm (see Figure 12 in Chapter 4).

Molecular Rayleigh scattering provides for scattered light over a wide distribution of angles. The angular scattering distribution is specified approximately by the relationship

$$f(\theta) = 1 + \cos^2\theta \qquad (5-3)$$

where θ is the scattering angle. Thus, forward and backward scattering are equally probable while the scattering distribution exhibits minimums at 90 and 270 deg. More detailed discussions on molecular Rayleigh scattering may be found in many sources including classic texts by Kondratyev [2] and Goody [7].

Aerosols provide another important source for scattering of solar light. Again these are largely important at lower altitudes although noctilucent clouds and/or polar mesospheric clouds may be found in the mesosphere. Indeed, the presence of these latter clouds has been shown to affect limb measurements of MUV radiance, easily dominating Rayleigh scattering (see the discussion in Huffman [5]).

The scattering cross sections for aerosols are dependent on both particle size and index of refraction and may be calculated through use of Mie theory [8] under the assumption of spherical particles. For constant index of refraction the controlling parameter in Mie theory is the size parameter, ρ

$$\rho = 2\pi \, a/\lambda \qquad (5-4)$$

where a is the particle radius. For particle sizes much smaller than the wavelength, $\rho < 1$, the scattering behavior is similar to Rayleigh scattering and exact in the limit of $\rho \to 0$. Alternatively for $\rho >> 1$, the scattering obeys geometric optics. The intermediate regime, often denoted as the Mie regime generally requires full evaluation of the Mie theory.

As the size parameter proceeds from the Rayleigh to the geometric limit the angular scattering distribution goes from near isotropic to highly forward scattered. This is shown in Figure 16a and b, excerpted from Kondratyev [2] which compares the scattering distribution in the Rayleigh limit to that predicted from Mie theory for a perfectly reflecting sphere ($m = \infty$) as a function of size parameter. The scattering distribution of atmospheric aerosols clearly will be controlled by their size distribution function which will typically range throughout the Rayleigh and Mie regimes.
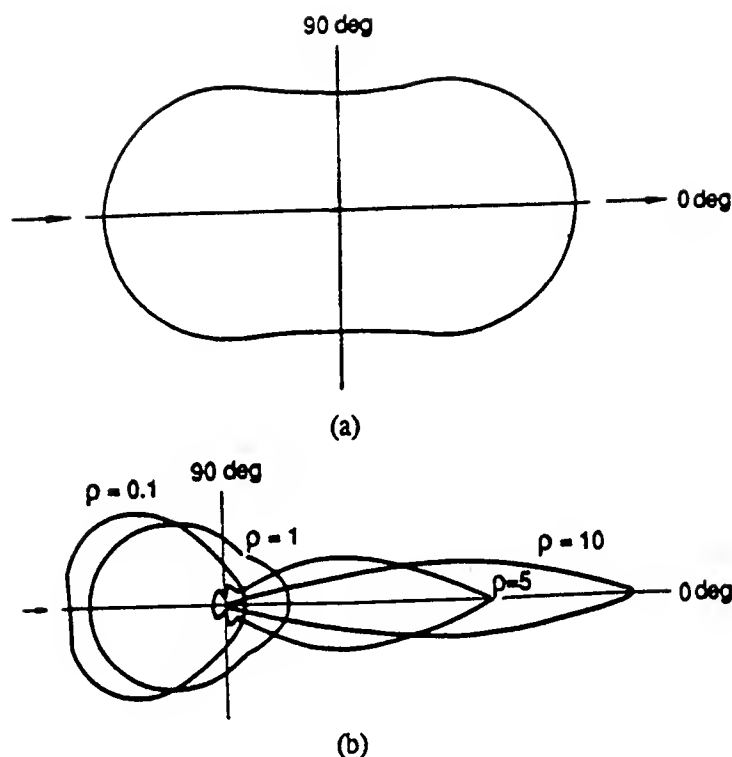
Figure 16.   (a) Rayleigh Scattering Function; (b) Scattering Function of Opaque Absolutely
               Reflecting Particles

Atmospheric aerosols are quite variable with altitude, geographical location, season, etc. For example, Figure 17 describes the variation of aerosol behavior with altitude. Different aerosol types will, of course, have differing indices of refraction and size distributions. A useful description of this variability is provided in Fenn et al. [4]. Aerosol scattering is particularly important in the stratosphere and troposphere. Much of the solar UV spectrum, below ≈ 300 nm, is largely attenuated prior to reaching these altitudes. Nonetheless, aerosols present an important scattering source, particularly for low altitude UV viewing.

COMPUTER MODELS

In general, detailed computer models are required for the prediction of UV backgrounds, particularly because of the complexities introduced by multiple scattering. At present there is no one code available which can predict UV backgrounds between 100 to 400 nm at all altitudes. (There is one under development however. See discussion on AURIC below.) There are several codes available which cover a wide range of the required parameter space.

The LOWTRAN code has for many years been the workhorse for prediction of atmospheric backgrounds at low spectral resolution, 20 cm^{-1}. The most recent embodiment of this code is LOWTRAN 7, Kneizys et al. [9].

Height (km) | Possible Dust Cloud in Orbit

```
200  — Meteor
              Flow
                  Deceleration
100  —  _____
 80  —  Noctilucent Clouds

 60  —  Zone of Slowly Settling
              Cosmic Dust
 40  —           Some Layered Structure
 30  —
 _____

 20  —  Jungle Layer(s)     { Aerosols of Volcanic Origin
                            { Some Photochemical Formation
 15  —
 _____
        Possible Layer Below    Tropopause
 10  —
  8  —
  6  —  _____
        Exponential Decrease
  4  —       with Height of
  3  —           Aerosol Concentration

  2  —  _____
        Aerosol Content Determined by Meteorological Conditions
  1  —  Water Vapor Content of Atmosphere Character of the Surface

  0  —
```

Figure 17. Characteristics of Atmospheric Aerosols. (Excerpted from Fenn et al. [4].)

LOWTRAN allows the prediction of atmospheric transmittance at low spectral resolution at wavelengths down to 200 nm including effects due to multiple scattering. The code embodies, among other things, the choice of six model atmospheres, a wide variety of aerosol and cloud models, general viewing geometries and variable solar parameters. The results are of course very specific to the specification of solar illumination conditions. Solar light will in general penetrate at a zenith angle, χ, i.e., angle relative to normal incidence which is defined by Brasseur and Solomon [3] as

$$\cos(\chi) = \cos(\phi) \cos(\delta) \cos(H) + \sin\phi \sin\delta \qquad (5\text{-}5)$$

where ϕ is the latitude, δ is the solar declination angle (seasonal) and H is the hour angle. This latter quantity is 0 deg at local noon and increases by 15 deg for every hour beyond noon. This quantity χ is required input to LOWTRAN 7, and indeed to any atmospheric transmittance code. LOWTRAN 7 does have some significant limitations in predicting UV backgrounds.

Specifically it does not include any atmospheric emissions, e.g., airglow, fluorescence, is limited to altitudes below 100 km and cannot be applied for wavelengths < 200 nm. Nonetheless it is a useful workhorse for reliably predicting UV backgrounds within its operational domain. An example of LOWTRAN 7 prediction contrasted with S3-4 satellite data is provided in Figure 18 [9]. As can be seen the comparison between model and data is quite good.

A higher resolution version of LOWTRAN has also been developed [11]. MODTRAN provides 2 cm^{-1} resolution capability while preserving the primary LOWTRAN capabilities. These codes are available from the National Climatic Data Center, NOAA, Environmental Data Services in North Carolina.

Another generally available "sky radiance" code, although limited to UV/visible transmittance, is UVTRAN [12]. Like LOWTRAN, it emphasizes lower altitude applications. It utilizes different aerosol parameterizations and includes NO_2 and SO_2 absorptions. This code is available through the U.S. Army Atmospheric Sciences Laboratory, White Sands, NM.

The aforementioned codes are user friendly, readily accessible and even available for use on PCs or PC clones. There are several other specialists' codes in use for predicting atmospheric UV radiances. Perhaps the most well known of these is the Naval Research Laboratory atmospheric radiance code LIMB [13,14] which includes dayglow down to 80 nm and Rayleigh scattering for wavelengths above 200 nm. There is also a specialized version of this code which calculates limb profiles of radiance from the oxygen atom resonance transition of 130.4 nm.
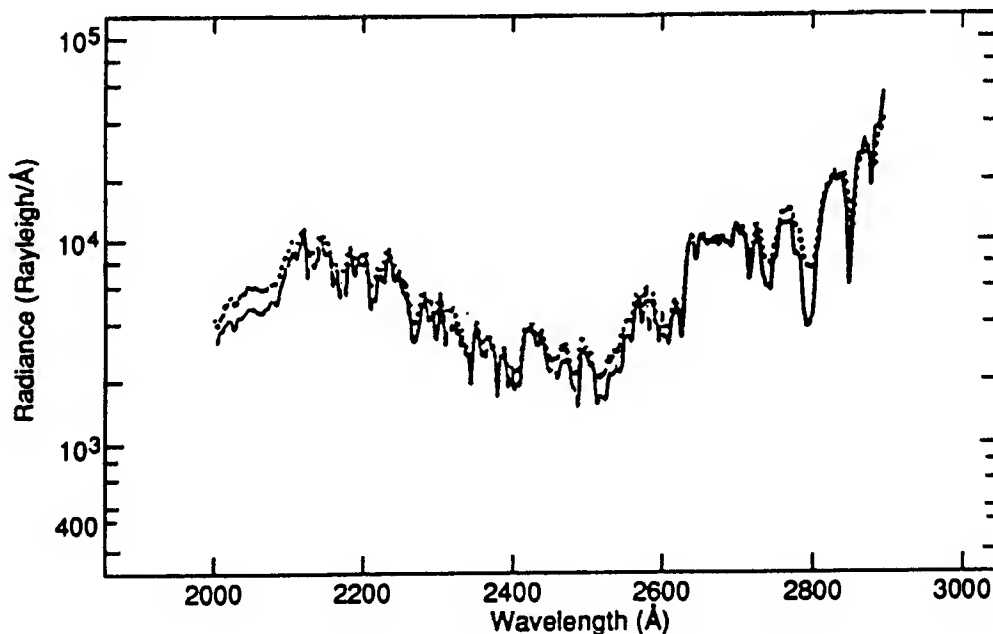
Figure 18.   Comparison of LOWTRAN 7 model (solid curve) and S3-4 satellite data (dashed curve) for UV radiance. Solar zenith angle (SZA) is 24 deg. (Excerpted from Huffman et al. [10].)

This code also provides good agreement with satellite observations. Figure 19 presents a comparison of LIMB code predictions [14] with recent satellite measurements [15] for a tangent altitude of 50 km. At this altitude, indeed below 90 km, the sky background due to Rayleigh scattering exceeds that of atmospheric emission and the code prediction can be seen to be quite reliable. Similar comparisons with data for higher altitudes, in the airglow dominated region, have also been presented by Strickland et al. [14]. At these altitudes the comparisons are fair although clear discrepancies are observed at some wavelengths.
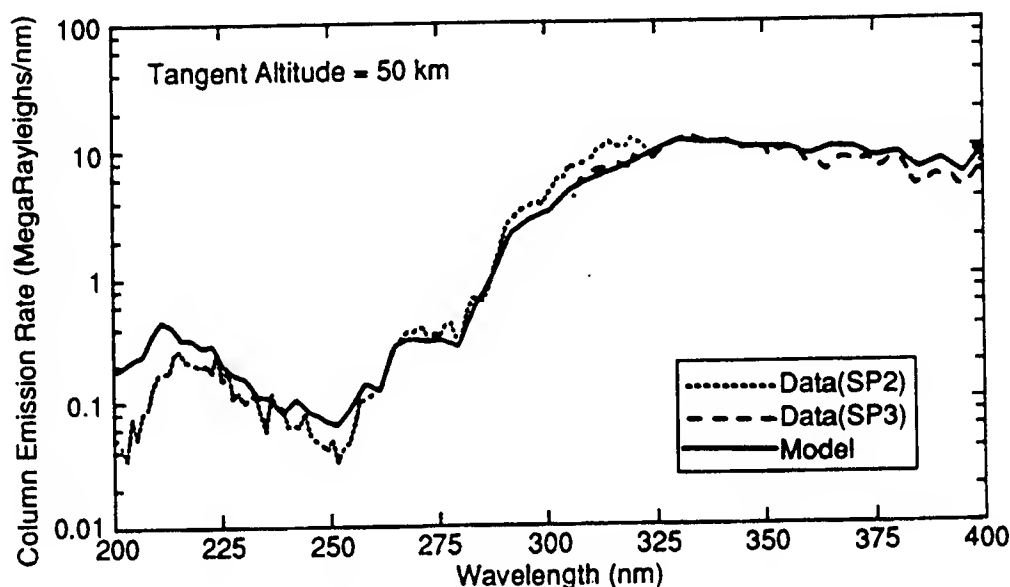
Figure 19. Measured and Calculated Spectral Radiances at a Tangent Altitude of 50 km and a Solar Zenith Angle of 50 deg. Units are MegaRayleighs/nm which come from scaling the intensity (photons cm^{-2} s^{-1} sr^{-1} nm^{-1}) by $4\pi/10^{12}$. (Exerpted from Strickland et al. [14].)

A very detailed model for the prediction of UV backgrounds, AURIC, the Atmospheric Ultraviolet Radiance Integrated Code is presently being developed at the Phillips Laboratory Geophysics Directorate under the direction of Dr. R.E. Huffman. Primary support is being provided by Computational Physics Inc., who also have played an important role in developing and exercising the Naval Research Laboratory LIMB code.

Planned AURIC capabilities are nicely described in Huffman [5]. The code will initially emphasize the spectral region of 100 to 400 nm with spectral resolution of 1 to 2 cm^{-1}. A detailed UV transmission model will be developed building from the LOWTRAN 7 capabilities. More advanced model atmospheres, such as MSIS 86, will be interfaced along with detailed Schumman-Runge band absorption, resonant line multiple scattering and detailed fluorescence modeling, e.g., NO (γ and δ bands), which is particularly important for predicting twilight backgrounds. The model will also include the appropriate chemistry to predict atmospheric airglows and, ultimately, auroral emissions.

69

The atmospheric chemistry/transmission modules, are necessarily complex, given the wealth of phenomenology described in earlier chapters. Figure 20 provides an overview of the components of AURIC 1.0, which was recently reviewed by Link et al. [16]. The model is presently limited to optically thin transmissions but includes an ion-neutral chemistry model and allows specification of appropriate geophysical parameters.

Figure 21 provides a comparison of AURIC predictions for the optically thin oxygen atom 135.6 nm atmospheric emissions compared with measurements taken from the Space Shuttle in 1982 using the Horizontal Ultraviolet Program (HUP) sensor [17]. Comparisons between prediction and data for two widely different solar angles are seen to be quite reasonable.

In sum, although significant model development and validation remains to be performed it appears that state-of-the-art UV atmospheric radiance models can provide an adequate representation of atmospheric UV backgrounds. Although at present there is no general user friendly code available for predicting UV backgrounds, i.e., LOWTRAN 7 is limited to lower altitudes without airglow, the planned development of AURIC should fill this void.
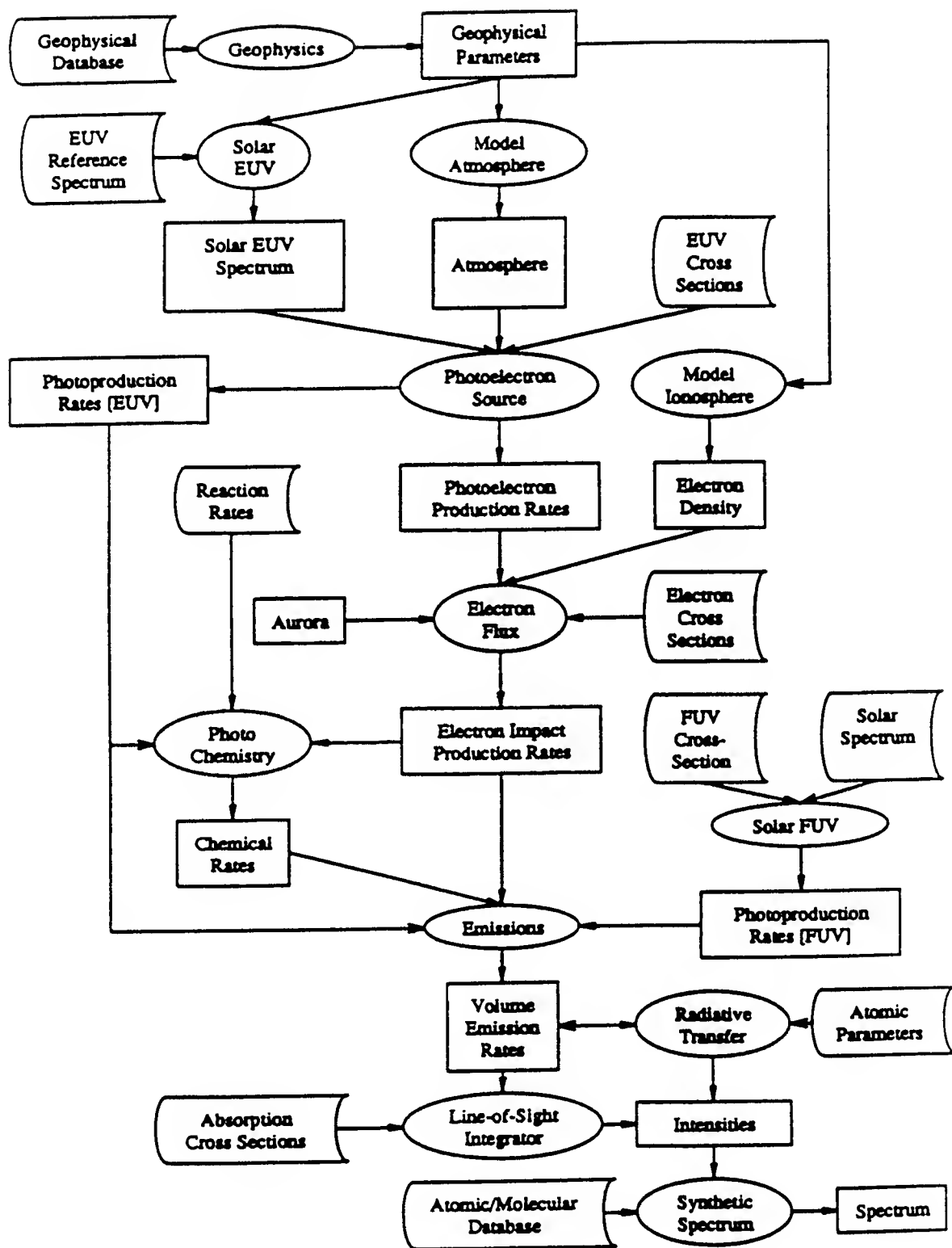
Figure 20. Overview of non-LTE Thermospheric AURIC. (Excerpted from Link et al. [16].)

71
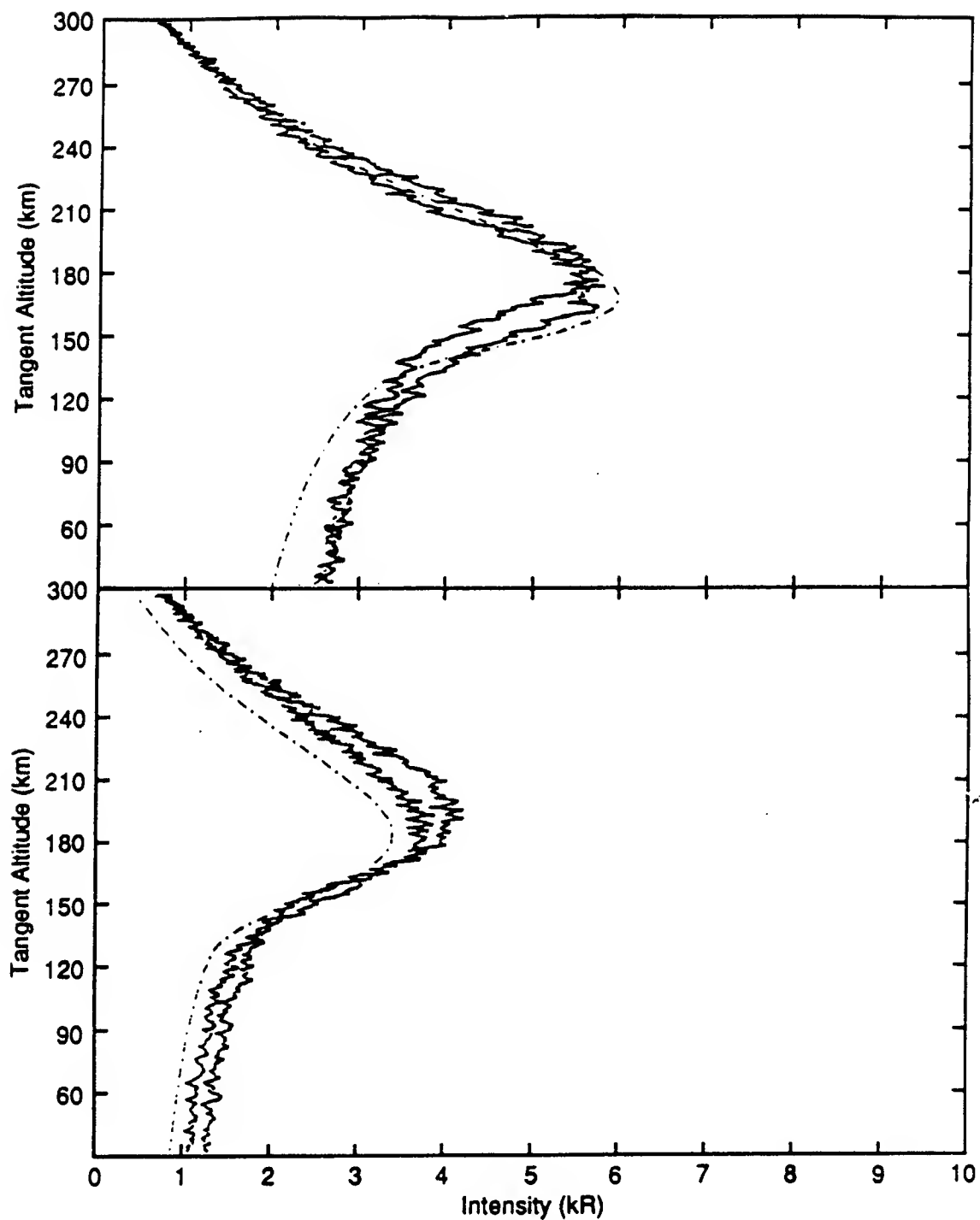
Figure 21.   HUP Horizon Scans (up and down) of 135.6 nm Oxygen Atom Emission
Observed from Shuttle Flight STS-4 at a Solar Zenith Angle of 12.2 (upper)
and 72.7 (lower) deg and Overlaid with the AURIC Version 1.0 prediction
(broken line). (Excerpted from LeBlanc et al. [17].)

72

CHAPTER 5 REFERENCES

1   Chandrasekhar, S., *Radiative Transfer*, Dover Publications, NY, 1960.

2   Kondratyev, K. Ya., "Radiation in the Atmosphere," *International Geophysics Series*, Vol. 12, Academic Press, NY, 1969.

3   Brasseur, G. and Solomon, S., *Aeronomy of the Middle Atmosphere*, Reidel, Dordrecht, 1984.

4   Fenn, R.W., Clough, S.A., Gallery, W.O., Good, R.E., Kneizys, F.X., Mill, J.D., Rothman, L.S., Shettle, E.P., and Volz, F.E., "Optical and Infrared Properties of the Atmosphere," Chapter 18 in *Handbook of Geophysics and the Space Environment*, ed. A.S. Jursa, 1985, AFGL-TR-85-0315, ADA167000.

5   Huffman, R.E., "Atmospheric Ultraviolet Remote Sensing", Vol. 52 in the International Geophysics Series, Academic Press, Boston, 1992.

6   Meier, R.R., "Ultraviolet Spectroscopy and Remote Sensing of the Upper Atmosphere", *Space Science Reviews* **58**, 1991.

7   Goody, R.M., *Atmospheric Radiation I, Theoretical Basis*, Oxford at the Clarendon Press, 1964.

8   Van de Hulst, H.C., *Light Scattering by Small Particles*, Wiley, Dover Publications, NY, 1957.

9   Kneizys, F.X., Shettle, E.P., Abreu, L.W., Chetwynd, J.H., Anderson, G.P., Gallery, W.O., Selby, J.E.A., and Clough, S.A., "Users Guide to LOWTRAN 7," AFGL-TR-88-0177, August 16, 1988, ADA206773.

10   Huffman, R.E., Hall, L.A., and LeBlanc, F.J., in *Ultraviolet Technology III*, ed. R.E. Huffman, SPIE Proceedings Vol. 1158, 10-11 August 1989, San Diego, CA, pp. 38-44.

11   Berk, A., Bernstein, L.S., and Robertson, D.C., "MODTRAN: A moderate Resolution Model for LOWTRAN 7," USAF Geophysics Laboratory Report GL-TR-89-0122, 30 April 1989, ADA214337.

12   Patterson, B.A. and Gillespies, J.B., "Simplified Ultraviolet and Visible Wavelength Atmosphere Propagation Model," *Appl. Opt.*, **28**, 425 (1989).

13   Strickland, D.J., Barnes, R.P., and Anderson, D.E., Jr., "UV Background Calculations: Rayleigh Scattered and Dayglow Backgrounds from 1200 to 3000 Å," AFGL-TR-88-0200, 24 August 1988, ADA201118.

14   Strickland, D.J., Barnes, R.P., Cox, R.J., Anderson, D.E., Jr., Carbary, J.F., and Meng, C.-I., "Analysis of UV Limb Data from Low Earth Orbit," in *Ultraviolet Technology III*, ed. R.E. Huffman, SPIE Proceedings Vol. 1158, 10-11 August 1989, pp. 59-68.

15   Carbary, J.F. and Meng, C.-I., "Limb Profiles from Low Earth Orbit," in *Ultraviolet Technology III*, ed. R.E. Huffman, SPIE Proceedings Vol. 1158, 10-11 August 1989, pp. 51-58.

16   Link, R., Strickland, D.J., and Daniell, R.E., Jr., "AURIC Airglow Modules: Phase I Development and Application," in *Ultraviolet Technology IV*, ed. R.E. Huffman, SPIE Proceedings Vol. 1764, 20-21 July 1992, pp. 132-150.

17   LeBlanc, F.J., DelGreco, F.P., Welsh, J.A., and Huffman, R.E., "Horizon UV Program (HUP) Atmospheric Radiance Measurements," in *Ultraviolet Technology IV*, ed. R.E. Huffman, SPIE Proceedings Vol. 1764, 20-21 July 1992, pp. 12-20.

CHAPTER 6. DOWNLOOKING BACKGROUNDS

INTRODUCTION

Substantial progress has been made in our understanding of the ionosphere and thermosphere over the last decade. New and improved instrumentation has been developed for sensing the ultraviolet wavelength region from satellites, and it has been demonstrated that UV atmospheric radiance, far UV auroral imagers, and extreme UV solar flux measurements can be used to characterize atmospheric compositions and emissions. Huffman [1] calls this the New Ultraviolet Space Weather Systems concept. He suggests a future network of satellites and ground based sensors which will give constant updates on 100 to 1000 km "weather" conditions as they change because of changes in the radiation and particle input from the sun. A space weather system will include models of important phenomenology in the form of codes which will, based on continuously updated remote sensing inputs, predict electron concentrations and expected emission in the 100 to 650 nm wavelength region. This code will likely be based on the Atmospheric Ultraviolet Radiance Integrated Code (AURIC) currently under development by the Phillips Laboratory Geophysics Directorate. See Refs. 6-2 and 6-3 for recent updates on the AURIC code.

This chapter contains a review of the literature of the past several years and emphasizes recent developments in remote sensing instruments, as well as information about nightglow, dayglow, and auroral emissions which has been obtained from those instruments. The 200 to 300 nm waveband of interest to the remote sensing of missile plumes has been emphasized.

During the past several years, UV imaging has become a standard method for observing the earth and the earth limb. CCD detector arrays have made it practical to do high resolution UV imaging from space or even a rocket probe. Imaging adds another physical dimension to observations and, of course, creates an enormous amount of data for resolving the spatial structure of emissions. It permits a new level of understanding for, in particular, auroral forms and spatial extent of other atmospheric emissions.

Spectrometers have been increased in spectral feature resolving power to sub-Angstrom wavelength resolution permitting clearer identification of emitting species. Photometers have improved spatial resolution and greater sensitivity for identifying lower order features in the airglow and aurorae allowing better definition of species concentrations in the atmosphere, including altitude profiles of electron densities.

The fact that many types of instruments are now flown on the same satellite and operated simultaneously in a coordinated fashion has dramatically enhanced the utility of atmospheric emission data. The Arizona Imager/Spectrograph (AIS) [4] and the Ultraviolet Plume Instrument (UVPI) [5] and Imaging Spectrometric Observatory (ISO) [6] are good examples of the current state of imaging measurement capability. For example, with an imager and a spectrometer, a spatial feature in an image can be further examined with a high resolution spectroscopic line scan at selected locations in the image. Furthermore, a satellite can take a sequence of images in

rapid succession, with a long observation window or return to approximately the same viewing location and geometry some time later which permits the time development and changes in emitting features to be observed. From these time-dependent measurements the spatial extent and altitude of features can be estimated. Both length scales and time constants of the emission features can be determined.

Carbary reviewed the existing data base of UV and visible observations from satellites in a presentation at a UV/VIS Special Topic Meeting on 10 September 1991 under BMDO (SDIO) sponsorship [7]. Missions potentially contributing to atmospheric UV data bases are listed in Table 8.

Table 8. Selected Orbital Observations Missions
(Greatly expanded from Ref. [7])

Sponsor	Orbital Missions
BMDO/SDIO	Delta 180, Delta 181, Delta Star, VUE, CIRRIS1A, AIS, UVPI Future: Clementine, UVISI
NASA	OGO, Atmospheric Explorers, Solar Mesospheric Explorer, Dynamics Explorers, ISO, Nimbus, Polar, several STS Missions, TOMS, SSBUV, UARS Future: SSBUV, EOS
Air Force and Navy	P78-1, S3-4, DMSP, HiLat, Polar Bear (AIRS), HUP, UVLIM HIRAAS/Mustant, FUV, (others) Future: AURA, RAIDS, GIMI, SUSSI, SSULT, DMSP, OOAM, POAM
Foreign	ISIS2, Meteor, ESRO, TD1, Kyokko, Viking, SPOT, Akebone

The objective of most of the work documented in the literature is to further the scientific understanding of the earth's atmosphere. In this chapter, a review of recent literature is completed from the point of view of emissions that a space-based surveillance platform would see for a background with anything from a nadir to limb view, while trying to identify the plume of a missile in boost phase. Papers were selected because they contained applicable data in the 200 to 300 nm wavelength range or because they described methods for using data to support the target acquisition function.

DAY AND NIGHT AIRGLOW

The spectral region between 200 and 300 nm is most useful for remote sensing of rocket launches because most of the solar radiation is absorbed by ozone and the earth appears black from above. This eliminates much of the surface and cloud features which are so important at many other wavelengths. The incredible complexity of the far UV region could also be avoided, although much structure still exists in the 200 to 300 nm range (see Chapter 4, Figures 11 and 13). The principal contributors of radiation are the NO δ and γ bands, the N_2 Vegard-Kaplan bands, and the O_2 Herzberg I, II, and III bands. Large differences exist, of course, between the

radiation levels of night and day airglow, and the actual emission details depend on the composition of the atmosphere. For night airglow, this means the recent history of solar irradiation and chemical reactions occurring the previous day and at night. For day airglow, the additional complications of solar flux and absorption depths of solar radiation as a function of wavelength all combine to create the current airglow.

In the decade between the late seventies and the late eighties there were relatively few new sources of data on atmospheric emissions in the 200 - 300 nm region, but further understanding of existing data was obtained through model development and more detailed and thorough analysis of existing data.

In an early paper on remote sensing of the ionosphere, Meng et al. [8] suggested a strategy of using ultraviolet optical measurements and in-situ ion concentration measurements for constantly updating input information to a detailed atmospheric model which would predict the atmospheric electron density as a function of altitude. For the daytime mid-latitude ionosphere where the main source of ionization is solar radiation, emission lines in the far ultraviolet were recommended to indirectly measure the O/N_2 density ratio and establish an electron density profile. The suggested FUV wavelength is 135.6 nm. For the nighttime mid-latitude region, 630 nm emission from O_2^+ recombination is recommended in combination with 135.6 nm emission. In the auroral region in daylight, solar radiation and auroral charged particle precipitation contribute about the same order of magnitude of ionization. In the nighttime more than 90% of the ionization is caused by incoming charged particles. Since electrons of different energies are absorbed at different altitudes a ratio of measured auroral spectral features such as 630 and 391.4 nm could be used to determine electron energies and total flux levels in auroral regions, establishing an electron density profile with altitude.

The recommended spectral features are summarized in Table 9, excerpted from Meng et al. with estimated ranges of emission rates. It is interesting that these features are not in the 200 - 300 nm range. A supplemental reference list of recent work emphasizing neighboring wavelengths, particularly the far ultraviolet (FUV) is included at the end of this chapter.

The ability to perform remote sensing in the 200 - 300 nm region clearly depends on understanding spectral features in that region and neighboring regions. In fact one might continuously monitor emissions in other regions in order to determine the "state" of the ionosphere for a continuous prediction of the background radiation to be expected at 200 - 300 nm.

At the BMDO UV/VIS Special Topic Meeting on 10 September 1991, Don Anderson provided an excellent review of the current state-of-knowledge of the UV attenuation problem [9]. Orbital platforms can probe altitudes down 18 - to 30 km depending on wavelength/bandpass and the local ozone column density. His conclusion was that we understand the composition and chemistry, but do not know the dynamics as well. In particular we have a poor understanding of the clutter in the auroral oval, the Power Spectral Density distributions of auroral features, and the structure of bright Polar Mesospheric Clouds which can have 10 kR/nm intensities. Ozone variability will also cause clutter that will have diurnal and

seasonal dependencies.

Table 9. Nominal Ranges of Column Emission Rates in Rayleighs as Observed from
~ 800 km Altitude (Excerpted from Ref. [8])

Feature	Dayglow	Low and Mid-Latitude Nightglow	Auroral Region
130.4 nm	1,000 - 20,000	0.2 - 200	1,000 - 10,000
135.6 nm	100 - 3,000	0.1 - 200	100 - 1,000
N_2LBH	5 - 200	*	10 - 1,000
391.4 nm, 337.1 nm	*	?	10 - 60,000 (night only)
630 nm	*	3 - 900	10 - 10,000 (night only)
* Lack of entry indicates feature is not applicable in given region.			

Sharp and Siskind [10] analyzed 3.5Å resolution spectrometer data from a 1984 rocket launch at White Sands Missile Range. Details of the ultraviolet nightglow in the Earth's limb at 90 to 110 km tangent altitudes were obtained from 267 to 304 nm and are shown in Figure 22. The resolution is sufficient in these measurements to identify clearly the O_2 Herzberg I and II band systems; resolution of the Herzberg III bands is also suggested. These measurements were taken during a period of high geomagnetic activity and during the Orionids Meteor shower. Some emission at 285.2 nm was suggested to be the Mg I resonance line indicating significant amounts of magnesium in the upper atmosphere from the vaporized meteoric solid material.

A more recent rocket experiment measured limb UV fluorescent emissions of NO in the lower thermosphere. The 1989 sounding rocket launch from Poker Flat, AK carried a high resolution UV spectrometer which viewed the limb dayglow from between 90 and 185 km altitude in the 212 to 250.5 nm wavelength range with sub-Angstrom resolution. Eparvier and Barth [11] developed a self-absorption model for NO and applied it to the $(1,0)\gamma$ band observations. They analyzed the rocket data assuming two conditions: (1) the atmosphere is optically thin at the NO $(1,0)\gamma$ band and (2) the NO is self-absorbing at that wavelength. They demonstrated that the second is clearly correct for altitudes below 120 km from a careful analysis of these high resolution data. Their conclusions are demonstrated in Figures 23 and 24. They point out that ignoring this self-absorption of NO can lead to underestimating the NO concentration below 120 km altitudes. Recent analysis of the UV Camera data from the AFP-675 mission on STS-39 [12] and from the rocket-borne MUSTANG spectrometer also exhibit this self-absorption.
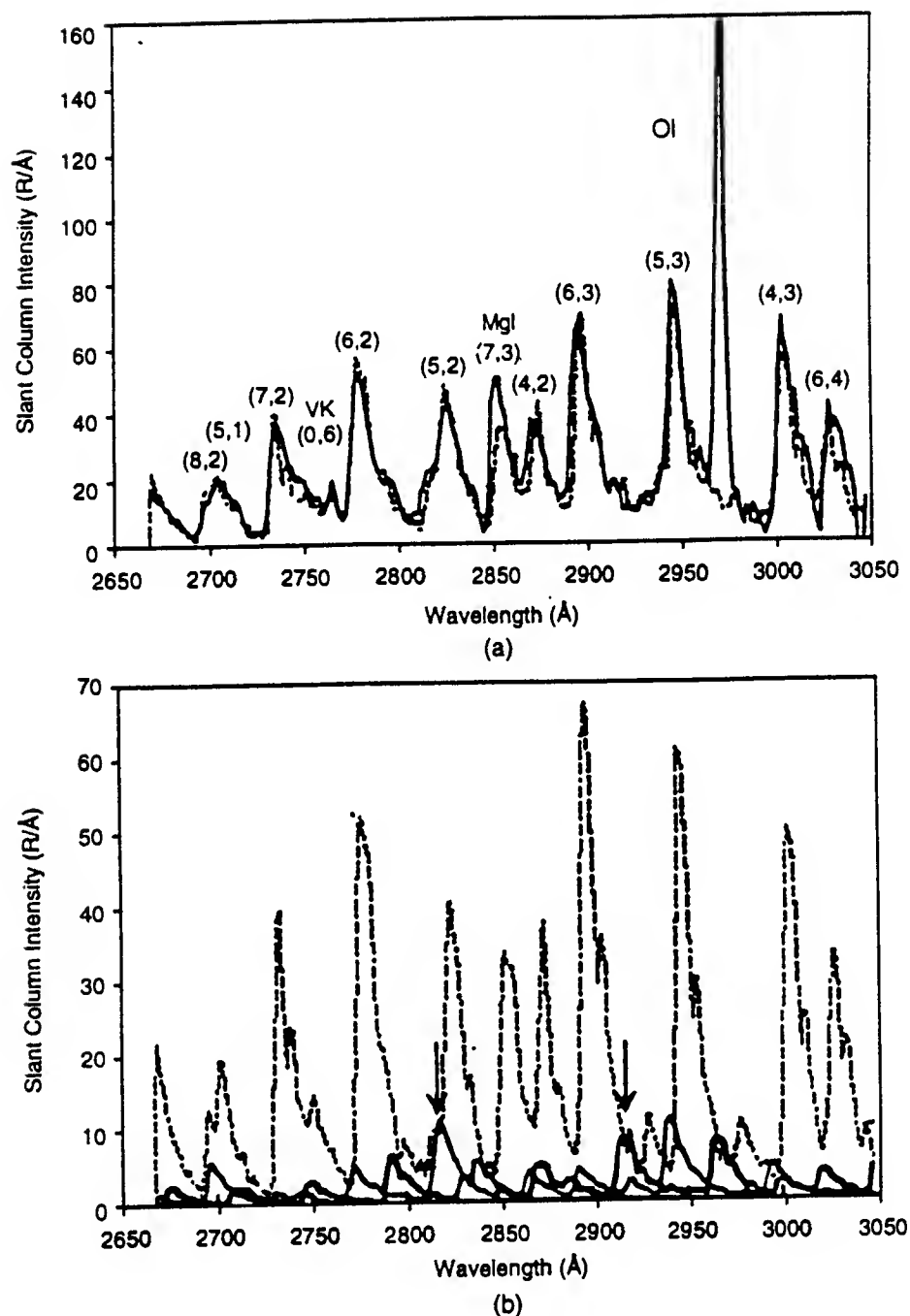
Figure 22.   (a) The data (solid line) obtained from the average of 41 spectral scans obtained while the field of view scanned the limb from approximately 90 to 110 km. Synthetic spectra for the Herzberg I, II, and III and the N_2 VK are summed together (dotted line) to compare with the data. (b) The individual synthetic spectra (on expanded vertical scale) for the Herzberg I (dotted line), Herzberg II (bold solid line) and Herzberg III (thin solid line) band systems. The two arrows label the Herzberg III (6,2) band at 2815Å and the Herzberg II (7,2) band at 2913Å. (Excerpted from Sharp and Siskind [10].)
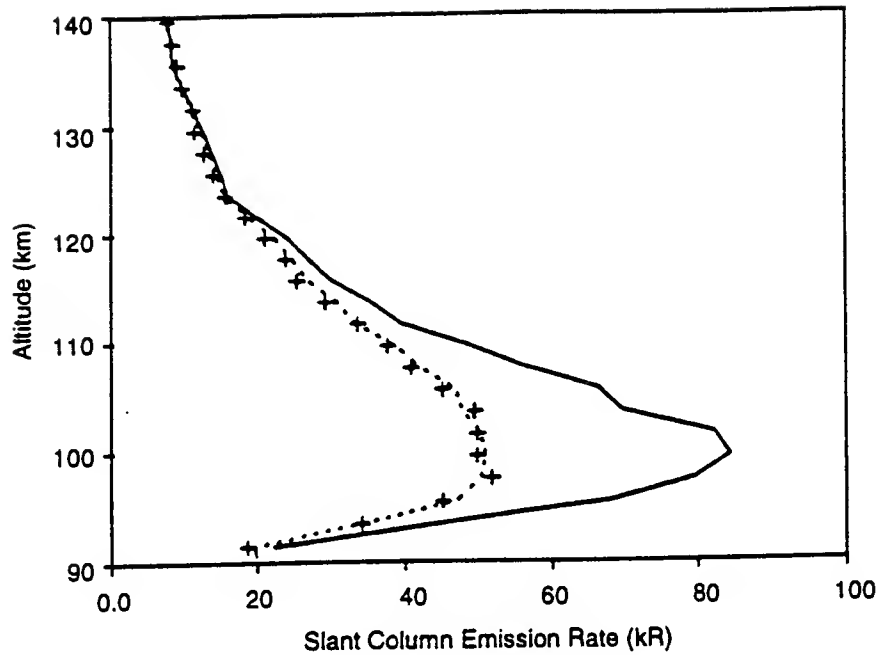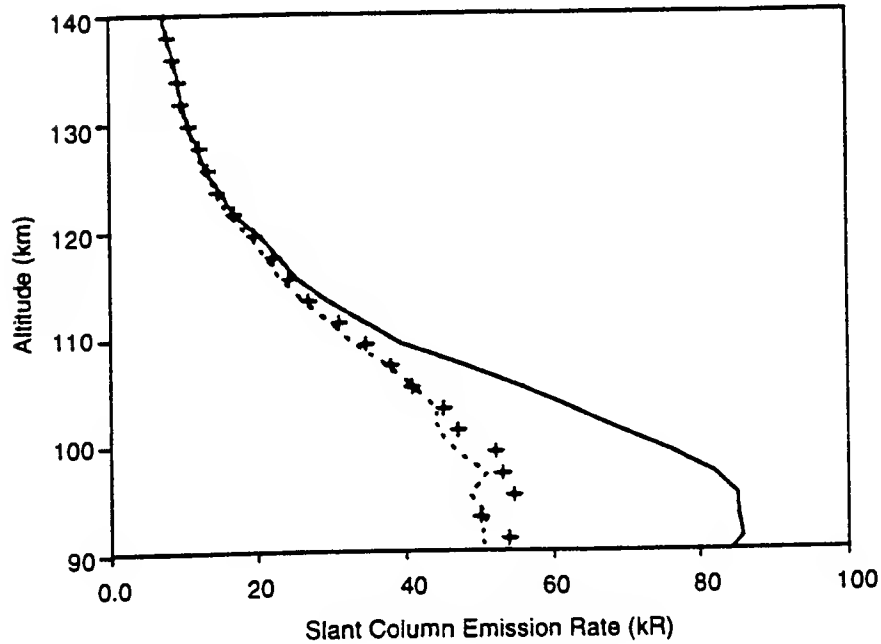
Figure 23. Slant column emission rates for the NO (1,0) γ band during the (a) upleg and (b) downleg of the flight. The crosses are the measured emission rates. The solid lines are the emission rates expected if the band were optically thin, and the dotted lines are the calculated self-absorbed emission rates. (Excerpted from Eparvier and Barth [11].)
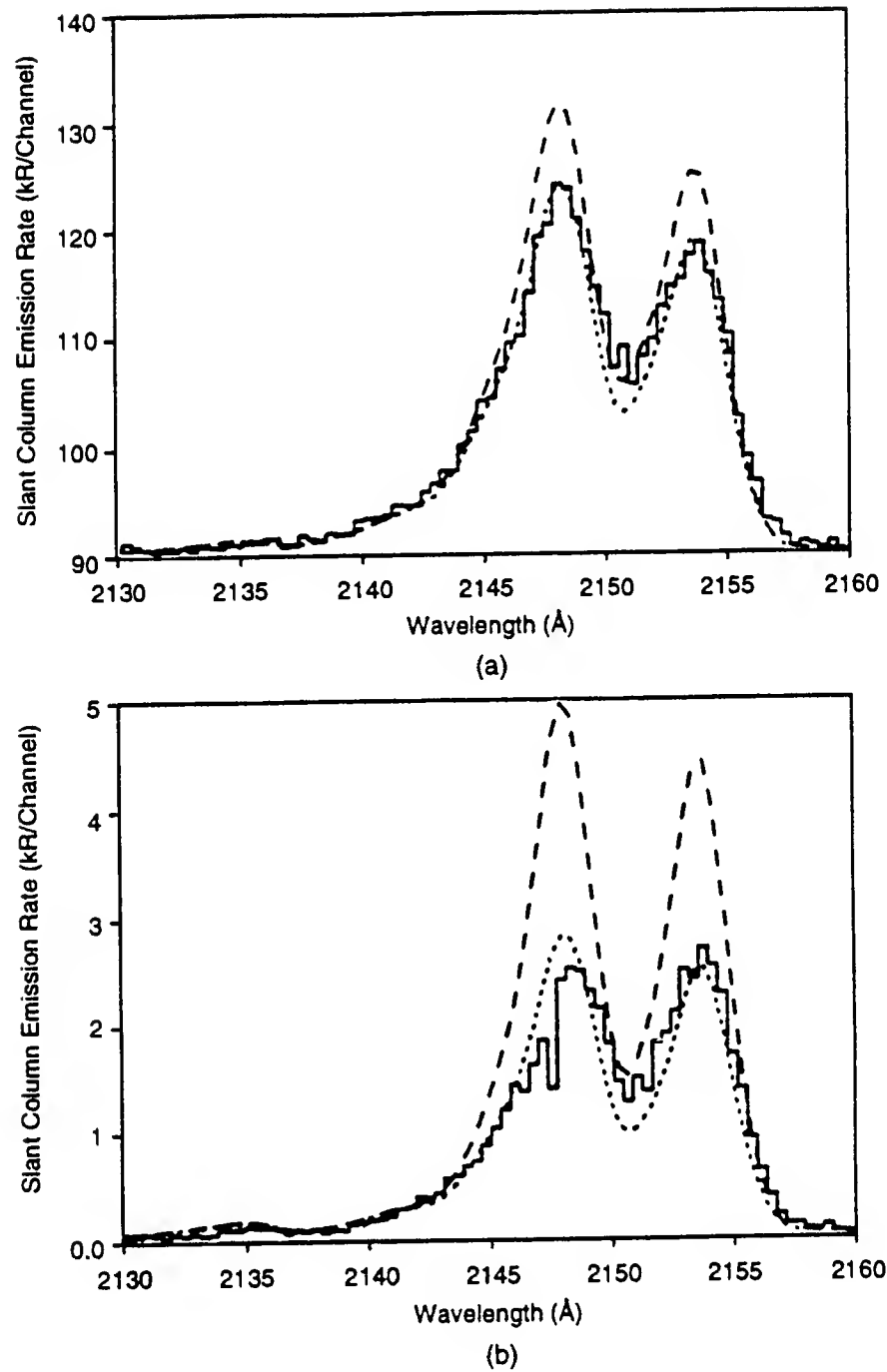
Figure 24.   Spectral fit of the self-absorbed NO (1,0)γ band at (a) 109.5 km and
(b) 93.5 km altitude. The solid lines are the data, the dashed lines are the
expected optically thin spectra, and the dotted lines are the calculated self-
absorbed spectra. (Excerpted from Eparvier and Barth [11].)

81

Huffman et al. [13] analyzed relatively old but valuable data in the 200 - 290 nm wavelength region taken in 1978 with the S3-4 satellite, viewing toward the center of the Earth. The LOWTRAN 7 transmission and radiance code calculations were in excellent agreement with the mid latitude daytime measurements (see Chapter 5, Figure 18). But the LOWTRAN 7 code does not include airglow and fluorescence emission and does not accurately describe the data which were taken under twilight conditions. They point out that the recent application/extension of LOWTRAN capabilities down to 200 nm in the ultraviolet included (1) atmospheric absorption by ozone, (2) molecular oxygen absorption in the Herzberg continuum and in the 0-0 and 1-0 Schumann-Runge bands, and (3) appropriate cross sections for Rayleigh scattering.

The onset of code failure under twilight conditions is shown in Figure 25 which is directly comparable to Figure 18 except that the solar zenith angle has increased to 94 deg. As the solar scatter decreases the total radiance falls dramatically and the familiar peaks due to NO and O_2 emission rise above the LOWTRAN 7 predictions between 200 and 290 nm. If LOWTRAN 7 were to be used for modeling background emissions for nighttime remote sensing applications, these NO and O_2 contributions would have to be added.
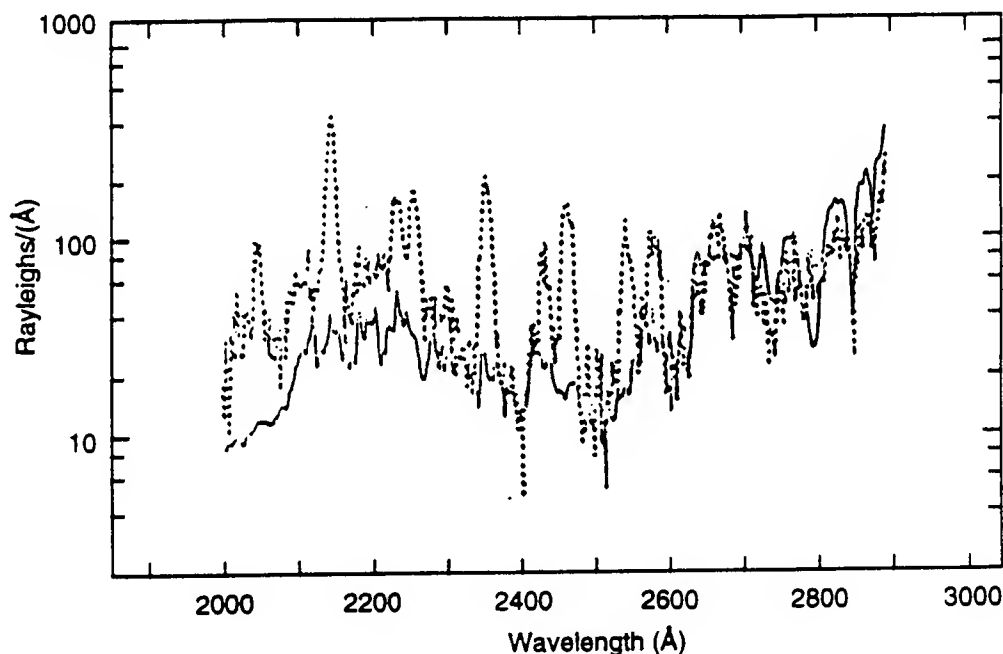
Figure 25.   Comparison of LOWTRAN 7 model (solid curve) and S3-4 satellite data (dash curve) for UV radiance. Solar zenith angle (SZA) is 94 deg. Dashed lines are measured radiances.

Trakhovsky et al. [14] have pointed out that both the LOWTRAN 7 and UVTRAN codes include O_2 continuum absorption but do not account for O_2 atmospheric absorption in the "solar blind" 230 - 290 nm region. They performed ground measurements of O_2 attenuation at relatively broad bands centered at 252, 255, and 264 nm yielding much greater O_2 absorption coefficients which they attribute to Herzberg I line absorption. These results are only important

at lower altitudes and they could be influenced by particulate scattering since they were obtained from near ground level path lengths.

Attempting to understand better the chemical reactions and numerous emissions which produce the ultraviolet nightglow, Eastes et al. [15] analyzed S3-4 satellite data taken in 1980 in the 160 - 295 nm wavelength range. They suggest that remote sensing of UV radiation in this range can be utilized to evaluate the concentration of atomic oxygen and nitrogen; which it is important to determine since it is involved in so many chemical reaction based emissions. The S3-4 satellite data were interesting to study because they included simultaneous O_2 and NO emissions over the same observation paths and the data were taken at sufficient sensitivity for high resolution observations at night. The prominent O_2 Herzberg I band emissions are produced by a three-body recombination of atomic oxygen while the other important NO nightglow is caused by a recombination of atomic nitrogen with atomic oxygen producing the NO δ and γ band emissions as noted in Chapter 4. Regardless of the success or failure of obtaining O and N concentrations in the atmosphere, these 1980 S3-4 satellite observations reduced in this way provide a quantitative measure of the 200 - 300 nm nightglow. The composite plot with background removed and presented in Rayleighs is shown in Figure 26 (repeated from Chapter 4, Figure 11).

The O_2 Herzberg emission peaks around 95 km while the NO emission is a maximum around 150 km. The S3-4 satellite was nadir viewing at altitudes ranging from approximately 200 - 270 km when these data were obtained.
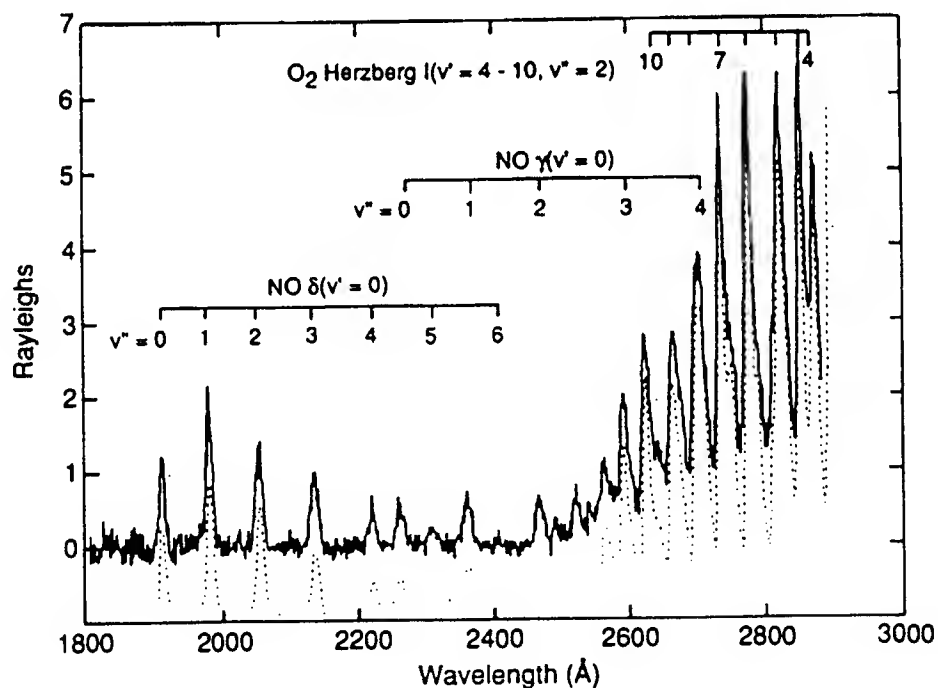
Figure 26.   Night Airglow Spectrum from the S3-4 Satellite   (Excerpted from Eastes et al. [15].)

By the late 1980's, imaging technology permitted fairly routine satellite UV images of the earth and earth limb. In early 1988, the Delta 181 mission launched a satellite which performed wavelength measurements of airglow in the 180 - 320 nm region. Measurements were made of the earth limb at noon, midnight, dawn and dusk, with simultaneous observation of the UV earth limb by an imager and spectrographs. The satellite pitched up and down observing tangent angles at altitudes of 100 - 250 km. The earth limb emissions were characterized vertically and spectrally. The results show that the UV nightglow is dominated by O_2 Herzberg I bands while the noon, dusk, and dawn glows are mainly due to solar-driven NO γ band radiation.

The limb viewing instruments permit a quantification of emission as a function of altitude. Strickland et al. [16] have analyzed these limb data at noontime solar levels. An optical backgrounds model was used which describes Rayleigh and aerosol scattering of sunlight as well as thermospheric emissions. The tangent column emission rate is given as a function of altitude from 0 to 80 km in Figure 27; for two 10-nm wide wavebands centered at 215 and 295 nm. These altitude emission profiles reach a maximum at around 50 km altitude where ozone and molecular oxygen begin to absorb large amounts of radiation. Variations with latitude and season in these profiles are expected.

At altitudes above 90 km, Rayleigh scattering of sunlight no longer dominates at wavelengths above 200 nm and dayglow becomes prominent. The dayglow emissions have lots of structure which becomes clearer at the higher altitudes although the overall emission levels decrease with further increases in altitude. This is shown by Figure 28, which is a comparison of tangent column emission rates at 100, 150, and 200 km with a solar zenith angle of 50 deg. The models compare favorably with the data particularly in the 200 - 300 nm wavelength region although the measured emission rates are higher than predicted.
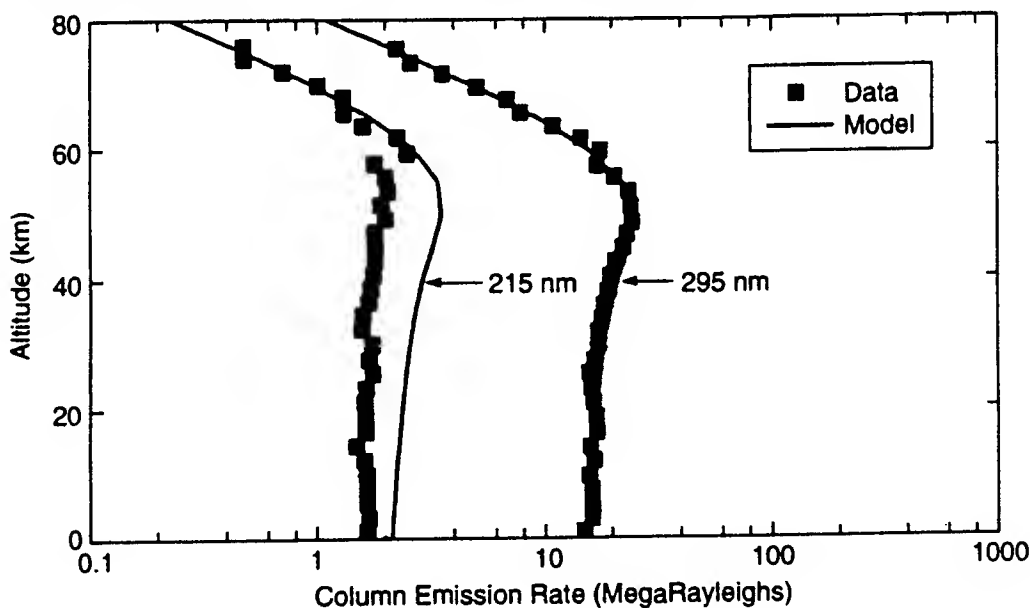
Figure 27. Measured and Calculated Limb Profiles over 10 nm Bands Centered at the Designated Wavelengths. (Excerpted from Strickland et al. [16].)
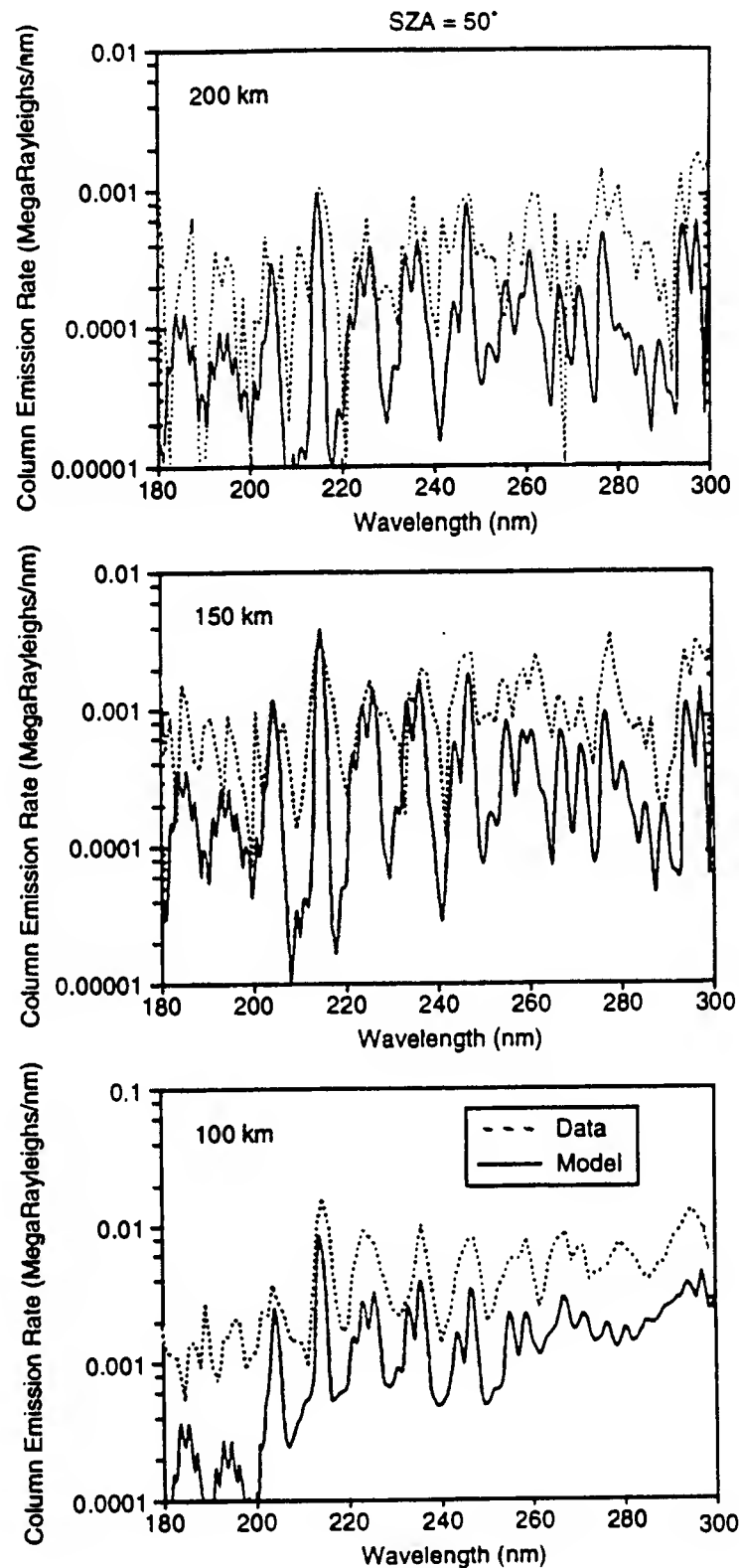
Figure 28.   Measured and Calculated Spectral Radiances at MUV Wavelengths and at
Tangent Altitudes of 200 km (upper panel), 150 km (middle panel), and 100 km
(lower panel). (Excerpted from Strickland et al. [16].)

85

The 1988 Delta 181 satellite data were also analyzed by Carbary and Meng [17] and produced some interesting comparisons of limb radiance profiles at different times such as noon, dusk, dawn, and midnight. These results give examples of the daily range of radiation levels seen in the earth limb. Figure 29a from Carbary and Meng shows the rapid changes in limb radiances at dusk over the 180 to 310 nm waveband. This is contrasted with Figure 29b for the same waveband at noon where there are almost no changes with solar zenith angle. The altitude profiles at midnight in the 180 to 310 nm waveband are included for comparison in Figure 29c where the O_2 Herzberg I band emissions above 250 nm dominate the nightglow as discussed earlier. Table 10 summarizes the dusk, dawn, noon, and midnight radiation levels observed.

Anderson, et al. [18] further analyzed the UV dayglow data from Delta 181 utilizing an improved model of noontime airglow emissions. The model now includes a description of "background" radiation due to off-axis Rayleigh scattering of sunlight from lower in the atmosphere. This was particularly important at target altitudes below 90 km. The data were analyzed by comparing with predictions of scattered sunlight and calculated dayglow spectra. This is a superior method than subtracting the background from the data and then comparing to the modeled dayglow.

In March 1992 the Imaging Spectrometric Observatory (ISO) was launched on the ATLAS-I mission. The ISO is a group of grating spectrometers using CCD arrays for detectors to obtain spectral and spatial information simultaneously. Owens et al. [6] reported the first comprehensive spatially-resolved spectral survey of nighttime airglow from 260 to 832 nm. They studied data from the 275 to 300 nm range to determine the variation with altitude of the O_2 Herzberg I bands. These recent ISO data have greater signal-to-noise ratios than the data analyzed by Siskind and Sharp [19]. Column densities were determined for $O_2(A)$ as a function of altitude. These results will put much tighter constraints on input parameters to the atmospheric models. An example spectrum from 260 - 300 nm is given in Figure 30 (taken from Reference 6).

Spectral dayglow data was also obtained from the ISO over a broad wavelength range (60 - 840 nm) as a function of altitude. The instrument's field of view was scanned down through the earth limb. Slant path intensities were obtained at different tangent heights. An example of the data obtained is shown in Figure 31 (from Torr et al. [20]) over a portion of the 200 - 300 nm wavelengths of interest here. Torr et al. made comparisons with ISO data at many wavelengths to their thermospheric model for conditions at the time of the ATLAS-I mission. They found generally good agreement between model predictions and these recent voluminous data. They suggest that photochemical processes controlling the thermospheric dayglow are now relatively well understood.

One additional dimension for limb radiance data was obtained from Delta 181 in early 1988 with the imaging data taken from low earth orbit. Ross et al. [21] report on CCD camera limb images of low latitude UV O_2 Herzberg I emission showing substantial structure in the UV nightglow. The limb emission shows patchy, sometimes periodic, spatial variations in amplitude of up to 20%, on a scale of about 15 kilometers in both the horizontal and vertical directions. They attribute the regular structure to gravity wave initiated temperature and
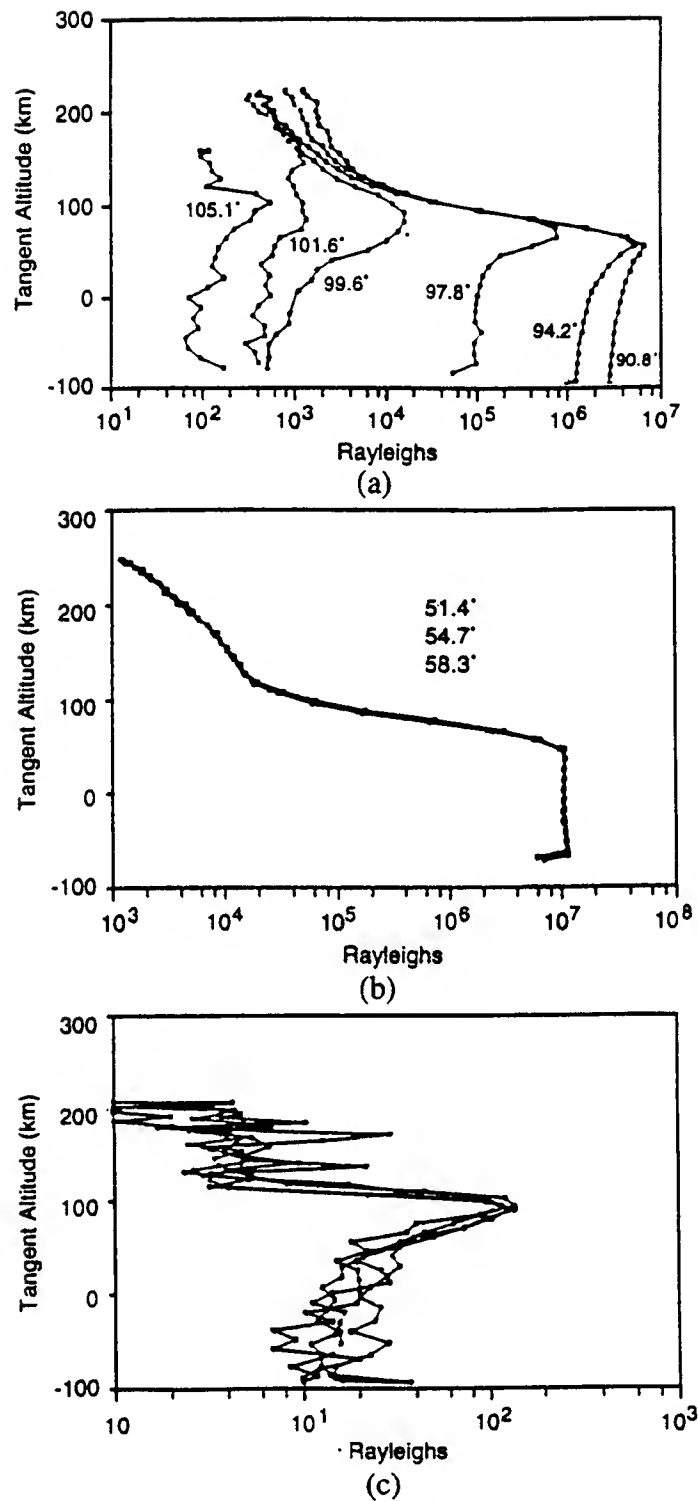
Figure 29.   Limb Altitude Profiles for the 180 to 310 nm Waveband. (a) Dusk limb altitude
profiles at six different solar zenith angles; (b) Noon limb altitude profiles at
three different solar zenith angles; (c) Midnight limb altitude profiles. Most of the
emission originates at wavelengths longer than 250 nm. (Excerpted from Carbury
and Meng [17].)

Table 10. LIMB Observational Summary (Excerpted from Carbury and Meng [17].)

	Tangent Altitude (km)	Intensity (180-310 nm) (R)	Dominant Spectral Features
Dusk Limb	-100	$\sim 2 \times 10^2 - 3 \times 10^6$	Solar Backscatter
	0	$\sim 1 \times 10^2 - 4 \times 10^6$	Solar Backscatter
	100	$5 \times 10^2 - 1 \times 10^6$	NO_γ, O_2 Herzberg I
	200	$< 9 \times 10^1 - 2 \times 10^2$	NO_γ
Dawn Limb	-100	$\sim 1 \times 10^2 - 4 \times 10^5$	Solar Backscatter
	0	$\sim 3 \times 10^2 - 6 \times 10^5$	Solar Backscatter
	100	$< 1 \times 10^2 - 2 \times 10^4$	NO_γ, O_2 Herzberg I
	200	$< 4 \times 10^2$	NO_γ
Noon Limb	-100	$< 1 \times 10^7$	Solar Backscatter
	0	$< 1 \times 10^7$	Solar Backscatter
	100	7×10^4	NO_γ, $NO\delta$, et al.
	200	4×10^3	NO_γ
Midnight Limb	-100	$\sim 1 \times 10^1$	Residual Airglow
	0	1×10^1	Residual Airglow
	100	$\sim 1 \times 10^2$	O_2 Herzberg I
	200	$\sim 4 \times 10^0$	Residual Airglow
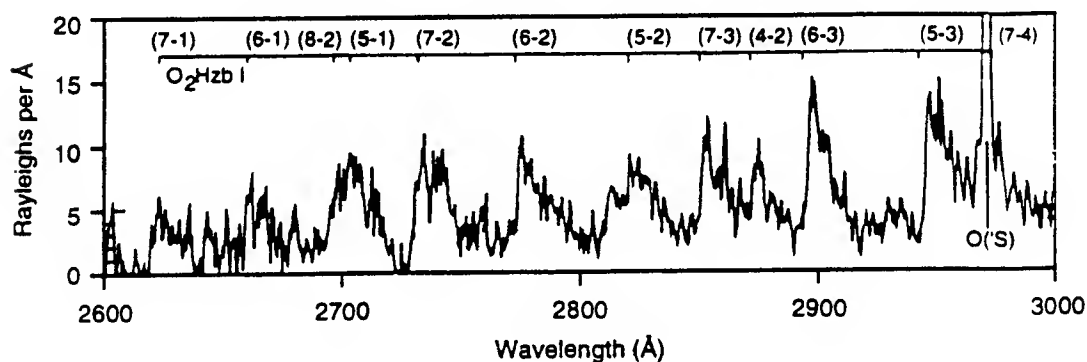
Figure 30. Spectral image of mesospheric nightglow over New Guinea measured by the ISO on ATLAS-1 at $\sim$ GMT 18:05 on day 88, 1992 at an altitude of $\sim$ 80 km. (Note: the structure is not noise.) (Excerpted from Torr et al. [20].)
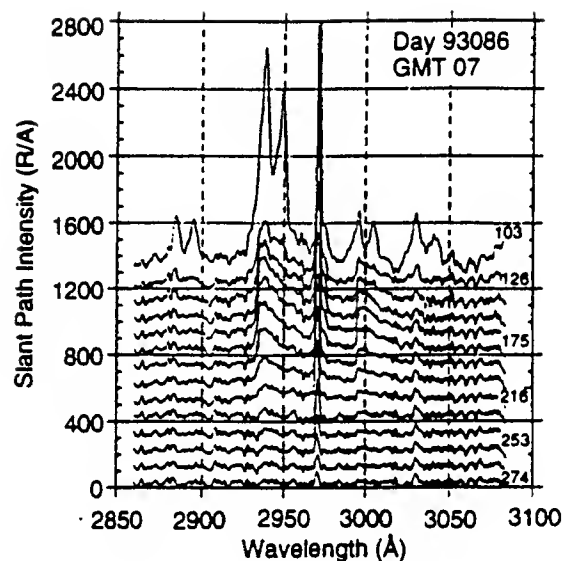
Figure 31.   Example of the spectra obtained at different tangent ray heights in the course of an ATLAS-I roll maneuver. While the absolute scale is the same for each, the various spectra have offsets added in order to display the data. (Excerpted from Torr et al. [20].)

composition oscillations in the limb. (Oscillations in the dynamic 82 - 90 km visible airglow layer have been traced via OH vibrational "Meinel band" emissions in the red. Fluctuations in temperature, and densities of oxygen and hydrogen atoms have been modeled to explain the large-scale wave structure observed.) Although the structure appears to be fully three-dimensional, its existence cannot be confirmed at altitudes very distant from the 95 km altitude where the UV O_2 Herzberg I emission is a maximum brightness. The Imaging Spectrometric Observatory on the ATLAS 1 Mission made limb scans of the O_2 Herzberg and Chamberlain bands over the 275 - 300 nm region. The altitude profiles of these bands were obtained at 2 km resolution between 80 and 110 km with 10 deg latitude resolution. The vibrational distribution remains invariant with altitude, bounding quenching rate coefficients [22]. Looking through the limb one sees an integrated emission over the entire path length so one tends to average over these "structured" emissions. Whether or not this structured nature of the night glow is of any consequence to nighttime remote sensing of missile targets is unknown. Spatial fluctuations in background radiation if large enough may have some effects on the ability of a space-based tracking system to find and track a target plume. At this time, however, they appear to be of minor significance at the low signal levels observed even though they may be scientifically fascinating.

AURORAL IMAGES AND EMISSIONS

Emissions from auroral activity are usually confined to polar regions although occasionally with large bursts of solar activity can be observed at latitudes corresponding to those of the continental United States. Auroral displays are important to remote sensing of missile launches. They also vary enormously in time and space, and are therefore a complicating factor in anticipating background radiation levels at all wavelengths. Auroral

emissions are brighter than night glow and are on the order of dayglow levels. Radiation in the 200 - 300 nm wavelength range are the VK bands of N_2, the N II band at 214.3 nm and N_2 LBH v=8 and 9 bands. Siskind and Barth [23] analyzed spectral data taken during a rocket launch into an auroral arc from Poker Flats, AK in 1983 with a horizontal viewing spectrometer between 90 and 195 km altitude. Figure 32 shows the measured spectra from 195 - 218 nm. The N II band at 214.3 nm is the overwhelming feature but the N_2 LBH bands are of significant brightness of 20 to 40 Rayleighs. Siskind and Barth used these data and 391.4 nm emission as a function of altitude to estimate precipitating electron cross sections and quenching rates for N_2. The peak emission rate at 214.3 nm is around 125 km altitude. The altitude dependence of that emission, of course, depends on the electron flux and the energy distribution of precipitating electrons.
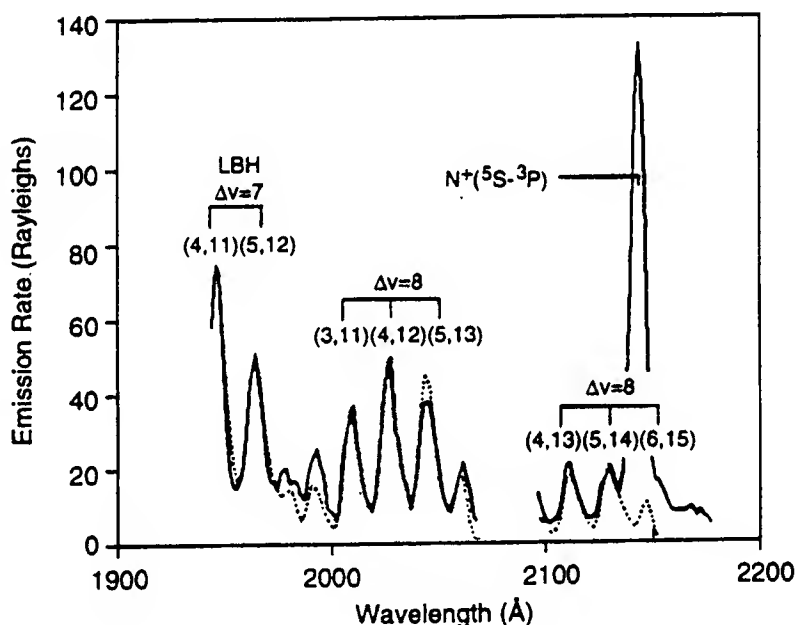
Figure 32.   Comparison of observed spectrum (solid line) and synthetic fit of the LBH bands (dotted line). Three LBH sequences and the NII doublet are identified. The data are a composite of 300 spectra obtained between 140 km and 170 km on the upleg portion of the rocket flight. No data were recorded between 2070 Å and 2095Å. (Excerpted from Huffman et al. [13].)

In a theoretical paper, Daniell and Strickland [24] examine the dependence of auroral middle UV emissions on the incident electron energy distribution and on the neutral atmosphere composition. They calculated emission rates for (1) N_2 VK bands, (2) N_2 2P bands and (3) the OI band at 297.2 nm for various incident electron energy distributions and fluences. Their purpose was to demonstrate the determination of the incident electron spectrum from optical observations. But the uncertainty in the atomic oxygen concentration profile with altitude leaves the determination uncertain. Daniell and Strickland calculate volume emission rates as a function of altitude of these three spectral features and then integrate these over altitude for column emission rates or what would be seen looking down from a satellite. They showed that

essentially all auroral emissions come from above 120 km for average energies. At low electron energies, most of the energy is deposited at high altitudes in the atomic oxygen controlled region. As the incoming electron energies increase, more of the energy is deposited at lower altitudes in N_2. The total emission still depends approximately on the total energy flux but the emitting layer is thinner and at lower altitudes for high energy electrons. This is straightforward if one is looking down, but complex if the line-of-sight is a slant or a limb view.

Ishimoto et al. [25] analyzed 1978 S3-4 satellite measurements of the N_2 LBH band at 192.8 nm and the N_2 VK band at 260.4 nm. Their purpose was to estimate the average energy and total energy flux of electrons by applying the models of Strickland et al. [26] and Daniell and Strickland [24] just discussed. The S3-4 satellite measured emissions of the nightside aurora in both the discrete and diffuse regions under a wide range of auroral activity with nadir viewing UV instruments from an altitude of 270 km. Ishimoto et al. chose the above two bands because they were relatively free from contamination by other emissions. They found that the N_2 LBH band emission was a good indicator of the average energy flux of electrons while the intensity ratio of the N_2 LBH emissions at 193 nm to the N_2 VK emissions at 260 nm was a good measure of the average energy of the electrons.

Auroral emissions vary from quiescent to very active with large changes in the emitted radiation. But it is not just the brightness which changes. Emissions have been observed at latitudes less than 60 deg during large magnetic disturbances so the area covered by the aurora enlarges and moves down to lower latitudes. The levels of emitted radiation rise and the relative levels of emission at various wavelengths changes with increasing solar activity and magnetic disturbances. On top of that, the radiation comes from a broader range of altitudes including much higher altitudes. Ishimoto et al. [27] analyzed UV auroral spectra which they describe as anomalous from the 1978 S3-4 satellite polar orbit observations at 270 km discussed earlier. These particular UV measurements were made during a particularly large magnetic disturbance. They examined the spectral content of these anomalous spectra and compared the low latitude auroral spectra with that from the more typical high latitude spectra. Typical diffuse auroral emissions are caused mostly by in-coming electrons with an energy spectrum of a Maxwellian type of distribution and an average energy of 3 keV. Peak emission levels are found at 110 - 120 km altitude [24]. In the midnight region most of this emission is caused by electrons with proton precipitation a minor contributor. The observed emission from the higher latitudes showed their usual characteristics. The anomalous spectra came from the low latitude regions (on the equator side of the diffuse auroral region). There the spectra were much higher in atomic emissions relative to molecular, and the N_2 molecular bands showed high vibrational and rotational temperatures. Ishimoto et al. suggested that the high altitude emission can be attributed to keV ion/neutral oxygen precipitation and collisions with N_2, rather than the more commonly observed proton initiated auroral emissions.

Being able to understand and model these emissions is of more than scientific interest. Prediction of auroral emissions are part of quantifying the background or clutter which may limit the capabilities of a future space-born platform to detect and track missile plumes. Auroral emissions are very variable in space, time and intensity and will be a significant challenge to characterize in near real-time for remote sensing.

BACKGROUNDS AND TARGET SENSING

Knowledge of the radiance sources of the ionosphere must be converted to forms which are useable to model, measure, or construct backgrounds against which missile plumes must be discriminated and tracked. The spectrometer, photometer and imaging data cannot be obtained in real time over just the right path lengths, angles, fields-of-view, and altitudes. Our understanding must be represented by models updated by frequent observations and then the backgrounds predicted or extrapolated forward in time in order to assist a surveillance satellite in identifying and tracking targets. The background radiance and all of its spatial and temporal variations must be available in a timely manner at some appropriate level of detail. This constantly varying signal is frequently called clutter or noise, from which the missile plume must be isolated.

Malkmus et al. [28] recently gave a review of models and measurements of the daytime limb radiance in the ultraviolet and visible regions, and calculated the background "clutter" for looking through the earth limb. The effects of molecular band emissions, atomic line emissions, fluorescence and Rayleigh scattering were included, as well as the importance of sun position, atmospheric composition and solar activity. The transmission through the limb as a function of tangent height was determined. A background clutter model was constructed by integrating over lines-of-sight in three wavelength regions: 200 to 300 nm, 300 to 400 nm and the 400 to 700 nm visible region during daytime conditions. An example of one of the steps in their calculations is shown in Figure 33, where the transmissivity of a line-of-sight from a target at various altitudes in the earth's limb out to space is plotted for several wavelengths and wavebands.

Using an average ozone concentration profile as a function of altitude for noontime conditions, and the computer code APART, the mean limb radiance as a function of altitude was calculated as given in Figure 34. A model for the high-altitude atmospheric radiance power spectral distribution was based on multiple sources of data on the scale size of atmospheric radiance emissions as a function of altitude as in Figure 35.

The expected variance in the UV clutter is determined from measured variations in the atomic oxygen profile, and the assumption that the radiance viewed by the observing platform is the sum along a line-of-sight of many statistically independent regions of the atmosphere. Malkmus et al. reduced this to a signal-to-noise ratio as a function of tangent height. Figure 36 shows an example calculation for the 200 - 300 nm waveband. Solid line (a) is the SNR for the estimated clutter, while the dashed lines above or below are for the clutter varying by $\pm 50\%$. Curve (b) is for the clutter set to zero. A corresponding calculation for the visible waveband shows that at tangent altitudes below about 80 km the 200 to 300 nm UV band offers higher signal-to-noise ratios than the visible band.

Although the clutter model just discussed, which is based on atmospheric composition variability, is preliminary, it is a good example of the kinds of calculations that will be required to make the current wealth of atmospheric/ionospheric emission data useful for target sensing, and to model and design the target sensing systems that will make target sensing a reality.
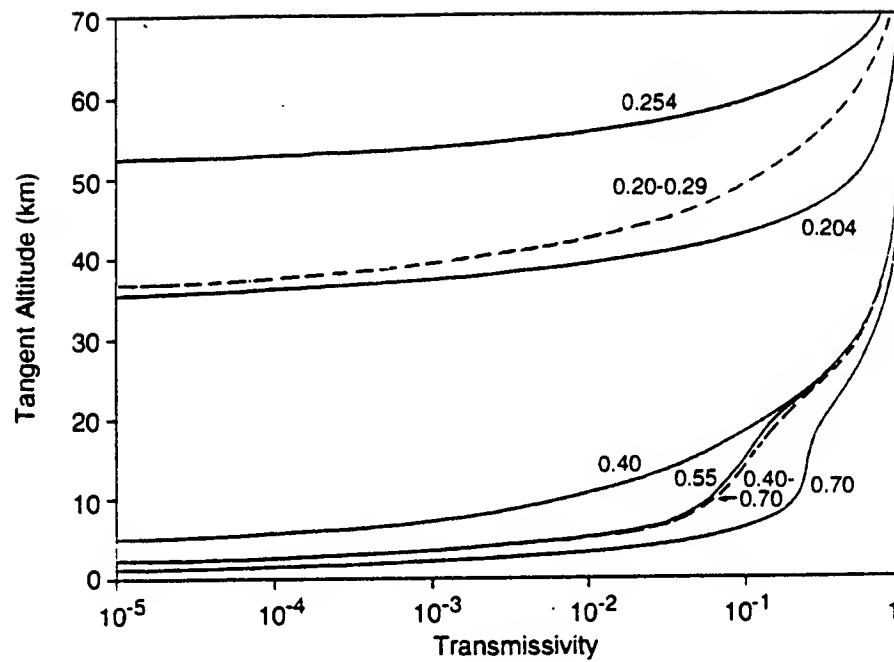
Figure 33.   Transmissivities from Space to Given Target Altitude at UV and Visible
            Wavelengths, and Averages over 0.20 to 0.29 and 0.40 to 0.70 μm Bandpasses.
            (Excerpted from Malkmas et al. [28].)
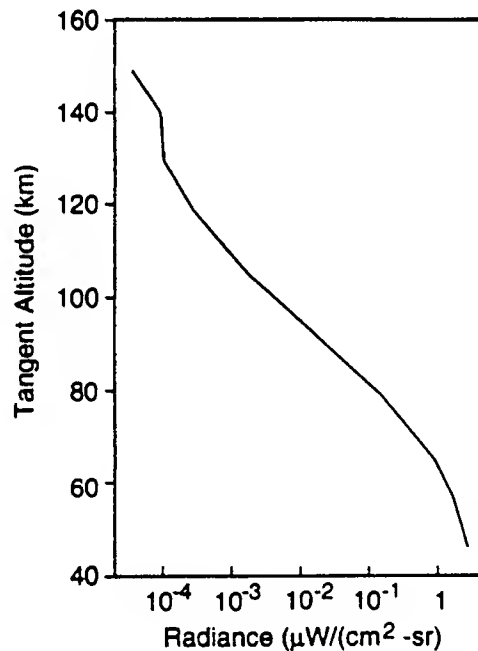
Figure 34.   Limb Radiance in the 2000 to 3000Å Band for Solar Zenith Angle of 30 deg and
            an Exospheric Temperature of 1000 K. (Excerpted from Malkmus et al. [28].)

93
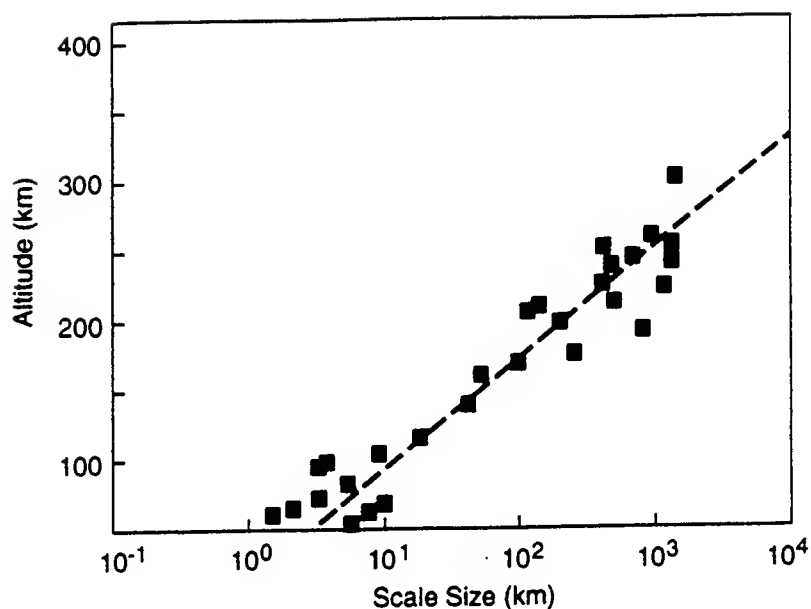
Figure 35.   The Altitude Distributions of the Measured Scale Sizes Adapted from Figure 18
(p. 101) of Humphrey et al. [39]
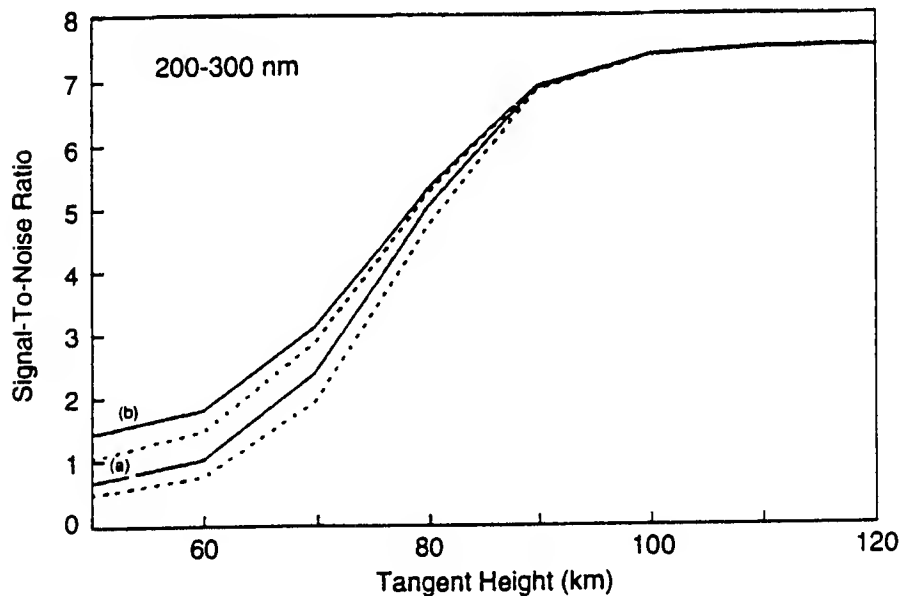
Figure 36.   Signal-to-Noise Ratio Calculation for an Object Viewed Against the Earthlimb in
the 2000 to 3000Å Band. Curve (a) is calculated from the estimated clutter. The
dashed lines represent the effect of varying the clutter estimate by ±50%. In
curve (b) the clutter has been set to zero.

94

Clutter can also be created by other atmospheric features such as polar mesospheric clouds (PMCs). These high altitude (~ 80 km) clouds will scatter solar radiation above the ozone attenuation layer. PMCs have optical thicknesses in the 10^{-4} or greater range. Reflected sunlight from a PMC could thus have significant upwelling radiances and significant spatial structure clutter. In a rocket-based mission, the UV Imaging Polarimeter detected the polarization of scattered sunlight at three angles from PMCs, at 265 nm, and determined the mean particle radius to be less than 40 nm [30]. Future missions will determine the radiances, seasonal occurrences, variabilities, and structure of PMCs.

The VUE System was an early SDIO UV bandpass radiometric payload mounted on an operational satellite. Multiple filters were used to view space, hard earth and targets. The nominal 200 to 300 nm filter provided much useful information, including earthlimb radiance profiles. Detectable signals up to 125 km were observed. Once corrected for dark counts, these compared favorably with the rate of radiance decrease with altitude predicted by a UV earthlimb model as shown in Figure 37 [31].
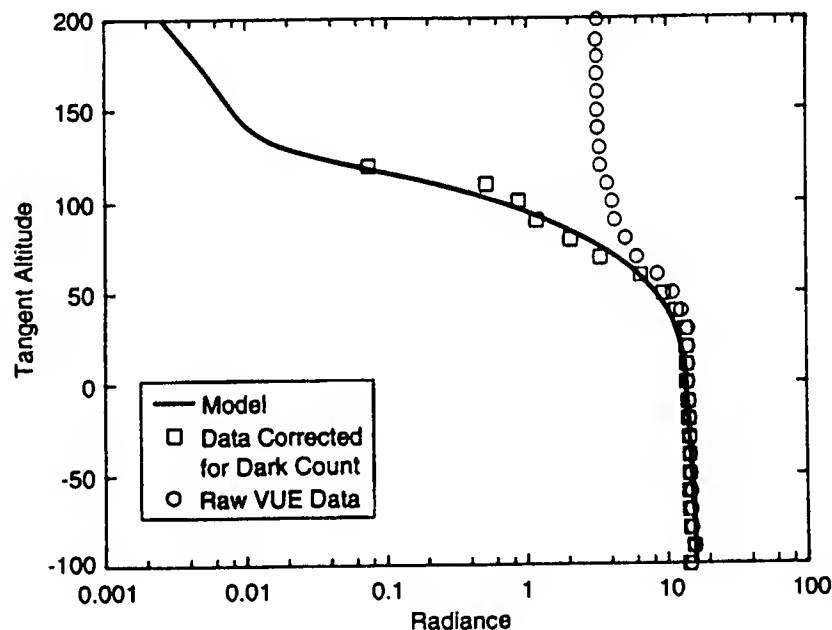
Figure 37.   Comparison of Normalized VUE Radiance Data with Atmospheric Model (Excerpted from Pritt [31].)

A recent paper by Smathers et al. [5] summarizes the capabilities of the Low-Power Atmospheric Compensation Experiment (LACE) satellite and the onboard Ultraviolet Plume Instrument (UVPI). This satellite was built by the Naval Research Laboratory for SDIO. Since its launch in 1990, the UVPI instrument has obtained high spatial resolution near UV/visible images of rocket plumes, and has been used to view aurora, the earth's limb, and other earth background phenomena. The UVPI has two CCD cameras co-aligned which share the same telescope. The tracker and plume camera specifications are given in Table 11 from Smathers et al. [5]. The dynamic range and sensitivity of the UVPI plume and tracker cameras were

Table 11. UVPI Instrument Characteristics (Excerpted from Smathers et al. [5].)

Parameter	Plume Camera	Tracker Camera
Telescope aperture	10 cm	10 cm
Telescope focal length	605 cm	60.5 cm
Spectral region	195 to 350 nm	255 to 450 nm
Available filters	4	1
Frame rate, normal	5 per sec	5 per sec
Pixels, normal	251 x 240	251 x 240
Frame rate, zoom*	30 per sec	30 per sec
Pixels, zoom*	91 x 112	91 x 112
Digitization	8 bits/pixel	8 bits/pixel
Image data rate	2.5 MB/s	2.5 MB/s
Field of view	0.18 x 0.137 deg	2.60 x 1.98 deg
Field of regard	100 x 97 deg	100 x 97 deg
Pixel field of view	12.8 x 10.0 μR	181 x 144 μR
System resolution	80 to 100 μR	220 to 250 μR
Pixel exposure time	33 ms	$\leq$ 33 ms (adj.)
*Reduced FOV		

designed for nighttime operation. The instrument is calibrated on orbit periodically by actively tracking stars with known spectra and magnitude. The LACE/UVPI cameras could be regarded as a prototype target acquisition and tracking device. However, it is really more experimental in that it is designed to evaluate various bandpasses in the UV to collect rocket plume imagery and the required complementary base-line data on earth backgrounds and limb. The five different filters for UV observations shown in Figure 38 give several different wavebands within or including the 200 - 300 nm range.

Some example earth limb night glow observations from the UVPI tracker camera over the broadest UV band (Filter TC covering almost all of the nightglow) are given in Figure 39. Altitude profiles of the nightglow radiance are shown for two different orbits. These data were taken at the same latitude, longitude, and local time, but only one day apart. The peak radiances vary by over 50% within a 24-hr period giving a good example of the changes in nightglow that will occur. Several UVPI radiance levels of nightglow are compared with other data in Table 12 from Smathers et al. [5]. The bandpasses are different for each data source so detailed comparisons are somewhat laborious to perform.

96
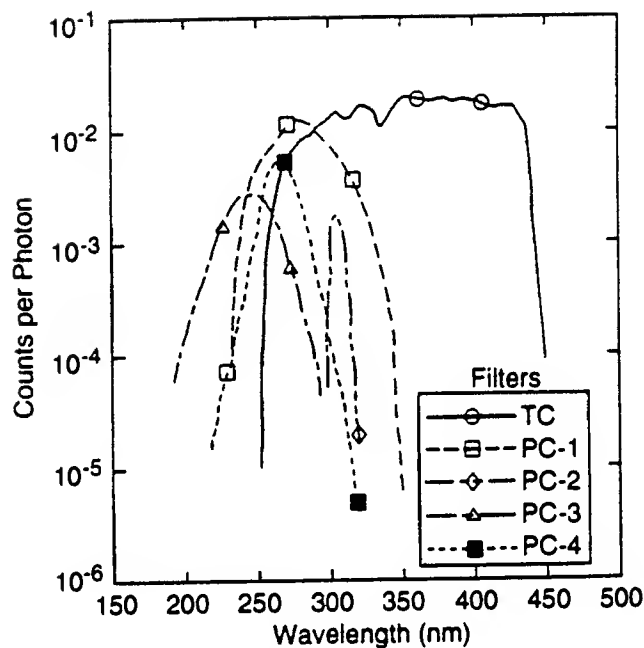
Figure 38.   Net Quantum Efficiency for the Tracker and Plume Cameras   (Excerpted from Smathers et al. [5].)

Samples of auroral observations by UVPI are shown in Figure 40 where two vertical profiles were obtained from different locations within the same image of a southern nighttime aurora on August 3, 1990. An auroral model was used to fit the profiles, permitting the number of auroral forms in the observed region, their locations, thickness and assumed precipitation electron spectra to vary. The model calculates altitude profiles of volume emissions from a user specified electron spectrum. Figure 41 is a reminder of the anticipated altitude of auroral emissions for different electron energies. Sorting out the origin of emissions from aurorae can be quite complex because the camera may be viewing multiple auroral forms at different locations. Good fits to these data were obtained by assuming that there were two auroral forms, a discrete auroral arc at the tangent point and a diffuse aurora between the tangent point and the spacecraft.

Each UVPI observation such as those listed in Table 13 provides a data set of several thousand images. Only a small amount of the data has been analyzed. The data are archived at the Naval Research Laboratory. Much more could be done with the data to develop a quantitative understanding of the complex task of finding and tracking a missile plume in the midst of all of these varying natural emissions.

97
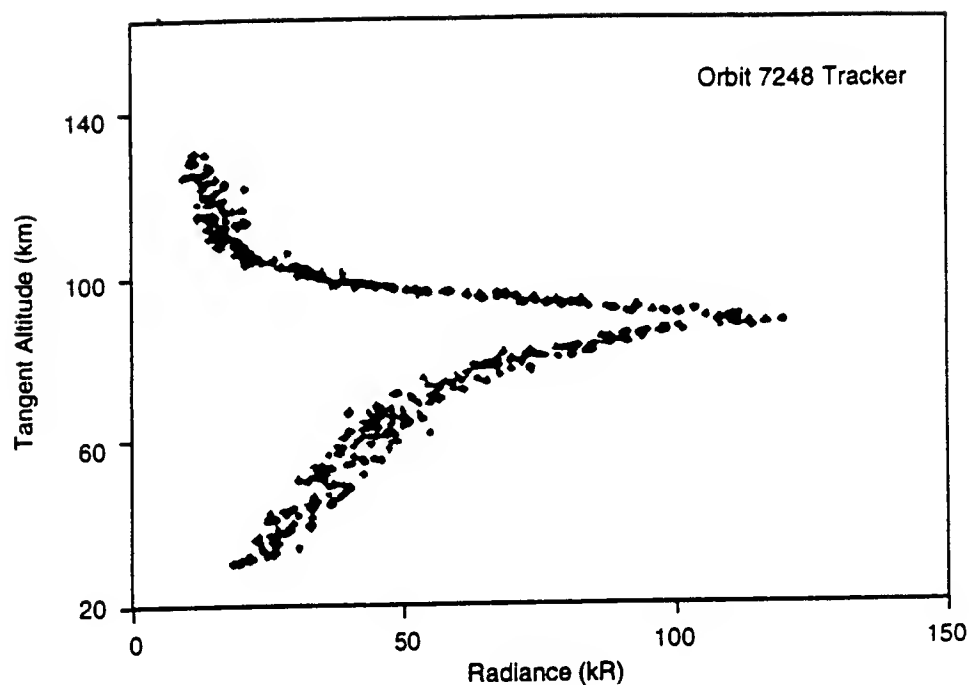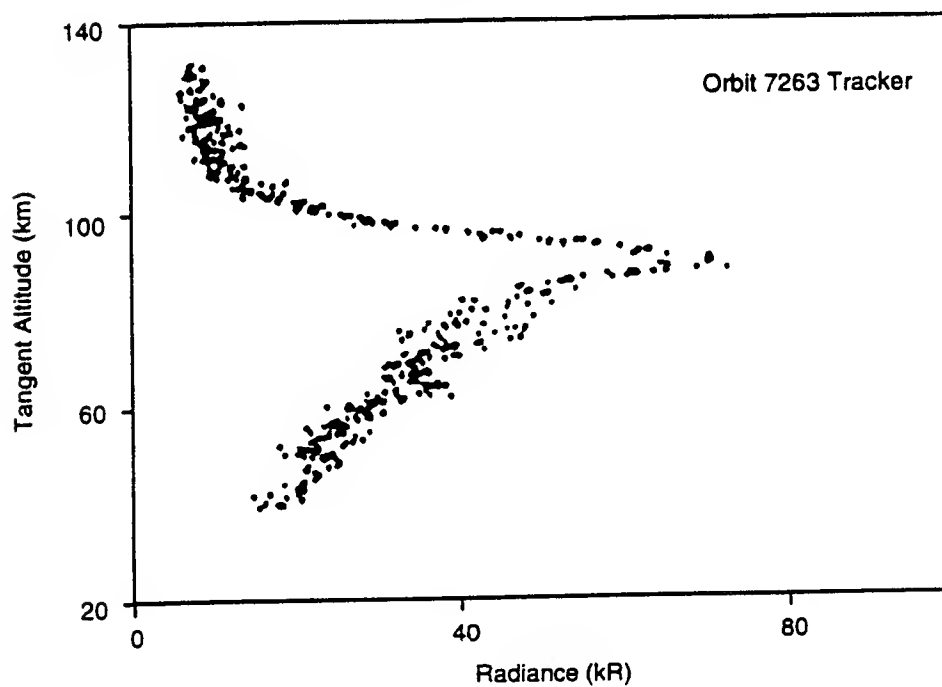
Figure 39.   UVPI Earthlimb Nightglow Data.   (a) Limb profile for orbit 7248, filter TC;
(b) Limb profile for orbit 7263, filter TC.   (Excerpted from Smathers et al.
[5].)

Table 12. Measurements of Nightglow Intensities (Excerpted from Smathers et al. [5].)

Source	Passband (nm)	Radiance (KR)
UVPI Tracker Camera, Orbit 2089	255-450	23-29[c]
UVPI Tracker Camera, Orbit 7248	255-450	100-120[c]
UVPI Tracker Camera, Orbit 7263	255-450	60-70[c]
UVPI Filter PC-4, Orbit 7248	235-350	65-75[c]
UVPI Filter PC-1, Orbit 7248	220-320	50-60[c]
Gerard, 1975	240-310	3.5-15[a]
Torr et al., 1985	312-320	29[a]
Sharp and Siskind, 1989	267-304	70[a]
Swenson et al., 1989	279-281	4.2[a]
Swenson et al., 1989	296-299	7.1[d]
Swenson et al., 1989	345-495	14[a]
[a]total Herzberg I [c]total Herzberg I + II & Chamberlain [d]total Herzberg I (50%) + $O(^1S)$(50%)		

VEHICLE INDUCED EMISSIONS AND CONTAMINATION

A brief review of both these effects is included as they affect the ability of the sensor to perform its designed mission to detect remotely upwelling earth radiance backgrounds.

The S3-4 platform was in an elliptical orbit and observed the hard earth with a nadir viewing UV spectrometer [32]. At altitudes near perigee an excess radiance from N_2 (a-X) LBH transitions was observed. These features scaled with atmospheric density cubed [33]. Although the exact mechanism has not been determined, it likely involves a stepwise dissociation, recombination and excitation of atmospheric nitrogen as it interacts at high relative velocities on and above spacecraft surfaces.
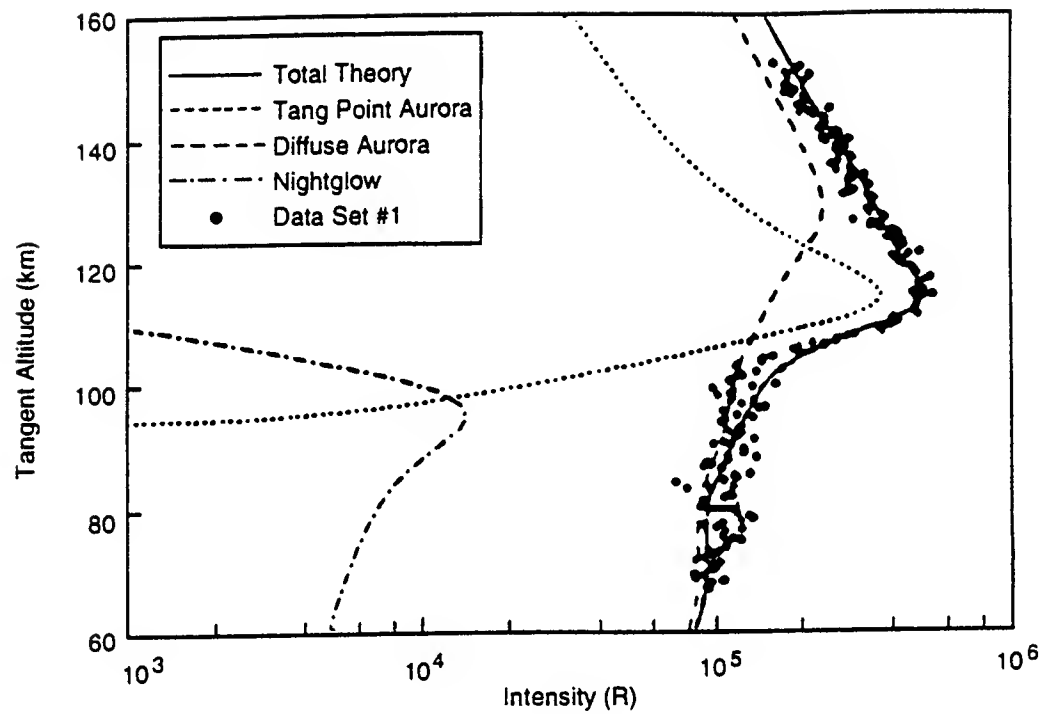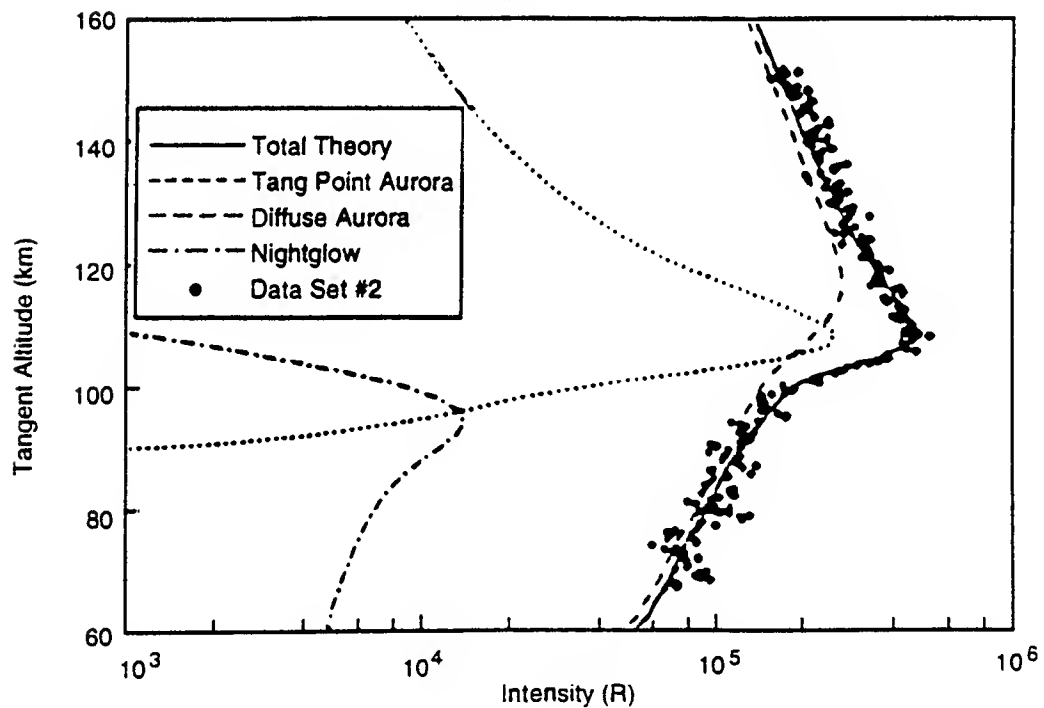
Figure 40. Vertical Emission Profiles from an Auroral Image. (a) Auroral profile #1 for orbit 2570, filter TC; (b) Auroral profile #2 for orbit 2570, filter TC. (Excerpted from Smathers et al. [5].)
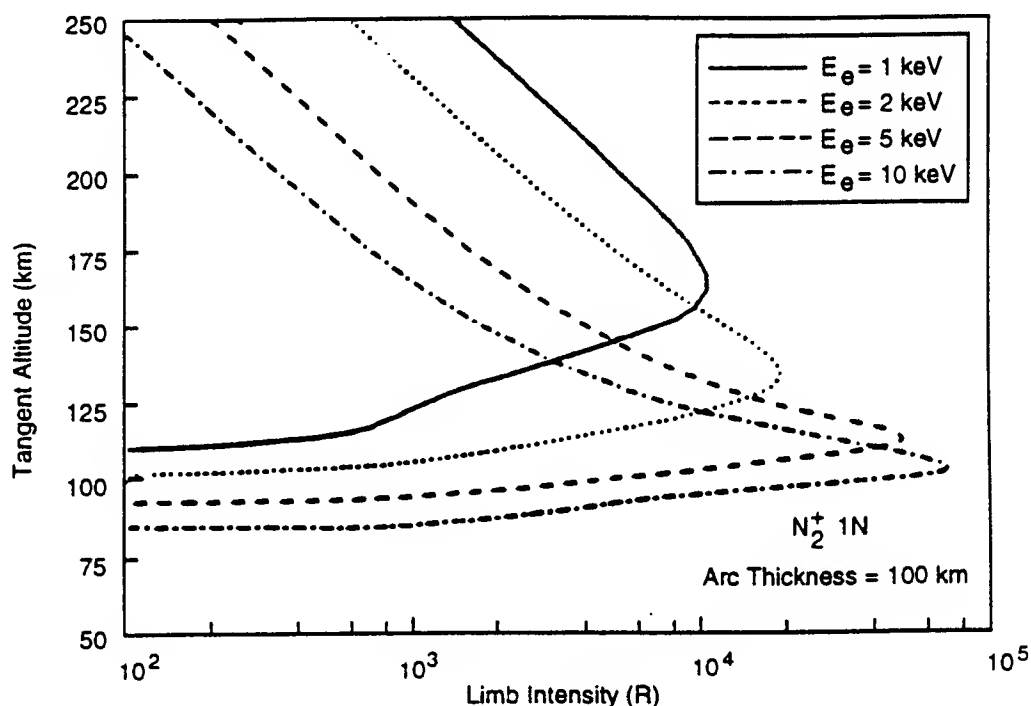
Figure 41.   Electron Energies for Various Altitude Aurora (Excerpted from Smathers et al. [5].)

Table 13. Summary of UVPI Observations

Type Observation	Number
1. Rocket Plume Obser. & Rehearsals	52
2. Beacon Tracking Tests	29
3. Star Calibration Observations	49
4. Night Limb Background Observations	46
5. Night Nadir Background Observations	21
6. Day Limb Background Observations	5
7. Day Nadir Background Observations	33
Total	235

The possibility of enhanced UV signatures due to the several km/s interaction of the atmosphere led to the UV Bow Shock missions. Although a primary goal of these missions is to address target signatures, they also observed enhanced near-field background radiances that arise from the interaction of the spacecraft with the tenuous upper atmosphere at ever increasing relative velocities. The Bow Shock experiments were performed at velocities of 3.5 and 5.1 km/s. Prominent interaction-induced signatures were observed. NO (A-X) transitions were the dominant MUV emission formed in the shock-excited air. OH (A-X) transitions and even N_2^+(B-X) emission at 391.4 nm were also observed in the interaction shock at altitudes approaching 100 km [34].

101

Spacecraft contamination can decrease system performance either by absorption of the far-field radiance or by creating scatter. The results from the VUE mission appear to have been compromised by contamination. Inspection on the ground revealed significant particulate contamination on the mirror. Although the mirror was cleaned, the rest of the telescope was not. The data from on-orbit indicated severe scattering problems. Apparently the particles remaining in the sensor were redistributed onto the mirror during the launch [35]. Thus the ability to launch clean UV sensors repetitively must be demonstrated in the future.

CHAPTER 6 REFERENCES

1   Huffman, R.E., "The New Ultraviolet: Global Space Weather Systems," in *Ultraviolet Technology IV*, ed. R.E. Huffman, SPIE Proceedings Vol. 1764, 20-21 July 1992, 152-160.

2   Link, R., Strickland, D.J., and Daniell, R.E., Jr., "AURIC Airglow Modules: Phase I Development and Application," in *Ultraviolet Technology IV*, ed. R.E. Huffman, SPIE Proceedings. Vol. 1764, 20-21 July 1992, pp. 132-150.

3   Huffman, R.E., "The Atmospheric Ultraviolet Radiance Integrated Code (AURIC): Validation of Version 1.0," in IRIS Proceedings, Targets, Backgrounds, and Discrimination, 1993, Vol. I, pp. 123-135.

4   Broadfoot, A.L., Sandel, B.R., Knecht, D., Viereck, R., and Murad, E., "A Panchromatic Spectrograph with Supporting Monochromatic Imagers," in *Ultraviolet Technology IV*, ed. R.E. Huffman, SPIE Proceedings Vol. 1764, 20-21 July 1992, pp. 2-11.

5   Smathers, H.W., Horan, D.M., Singh, M., Cardon, J.G., Bakeris, D.F., and Swanson, R.A., "Satellite Observations with the UVPI Instrument," in *Ultraviolet Technology IV*, ed. R.E. Huffman, SPIE Proceedings Vol. 1764, 20-21 July 1992, pp. 36-47.

6   Owens, J.K., Torr, D.G., Torr, M.R., Chang, T., Fennelly, J.A., Richards, P.G., Morgan, M.F., Baldridge, T.W., Fellows, C.W., Dougani, H., Swift, W., Tejada, A., Orme, T., Germany, G.A., and Yung, S., "Mesospheric Nightglow Spectral Survey Taken by the ISO Spectral Imager on Atlas I," *Geophys. Res. Ltrs.*, **20**, 515-518, 1993.

7   Carbary, J., at the UV/VIS Special Topic Meeting, Crystal City VA, 10 Sept. 1991, sponsored by SDIO.

8   Meng, C-I, Huffman, R.E., Strivanek, R.A., Strickland, D.J., and Daniell, R.E., Jr. "Remote Sensing of Ionosphere by Using Ultraviolet and Visible Emissions," in *Ultraviolet Technology*, ed. R.E. Huffman, SPIE Proceedings Vol. 687, 1986, pp. 62-72.

9   Anderson, D., at the UV/VIS Special Topic Meeting, Crystal City VA, 10 Sept. 1991, sponsored by SDIO.

10   Sharp, W.E. and Siskind, D.E., "Atomic Emission in the Ultraviolet Nightglow," *Geophys. Res., Ltrs.*, **16**, 1453-1456, 1989.

11   Eparvier, F.G. and Barth, C.A., "Self Absorption Theory Applied to Rocket Measurements of the Nitric Oxide (1,0)γ Band in the Daytime Thermosphere," *J. Geophys. Res.*, **97**, 13,723-13,731, 1992.

12   Mc Coy, R.P., Carruthers, G.R., Dorner, M.A., and Michael, A.L., "Ultraviolet Imagery of the NO Delta Band Nightglow Observed During the AFP-675 Mission on STS-39," *EOS Trans.* **74**(43), 474 SA51B-3 (1993).

13   Huffman, R.E., Hall, L.A., and LeBlanc, F.J., in *Ultraviolet Technology III*, ed. R.E. Huffman, SPIE Proceedings Vol. 1158, 10-11 August 1989, San Diego, CA, pp. 38-44.

14   Trakhovsky, E., Ben-Shalom, A., and Devir, A.D., "Measurements of Tropospheric Attenuation in the Solar Blind UV Spectral Region and Comparison with the LOWTRAN-7 Code," in *Ultraviolet Technology III*, ed. R.E. Huffman, SPIE Proceedings Vol. 1158, 10-11 August 1989, San Diego, CA, pp. 357-365.

15   Eastes, R.W., Huffman, R.E., and LeBlanc, F.J., "NO and O_2 Ultraviolet Nightglow and Spacecraft Glow from the S3-4 Satellite," *Planet. Spa. Sci*, **40**, 481-493, 1992.

16   Strickland, D.J., Barnes, R.P., Cox, R.J., Anderson, D.E., Jr., Carbary, J.F., and Meng, C.-I., "Analysis of UV Limb Data from Low Earth Orbit," in *Ultraviolet Technology III*, ed. R.E. Huffman, SPIE Proceedings Vol. 1158, 10-11 August 1989, pp. 59-68.

17   Carbary, J.F. and Meng, C.-I., "Limb Profiles from Low Earth Orbit," in *Ultraviolet Technology III*, ed. R.E. Huffman, SPIE Proceedings Vol. 1158, 10-11 August 1989, pp. 51-58.

18   Anderson, D.E., Jr., Strickland, D.J., Evans, J.S., Paxton, L.J., Carbary, J.F., and Meng, C.-I., "A Study of Earth Limb Optical Backgrounds and Remote Sensing Techniques Using Middle UV Data from a Low-Altitude DoD Satellite Experiment," in IRIS Proceedings, Targets, Backgrounds, and Discrimination, 1992, Vol. I, pp. 131-150.

19   Siskind, D.E. and Sharp, W.E., "A Vibrational Analysis of the $O_2A^3\Sigma_u^+$ Herzberg I System Using Rocket Data," *Planetary Space Sci.*, **38**, 1399-1408, 1990.

20   Torr, D.G., Torr, M.R., and Richards, P.G., "Thermospheric Airglow Emissions: A Comparison of Measurements from ATLAS-1 and Theory," *Geophys. Res. Ltrs.*, **20**, 519-522, 1993.

21   Ross, M.N., Christensen, A.B., Meng, C-I, and Carbary, J.F., "Structure in the UV Nightglow Observed From Low Earth Orbit," *Geophys. Res. Ltrs.*, **19**, 985-988, 1992.

22   Torr, D.G., Torr, M.R., Owens, J.K., and Chang, T., "Analysis of Mesospheric O_2 Herzberg Emissions Observed by the Imaging Spectrometric Observatory on ATLAS 1 Mission," *EOS Trans.* **74**(16), 219, SA11A-12 (1993).

23   Siskind, D.E. and Barth, C.A., "Rocket Observation of the NII 2143 A Emission in an Aurora," *Geophys. Res. Ltrs.*, **14**, 479-482, 1987.

24   Daniell, R.E., Jr. and Strickland, D.J., "Dependence of Auroral Middle UV Emissions on the Incident Electron Spectrum and Neutral Atmosphere," *J. Geophys. Res.*, **91**, 321-327, 1986.

25   Ishimoto, M., Meng, C-I, Romick, G.J., and Huffman, R.E., "Auroral Electron Energy and Flux from Molecular Nitrogen Ultraviolet Emissions Observed by the S3-4 Satellite," *J. Geophys. Res.*, **93**, 9854-9866, 1988.

26   Strickland, D.J., Jasperse, J.R., and Whalen, J.A., "Dependence of Auroral FUV Emissions on the Incident Electron Spectrum and Neutral Atmosphere," *J. Geophys. Res.* **88**, 8051-8062, 1983.

27   Ishimoto, M., Meng, C-I, Romick, G.R., and Huffman, R.E., "Anomalous UV Auroral Spectra During a Large Magnetic Disturbance," *J. Geophys. Res.*, **94**, 6955-6960, 1989.

28   Malkmus, W., Filice, J.P., and Ludwig, C.B., "Earthlimb Radiances, Transmissivities, and Clutter," in *Ultraviolet Technology III*, ed. R.E. Huffman, SPIE Proceedings Vol. 1158, 10-11 August 1989, San Diego, CA, pp. 69-83.

29   Humphrey, C.H., et al., "Atmospheric Infrared Radiance Variability," AFGL-TR-81-0207, 1981, ADA109928.

30   Thomas, G.E., Kohnert, R., Lawrence, G.M., and Westfall, J., "Observations of Polar Mesospheric Clouds with an Ultraviolet Imaging Polarimeter," *EOS Trares* **74**(43), 459, SA22B-1 (1993).

31   Pritt, A.T., "VUE Review," at Joint PSAG Meeting, ANSER Arlington VA, 9 July 1991.

32   Huffman, R.E., Leblanc, F.J., Larrabee, J.C., and Paulsen, D.E., "Satellite Vacuum Ultraviolet Airglow and Auroral Observations," *J. Geophys. Res.*, **85**, 2201 (1980).

33   Conway, R.R., Meier, R.R., Stroebel, D.F., and Huffman, R.E., "The Far Ultraviolet Glow of the S3-4 Satellite," *Geophys. Res. Lett.*, **14**, 628, (1987).

34   Caveny, L. and Mann, D., "Shock-Layer Induced UV Emissions Measured by Rocket Payloads," SPIE Aerospace Sensing Conf. Proc. Paper 1479-11 [Apr. 1991].

35   Betts, T. and Friedman, R., "Non-Rejected Earth Radiance Performance of the VUE Sensor," SPIE Aerospace Sensing Conf. Proc. Paper 1479-14 [Apr.1991].

Bowers, C.W., Feldman, P.D., Tennyson, P.D., and Kane, M., "Observation of the OI Ultraviolet Intercombination Emissions in the Terrestrial Dayglow," *J. Geophys. Res.* **92**, 239-245, 1987.

Chiu, Y.T., Robinson, R.M., Collin, H.L., Chakrabarti, S., and Gladstone, G.R., "Magnetospheric and Exospheric Imaging in the Extreme Ultraviolet," *Geophys. Res. Ltrs.* **17**, 267-270, 1990.

Conway, R.R., Anderson, D.E. Jr., Budzien, S.A., and Feldman, P.D., "Ultraviolet Limb Imaging Experiment," in *Ultraviolet Technology III*, ed. R.E. Huffman, SPIE Proceedings Vol. 1158, 10-11 August 1989, pp. 2-15.

Cox, R.J., Strickland, D.J., Barnes, R.P., and Anderson, D.E. Jr., "A Model for Generating UV Images at Satellite Altitudes," in *Ultraviolet Technology IV*, ed. R.E. Huffman, SPIE Proceedings Vol. 1764, 20-21 July 1992, pp. 177-189.

Eastes, R.W. and Feldman, P.D., "The Ultraviolet Dayglow at Solar Maximum: 1. Far UV Spectroscopy at 3.5Å Resolution," *J. Geophys. Res.* **90**, 6594-6600, 1985.

Feldman, P.D., Davison, A.F., Blair, W.P., Bowers, C.W., Durrance, S.T., Kriss, G.A., Ferguson, H.C., Kimble, R.A., and Long, K.S., "The Spectrum of the Tropical Oxygen Nightglow Observed at 3Å Resolution with the Hopkins Ultraviolet Telescope," *Geophys. Res. Ltrs.* **19**, 453-456, 1992.

Frank, L.A., Sigwarth, J.B., and Craven, J.D., "Search for Atmospheric Holes wit the Viking Cameras," *Geophys. Res. Ltrs.* **16**, 1457-1460, 1989.

Gladstone, G.R., "UV Resonance Line Dayglow Emissions on Earth and Jupiter," *J. Geophys. Res.* **93**, 14,623-14,630, 1988.

Huguenin, R., Wohlers, M., Weinberg, M., Huffman, R., Eastes, R., and Delgreco, F., "Spatial Characteristics of Airglow and Solar Scatter Radiance from the Earth's Atmosphere," in *Ultraviolet Technology III*, ed. R.E. Huffman, SPIE Proceedings Vol. 1158, 10-11 August 1989, pp. 16-27.

Ishimoto, M., Meng, C.-I., Romick, G.R., and Huffman, R.E., "Doppler Shift of Auroral Lyman α Observed from a Satellite," *Geophys. Res. Ltrs.* **16**, 143-146, 1989.

Link, R., Gladstone, G.R., Chakrabarti, S., and McConnell, J.C., "A Reanalysis of Rocket Measurements of the Ultraviolet Dayglow," *J. Geophys. Res.* **93**, 14,631-14,648, 1988.

Meier, R.R., Conway, R.R., Anderson, D.E. Jr., Feldman, P.D., Eastes, R.W., Gentieu, E.P., and Christensen, A.B., "The Ultraviolet Dayglow at Solar Maximum: 3. Photoelectron-Excited Emissions of N_2 and O," *J. Geophys. Res.* **90**, 6608-6616, 1985.

Meng, C.-I. and Huffman, R.E., "Ultraviolet Imaging from Space of the Aurora Under Full Sunlight," *Geophys. Res. Ltrs.* **11**, 315-318, 1984.

Newell, P.T., Meng, C.-I., and Huffman, R.E., "Determining the Source Region of Auroral Emissions in the Pre-noon Oval Using Coordinated Polar BEAR UV-Imaging and DMSP Particle Measurements, *J. Geophys. Res.* **97**, 12,245-12,252, 1992.

Oznovich, I., McEwen, D.J., and Eastes, R.W., "Stereoscopic Auroral Intensity Measurements from Ground and Space," *Geophys. Res. Ltrs.* **20**, 1995-1998, 1993.

Robinson, R., Dabbs, T., Vickery, J., Eastes, R., DelGreco, F., Huffman, R.E., Meng, C.-I., Daniell, R., Strickland, D., and Vondrak, R., "Coordinated Measurements Made by the Sondrestrom Radar and the Polar Bear Ultraviolet Imager," *J. Geophys. Res.* **97**, 2863-2871, 1992.

Strickland, D.J., Jasperse, J.R., and Whalen, J.A., "Dependence of Auroral FUV Emissions on the Incident Electron Spectrum and Neutral Atmosphere," *J. Geophys. Res.* **88**, 8051-8062, 1983.

Strobel, D.F., Meier, R.R., Summers, M.E., and Strickland, D.J., "Nitrogen Airglow Sources: Comparison of Triton, Titan, and Earth," *Geophys. Res. Ltrs.* **18**, 689-692, 1991.

Wilson, G.R., "Inner Magnetospheric Imager (IMI) Instrument Heritage," NASA Contractor Report 4498, 1993.

CHAPTER 7. SUMMARY AND FUTURE DIRECTIONS

The BMDO has played an effective role in advancing the capabilities of on-orbit UV sensing by sponsoring the development of advanced sensor arrays, and by rapidly demonstrating these sensors' capabilities on-orbit. The altitude profiles, variabilities and minor emitters are much better characterized today than they were a decade ago. Moreover, the BMDO has developed the broad Strategic Scene Generation Model (SSGM) to couple effectively this enhanced understanding into its effects on a wide range of strategic scenarios. This will permit sensors' and systems' performance to be simulated and tested against a variety of stressing scenes [1]. The lessons learned from the observations during the missions discussed above are being used to validate the backgrounds codes in the Strategic Scene Generation Model. This model can then be exercised to define operational regimes where better information is required, thus focussing future measurements programs. Atmospheric radiance predictions from the lower atmosphere are created using the GENESIS and CLOUDSIM modules. These have been complemented by a UV extended version of MODTRAN complete with improved absorption, solar radiance models, and atmospheric layering. The AURIC high altitude UV Radiance model is also nearing completion and will be included into the SSGM.

The most important unfilled data base is the accurate determination of the clutter structure for below the horizon (BTH) viewing geometries in MUV at scales required for hard body track and location pinpointing. In addition to the natural atmospheric radiance variability, the magnitudes and statistics of the variations induced by transient atmospheric events such as aurora, PMCs, stratospheric warmings need to be acquired. Detailed understanding requires a global database on these variabilities. UVISI on MSX will be is able to address many of these issues. MSX will be in a 898 km near sun-synchronous polar orbit. Radiances from all latitudes will be detected over all seasons. The nominal 5-year mission will permit the development of a good statistical data base and extraction of the effects of solar activity. The effects of line-of-sight and solar scatter angles will be deduced from the large data base, in addition to the effects of seasons, latitudes, terrain, and cloud types.

UVISI is comprised of five spectral imagers and four bandpass imagers. It will view the limb and hard earth with 0.9 to 1.8 nm spectral resolution in the MUV (200 - 300 nm) region. A spatial resolution of 90 μrad (7.9 x 10^{-9} sr) will be achieved with a sensitivity of two photons/cm^2-s per pixel. This spatial resolution is a factor of two better than the UVPI camera. The narrow field UV imager can operate with four bandpasses 200 to 300 nm (open), 200 to 230 nm, 230 to 260 nm, and 260 to 300 nm. An auroral hot-spot tracker will permit intense features to be imaged spatially and spectrally simultaneously [2,3]. Image region will be automatically processed to extract the spatial moments from the probability density function and PSD distributions [4]. The performance specifications for the imagers and spectrographic imagers are given in Table 14.

UVISI was assembled and integrated in a Class 100 Cleanroom environment and carefully

Table 14. UVISI Imager Specifications (Excerpted from Carbury [5].)

Imagers				
Item	IUN	IUW	INV	IVW
Filter (nm)				
Open	180 to 300	110 to 180	300 to 900	380 to 900
Attenuated	180 to 300 $(x\ 10^{-3})$	110 to 180 $(x\ 10^{-3})$	300 to 900 $(x\ 10^{-4})$	380 to 900 $(x\ 10^{-4})$
WB1	200 to 230	117 to 127	305 to 315	426 to 429
WB2	230 to 260	128 to 138	350 to 440	529 to 631
WB3	260 to 300[1]	145 to 180	470 to 640	380 to 900[2]
Sensitivity (p/cm²-s)				
Open	2	5	1	6
Attenuated	400	25000	12000	57000
WB1	3	90	18	9
WB2	4	100	3	5
WB3	N/A	90	1	N/A
Photocathode (window)	RbTe (MgF_2)	CsI (MgF_2)	ExtS20 (SiO_2)	ExtS20 (SiO_2)
A_d (cm²)	130	25	130	25
Ω_p (sr)	7.92×10^{-9}	6.68×10^{-7}	7.92×10^{-9}	6.68×10^{-7}

Spectrographic Imagers					
Item	SPIM1	SPIM2	SPIM3	SPIM4	SPIM5
Waveband (nm)	110 to 170	165 to 258	251 to 387	381 to 589	581 to 900
λ Resolution (nm)					
wide slit	0.8	1.2	1.8	2.8	4.3
narrow slit	0.5	0.9	1.5	2.1	2.9
Sensitivity (phot/cm²s)	5	2	3	1	1
Photocathode (window)	CsI (MgF_2)	RbTe (MgF_2)	BiAlk (SiO_2)	ExtS20 (SiO_2)	ExtS20 (SiO_2)
A_d (cm²)	110	110	110	110	110
Ω_p** (sr)	3.81×10^{-7}	3.81×10^{-7}	3.81×10^{-7}	3.81×10^{-7}	3.81×10^{-7}

*Center λ with Δλ = resolution for wide slit; Δθ assumed 0.10 deg.
**Pixel size for small slit (0.05 deg) and best along-slit resolution (1 deg/40)

baked out to avoid molecular and particulate contamination affecting its mission performance.

A future NASA and NRL Mission will observe the OH and NO A-X transitions at 0.01 nm spectral resolution to obtain the spatial structure dependence and its effect on radiance and the molecular internal distribution in the airglow. Highly non-equilibrium OH and NO rotational distributions have been observed by CIRRIS1A in the infrared, and these distributions may also be detected in their UV emission signatures.

The near-term missions will rely upon evolutionary improvements in the state of imaging arrays and intensifiers such as microchannel plates. Future long-term missions will require further advances in detector technologies. Sensor systems will need to be hardened against natural and offensive radiation threats to levels far in excess of those currently possible. This may require the use of non-silicon-based detection techniques and new electron multiplier technologies. Filters for UV detection systems have stringent out-of-band rejection requirements approaching 10^8 over the entire surface of the filter. Better process control or techniques will be required for future systems.

The advances in data fusion techniques and the recent progress in infrared detector arrays suggest that simultaneous scene observation in several colors from UV through IR spectral regions should be possible with identical spatial resolution, temporal resolution, and co-registration.

This material represents the status of the field as of late 1993. Analysis of the field observations data and the models from the many BMDO sponsored program elements is ongoing, and continuous improvement in our understanding of the UV atmospheric radiance variability and ability to predict its global and spatial/temporal behavior is expected.

CHAPTER 7 REFERENCES

1. Heckathorn, H., "SSGM Update," at PSAG Backgrounds Interest Group Meeting, at the Aerospace Corporation, 13-14 February 1992.

2. Mill, J., O'Neil, R.R., Price, S., Romick, G. "The Midcourse Space Experiment, An Introduction to the Spacecraft, Instruments, and Scientific Objectives," J. Spacecraft 31, 5, Sept 1994.

3. Anderson, D., "MSX Shortwave Terrestrial Backgrounds Experiments," at PSAG Backgrounds Interest Group Meeting, at the Aerospace Corporation, 13-14 February 1992.

4. Romick, G. and Anderson, D., "Short-Wavelength Terrestrial Backgrounds," at the Midcourse Space Experiment Technical Interchange Meeting, at JHU Applied Physics Laboratory, March 1993.

5. Carbary, J., "UVISI Instrument Tutorial" APL-S1G-R92-04 at MSX PI Meeting June 1992.

BLANK

PART THREE

INFRARED EMISSION FROM NO$^+$ BY ELECTRON IRRADIATION OF THE ATMOSPHERE

INTRODUCTION

The presence of infrared radiation from NO$^+$ in the upper atmosphere has often been invoked to account for prompt radiation observed in the vicinity of 4.3 micrometers. However, attempts to measure NO$^+$ infrared emission characteristics have not been fruitful. The only atmospheric measurements of NO$^+$ were from an aircraft-borne, free-running, low-resolution interferometer during the 1963 Fish Bowl nuclear test series reported by Stair et al. [1] and a field-widened interferometer rocket probe of the aurora reported by Picard et al. [2]. Earlier EXCEDE measurements by O'Neil et al. [3] tenitively identified NO$^+$ emissions but later Lee et al. [4] corrected the identification and attributed the emission to CO. All of these observations are somewhat ambiguous. In part, the failure to observe NO$^+$ emission stems from its close spectral proximity to the CO_2 (001-000) band. For typical upper atmospheric temperatures of 220 degrees K, the $CO_2(\nu_3)$ band overlaps the emission of NO$^+$ fundamental band emanating from its first excited vibrational level. Fortunately, due to its anharmonic nature, emission from higher vibrational levels fall to the long wavelength side of $CO_2(\nu_3)$ and may be more easily measured.

Several candidate chemical reactions for producing NO$^+$ are sufficiently exothermic to populate very high vibrational levels. Unfortunately, the majority of the reactions are undetermined as to the distribution of energy partitioned into the vibrational states of NO$^+$ and the reactant products. Consequently, it has been uncertain if emission from higher vibrational levels of NO$^+$ is produced in the upper atmosphere. Even laboratory attempts such as Henninger et al. [5] to collect infrared data on NO$^+$ have been sparce. Laboratory measurements are hampered by the inability to generate and maintain the excited ion at sufficient concentrations and it appears unlikely that the reactions producing vibrationally excited NO$^+$ will be quantified soon. Hence, a rocket-borne electron beam experiment, EXCEDE III, as described by Paulsen et al. [6] was conducted with one of its important objectives being to perform a series of spectral measurements at different altitudes in the atmosphere to characterize the emission spectra of NO$^+$.

EXPERIMENT DESCRIPTION

On 27 April 1990 at 01:00:59 MDT, an Aries booster carried the EXCEDE III payload into the night sky at White Sands Missile Range, NM. Figure 1 gives a pictorial representation of critical events during the flight. The payload consisted of two parts, an electron accelerator or electron gun module, and a sensor module. Following booster separation the two modules were uncoupled, the modules were re-oriented with the gun module beam pointed along the earth's magnetic field lines and the sensor module was aimed with its sensors pointed initially about 60 meters along the electron beam. Pointing of the sensors was achieved by a pre-programmed, precision attitude control system with real-time override based on on-board video and ground-

based commands.

DOWNRANGE DISTANCE (KM)
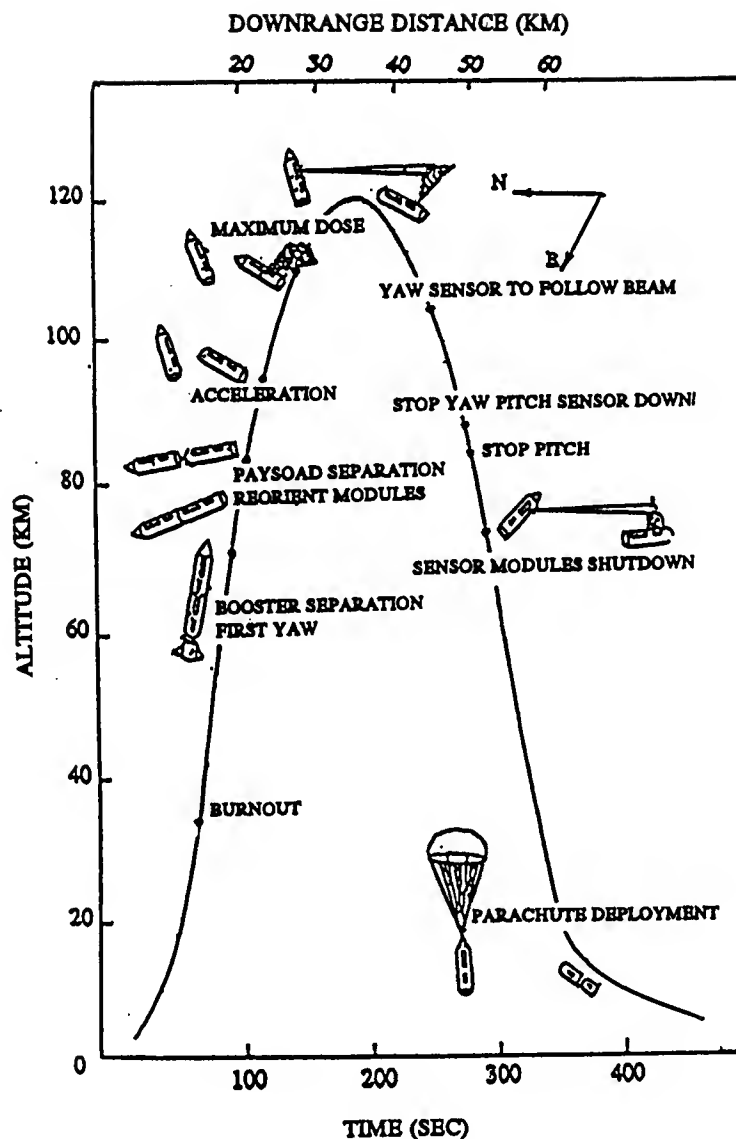
Figure 1. Payload Trajectory Showing Key Events.

Figure 2 shows a conceptual diagram of the two major payload components. The accelerator system which produced the electron beam consisted of two separate accelerator bays. Protection of each bay was provided by a load-fault detector which disabled the bay for about 0.1 sec and implemented a re-start at a lower voltage. Three high voltages at 2.6, 2.1 and 1.5 kV were available. All of the data reported here were taken with the highest gun voltage. The gun design was intended to produce an uncollimated beam of electrons of approximately 18 amps at 2.6 kV. The electron density at maximum energy deposition near 103 km was about 1.0×10^9 cm^{-3} which is much greater than that in the ambient or even a Class III aurora, which would be about 1.0×10^6 electrons cm^{-3} according to Whalen [7]. Actual beam performance was monitored by several devices observing voltages, currents; with emission intensities measured by photometers and cameras from on-board and from ground-based telescopes.

112

The sensor module carried a Michelson-type interferometer-spectrometer pointed at the beam and three Circular Variable Filter (CVF) spectrometers. One CVF was pointed at the beam, the second CVF was pointed 8 degrees into the afterglow and the third CVF is pointed 20 degrees into the afterglow. Also, on-board the sensor module were ultraviolet and visible spectrometers with co-aligned photometers, a spatially scanning photometer package (3914 Å) to sweep over the beam and several other sensors. The work presented here is primarily concerned with the measurements from the interferometer looking at the beam, and the measurements of the intensity profile of the N_2^+ 3914 Å emission.

The high resolution spectrometer designed to perform the infrared spectral measurements was a modified Michelson interferometer built by Thurgood and Huppi [8] at Utah State University. The principal modification to a conventional Michelson interferometer was the use of two separate front-end optical systems which were treated independently but shared a common translating element. Figure 3 shows the mechanical layout of the interferometer. The unique aspect of this configuration was the rotation of two mirrors about a pivot point so that as one mirror advanced the other retreated. As can be seen, the moving mirrors share a common drive and constitute a dual optical cube which in essence yields two interferometers. Each beam in these two interferometers was separated spectrally by dichroic beam splitters (not shown) to produce four channels of infrared radiation, each of which was directed onto one of four separate detectors. The four spectral channels were spectrally isolated to the regions of 2.2 - 3.8, 3.8 - 7.5, 7.1 - 12.2 and 12.2 - 21.3 micrometers, designated channels 1 - 4 respectively. Only data from channel 2 are reported here.
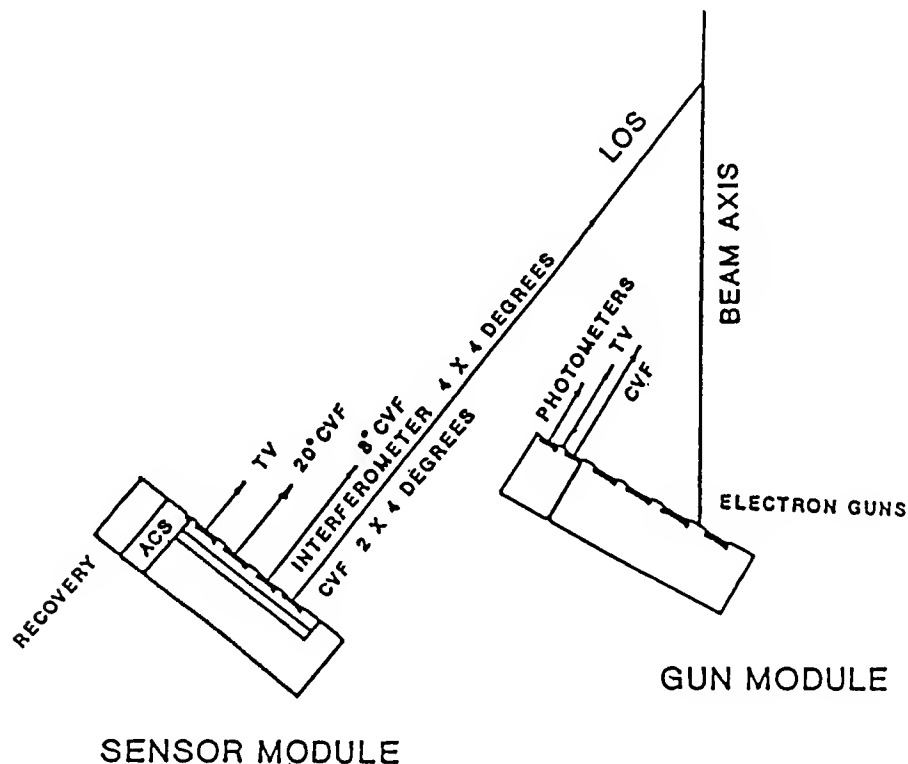
Figure 2. Payload Showing The Sensor Module and Gun Module.

Since an interferometer is usually intended for observation of stationary sources, the measurements were synchronized to the pulses of the electron gun. The timing of the moving mirrors to begin a measurement relative to the electron gun event is shown in Figure 4. In the beam-on condition, two full scans with the movable mirror covering maximum extension in optical path difference were recorded. During the beam-off condition, one full measurement to the maximum optical path difference was followed by a short scan and scan/retrace to be in position for the next beam-on pulse. Thus, four interferograms were obtained each cycle of the electron gun. The resolution for the three long scans with the moving mirror is 1.8 cm^{-1} and the field of view is approximately 3.6 x 3.6 degrees.

A continuous scanning photometer with a 10 Å bandpass centered at 3914 Å was used to monitor the N_2^+ emission. This photometer swept from -15 degrees south of the beam to 30 degrees north of the beam with full angular coverage in one second. The instantaneous field-of-view was 0.1 degree and provided for a spatial resolution of a meter or less at the beam. Details on on the measurement of the 3914 Å radiation is given by Rieder et al. [9].

The Aries launch was from north to south in order to direct the beam up the earth's magnetic field lines and away from the degassant plume. Payload separation from the booster (having a down range velocity of 279 m/s) occurred at 68 km and followed a ballistic trajectory reaching an apogee of 115 km. Following separation, the sensor and gun modules were de-coupled from each other at 82 km with a relative velocity of 3.17 m/s. The initial beam cycle occurred at 120.4 s after launch corresponding to an altitude of 89 Km. In all, 23 useful beam cycles were generated with the final pulse on down-leg occurring near 62 km.
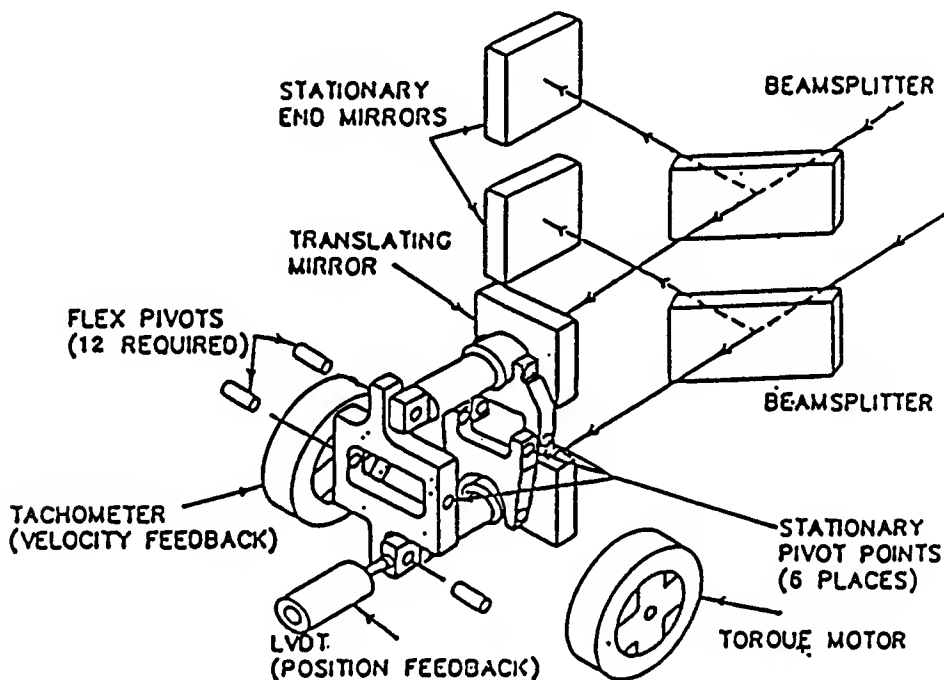
Figure 3. Schematic of the Interferometer Optics and Drive Mechanism (Reference 8).

114
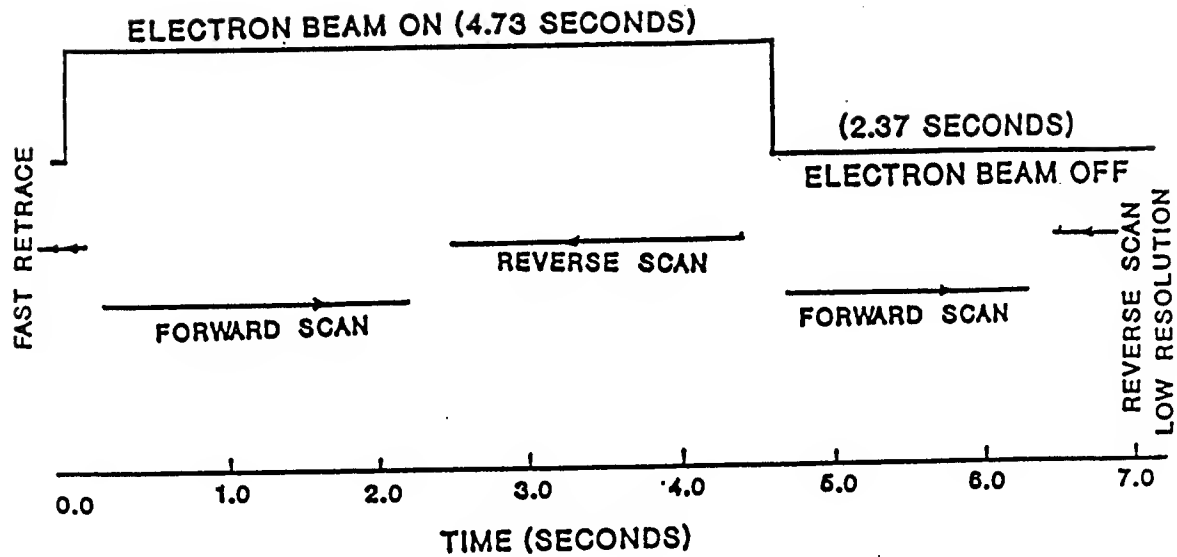
Figure 4. Interferometer Scans Synchronized to the Electron Beam.

SPECTRAL DATA

Data collected from the interferometer are interferograms, F(x), each produced over a single scan of the moving mirror. An interferogram is the autocorrelation of the incident radiation falling on the entrance aperture of the interferometer. Spectral recovery is accomplished by performing a Fourier transform of each interferogram, that is

$$B(\sigma) = \int_{-\infty}^{\infty} F(x)A(x)\exp[2\pi\sigma x + ip(\sigma)] \qquad (1)$$

with

$$A(x) = \frac{1.0}{\underset{-L \qquad L}{\underbrace{}}} \qquad (2)$$

where B(σ) is the spectral density of the incident radiation at wavenumber σ, x is the optical path difference of the interfering optical beams in the interferometer with extremes at distances -L and L and p(σ) is a phase function usually related to the instrument. Interferograms were phase-

115

corrected by the Foreman et al. [10] method which permits spectral recovery through the cosine Fourier transform,

$$B(\sigma) = \int_0^\infty A(x)F(x)\cos(2\pi\sigma x)dx \qquad (3)$$

Figure 5 shows the spectrum obtained at an altitude of 102 km where the highest electron energy deposition occurred. The brightest emission features are from the electronic ground state nitric oxide fundamental bands; the features shown near 2020, 1990 and 1960 are bandheads beonging to the NO fundamental bands. The emission from $CO_2(\nu_3)$ centered near 2340 cm^{-1} is also very bright. Unfortunately, the radiation of primary interest namely, the NO$^+$ fundamental band, 1 - 0 vibrational transition, falls in and around the envelope of the $CO_2(\nu_3)$ emission making identification difficult. The spectrum of the beam-off quiescent background radiation taken approximately two seconds later is shown in the same figure. Similarly, Figures 6a and b show the beam-on and beam-off spectra taken at the 115 km apogee. Note that the signal level is reduced by about ten over that of Figure 5. At apogee the contribution from $CO_2(\nu_3)$ is substantially reduced and the emission features appear to be predominantly from NO$^+$. To improve the signal to noise, 12 interferograms taken at altitudes greater than 113 km were co-added. Figure 7 shows the co-added spectrum with background removed in the spectral region from 2250 to 2400 cm^{-1}. This spectral region contains lines from the (1-0) and (2-1) bands of the $\Delta v = 1$ sequence of NO$^+$. Over forty individual vibration-rotation lines belonging to NO$^+$ are shown giving very positive identification. The local N_2^+ density has been derived from the 3914 Å scanning photometer measurements.
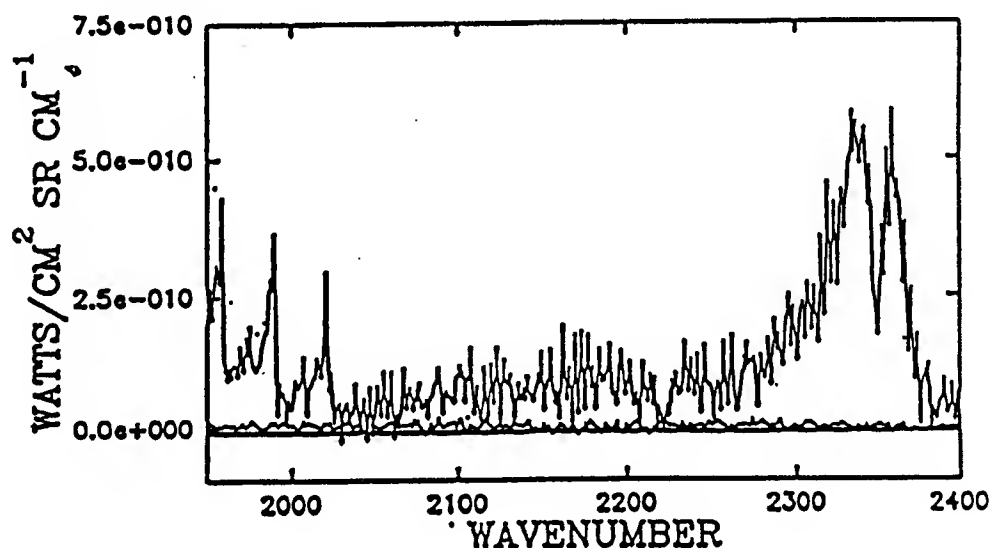
Figure 5. Spectrum of Electron Irradiated Air at 102 km Showing NO, CO_2 and the NO$^+$ Spectral Region.
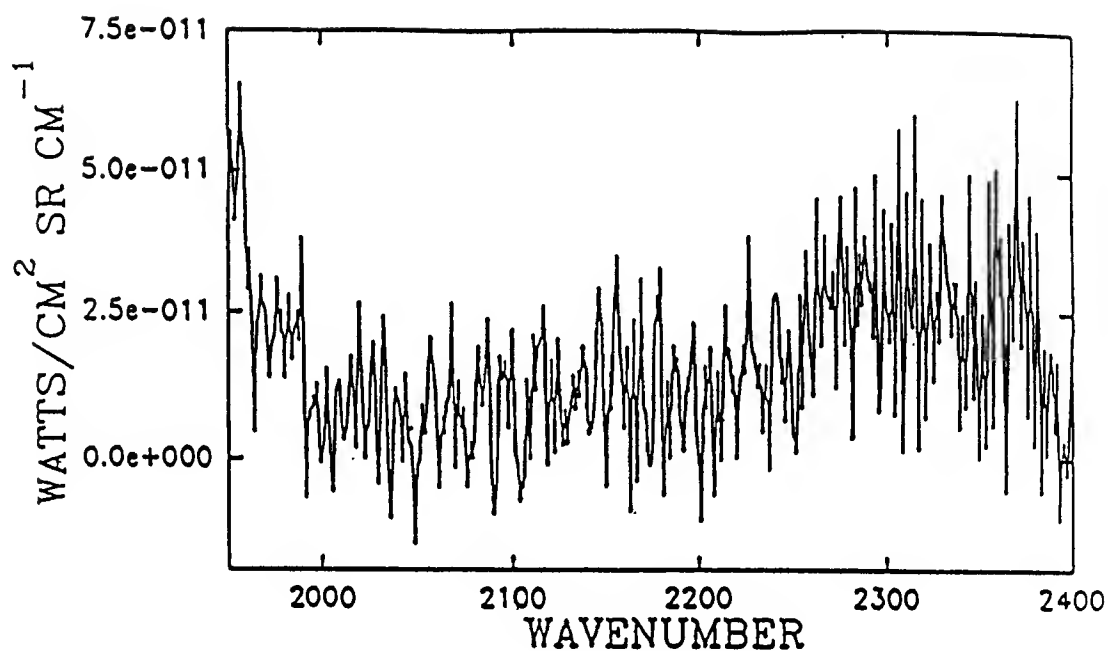
Figure 6a. Spectrum of Electron Irradiated Air at 115 km Showing NO Bandheads and the NO+ Spectral Region.
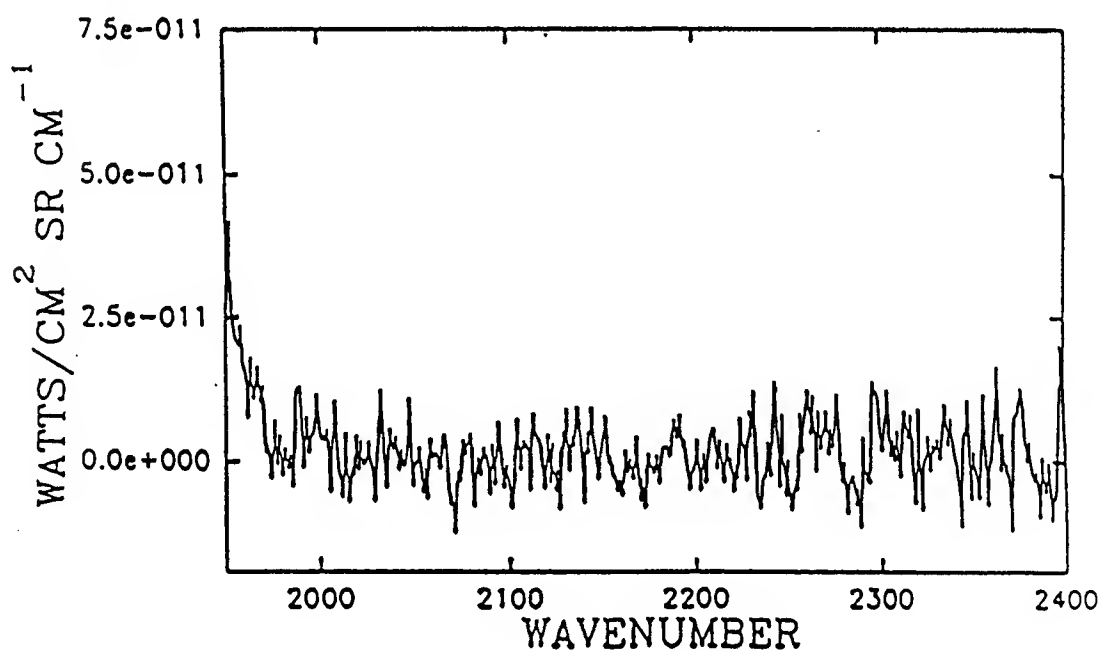
Figure 6b. Spectrum of Quiescent Night Sky Taken Just After The Spectrum Shown in Figure 6a.
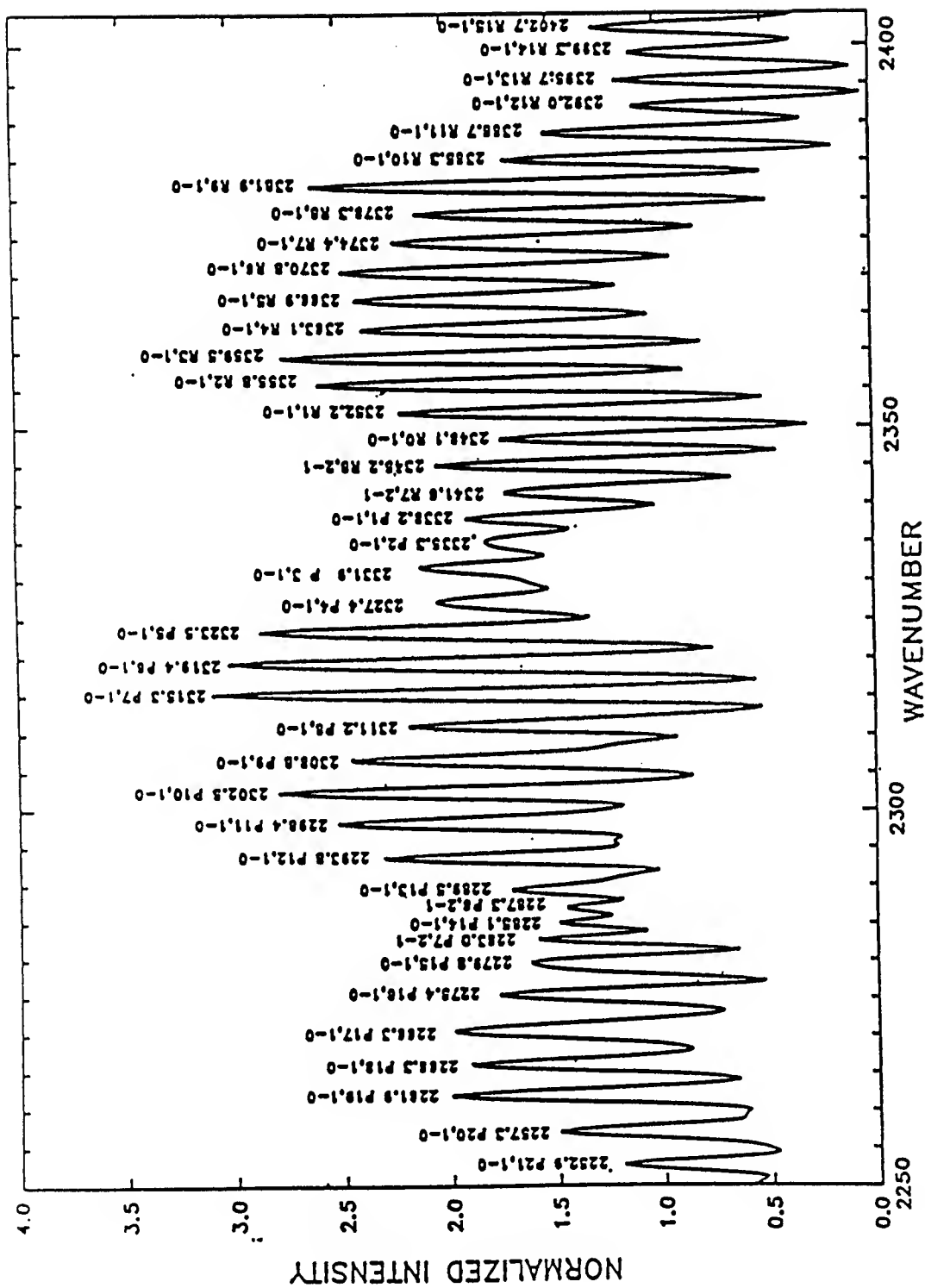
Figure 7. Co-added spectrum near 115 km, beam-on. NO+ vibration-rotation lines are identified.

118

A complete scan across the beam of the prompt 3914 Å radiation was made in one second intervals. These radiance profiles permit determination of the local N_2^+ density which in turn yields the energy deposition per unit volume. Two profiles of the N_2^+ density are given by Rieder et al. [9] for each scan of the interferometer during the beam-on condition.

NO$^+$ CHEMISTRY AND MODELING

NO$^+$ is the terminal E-region ion and models of its chemical production by very fast ion-molecule reactions show it to be formed very rapidly. Winick and collaborators [11, 12b] have predicted the production of NO$^+$ for the quiescent atmosphere and for various aurora intensity levels. For a Class III aurora, the NO$^+$ concentration is increased dramatically and under the conditions reached with the EXCEDE III electron irradiation of the atmosphere, NO$^+$ would be expected to have an even larger production rate. Low in the atmosphere where the mole fraction of [O_2] exceeds that of [O], the principal production reactions are:

$$N^+ + O_2 \longrightarrow NO^+(v) + O(^3p) \qquad v \leq 28 \qquad (4)$$

$$N^+ + O_2 \longrightarrow NO^+(v) + O(^1D) \qquad v \leq 18 \qquad (5)$$

$$N^+ + O_2 \longrightarrow NO^+(v) + O(^1S) \qquad v \leq 8 \qquad (6)$$
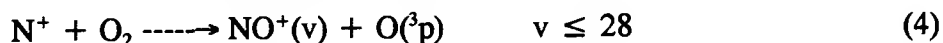
which are sufficiently exothermic to populate the vibrational levels indicated. The nascent vibrational distribution for the reaction of N^+ with O_2 reported by Smith et al. [13] has a bi-modal nature with peaks at $v=7$ and 13. Since the radiative transition probabilities for the fundamental bands increase with v, it may be expected that spectral features would be present up to and beyond 5 μm.

At higher altitudes where [O]/[O_2] becomes larger, the primary source of NO$^+$ is expected to result from the reactions:

$$N_2^+ + O \longrightarrow NO^+(v) + N(^2D) \qquad v \leq 2 \qquad (7)$$

$$N_2^+ + O \longrightarrow NO^+(v) + N(^4S) \qquad v \leq 8 \qquad (8)$$
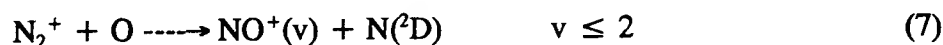
again exothermic and capable of producing the vibrational levels shown. A branching ratio of 0.9 for the reactions of 7 and 8 has been estimated by Winick et al. [11] based on modeling considerations of NO. Hence, the majority of emission from NO$^+$ from this reaction would come from the lowest two excited vibrational levels with radiation concentrated in the vicinity of 2300 - 2400 wavenumbers.

Additional chemical reaction sources include

$$O_2^+ + NO \longrightarrow NO^+(v) + O_2(x) \qquad v \leq 9 \qquad (9)$$

$$O_2^+ + NO \longrightarrow NO^+(v) + O_2(^1\Delta) \qquad v \leq 6 \qquad (10)$$

119

$$O_2^+ + NO \longrightarrow NO^+(v) + O_2(^1\Sigma) \qquad v \leq 4 \qquad\qquad (11)$$

although no evidence of vibrational excitation from reactions 9-11 has been observed, and the vibrational excitation of the product is less likely for a charge transfer reaction where no new bond is formed. Other possible sources for $NO^+(v)$ involve excited state reactants as for example given by Piper [14] such as,

$$N(^2P) + O \longrightarrow NO^+ + e \qquad v \leq 2 \qquad\qquad (12)$$

or

$$O^+(^2D) + N_2 \longrightarrow NO^+(v) + N \qquad v \leq 17 \qquad\qquad (13)$$

and need consideration.

Still other reactions such as

$$O_2^+ + N \longrightarrow NO^+(v) + O \qquad\qquad (14)$$

although shown to be fast by Fehsenfeld et al. [15] have concentrations too low to be significant and

$$O^+ + N_2 \longrightarrow NO^+(v) + N \qquad\qquad (15)$$

is too slow [16] at thermal energies to be important for this experiment.

The principal destruction mechanism for $NO^+(v)$ is by recombination since the electron density is relatively high. The vibrational energy residing in NO^+ may be lost through radiative emission or by collisions with other molecules, that is for example

$$NO^+(v) + N_2 \longrightarrow NO^+(v\text{-}1) + N_2 \qquad\qquad (16)$$

$$NO^+(v) + O_2 \longrightarrow NO^+(v\text{-}1) + O_2. \qquad\qquad (17)$$
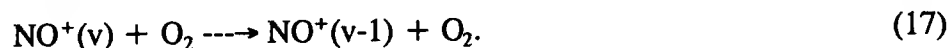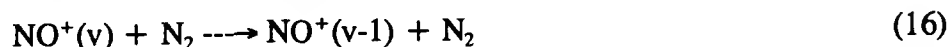
Quenching of NO^+ at altitudes below 100 km is important with importance decreasing at higher altitudes; the V-T transfer has been measured by Federer et al. [17] to be, for $v = 1$, 7 x 10^{-12} cm^{-3} s^{-1} with N_2 and $< 10^{-12}$ cm^{-3} s^{-1} with O_2. Even lower quenching rates were obtained by Morse et al. [18]. Although there are no measured rates for $v > 1$, it may be assumed that they are at least as fast.

Synthetic emission spectra of vibrationally excited NO^+ were generated according to the relation,

$$I(\sigma,v,j) = hc\sigma N(v,j)A(v,j)/4\pi \qquad\qquad (18)$$

where h is Planck's constant, c is the velocity of light, σ the wavenumber, $A(v,j)$ is the radiative transition probability, and $N(v,j)$ is the number density of NO^+ in vibrational level v and rotational level j. The line positions and transition probabilities of Werner and Rosmus [19] were used. Populations of the vibrational levels and rotational states could be produced from a Boltzmann temperature, from independent temperatures for each, or arbitrarily populated. Twelve vibrational and forty rotational levels were included for each of the P and R branches of NO^+ in the ground singlet-sigma state. The model spectral output of NO^+ was convolved with an instrument function of adjustable resolution which was matched to the line profiles for the interferometer.

ANALYSIS

Prior to analyzing the field data a first order correction to the observations is required due to the motion of the e-beam and sensors. The spatial profile of the electron energy deposited is available from the prompt $N_2{}^+$ 3914 Å scanning photometer. However, the NO^+ radiation lifetime is relatively long, necessitating a substantial correction. Because of the low momentum transfer of the electrons, the energy deposited into the ambient atmosphere remains essentially fixed in space for early times. The motion of the accelerator module through the atmosphere causes the electron beam to impact the air and leave a trail of excited and reacting gas behind it. The co-moving sensor module observes the leading edge of the beam deposition volume and all prior energy depositions within the field-of-view, so that the sensor sees a superposition of beam profiles; each previous profile having spread by some diffusion which depends upon its age since formation. Each of these aging profiles must also be weighted by the exponential decay rate function of any particular NO^+ radiating state. A lower bound estimate of the fraction of radiation lost because of the transverse motion of the sensor may be found, neglecting diffusion. The resulting shape of this radiating profile is a convolution of the 3914 Å profile with an exponential decay, depending on the ratio of the Einstein radiative decay rate and the transverse beam velocity, v. The radiating species spatial transverse profile $p(y)$ is given by

$$p(y) = \alpha \int_{-\infty}^{\infty} g(x)\,step(y-x)\exp[-\alpha(x-y)]dx$$

(19)

where $g(x)$ is the 3914 Å beam profile as a function of transverse x distance and α is the ratio of the transition probability to the velocity, A/v. The step function is unity everywhere its argument is positive, and vanishes otherwise. The integral is taken over the entire transverse beam extent, with motion along the beam axis assumed not to affect the integral; the loss at one end of the leading axial window being replaced by an equivalent gain at the trailing axial window edge. Figure 8 shows the application of this process to the 3914 Å electron beam profile, and the resulting NO^+ radiation profile for the $1 \rightarrow 0$ transition. The peak is shifted away from the direction of transverse motion, the motion spreading out the profile due to the longer radiative lifetime of the infrared transitions of NO^+ compared to the 62 ns radiative lifetime of the ultraviolet 3914 Å transition.

The correction must account for the fraction of radiation observed within the sensor field of view. A second integral over this field-of-view of $p(y)$ must be performed and divided by

the entire integral of p(y) unrestricted by sensor limitations. For example, in Figure 8 only 46 percent of the NO^+ radiation profile is within the sensor window from -12 meters to 12 meters. With y_o the window half width the window fraction F is

$$F = \int_{-y_o}^{y_o} p(y)dy / \int_{-\infty}^{\infty} p(y)dy \qquad (20)$$
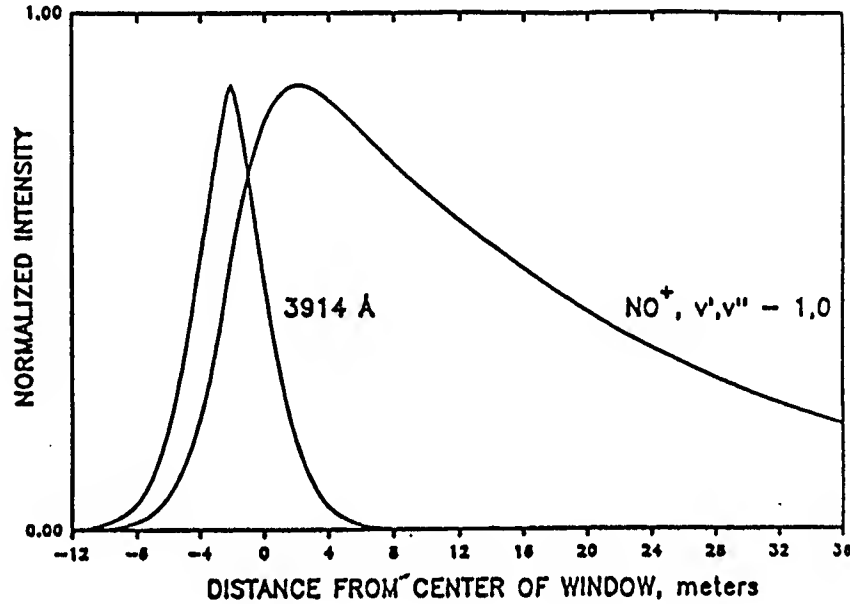
Figure 8. Emission Profiles of the N_2 3914Å Radiation and NO^+ Fundamental Band (1-0). The Beam Advances To The Left at 245 m/s.

If the expression for p(y) is inserted into expression 20 and the order of integration reversed, the result is,

$$F = \int_{-\infty}^{\infty} g(x) \int_{-y_o}^{y_o} \alpha \ step(y-x)exp[-\alpha(x-y)]dydx \qquad (21)$$

where the integral over infinity of p(y) is unity. The inner integral may be written as a convolution,

$$\int_{-\infty}^{\infty} rect(y/2y_0)\alpha step(y-x)exp([-\alpha(y-x)]dy \qquad (22)$$

ie., a transmission of the window in the transverse beam direction. Over the window region this may be integrated exactly, making the window fraction numerically easier to calculate as,

$$F = \int_{-y_0}^{y} g(x) \ (1 \ - \ exp[-\alpha(x-y)])dx \qquad (23)$$

122

The above correction, giving a lower bound, was applied to all analysis of vibrational levels when comparing with the 3914 Å emission. Inspection of the co-added spectrum, obtained from the interferometer, showed that the vibrational levels 1 and 2 are populated more than the higher levels. A model spectrum for the lower vibrational levels was generated. Based on a least squares fit to the data, a rotational temperature of 300 degrees K was determined over the spectral region free from overlap by the higher vibrational level emission. The modeled spectrum and interferometer spectrum were normalized and subtracted from one another. The residual spectrum exhibited emission in the region around 2350 cm^{-1} having a shape which was recognizable as belonging to the $CO_2(v_3)$ band. Synthetic spectra for $CO_2(v_3)$ was generated and fit to the residual spectrum and removed from the co-added interferometer spectrum. Co-addition of spectra improved the signal to noise by about a factor of 3 bringing the noise level to approximately 3 x 10^{-12} W/cm^{2}sr cm^{-1}. The spectrum, after removal of the small contributions from CO_2 is shown as the lower trace in Figure 9. From the emission lower than 2250 cm^{-1}, it is apparent that there are higher vibrational levels present, with a non-thermal vibrational distribution. The upper trace in Figure 9 is a best fit model to the field spectrum; derived with a rotational temperature of 300 degrees K and populations for the vibrational levels as indicated in Table 1. The uncertainty associated with each of the vibrational populations relative to level v = 1 is also given in Table 1. The presence of emission from higher v levels requires that a fraction of the NO$^+$ production must be from a mechanism other than reactions 7 or 12.
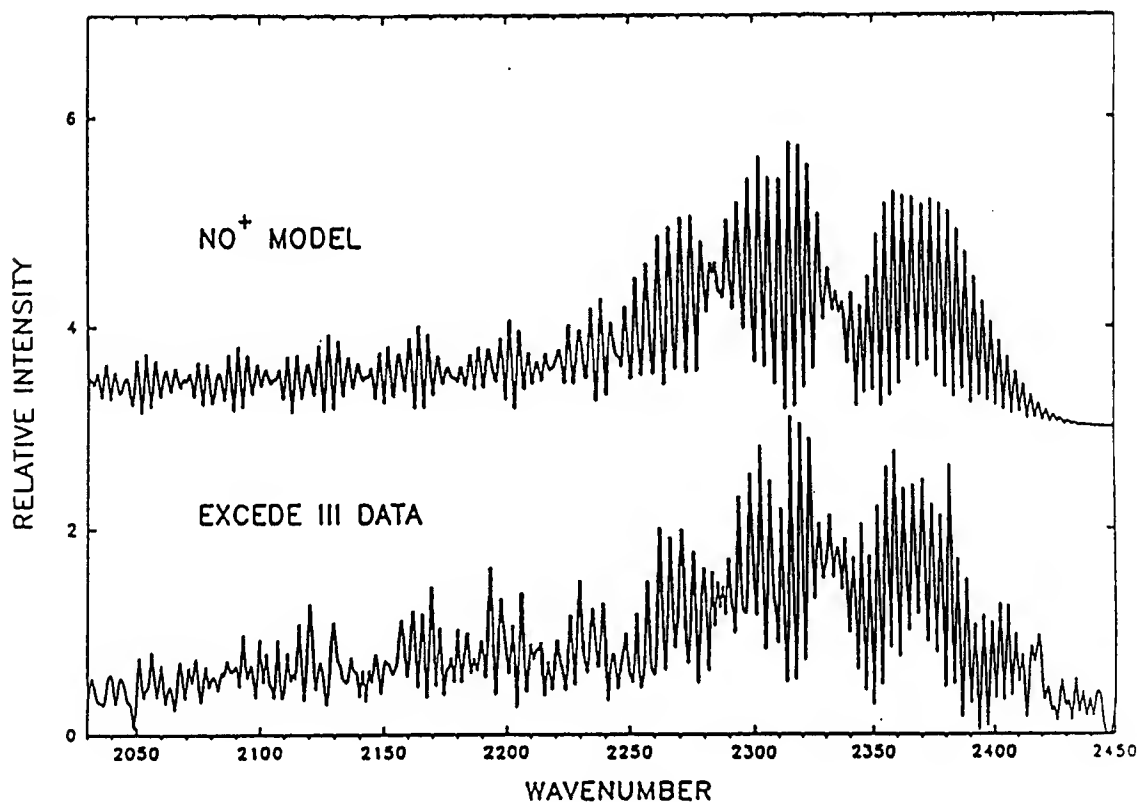
Figure 9. Comparison of NO$^+$ Measured Spectrum and Model Spectrum.

123

Table 1.

Relative Population of NO$^+$ Vibrational Levels

Vibrational Level

	1	2	3	4	5	6	7	8
Population	1.0	.218	.013	.017	.015	.010	.014	.004

At lower altitudes the emission from $CO_2(v_3)$ dominates the spectra. The spectrum obtained from the interferometer at maximum dose in the spectral region of interest, shown in Figure 5, indicated emission, but of uncertain origin. In addition to $CO_2(v_3)$, potential radiators in this spectral region include $O_3(v_1+v_3)$ combination band, CO fundamental bands, a fundamental band of N_O, and bands belonging to electronically excited molecular nitrogen. Consequently, attempts to isolate the spectral contribution of NO^+ were not made.

PHOTON EFFICIENCY

A quantity of atmospheric importance for modeling purposes and simple estimates of energy distribution is the rate of photon production from NO^+ relative to the rate of ion production. This ratio for the fundamental bands of NO^+ is given by

$$F = \Sigma_v[NO^+(v)]A(v,v-1)/Q_c \tag{24}$$

or alternatively in terms of the ratio of output energy to input energy, referred to as efficiency, ϵ

$$\epsilon = 3.65 \times 10^{-2} \Sigma_v[NO^+(v)]A(v,v-1)/Q_c \times \Gamma(v) \tag{25}$$

where Γ is the central wavelength in micrometers for each vibrational transition in the fundamental sequence and Q_c is the ion pair creation rate.

Since the NO^+ emission is optically thin, the number of photons produced may be obtained directly from the spectrometer measurements. Likewise the N_2^+ production may be derived from the 3914 Å scanning photometer measurements by Rieder et al. [9]. For the conditions created by the EXCEDE III electron irradiation at altitudes near 115 km, the ratio of the production rate of NO^+ fundamental-band photons relative to the production of 3914 Å photons is 1.6 ± 0.9 where the motion correction introduced by Eq. 23 has been applied to the NO^+ emission.

The rate of $[N_2^+]$ production relative to the total ionization can be estimated (unpublished May 3, 1987 RDA memo by F. Gilmore) as,

$$\{N_2^+\}/Q_c = 1.62\{N_2\}/(2\{N_2\} + 2\{O_2\} + \{O\}) \tag{26}$$

where the curly brackets denote mole fraction. The atmospheric concentrations on launch day, as taken from MSIS [20] for 115 km, were the $[O] = 1.622 \times 10^{11}$, $N_2 = 6.722 \times 10^{11}$, and $[O_2] = 9.922 \times 10^{10}$ cm^{-3} and together with the measured 3914 Å radiation gives,

$$Q_c = 22.1 \times 3914 \text{ Å photon rate} = 3.6 \times 10^{11} \text{ cm}^{-3} \text{ s}^{-1} \tag{27}$$

where 14.1 N_2^+ ions are required to produce one photon of 3914 Å radiation. From Eq. 25 the energy efficiency was found to be $(6.1 \pm 3.4) \times 10^{-4}$ (which also corresponds to $0.072 \pm .040$ NO^+ photons/ion pair).

125

This efficiency is significantly smaller than found in the aurora by Caledonia et al. [21]. Although the energy deposition is much higher in the EXCEDE III experiment, the emission is severely quenched that is, the excited NO^+ undergoes recombination before it can radiate. As the electron density increases relative to an aurora situation, the production of N_2^+ and consequently the 3914 Å emission will continue to scale linearly. The production of NO^+ will scale as the square root of the energy deposition as recombination becomes more dominant. Hence, even though the production of NO^+ increases as in the EXCEDE III experiment, the photon efficiency relative to 3914 Å emission will decrease, in agreement with the efficiency determination above.

CHEMICAL KINETICS

$NO^+(v)$ can be removed by recombination with an electron with a characteristic rate $1/\tau$ which is related to the product of the NO^+ electron recombination rate, k_e and electron number density, $[e]$ ie., $1/\tau = k_e[e]$. For electron densities on the order of 1×10^9 cm^{-3}, the characteristic rate, $1/\tau$ for NO^+ recombination is on the order of

$$1/\tau = k_e[e] = 2 \times 10^{-7} \times 1 \times 10^9 = 200 \text{ s}^{-1} \tag{28}$$

Also, at altitudes near 115 km quenching of $NO^+(v)$ by N_2 as given by Eq. 16 has a characteristic rate

$$1/\tau = k_{N2}[N_2] = 7 \times 10^{-12} \times 8 \times 10^{11} = 5.6 \text{ s}^{-1} \tag{29}$$

where the quenching rate is taken from Federer et al. [17]. These characteristic rates must be compared to the radiative transition probability of vibrationally excited NO^+, for example $A(1-0)$ is 10.9 s^{-1} showing that recombination dominates.

Recombination rapidly removes $NO^+(v)$ before radiative cascade or collisional relaxation can appreciably alter the vibrational distribution. Therefore, the vibrational populations given in Table 1 must reflect the nascent vibrational distribution of NO^+ as it was produced. If NO^+ were produced by the reaction of N^+ and O_2, emission from vibrational levels greater than eight would be expected in accordance with the nascent distribution reported by Smith et al. [13]. The population from this reaction extends well beyond the eighth level and has relative maxima at the seventh and thirteenth levels. NO^+ emission from vibrational levels greater than eight was not observed. Alternatively, given the intensity from $v=7$, with the Smith distribution for N^+ + O_2, a much smaller fraction of the observed emission from vibrational levels 1 and 2 would have been present. Hence, reactions 4-6 are not significant production mechanisms for $v = 1,2$ under these conditions and at altitudes near 115 Km.

As a further investigation of the production sources for NO^+, a chemical kinetic computer code SHARC/AARC [22, 11] was employed following the modifications of Duff et al. [23]. A set of chemical rate equations was solved using a Runge-Kutta integration technique. The chemistry set of coupled, first order, non-linear differential equations involving the production and loss functions for 40 species was solved as a function of time. Initial excitation conditions

were taken to correspond to the electron irradiation generated by the EXCEDE III experiment interacting with air at 115 Km. Production of $NO^+(v)$ from reactions 4 - 6 was taken from Smith et al. [13] and the vibrational distribution for reactions 7 and 8 was taken from Table 1. No initial production into the lowest vibrational level ($v=0$) was assumed for the reactions, hence the vibrational populations correspond to an upper limit. Population gain and loss into vibration levels from radiative relaxation were determined using Werner and Rosmus [19] transition probabilities which become marginally significant relative to the electron recombination process at the higher vibrational levels. Single step vibrational quenching of $NO^+(v)$ was also included in the reaction set. Figure 10 shows the build-up and decay of the major species.
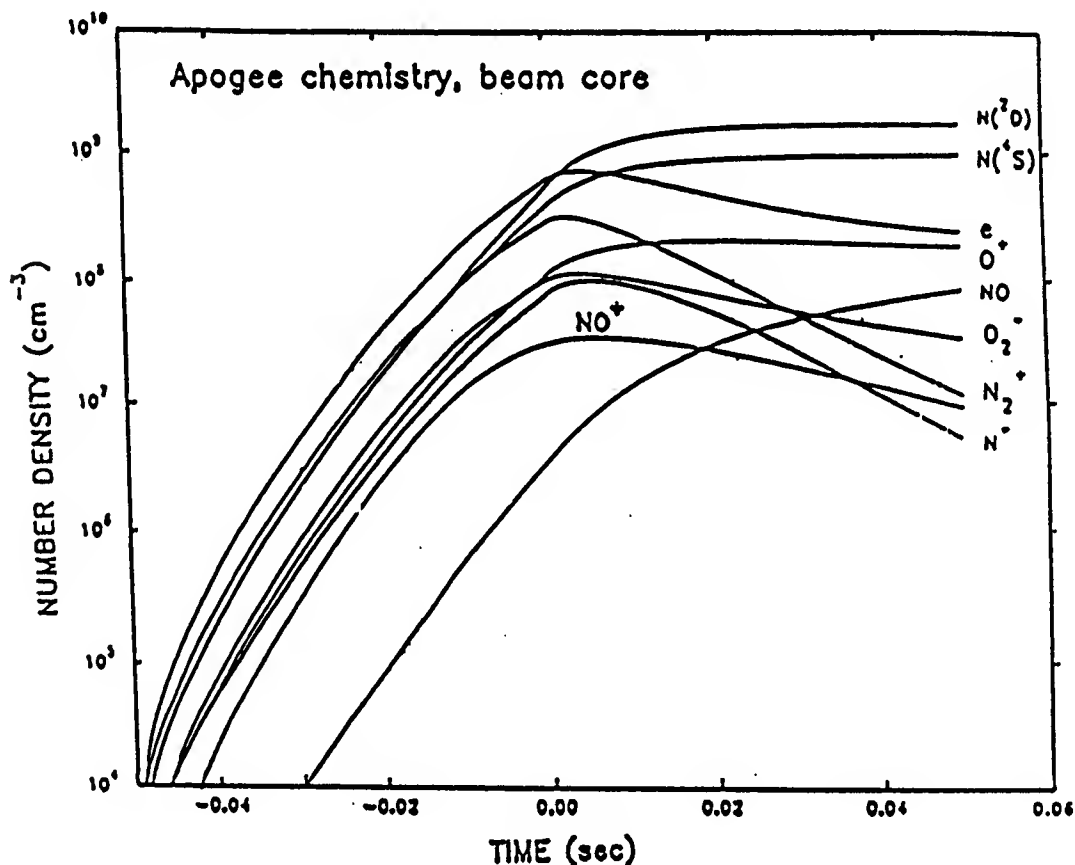
Figure 10. Calculated Evolution of Species Concentrations With Time.

The computer code can generate the population history of $NO^+(v)$. The reactions 4-6 and 7-8 were alternately suppressed in the chemical kinetics code in an attempt to ascertain their relative production importance. Figure 11 shows the time history of each of the individual vibrational levels of NO^+ where the $N^+ + O_2$ reactions (4-6) have been suppressed. A similar plot is given in Fig. 12 where the $N_2^+ + O$ reactions (7-8) have been suppressed. As anticipated, the relative vibrational populations of NO^+ are almost completely frozen with their respective nascent distributions with only slight discrepancies later in time due to radiative relaxation. Most significant is the relative contribution to levels 1 and 2 where reaction 7 clearly

127

dominates. Therefore, reactions 7 and 8 must be making the major contribution to the $NO^+(1,2)$ populations as concluded previously.
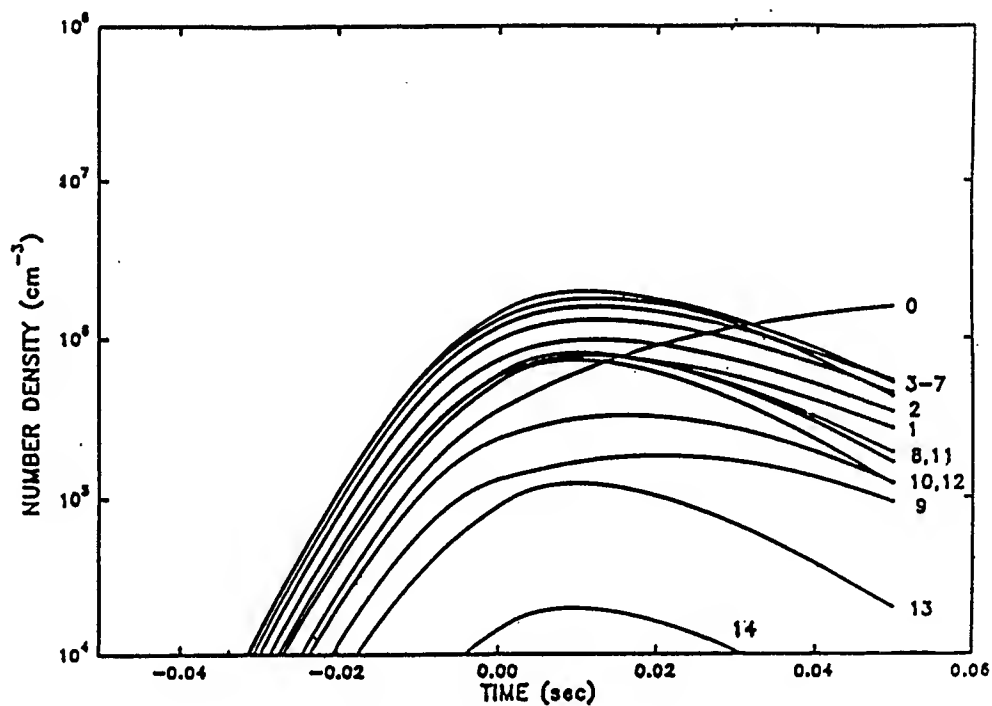
Figure 11. Calculated Evolution of the Vibrational Levels of $NO^+ + O_2$ in the Beam Core.
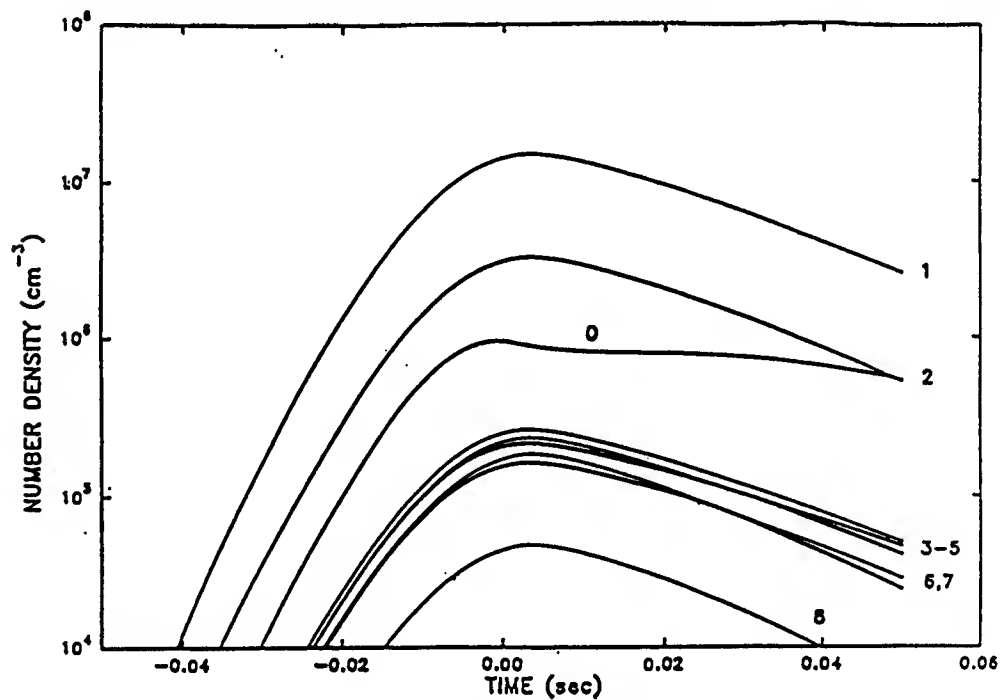
Figure 12. Calculated evolution of the vibrational levels of NO^+ From the Reaction $N_2 + O$ in the Beam Core.

128

The chemi-ionization reaction 12 is a possible source of $NO^+(v=1,2)$. This reaction has been suggested by Caledonia et al. [21] as being a source of auroral emission with a contribution as large as 10 - 15 % of the NO^+ radiation produced. The population distribution into the vibrational levels is unknown, particularly the fraction of NO^+ produced in $v=0$. The chemistry code was used to explore the predicted concentrations of $N(^2P)$. The prediction of $N(^2P)$ is sufficiently small that any contribution from this chemi-ionization reaction to the populations of $v=1,2$ has been ignored.

As a further examination of the source mechanism for the $NO^+(v)$, a linear extrapolation of the observed populations from levels 3 - 8 to levels 1 and 2 was projected to give the contribution to levels 1 and 2 by reaction 8. The branching ratio for reactions 7 and 8 with this projection is

$$\frac{R(7)}{R(7) + R(8)} = \frac{P_7(1) + P_7(2)}{[P_7(1) + P_7(2) + P_8(v=1,8)]} = \frac{0.976 + 0.197}{(0.976 + 0.197) + 0.118}$$

where $P_7(v)$ represents the relative population in level v from reaction 7 and so forth. The branching ratio value is 0.91, in excellent agreement with other determinations. Thus, reaction 8 is sufficient to account for the observed radiation at higher vibrational levels and it is not necessary to attribute the radiation to an additional source. It is therefore reasonable to take the NO^+ emission as predominantly due to reactions 7 and 8, in which case the nascent distribution in Table 1 is directly proportional to the detailed reaction rates.

CONCLUSIONS

Spectral measurements of the emission produced by energetic electrons impacting the atmosphere have been examined for infrared radiation from NO^+. High resolution measurements by a Michelson-type interferometer spectrometer have produced spectra having about 2 cm^{-1} spectral resolution. An interferometer spectrum has permitted identification of over 40 vibration-rotation lines belonging to NO^+; thus, its identification has been established. From the spectrometer measurements and an ancillary measurement of the N_2^+ 3914 Å emission, approximately 1.6 ± 0.9 NO^+ photons per 3914 Å photon was derived. The energy efficiency of NO^+ photons produced relative to ion pair production was determined to be $6.1 \times 10^{-4} \pm 3.4 \times 10^{-4}$. The emission from NO^+ was severely quenched by electron recombination. A spectral model was developed and used to analyze the measured radiation. Analysis shows the emission is non-Boltzmann with high level vibrational levels being populated, but with a preponderance in levels 1 and 2. Source mechanisms were reviewed, with most-likely production mechanism of NO^+ identified as the reaction of N_2^+ and O. The vibrational populations derived from the spectrum reflect the nascent distribution and the vibrational dependent reaction rates.

129

REFRENCES

1 Stair, A.T., Jr., and H.P. Gauvin, *Aurora and Airglow*, Proceedings NATO Advanced Study Institute, University Keele, B.M. McCormac, Ed., Reinhold, New York, 365-378, 1967.

2 Picard, R.H., J.R. Winick, R.D. Sharma, A.S. Zachor, P.J. Espy and C.R. Harris, Interpretation of Infrared Measurements of The High-Latitude Thermosphere from A Rocket-Borne Interferometer. Adv. Space Res. 7, 10, 23-30, 1987.

3 O'Neil, R.R., A.T. Stair, Jr., W.R.Pendleton, Jr. and D.A.Burt, The EXCEDE Spectral Artificial Auroral Experiment: An Overview, *Artificial Particle Beams in Space Plasma Studies*, Bjorn Grandal Ed., 207-215 Plenum Press New York, 1982.

4 Lee, E.T.P., F. Bien, M. Zahniser, R. Lyons, C. Kolb and R.R. O'Neil, EXCEDE: Spectral Final Report, *AFGL-TR-85-0125, Environ. Research Papers No. 920*, 1985

5 Henninger, M., S. Fenistein, M. Durup-Ferguson, E.E. Ferguson, R. Marx and G. Mauclaire, Radiative Lifetime for $v=1$ and $v=2$ Ground State NO^+ Ions, *Chem. Phys. Let.* 131, 6, 439-443, 1986.

6 Paulsen, D.E., P.S. Armstrong, S.J. Lipson, J. Lowell, W.A.M. Blumberg, M.E. Fraser, W.T. Rawlins, B.D. Green, R.E. Murphy, F. Bien, J. W. Duff, R. J. Rieder, R.A. Armstrong, and M. H. Bruce, Overview of Infrared Observations from EXCEDE III, *Proc. IRIS Targets, Backgrounds and Discrimination*, 1, 91-103, 1994.

7 Whalen, J. A., Aurora, *Handbook of Geophysics and the Space Environment*, A.S. Jursa Editor, 12-16, AFGL ADA 167000 1985.

8 Thurgood, V.A., and R.J. Huppi, A Cryogenic Infrared Dual Optical Channel Interferometer-Spectrometer for Upper Atmospheric Measurements, *SPIE*, 1145,591-594,1989.

9 Rieder, R.J., R.L. McNutt, S.A. Rappaport and D.E. Paulsen, A Characterization of Energy Deposition by The Primary Electron Beam on The EXCEDE III Experiment. *Visidyne Report 2067*, 1993.

10 Foreman, M.L., W.H. Steel and G.A. Vanasse, Correction of Asymmetric Interferograms Obtained in Fourier Spectroscopy, *J. of Opt. Soc. Amer* 56, 59-63 1966.

11 Winick, J.R., R.H. Picard, R.A. Joseph, R.D. Sharma, and P.P. Wintersteiner, An Infrared Spectral Radiance Code for the Auroral Thermosphere, (AARC) *AFGL-TR-87-0334*, 1987a, ADA202432.

12 Winick, J.R., R. H. Picard, R.D. Sharma, R.A. Joseph and P.P. Wintersteiner, Radiative Transfer Effects on Aurora Enhanced 4.3 Micron Emission, *Adv. Space Res.*, 7, 10, 17-21, 1987b.

13 Smith, M.A., V.M. Bierbaum, and R.S. Leone, Infrared Chemiluminescence from Vibrationally Excited NO^+: Product Branching in The $N^+ + O_2$ Ion-molecule Reaction, *Chem. Phys. Lett.* 94, 398-403, 1983.

14 Piper, L.G., The Reactions of $N(^2P)$ with O_2 and O. *J. Chem. Phys.* 98, 8560-8564, 1993.

15 Fehsenfeld, F.C.. The Reaction of O_2^+ with Atomic Nitrogen and $NO^+ \cdot H_2O$ and NO_2^+ with Atomic Oxygen, *Plant. Space Sci.*, 25, 195-196, 1977.

16 Burley, J.D., K.M. Ervin and P.B. Armentrout, Translational Energy Dependance of $(^4S) + N_2 \to NO^+ + N$ from Thermal Energies to 30 eV, *J. Chem. Phys.*, 86, 1944-1953, 1987.

17 Federer, W., W. Dobler, F. Howorda, F. Lindinger, M. Durup-Ferguson, and E.E. Ferguson, Collisional Relaxation of Vibrationally Excited $NO^+(v)$ Ions, *J. Chem. Phys.* 83 1032-1038, 1985.

18 Morris, R.A., A.A. Viggiano, F. Dale and J.F. Paulsen, Collisional Vibrational Quenching of $NO^+(v)$ Ions, *J. Chem. Phys.* 88, 4772-4778, 1988.

19 Werner, H.J. and P. Rosmus, Ab Initio Calculations of Radiative Transition Probabilities in The $^1\Sigma_+$ Ground State of NO^+ Ion, *J. Molec. Spect* 96, 362-367, 1982.

20 Hedin. A.E., MSIS-86 Thermospheric Model, *J. Geophys. Res*, 92, 4649-4662, 1987

21 Caledonia, G.E., R.E. Murphy, R.M. Nadile and A.J. Ratkowski, Analysis of Auroral Infrared Emissions Observed During The ELIAS Experiment, Accepted for publication Ann. Geophys. 1994

22 Sharma, R.D., A.J. Ratkowski, R.L. Sundberg, J.W. Duff, L.S. Bernstein, P.K. Acharya, J.H. Gruninger, D. C. Robertson and R.J. Healey, Description of SHARC, The Strategic High-Altitude Radiance Code, *GL-TR-89-0229, Environmental . Research. Papers*, No. 1036, 1989. ADA213806

23 Duff, J.W., F. Bien, P. De and D.E. Paulsen, Analysis of Time-Dependent NO Infrared Emission Observed During EXCEDE III, *Proceedings IRIS Targets, Backgrounds and Discrimination* 1, 241-249, 1993.

BLANK

PART 4

EXCEDE III SELECT SPECTRA

INTRODUCTION

The data returned from the EXCEDE III rocket borne measurement of the emissions produced by the action of a 2.6 KeV, 18 amp electron beam bombarding the atmosphere is very extensive. Presently the data base is being developed from the measurements by many instruments carried on board the experiment. Of this data, much interest is in the spectral measurements made with the Michelson type interferometer-spectrometer. By the nature of the interferometer, the data is extensive and requires substantial computer manipulations and detailed hand calculations in order to produce validated spectra. The process to produce the interferometer data base has recently been initiated but is as yet not complete. However, in the meantime, it has been suggested that it would be very beneficial to provide a sampling of the spectral data to permit judgment as to its applicability to a host of problems related to high altitude nuclear burst phenomenology. The purpose of this presentation is to make available a smattering of the spectra recovered from the experiment which covers the full spectral range (2 - 22 micrometers) at the best resolution the data will accommodate. The resolution capability of the instrument is about 2 cm^{-1} but the signal-to-noise is not always sufficient to warrant producing the recovered spectra to that resolution. When the signal level is marginal the spectral resolution can be reduced in the computer calculations to give an improved signal to noise ratio in the recovered spectra.

Three samplings of the spectral data from the interferometer are presented. They correspond to the occurrence of maximum energy dosing of the atmosphere by the bombarding electrons at an altitude of about 103 Km at IRIG time 7:03:23 of the day of the flight. The second series of spectra corresponds to the apogee of the flight, near 115 Km, occurring at IRIG time 7:04:10. The third series of spectra was collected on down-leg at 103 Km at an IRIG time of 7:05:07. In addition, spectra of the quiescent background for channel 2 at IRIG time 7:03:18 is provided since the natural background intensity is so important to the data in that spectral region. The channel 2 background emission shows relatively little change over the altitude of the flight, decreasing very slightly with altitude.

The raw field data interferograms have undergone correction which includes de-trending, spike removal, ripple removal, hand filtering and so on. The spectra from channels 1 and 2 are the result of 8192 data points with triangular apodization. Channel 3 and 4, sampled at twice the interval are the result of 4096 point transforms corrected using the Mertz technique. The plots for 4 channels 1 and 2 have been interpolated by five using the zero fill method so that there are output points at about 0.2 cm^{-1}. Likewise, channels 3 and 4 are interpolated so that there are output points at about the same interval in wavenumbers. Thus, the output points in the plotted spectra are about ten times that of the spectral resolution.

Absolute intensity values are presented in the display and were obtained with the pre-flight calibration data supplied by Utah State University and, therefore, must be considered as preliminary. A complete post flight calibration would give more reliable absolute values for the spectral data. It is anticipated that such a post-flight calibration will be performed to give the more accurate values for the spectral radiance. With this calibration the final spectral measurements will be generated in absolute units.

The spectra are presented as linear plot os radiance vs. wavenumber and simi-log plots of the same quantities. The nature of the plots easily permits identification of the intensity scales. Interesting spectral features are expanded to show the spectral features in more detail. The spectral channel and IRIG time are shown at the top of each plot. The format is to give the spectral events as designated by IRIG time. The resolution on the spectral plots of channel 1 for events 4:10 and 5:07 include degrading the resolution to 12 and 50 wavenumbers due to the very weak intensity of the emission. This spectral resolution change is made very obvious by text included on these few plots.

EXCEDE III

INTERFEROMETER CHANNELS 1 -4

BEAM ON
IRIG TIME 7:03:23   103 KM

EXCEDE III

CHANNEL 1   7:03:23
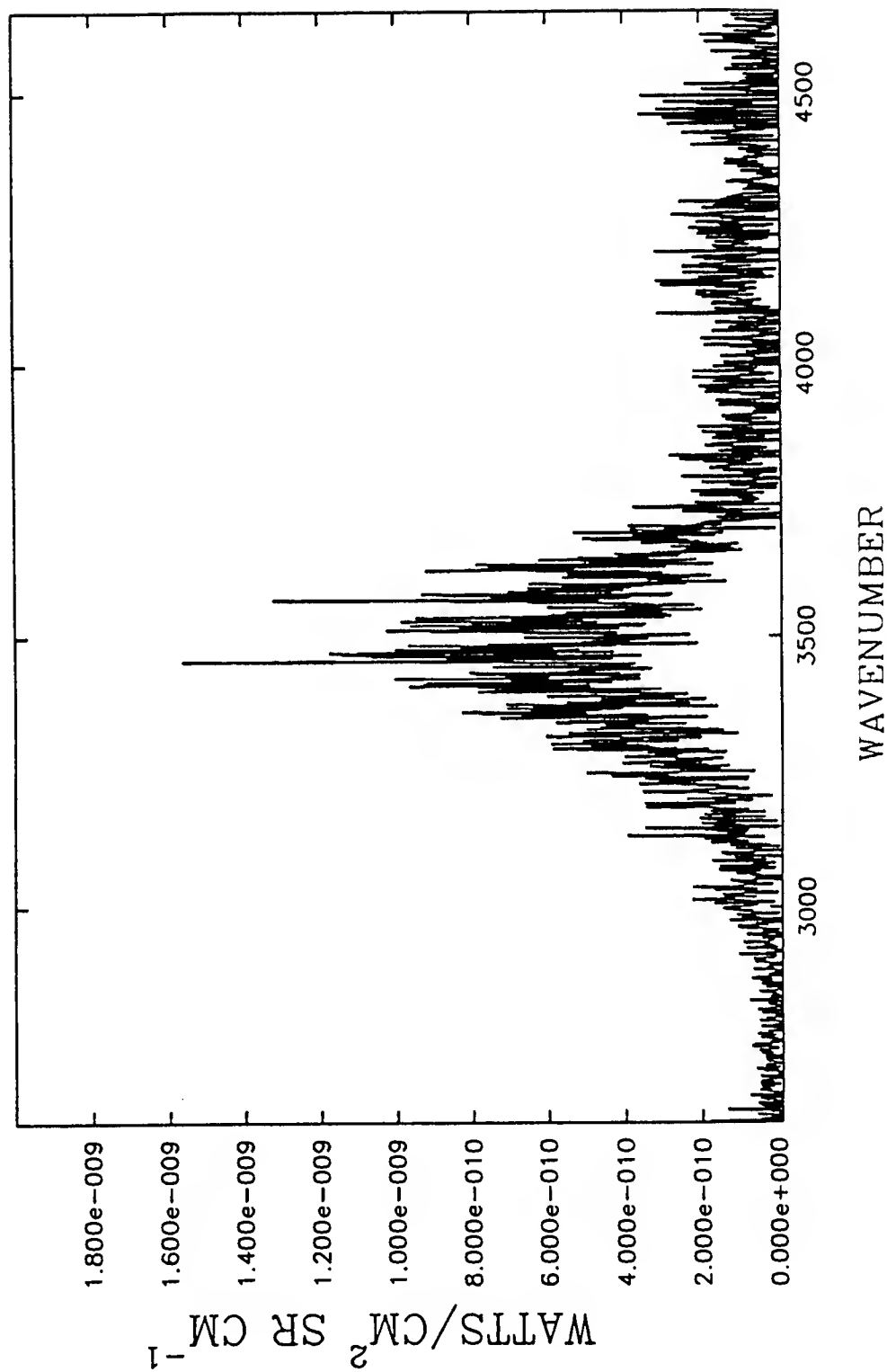
Figure 1. EXCEDE III spectra -- beam-on IRIG time 7:03:23, 103 km, channel 1
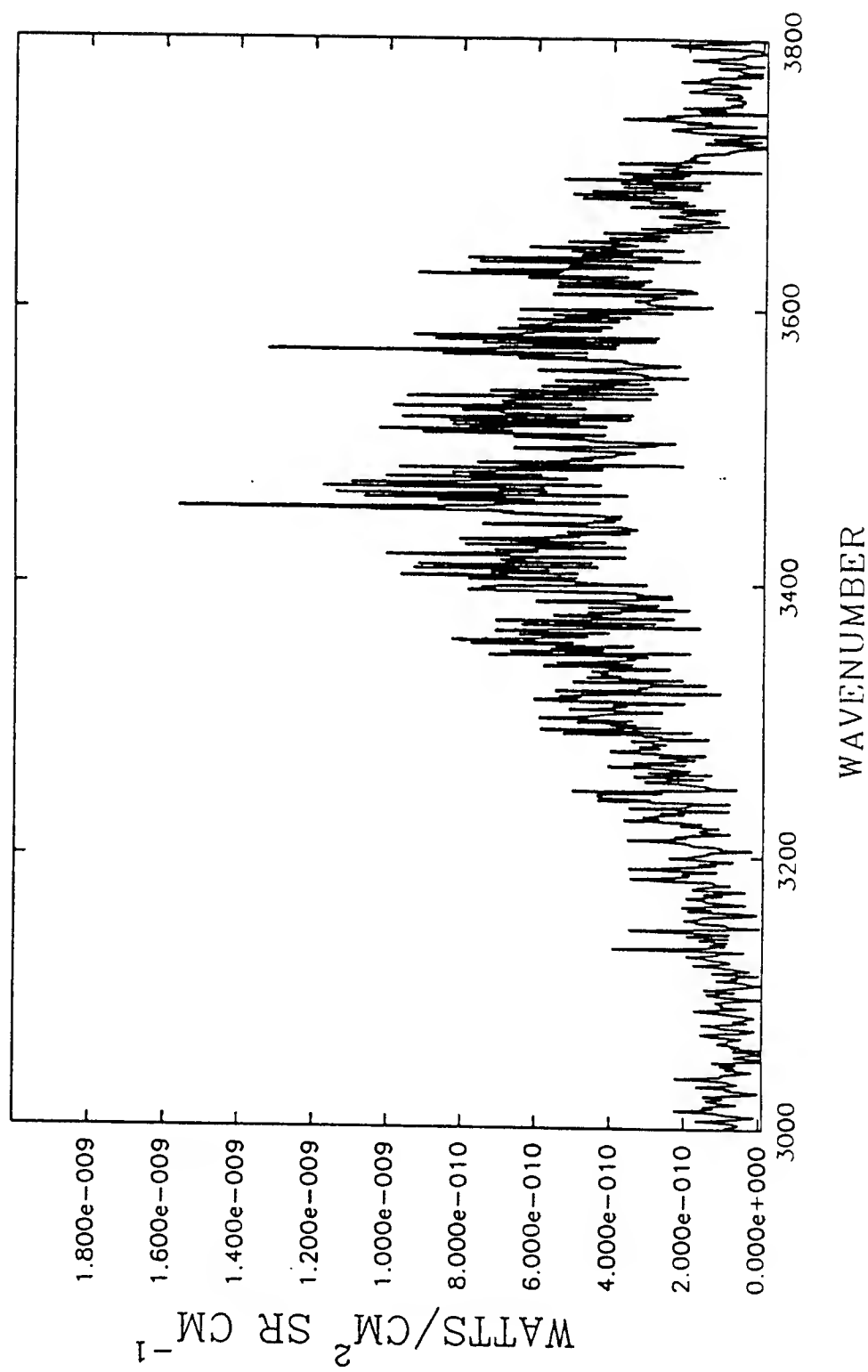
Figure 2. EXCEDE III spectra -- beam-on IRIG time 7:03:23, 103 km, channel 1

137
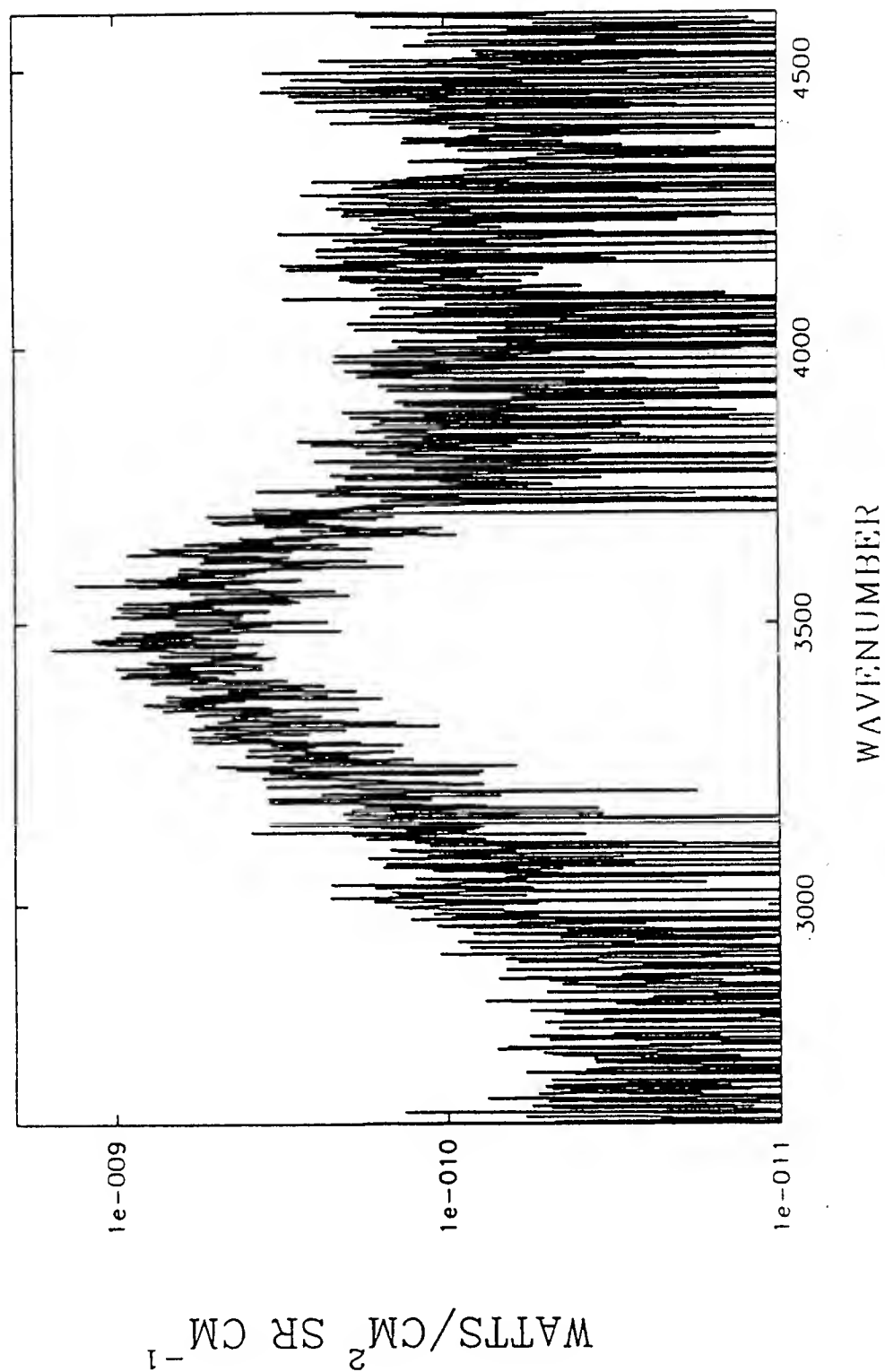
Figure 3. EXCEDE III semi-log spectra -- beam-on IRIG time 7:03:23, 103 km, channel 1

138
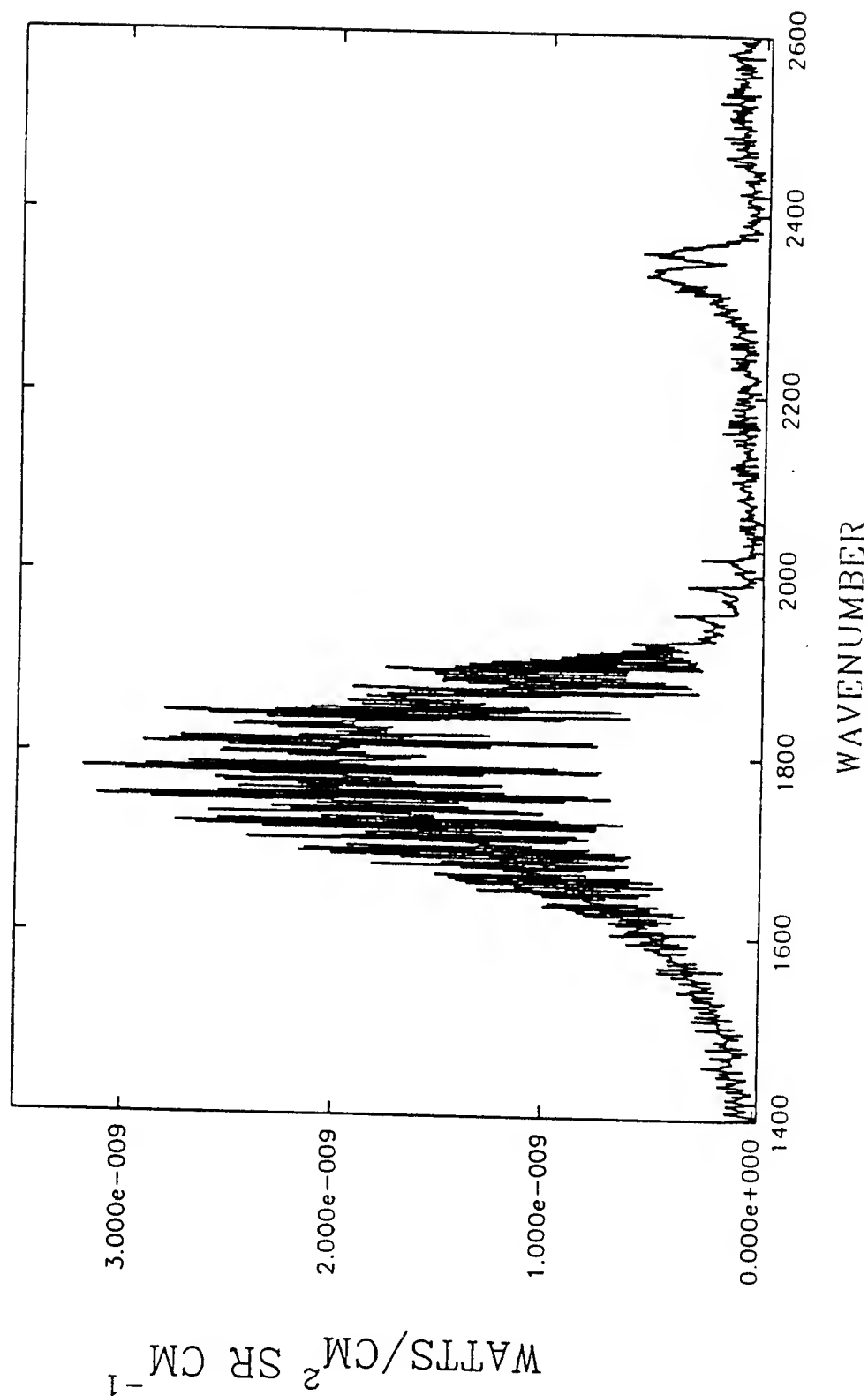
Figure 4. EXCEDE III spectra -- beam-on IRIG time 7:03:23, 103 km, channel 2.
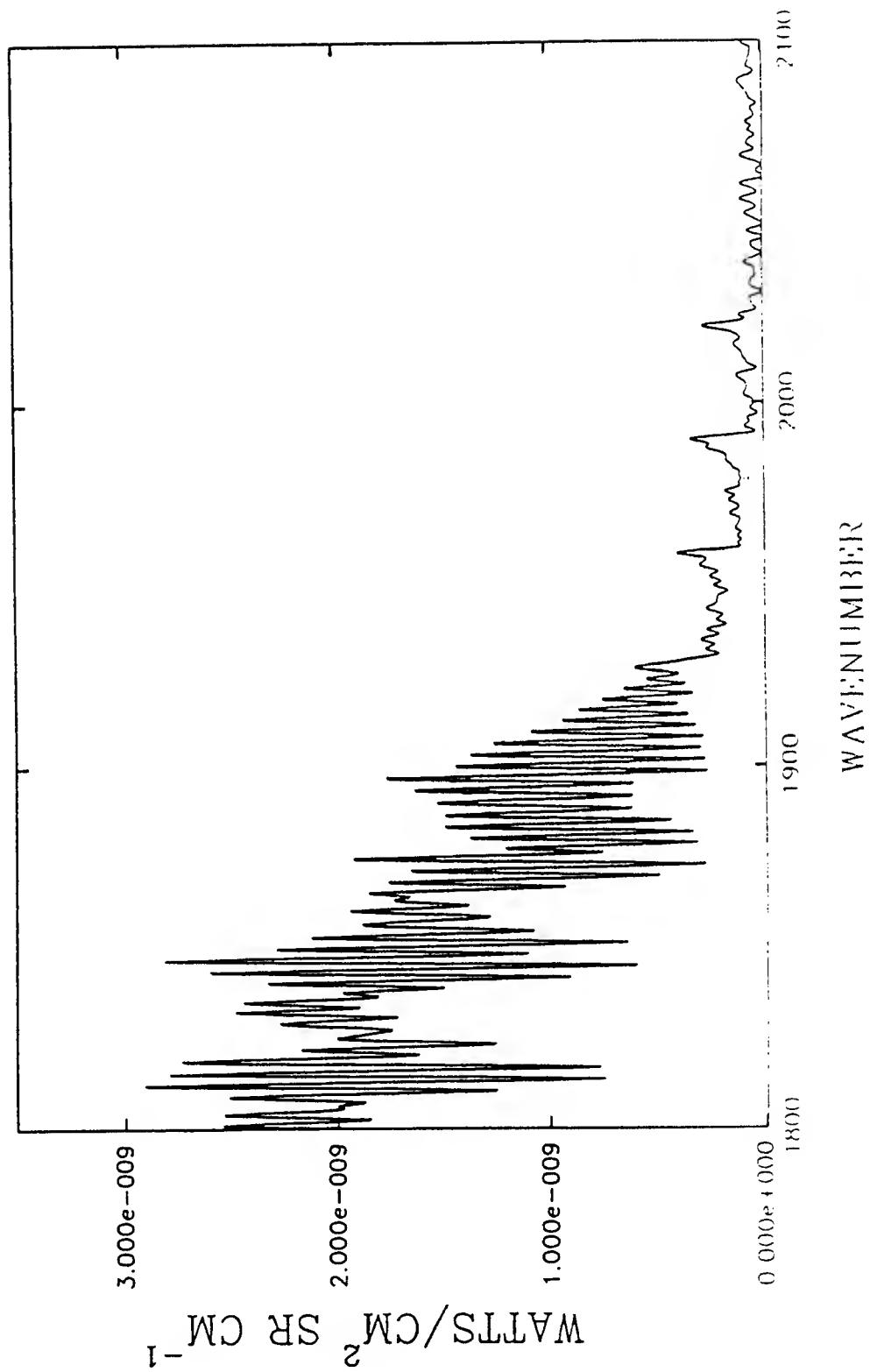
Figure 5. EXCEDE III spectra -- beam-on IRIG time 7:03:23, 103 km, channel 2.

140

EXCEDE III
CHANNEL 2   7:03:23
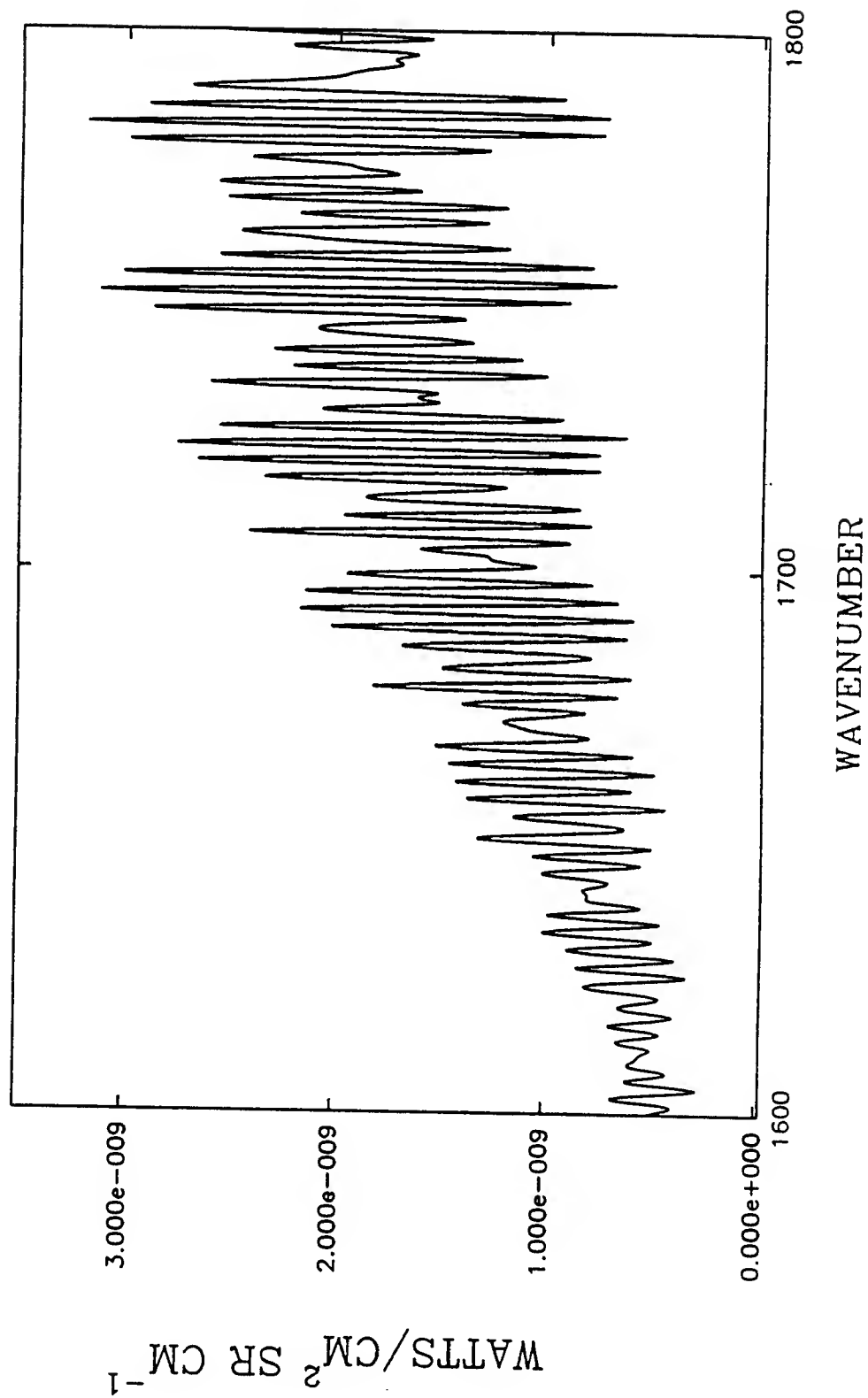
Figure 6.   EXCEDE III spectra -- beam-on IRIG time 7:03:23, 103 km, channel 2

EXCEDE III
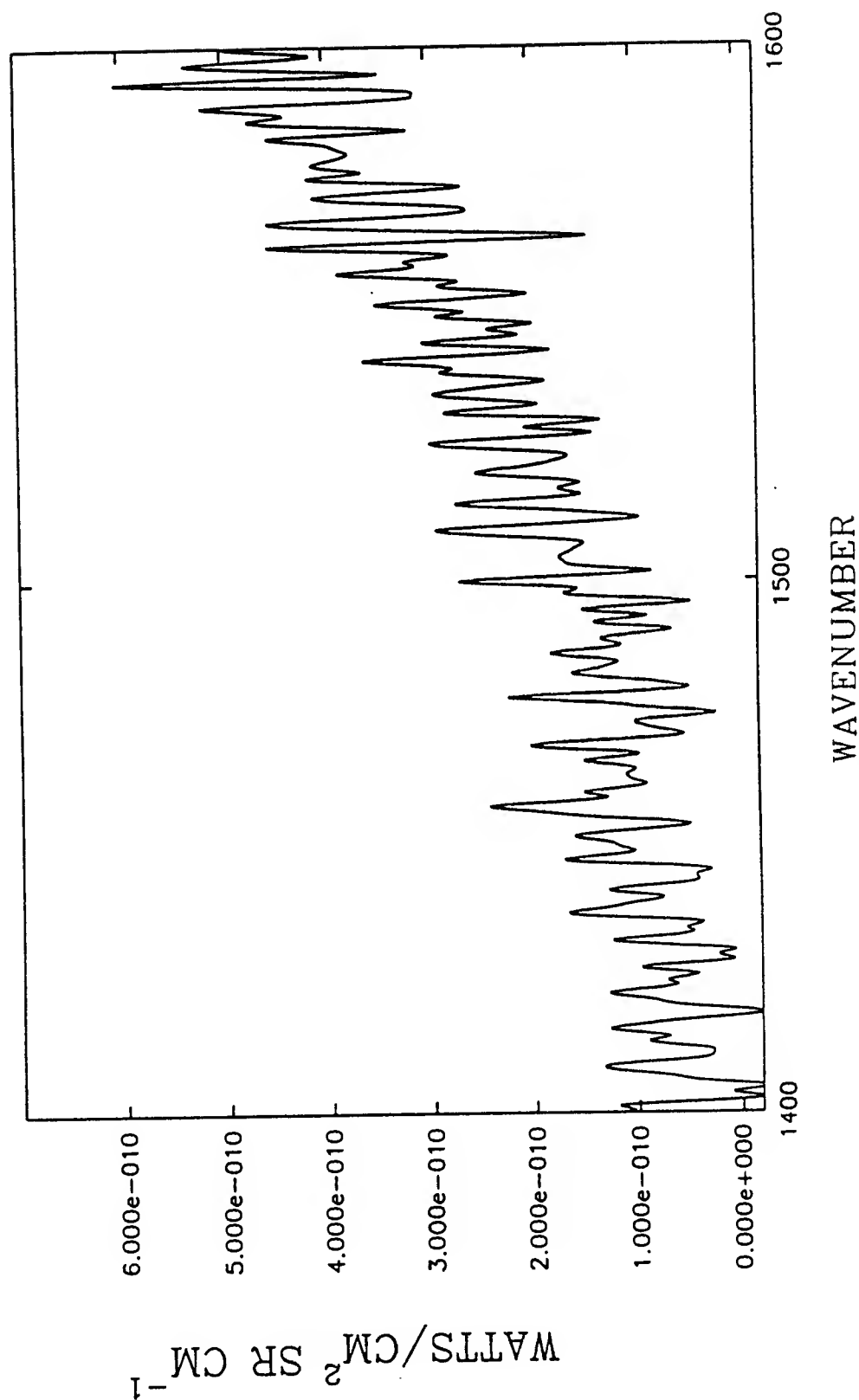
CHANNEL 2   7:03:23

Figure 7. EXCEDE III spectra -- beam-on IRIG time 7:03:23, 103 km, channel 2

142

EXCEDE III
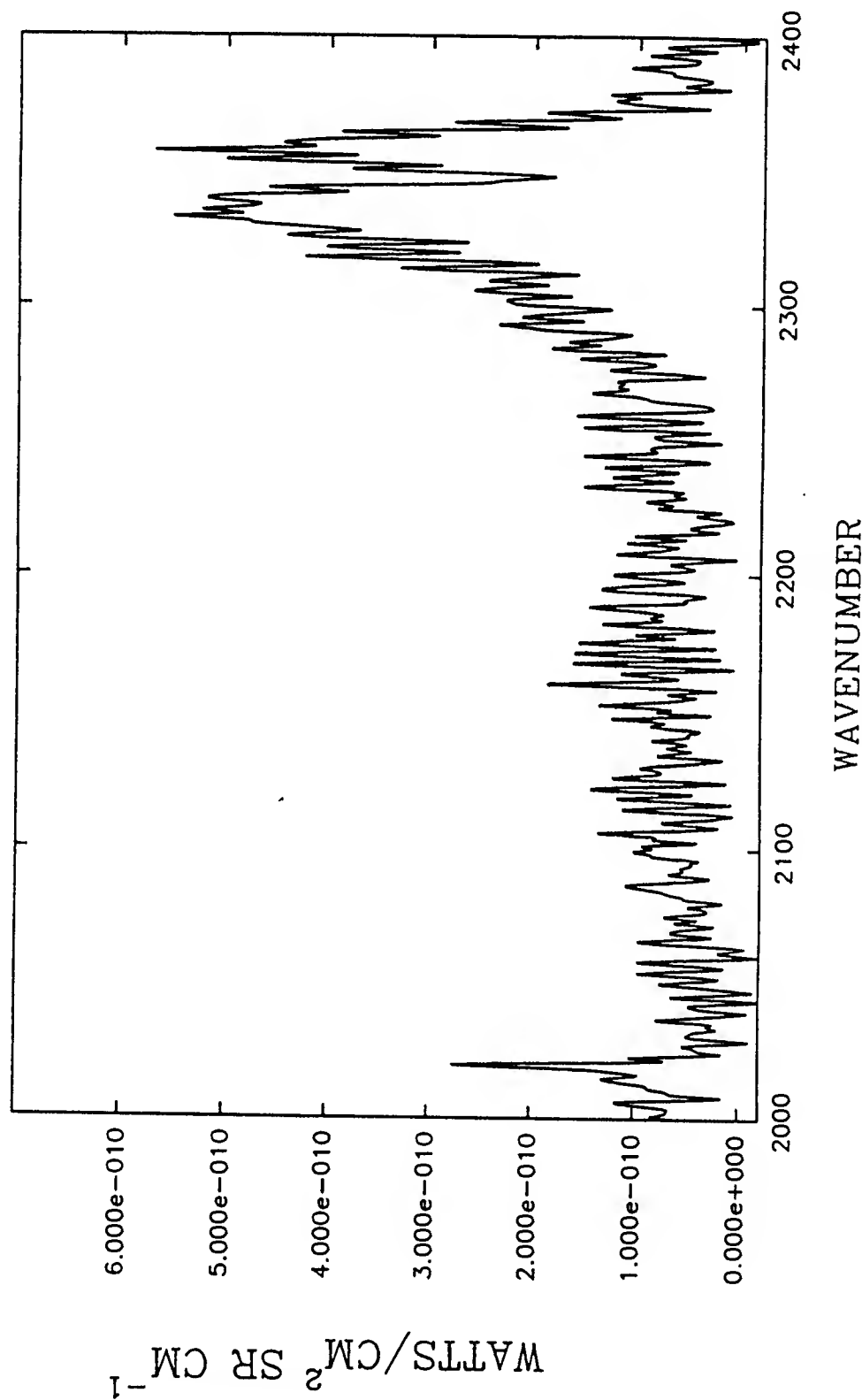
CHANNEL 2   7:03:23

Figure 8.   EXCEDE III spectra -- beam-on IRIG time 7:03:23, 103 km, channel 2

143
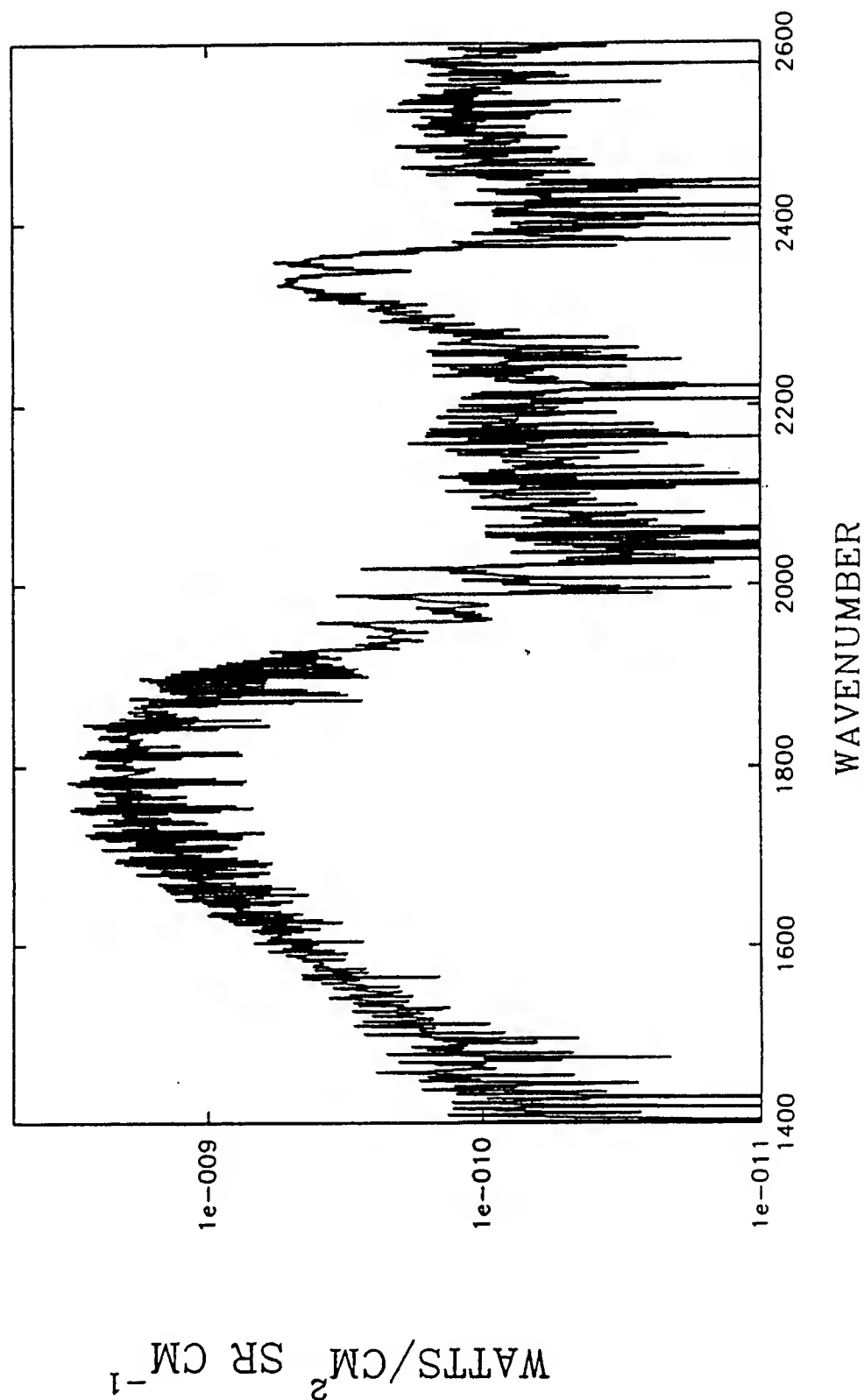
Figure 9. EXCEDE III semi-log spectra -- beam-on IRIG time 7:03:23, 103 km, channel 2.

EXCEDE III
CHANNEL 3   7:03:23
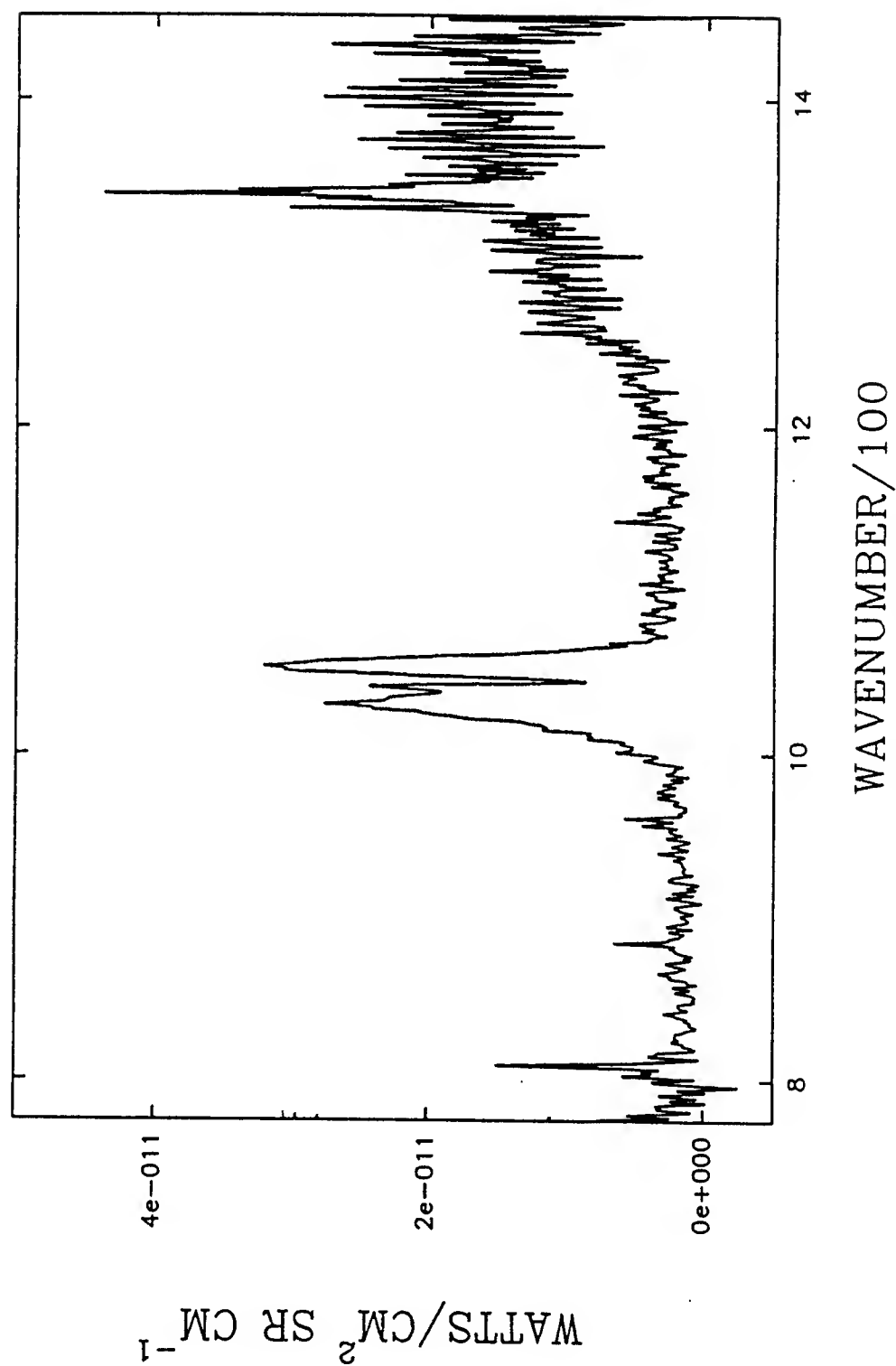
Figure 10. EXCEDE III spectra -- beam-on IRIG time 7:03:23, 103 km, channel 3.

145
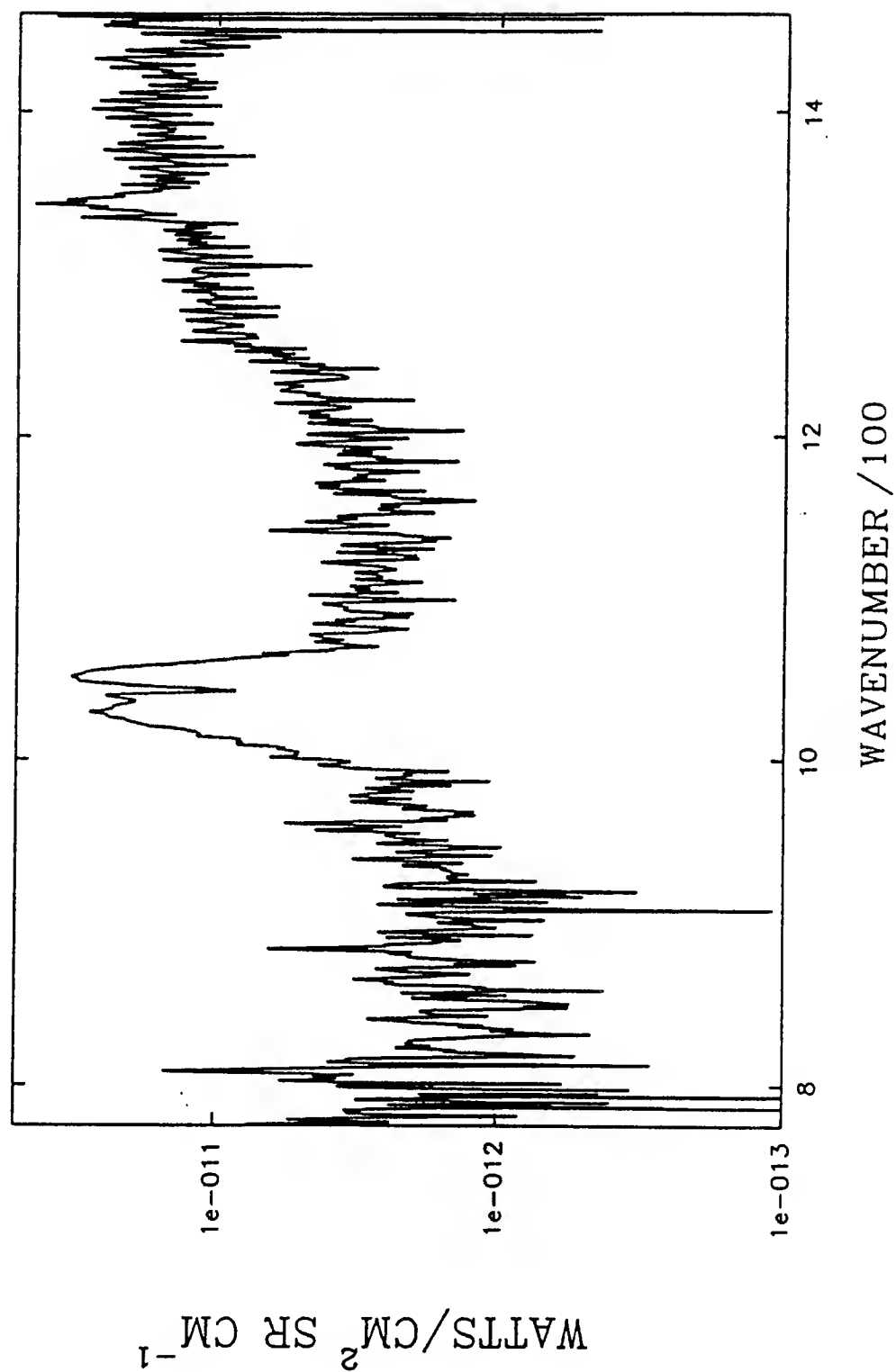
Figure 11. EXCEDE III semi-log spectra -- beam-on IRIG time 7:03:23, 103 km, channel 3
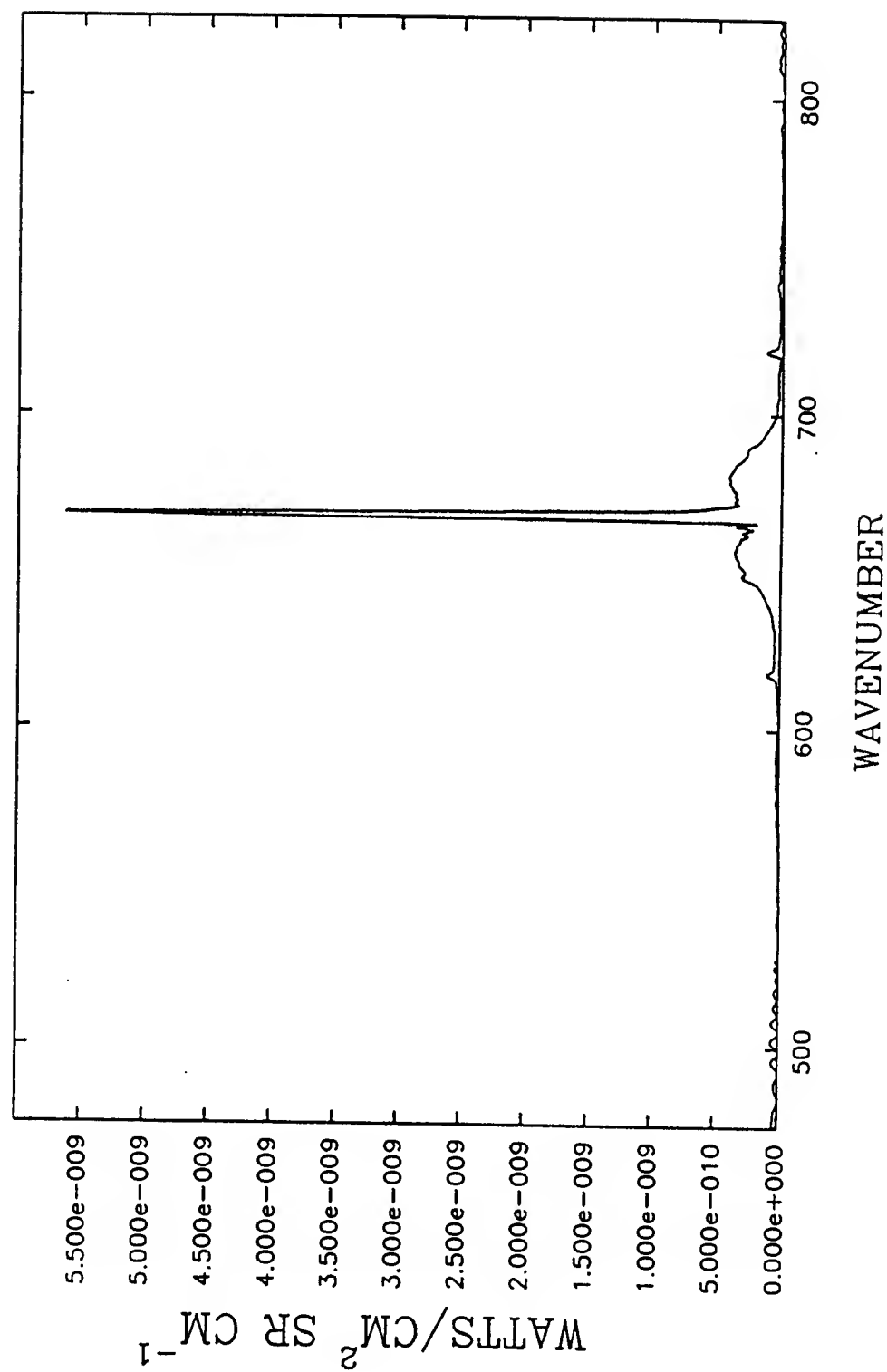
Figure 12. EXCEDE III spectra -- beam-on IRIG time 7:03:23, 103 km, channel 4.

147
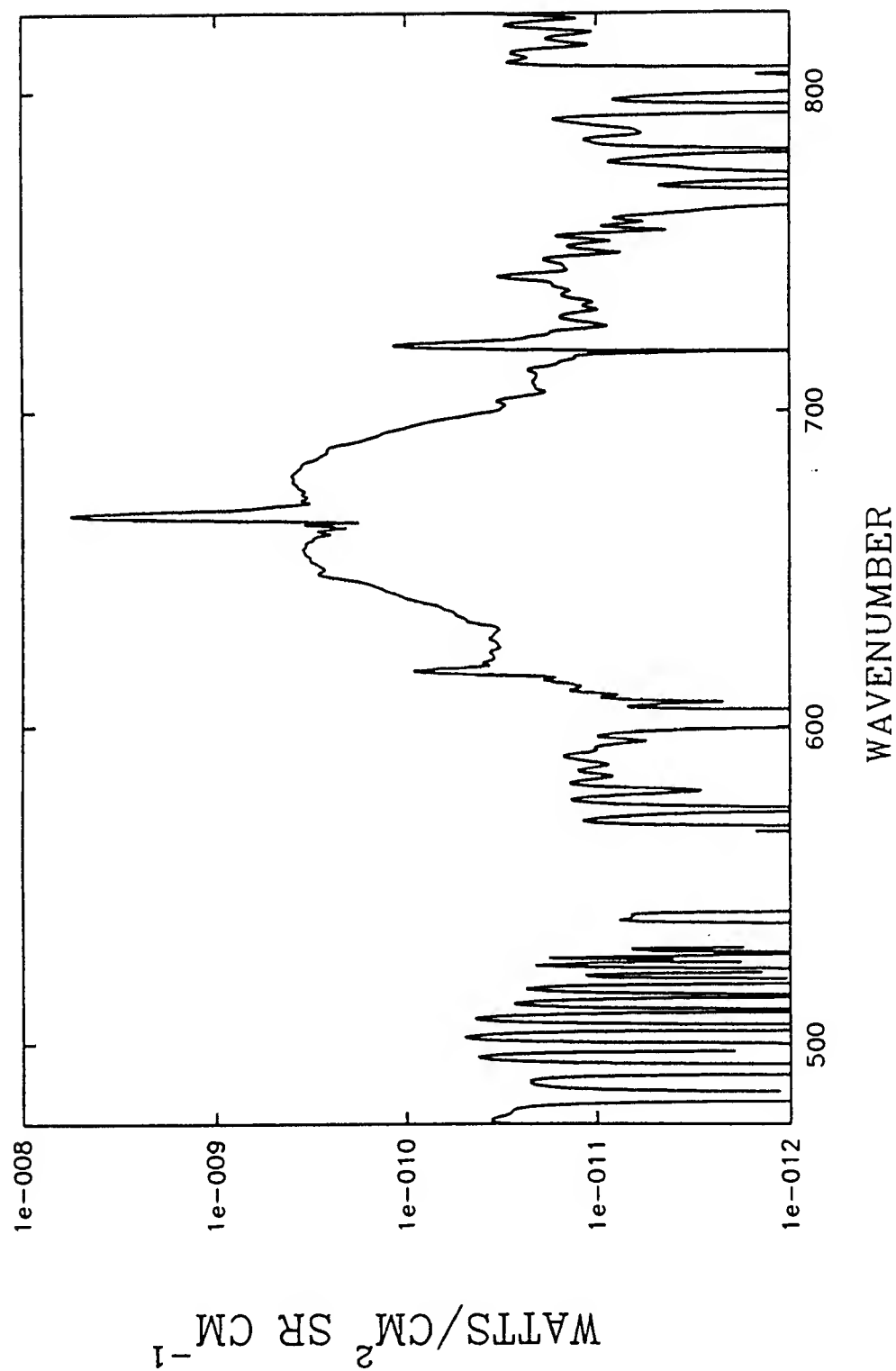
Figure 13. EXCEDE III semi-log spectra -- beam-on IRIG time 7:03:23, 103 km Channel 4.

148

EXCEDE III

INTERFEROMETER CHANNELS 1 –4

BEAM ON
IRIG TIME 7:04:10   115 KM

149

EXCEDE III

CHANNEL 1   7:04:10

50 WAVENUMBER RESOLUTION
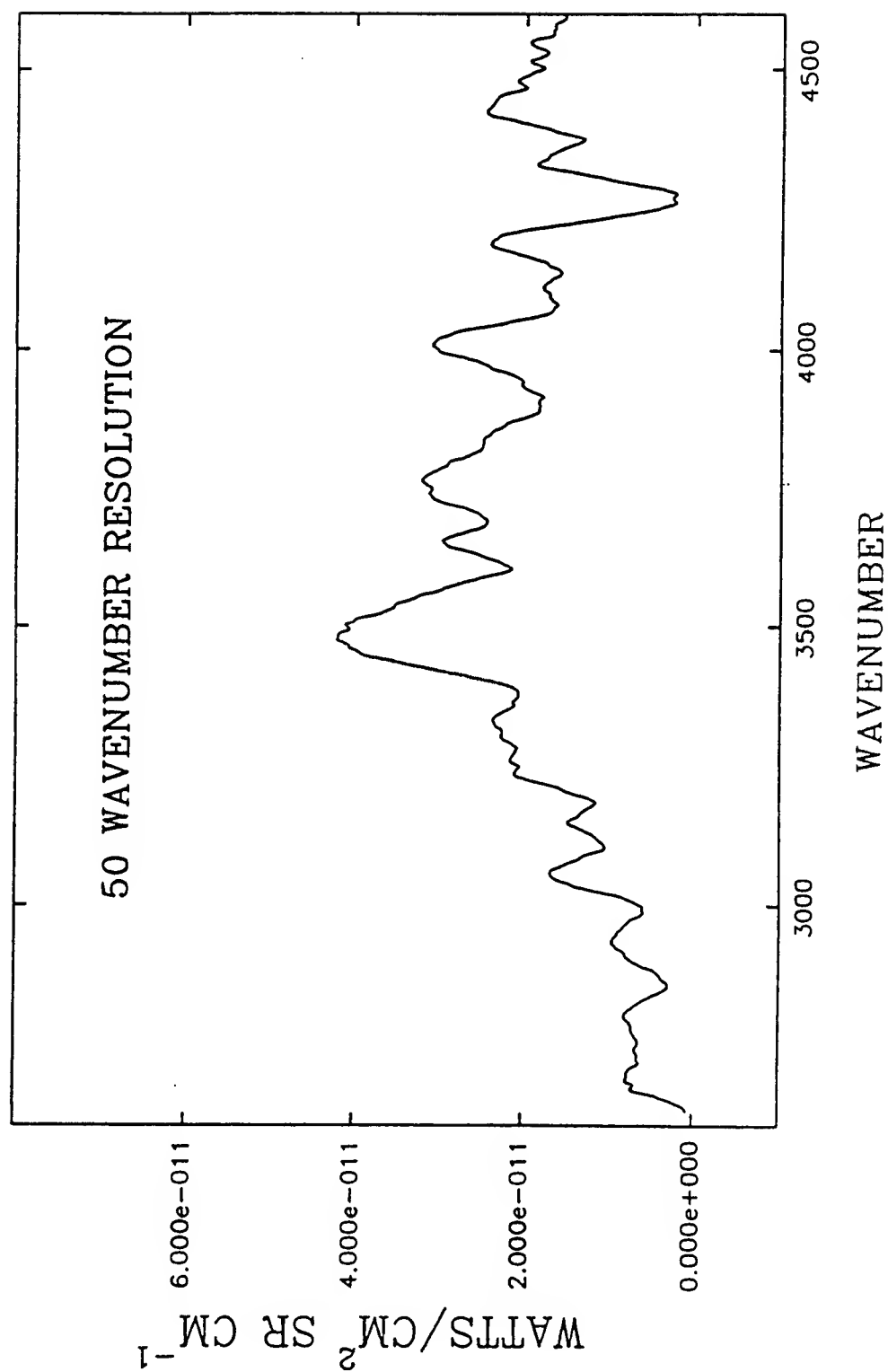
Figure 14.   EXCEDE III spectra -- beam-on IRIG time 7:04:10, 115 km Channel 1.
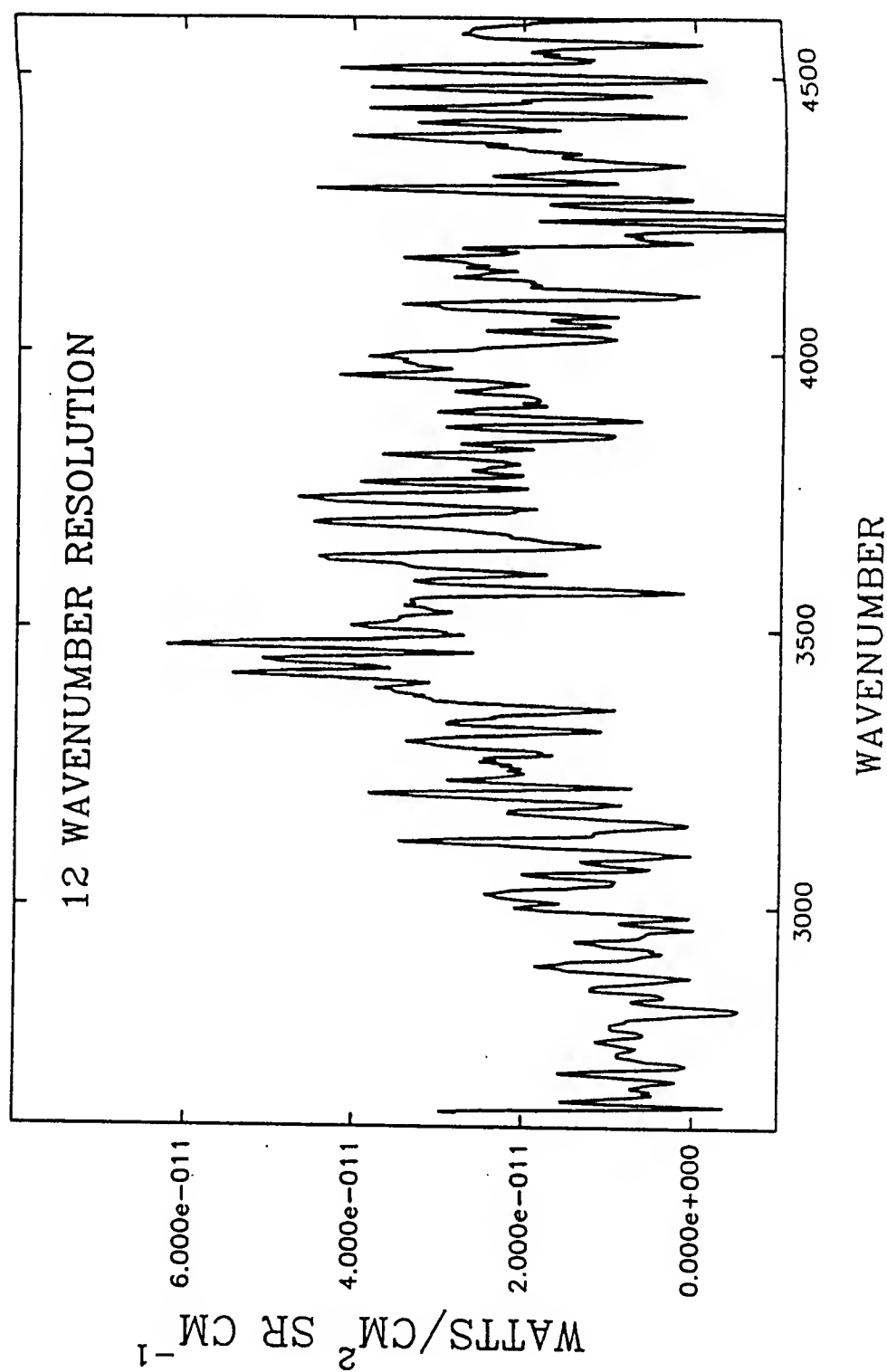
Figure 15. EXCEDE III spectra -- beam-on IRIG time 7:04:10, 115 km Channel 1.

151
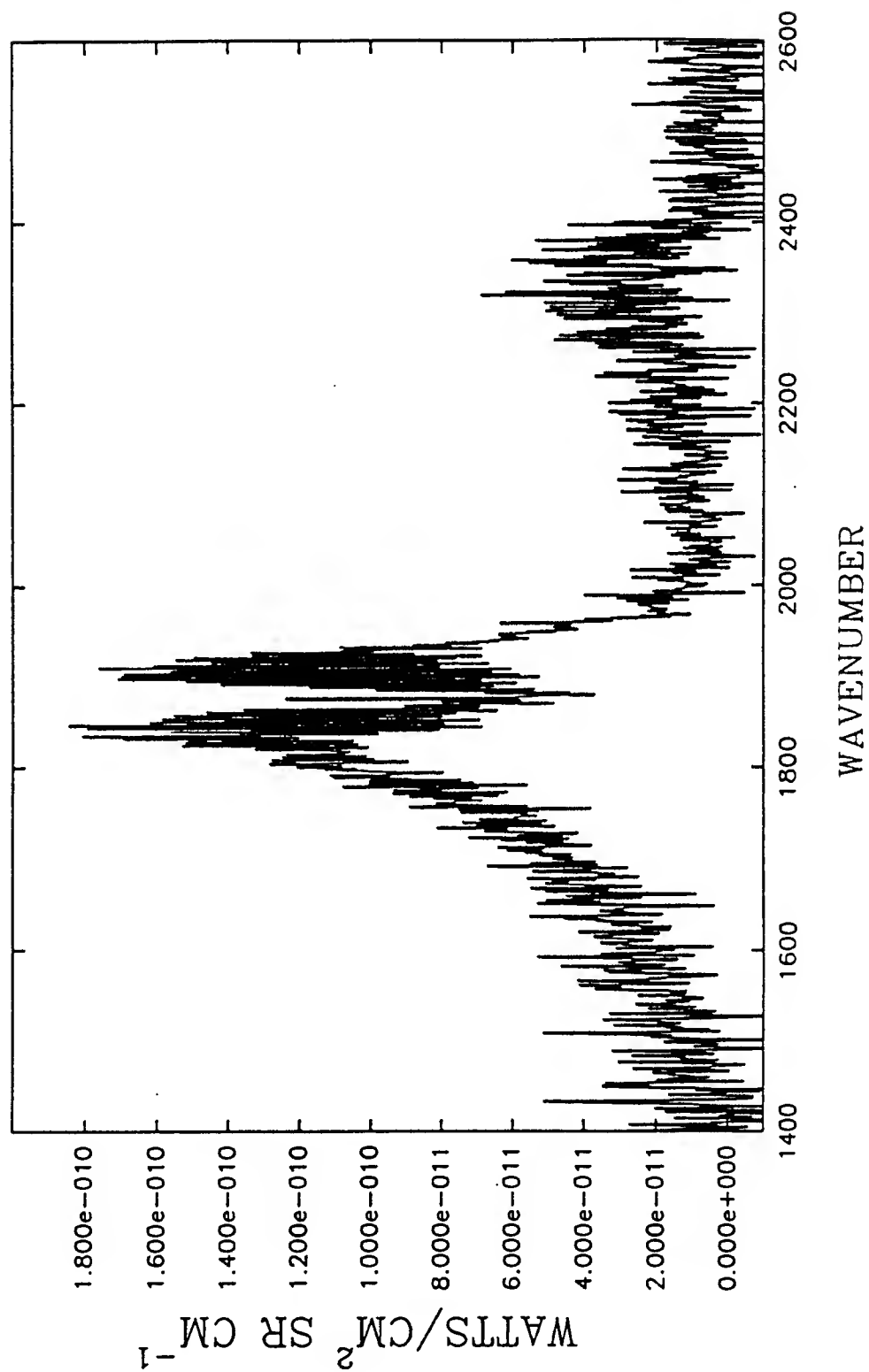
Figure 16.   EXCEDE III spectra -- beam-on IRIG time 7:04:10, 115 km Channel 2.
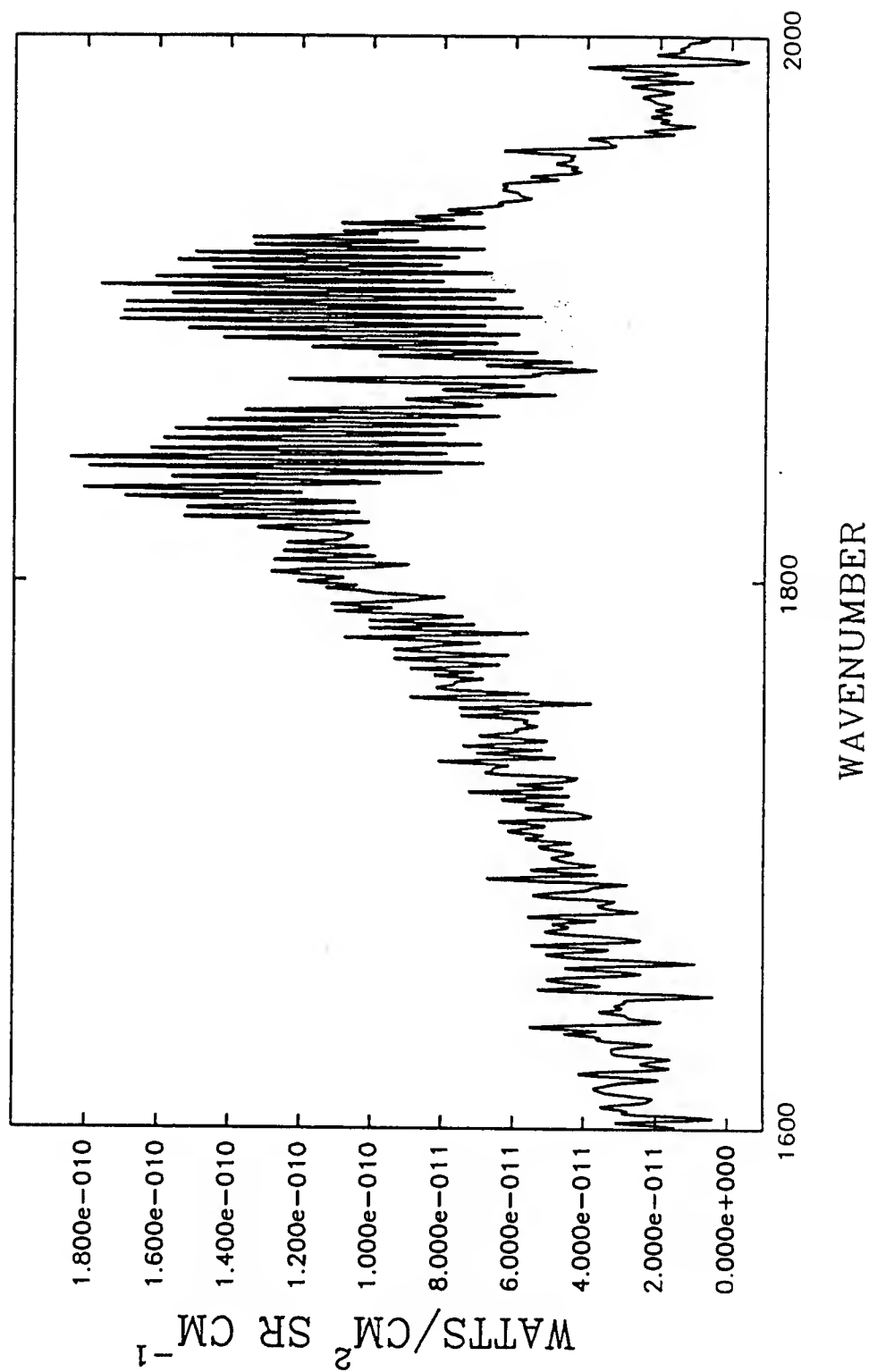
Figure 17. EXCEDE III spectra -- beam-on IRIG time 7:04:10, 115 km Channel 2.

153

EXCEDE III 7:04:10
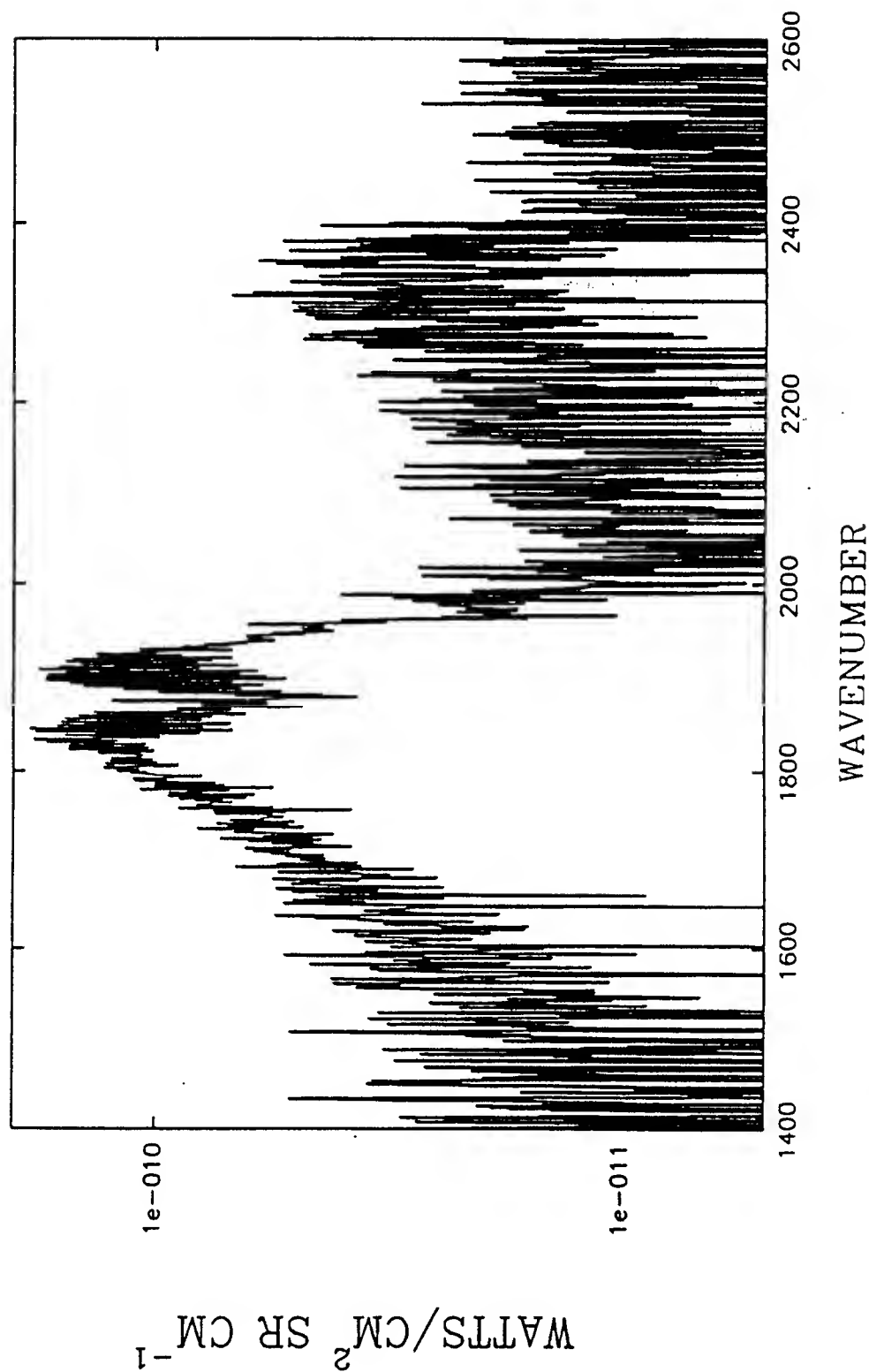
CHANNEL 2

Figure 18.   EXCEDE III semi-log spectra -- beam-on IRIG time 7:04:10, 115 km Channel 2.

154
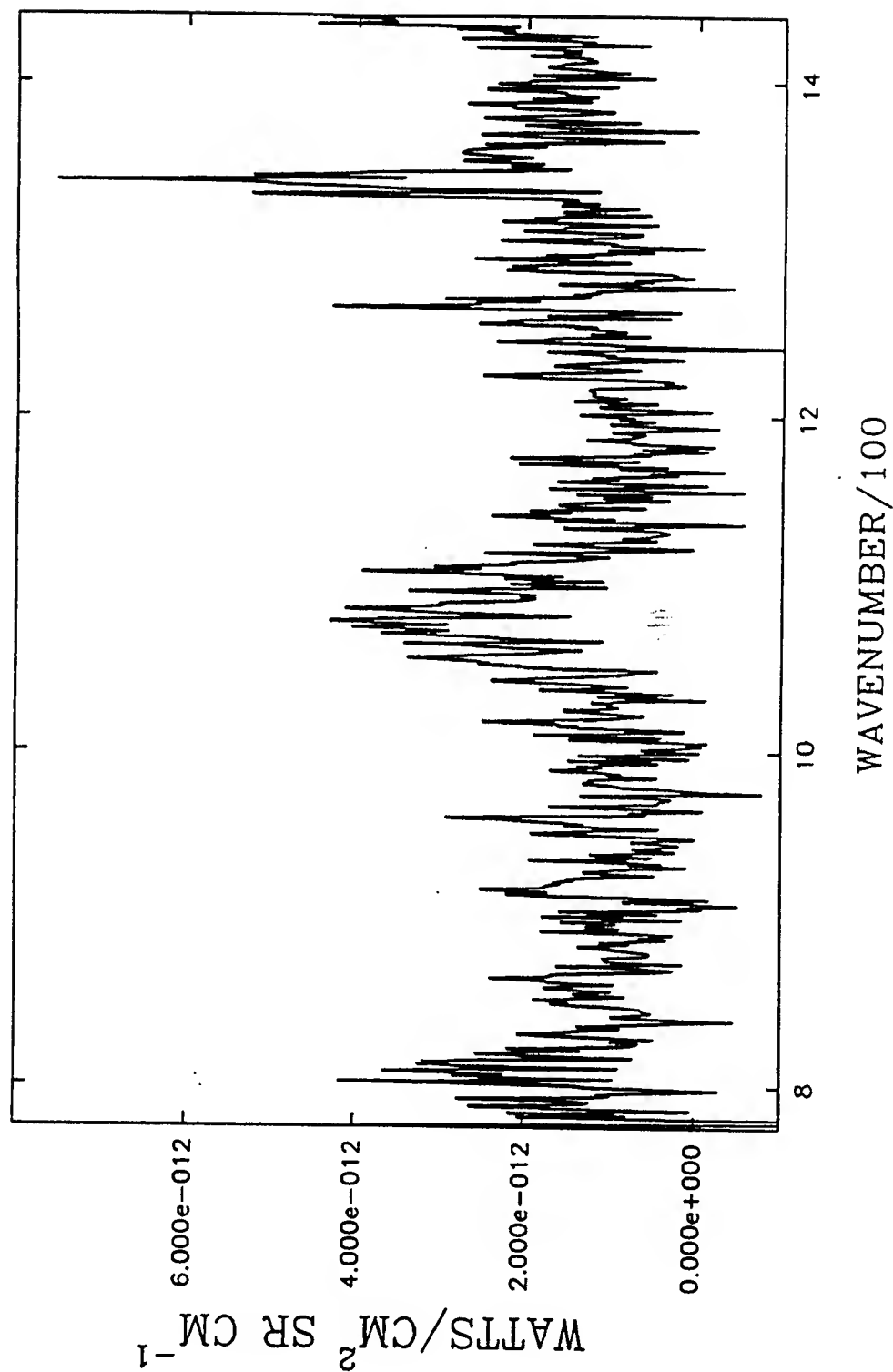
Figure 19.   EXCEDE III spectra -- beam-on IRIG time 7:04:10, 115 km Channel 3.

155

EXCEDE III   7:0 4:10
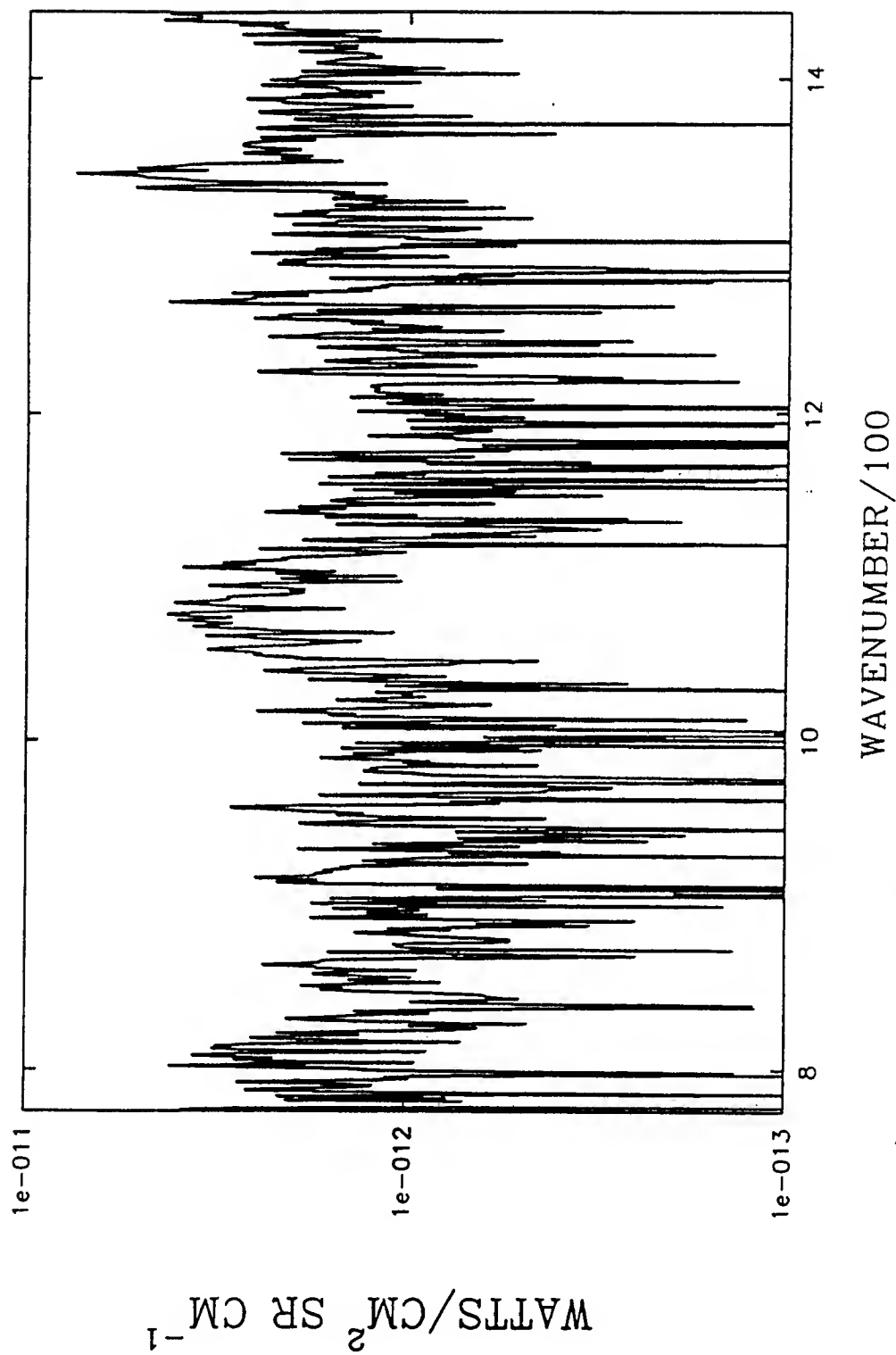
CHANNEL 3

Figure 20. EXCEDE III spectra -- beam-on IRIG time 7:04:10, 115 km Channel 3.

Figure 21. EXCEDE III spectra -- beam-on IRIG time 7:04:10, 115 km Channel 4.

157

EXCEDE III

CHANNEL 4   7:0 4:10

WATTS/CM² SR CM⁻¹

WAVENUMBER
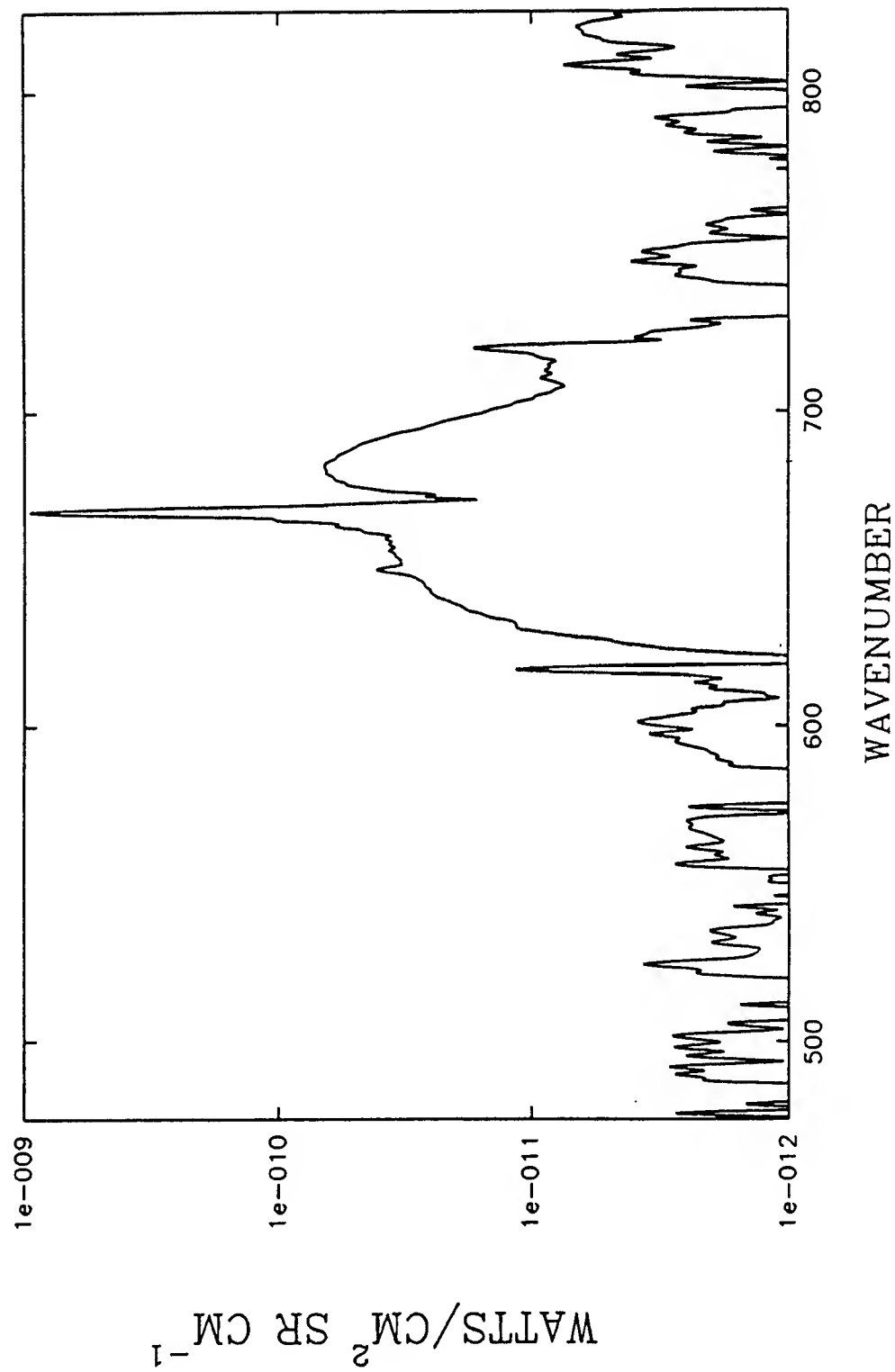
Figure 22.   EXCEDE III semi-log spectra -- beam-on IRIG time 7:04:10, 115 km Channel 4.

EXCEDE III

INTERFEROMETER CHANNELS 1 -4

BEAM ON
IRIG TIME 7:05:07   103 KM
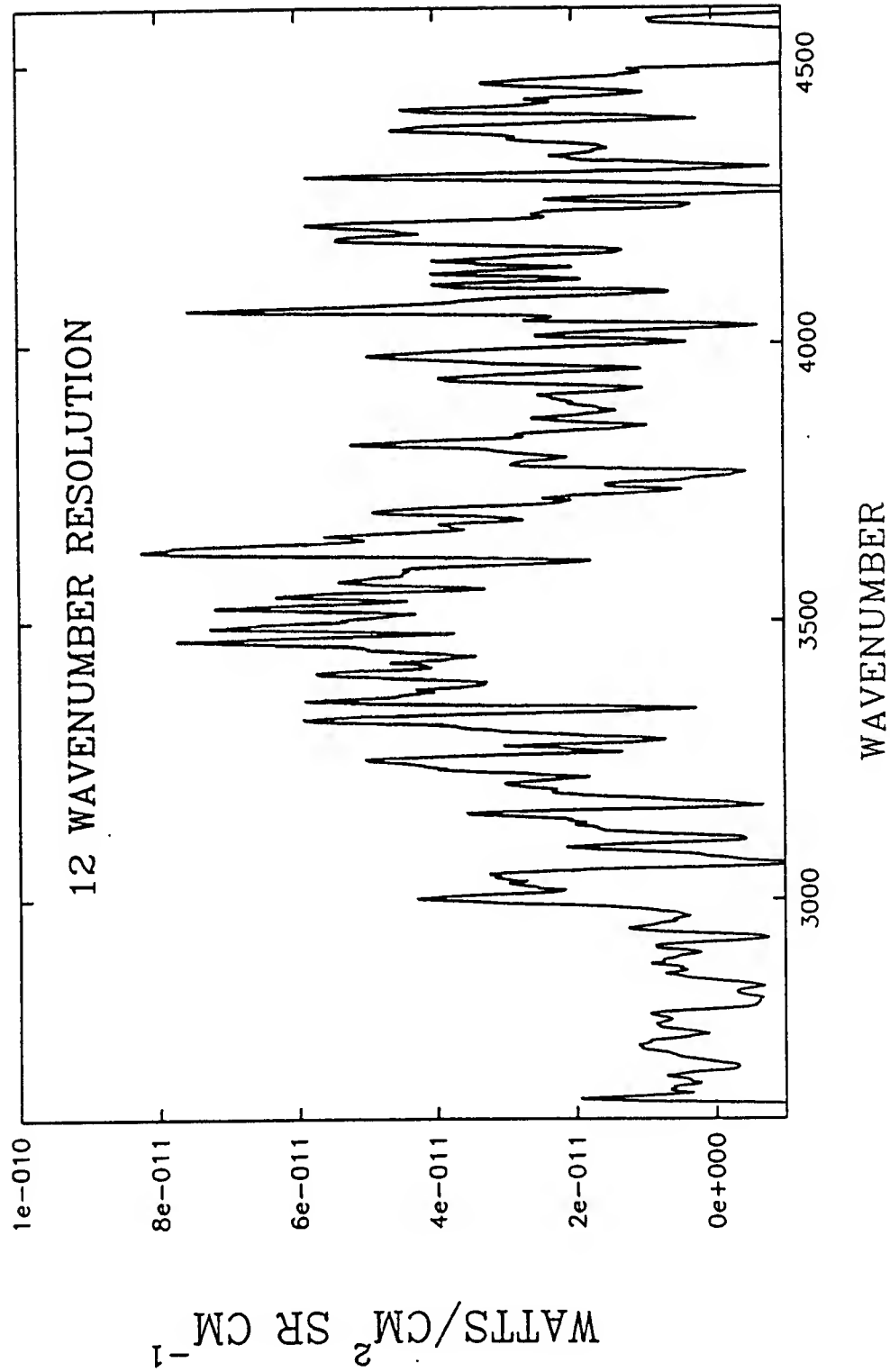
Figure 23. EXCEDE III spectra -- beam-on IRIG time 7:05:07, 103 km Channel 1.

Figure 24.   EXCEDE III spectra -- beam-on IRIG time 7:05:07, 103 km Channel 2.

161

Figure 25. EXCEDE III spectra -- beam-on IRIG time 7:05:07, 103 km Channel 2.

162

EXCEDE III

CHANNEL 2   7:05:07
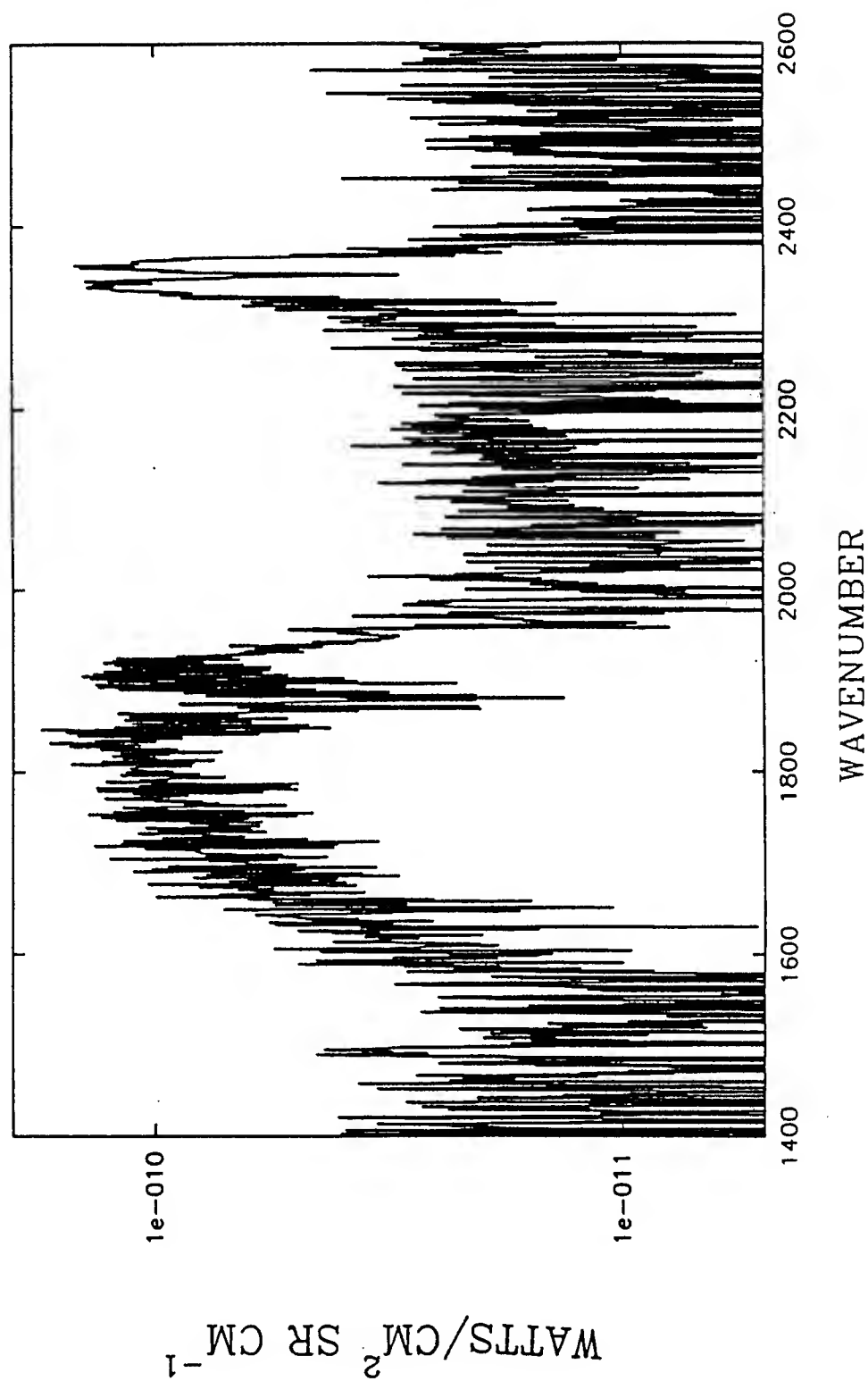
Figure 26.   EXCEDE III semi-log spectra -- beam-on IRIG time 7:05:07, 103 km Channel 2.

163
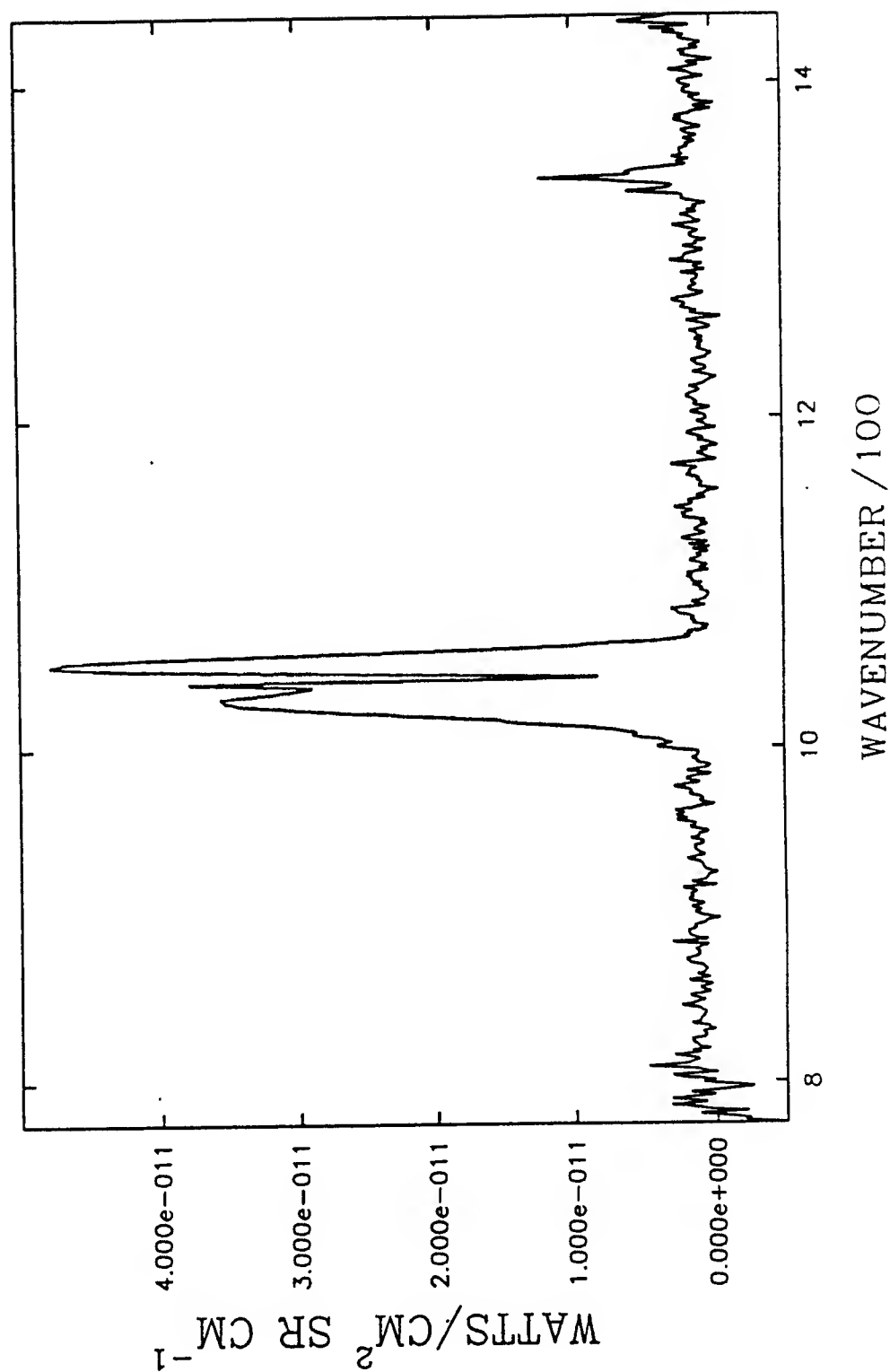
Figure 27. EXCEDE III spectra -- beam-on IRIG time 7:05:07, 103 km Channel 3.
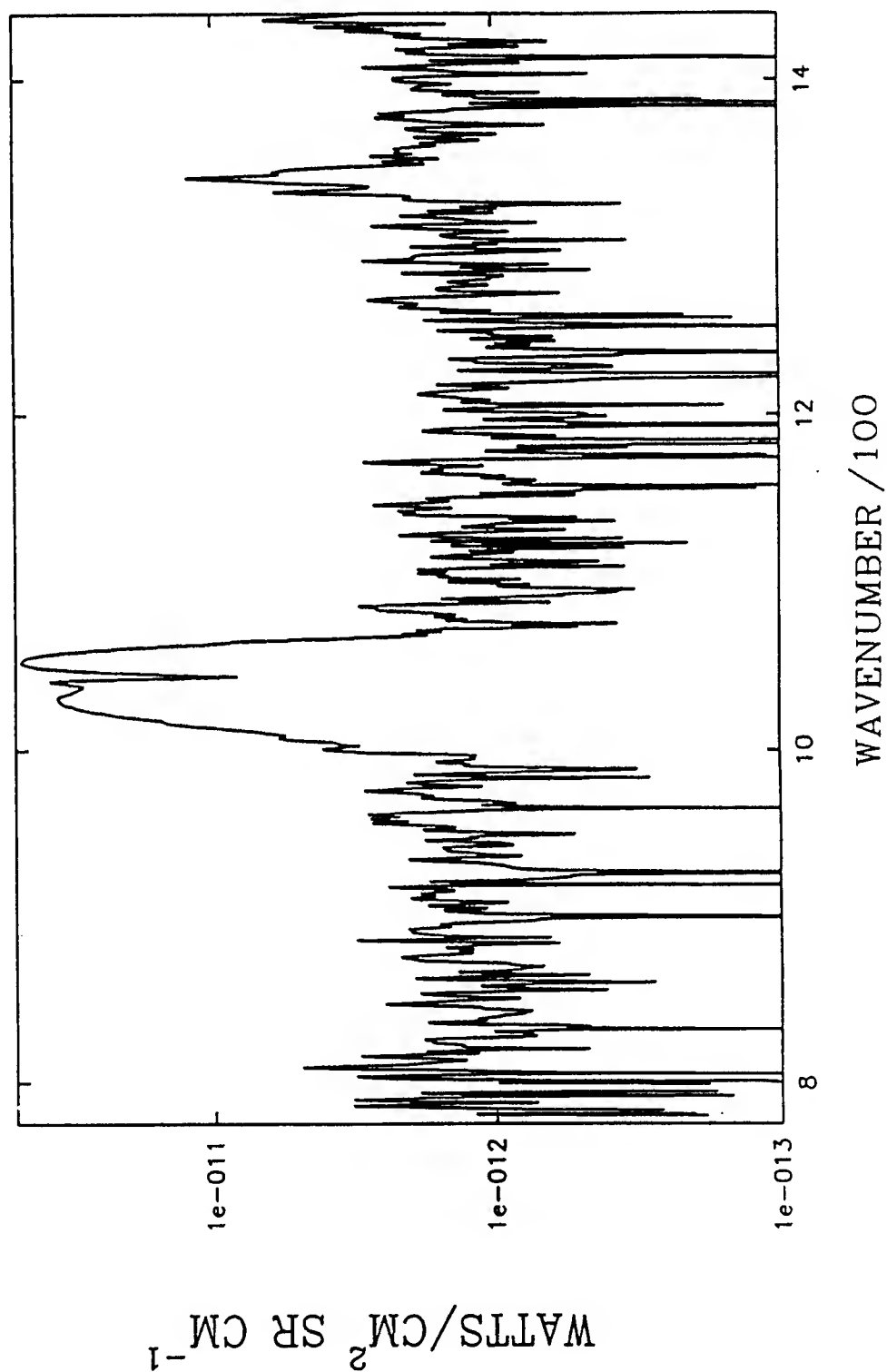
Figure 28. EXCEDE III semi-log spectra -- beam-on IRIG time 7:05:07, 103 km Channel 3.

165
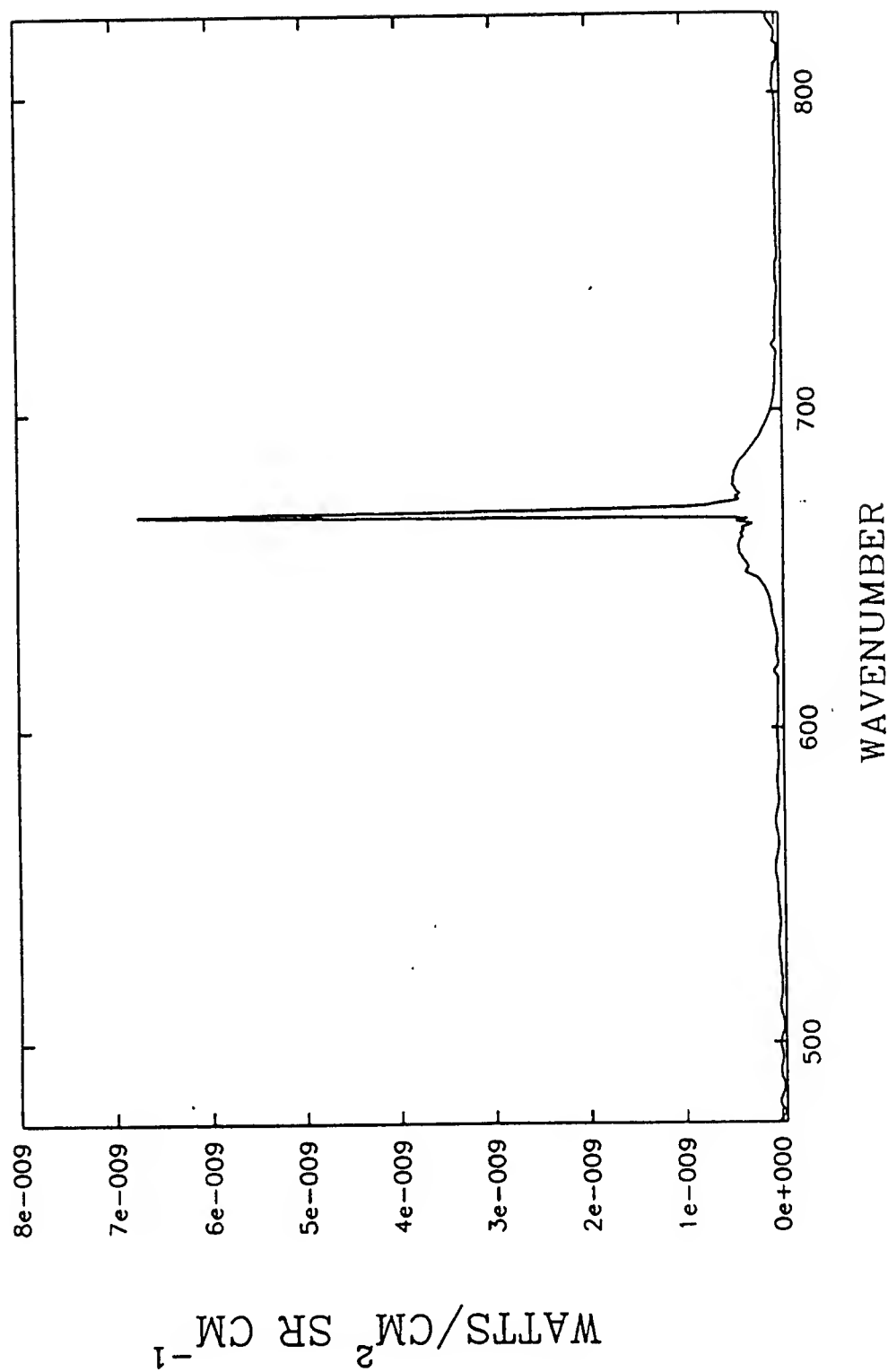
Figure 29. EXCEDE III spectra -- beam-on IRIG time 7:05:07, 103 km Channel 4.
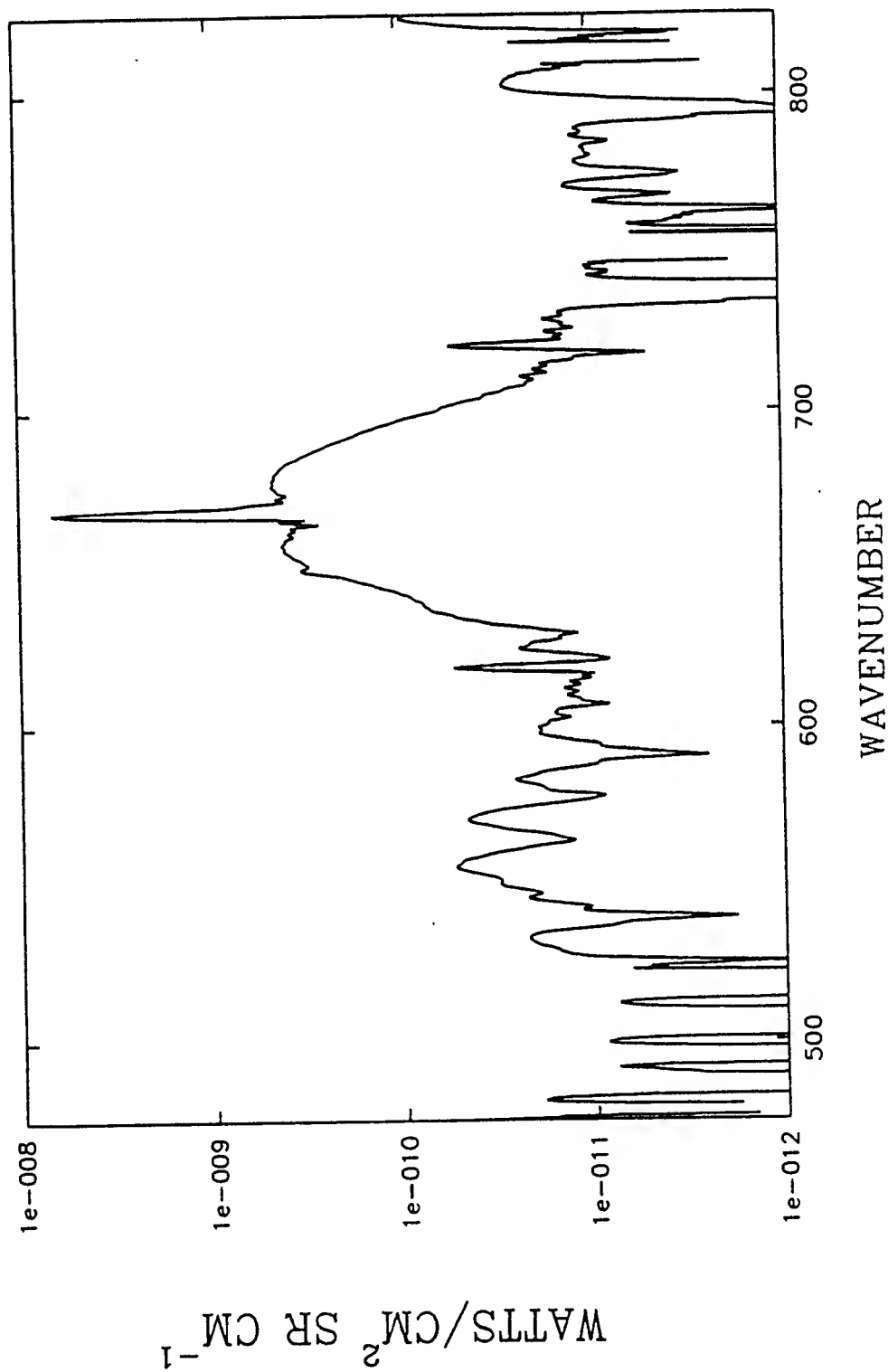
Figure 30.   EXCEDE III semi-log spectra -- beam-on IRIG time 7:05:07, 103 km Channel 4.

167

EXCEDE III

INTERFEROMETER CHANNEL 2

BEAM OFF
IRIG TIME 7:03:18   100 KM

Figure 31. EXCEDE III spectra -- beam-off IRIG time 7:03:18, 100 km Channel 2.

169

EXCEDE III
CHANNEL 2   7:03:18
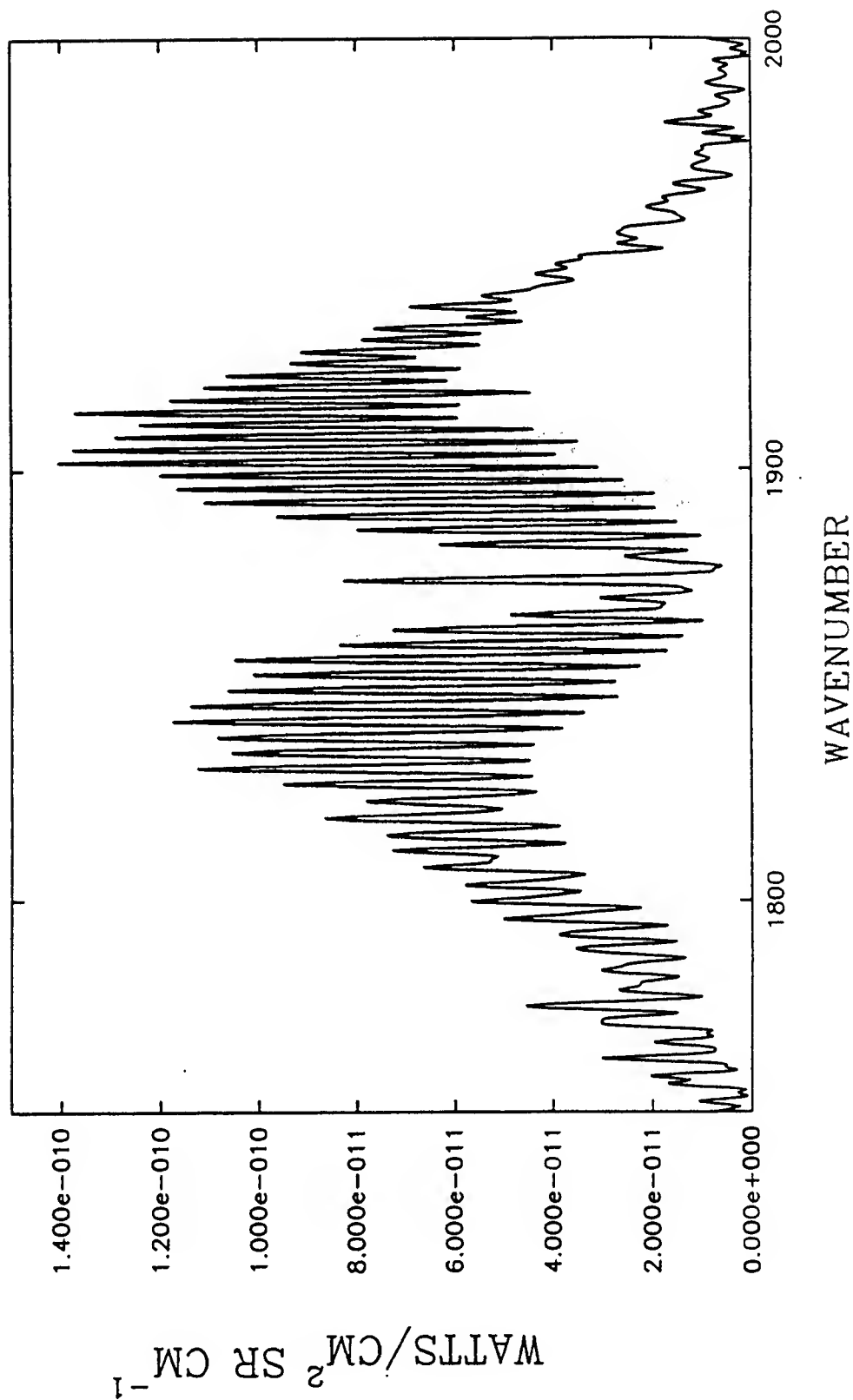
Figure 32.   EXCEDE III spectra -- beam-off IRIG time7:03:18, 100 km Channel 2.

EXCEDE III   7:03:18

CHANNEL 2   7:03:18

WAVENUMBER

WATTS/CM² SR CM⁻¹
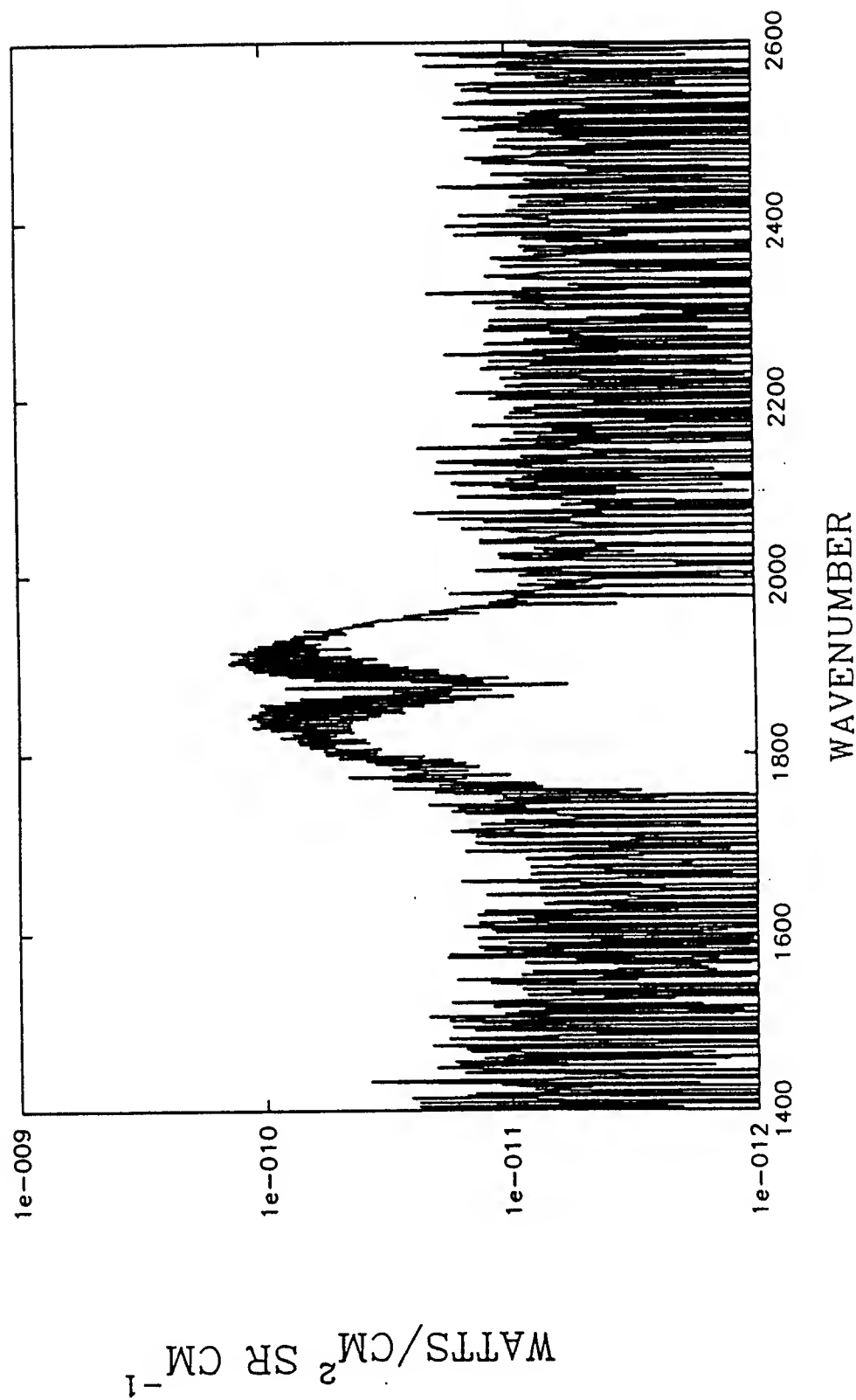
Figure 33.   EXCEDE III spectra -- beam-off IRIG time 7:03:18, 100 km Channel 2.

171

BLANK

APPENDICES

APPENDIX A

Model for NO$^+$ Spectra

APPENDIX B

Program Interperet

APPENDIX C

Program Band

APPENDIX D

Chemistry Code

BLANK

APPENDIX A

```
REM                     MODEL FOR NO+ SPECTRA

REM THE EXCEED INTERFEROMETER HE-NE LASER WAVENUMBER IS 15798.0117 CM-1 ,
REM WHICH IS 10000/15798.0117 MICRONS = 0.63299105 x 10-6 M =
REM 6329.9105 ANGSTOMS . THEN FOR LAMDA/2 SAMPLING FOR 8192 POINTS
REM THE DRIVE IS L = 6329.9105 x10-8 x8192 CM = 0.259273134 CM , AND THE
REM OPTICAL PATH DIFFERENCE OPD = 2L = 2x0.259273134 = 0.518546268 CM .
REM THE SINC SQUARED RESOLUTION IS THEN RESL = 1/(2L) = 1.928468222  CM-1 .
REM THE SPECTRAL SAMPLING IS THE 1.928468222/2 = 0.964234111 CM-1/POINT .
REM WN(I)=1024.017+0.96423411*(I-1), SO DELTA WN=0.96423411 CM-1
REM I = 1 + INT( (WN-1024.017)/0.96423411+0.5), I=1 TO 2048 ,
REM THE SAME INTERVAL AS THE "BAND.EXE" APPLIED TO EXCEED 8192 SPECTRA
REM FILES. THEN WN(1)=1024.017 CM-1, WN(2048)=2997.804 CM-1 .
REM THE SPECTRAL SAMPLING IS 0.96423401 CM-1/INTERVAL, NO INTERPOLATION.

REM IF WE LET WN(I)=1024.017*(I-1)/2 = 1024.017+0.482117005*(I-1)
REM WN(1)=1024.017 , WN(4096)=2998.286 CM-1,WHICH CORRESPONDS TO THE
REM EXCEED SPECTRA FROM "BAND.EXE" APPLIED TO A 8192 POINT INTERFEROGRAM
REM WITH A FACTOR OF TWO INTERPOLATION.

REM ALTERNATIVELY, FOR A FACTOR OF FOUR INTERPOLATION THEN
REM WN(I)=1024.017+0.96423401*(I-1)/4 WHICH EQUALS
REM WN(I)=1024.017+0.241058502*(I-1) ,
REM THEN    I=1+INT(4.148370589*(WN-1024.017)+0.5)
REM AND WN(1)=1024.017, WN(8192)=2998.527 CM-1 .

REM DELTA WAVENUMBER SAMPLING = DWN , CM-1 / POINT
REM DWN = .482117005, AND I = 1 + INT(2.07418529# * (WN - 1024.017)+.5)
REM DWN = .241058502, AND I = 1 + INT(4.148370589# * (WN -1024.017 )+.5)

'FOR TRIANGULAR LINE SHAPE
'G4 = 0.00
'G3 = .25
'G2 = .5
'G1 = .75
'G0 = 1.00
'FOR EXAMPLE, FOR A SINC SQUARED LINE SHAPE, RESOLUTION = 3.86 CM-1
'G3 = .0901
'G2 = .4053
'G1 = .8106

OPEN "D:\QB45\NOPLUS.DAT" FOR INPUT AS #1
'DIM W(3000), SIGMA(3000)
'DIM BRAN$(3000), ROT(3000)
'DIM MULT(3000), VIB(3000)
DIM G(20), PHOTON(8202)', SIGMA(8202)
K = 0
E0(0) = 0!
E0(1) = 2344.16
E0(2) = 4655.688
E0(3) = 6934.433
E0(4) = 9180.357
E0(5) = 11393.35#
E0(6) = 13573.32#
E0(7) = 15720.17#
E0(8) = 17833.81#
PREL(0) = 1
'PREL(1) = 1!
'PREL(2) = .3
'PREL(3) = .07
```

```
'PREL(4) = 0!
'PREL(5) = 0!
'PREL(6) = 0!
'PREL(7) = 0!
'PREL(8) = 0!
'TR = 320

PRINT "ENTER TR, PREL(1), PREL(2), PREL(3), PREL(4), PREL(5), RESL, C, N"
INPUT TR, PREL(1), PREL(2), PREL(3), PREL(4), PREL(5), RESL, C, N

B = 1.997
QR = TR / (1.4387 * B)
QV = PREL(0) + PREL(1) + PREL(2) + PREL(3) + PREL(4) + PREL(5)
PI = 3.1415926#
DWN = .241058502#
'DWN = .482117005#
'DWN = .96423401#

FOR J = 1 TO 10
G(J) = (SIN(PI * J * DWN / RESL) / (PI * J * DWN / RESL)) ^ 2
NEXT J

SUM = 0
FOR J = 1 TO 10
SUM = SUM + G(J)
NEXT J
SUM = 1 + 2 * SUM

WHILE NOT EOF(1)
LINE INPUT #1, A$
IF VAL(MID$(A$, 36, 8)) - VAL(MID$(A$, 44, 8)) = 2 THEN GOTO SKIP
IF MID$(A$, 59, 1) <> "+" THEN GOTO SKIP
IF VAL(MID$(A$, 36, 10)) > 5 THEN GOTO SKIP
B$ = LEFT$(A$, LEN(A$) - 1)
K = K + 1
WN = VAL(LEFT$(A$, 10))
REM N IS AN ASSIGNED "SLIPPAGE" OF THE MODEL SPECTRUM FOR BEST FIT WITH DATA
IF WN < 1024.017 THEN N = 0
IF WN > 2998.527 THEN N = 0
I = 1 + INT(4.148370589# * (WN - 1024.017) + .5) + N
'I = 1 + INT(2.07418529# * (WN - 1024.017) + .5)
'I = 1 + INT((WN-1024.017) / .96423401# + .5)
E = VAL(MID$(A$, 26, 10))
EE = WN + E
VV = VAL(MID$(A$, 36, 8))
IF PREL(VV) = 0! THEN GOTO SKIP
'VIB(I) = VV
WRITE I, VV ', VIB(I)
EREL = EE - E0(VV)
J = VAL(MID$(A$, 65, 5))
'ROT(I) = J
IF MID$(A$, 64, 1) = "P" THEN
JJ = J - 1
'BRAN$(I) = "P"
'MULT(I) = MULT(I) + 1
END IF
IF MID$(A$, 64, 1) = "R" THEN
JJ = J + 1
'BRAN$(I) = "R"
'MULT(I) = MULT(I) + 1
```

```
END IF
F = (2 * JJ + 1) * EXP(-1.4387 * EREL / TR) / QR
INTEN = F * VAL(MID$(A$, 11, 10)) * PREL(vv) / Qv
IF WN < 1024.017 THEN GOTO SKIP
'SIGMA(I) = WN
P = INTEN / SUM
PHOTON(I) = PHOTON(I) + P

FOR J = 1 TO 10
PHOTON(I - J) = PHOTON(I - J) + G(J) * P
PHOTON(I + J) = PHOTON(I + J) + G(J) * P
NEXT J

SKIP:
WEND
CLOSE #1

FOR I = 1 TO 10
WRITE "I, G(I) =", I, G(I)
NEXT I

'OPEN "NOPLUS.X" FOR OUTPUT AS #1
'FOR I = 1 TO 8192
'FOR I = 1 TO 4096
'FOR I = 1 TO 2048
'WRITE #1, I, VIB(I), ROT(I), BRAN$(I), SIGMA(I), PHOTON(I), MULT(I)
'WRITE #1, I, SIGMA(I), C*PHOTON(I)
'NEXT
'CLOSE #1

OPEN "NOPLUS.S" FOR OUTPUT AS #1
FOR I = 1 TO 8192
'FOR I = 1 TO 4096
'FOR I = 1 TO 2048
WRITE #1, C * PHOTON(I)
NEXT
CLOSE #1
```

BLANK

APPENDIX B

```
          $DEBUG
$LARGE
          PROGRAM INTERP

C RESEARCH SCIENCES CORPORATION
C MHB 5/5/92

C USES 2048 POINT FILE OF ONLY THE INBAND SPECTRAL POINTS
C ORIGINALLY FROM 8192 POINT EXCEED SPECTRA AND INTERPOLATES
C BY FACTORS OF 2 OR 4 AND WRITES TO CORRESPONDING FILE.

C  N1=1338 AT 1289.181 CM-1,
C  N2 = 2834 AT 2732.639 CM-1, WHERE WN(I)= 0.0 + 0.96423401*(I-1)
C  NEW START (I=1) AND END WAVENUMBERS OF 2048 FILE ARE
C  FROM WN(I)=1289.181+0.96423401*(I-276), THEN I=276 GIVES 1289.181 CM-1,
C  I=1772 GIVES 2731.675, SO I=1 GIVES 1024.017 CM-1, AND FINALLY
C  I=2048 GIVES 2997.804
C  THE NEW 4096 OUTPUT FILE THEN HAS THE ORIGINAL WAVE NUMBER WN(I) AT
C  THE POINT 2*I-1 .

          REAL*4 INBUF(8194),OUTBUF(16386)
          COMPLEX*8 BUF(4096),BUF2(8192)
          COMMON /BLOCK1/ NDP,NDP2

          M=2
          K1=11
          K2=12
          I1=1024
          L1=2048
          L2=4096
          NDP=8192
          NDP2=16384

C AQUIRE EXTERNAL FILE AND LOAD INTO INBUF

          WRITE(*,*)'AQUIRE INPUT FILE'
          WRITE(*,*)'ASC OR BINARY INPUT FILE ? (A/B))'
          READ(*,'(A)')Q
          IF((Q.EQ.'A').OR.(Q.EQ.'A'))GOTO 5
          CALL READBN(INBUF,L)
          GOTO 7
5         CALL READAS(INBUF,L)
7         WRITE(*,*)'NUMBER OF POINTS IN FILE =',L

C MAKE COMPLEX BUF FROM INBUF

10        DO 111 I=1,L1
          BUF(I)=INBUF(I)
111       CONTINUE

C***-1B MAKE REAL OUTBUF FOR TEST
C         DO 105 I=1,2048
C105       OUTBUF(I)=REAL(BUF(I))

C TEST OF BUF: WRITE OUTBUF TO FILE
C         CALL MKASC(OUTBUF,L1)
C         GOTO 120
C***-1E

C DO COMPLEX FT ON BUF
```

```
C RETURNS REAL PART AS = BUF(2*I), IMAG PART AS BUF(2*I-1)

        CALL CFFT(BUF,K1,1,1.0)

C***0B MAKE REAL OUTBUF
C       DO 107 I=1,2048
C107    OUTBUF(I)=REAL(BUF(I))

C TEST OF CFFT BUF: WRITE OUTBUF TO FILE
C       CALL MKASC(OUTBUF,L1)
C       GOTO 120
C***0E

C ADD ZEROS TO BUF(I)

        I2=2*I1
        I3=3*I1
        I4=4*I1
        I11=I1+1
        I31=I3+1
        DO 300 I=1,I1
300     BUF2(I)=BUF(I)
        DO 302 I=I11,I3
302     BUF2(I)=(0.0,0.0)
        DO 304 I=I31,I4
304     BUF2(I)=BUF(I-I2)

        CALL CIFT(BUF2,K2,1,1.0)

C MAKE REAL OUTBUF

        DO 113 I=1,L2
113     OUTBUF(I)=REAL(BUF2(I))

C***1B
C       WRITE(*,*)'TEST OF ADD ZEROS'
C TEST OF ADD ZEROS: WRITE OUTBUF TO FILE
C       CALL MKASC(OUTBUF,L2)
C       GOTO 120
C***1E

C WRITE EXTRAPOLATED SPECTRUM TO FILE OR INTERPOLATE AGAIN

        WRITE(*,*)' INTERPOLATION FACTOR IS',M
        WRITE(*,*)' WRITE TO FILE OR INTERPOLATE AGAIN ? (W/I)'
        READ(*,'(A)')Q
        IF((Q.EQ.'I').OR.(Q.EQ.'i'))GOTO 116

109     WRITE(*,*)'ASC OR BINARY OUTPUT FILE ? (A/B))'
        READ(*,'(A)')Q
        IF((Q.EQ.'A').OR.(Q.EQ.'a'))GOTO 115

        CALL MKBIN(OUTBUF,L2)
        GOTO 120

115     CALL MKASC(OUTBUF,L2)
        GOTO 120

116     DO 117 I=1,L2
117     INBUF(I)=OUTBUF(I)
```

```
          I1=2*I1
          K1=K1+1
          K2=K2+1
          L1=2*L1
          L2=2*L2
          M=2*M
          GOTO 10

120       CONTINUE
          END

C --------------------------------
          SUBROUTINE READAS(X,L)

C         READS AN ASCII 10000 POINT SINGLE COLUMN FILE

          REAL*4 X(10000)
          CHARACTER*30 INFILE

5         WRITE(*,*) ' ENTER ASCII INPUT FILE NAME '
          READ(*,'(A)') INFILE
          OPEN(1,FILE=INFILE,STATUS='OLD',FORM='FORMATTED')

          WRITE(*,*)'ENTER NUMBER OF INITIAL POINTS IN FILE TO BE SKIPPED'
          READ(*,*) NSKIP

C  FIRST NSKIP LINES ARE NOT WRITTEN TO FILE

          I1=1+NSKIP
          DO 20 I=1,10000
          M=I
          READ(1,*,END=200) XVAL
          IF(I.LE.NSKIP)GOTO 20
          IS=I-NSKIP
          X(IS)=XVAL
20        CONTINUE
200       L=M-1-NSKIP

          WRITE(*,*) 'ALL DATA READ '
          CLOSE(1)

          RETURN
          END
C         --------------------
          SUBROUTINE MKASC(INBUF,L)

C OPENS AN ASCII FILE AND WRITES TO IT. L IS NUMBER OF POINTS.

          REAL*4 INBUF(1)
          CHARACTER*30 OUTFILE

          WRITE(*,*) ' ENTER OUTPUT FILE NAME '
          READ(*,'(A)') OUTFILE
          OPEN(1,FILE=OUTFILE,STATUS='NEW',FORM='FORMATTED')

100       FORMAT(E13.6)

9         DO 7 I=1,L
7         WRITE(1,100) INBUF(I)
```

181

```
11        WRITE(*,*) 'ALL DATA WRITTEN TO FILE '

          CLOSE(1)

          RETURN
          END
C ---------------------------------
          SUBROUTINE READBN(INBUF,K)

          CHARACTER*30 INFILE
          REAL*4 INBUF(1)

C READS A REAL*4 (RECORD LENGTH = RECL = 4 BYTES) BINARY INPUT FILE

          WRITE(*,*)'ENTER INPUT FILE NAME'
          READ(*,'(A)') INFILE

          N=10000

          WRITE(*,*)'ENTER NUMBER OF INITIAL POINTS IN FILE TO BE SKIPPED'
          READ(*,*) NSKIP

          OPEN(1,FILE=INFILE ,ACCESS='DIRECT', RECL=4,STATUS='OLD')

C   FIRST NSKIP LINES ARE NOT WRITTEN TO FILE

          I1=1+NSKIP
          DO 5 I=I1,N
          M=I
          READ(1,REC=I, END=6) XVAL
          INBUF(I-NSKIP)=XVAL
5         CONTINUE
6         K=M-1-NSKIP

          CLOSE (1)
          RETURN
          END
C -------------------------
          SUBROUTINE MKBIN(X,L)

C         OPENS A BINARY FILE AND WRITES TO IT .

          REAL*4 X(1)
          CHARACTER*30 OUTFILE
          LOGICAL EX

5         WRITE(*,*) ' ENTER NEW OUTPUT FILE NAME '
          READ(*,'(A)') OUTFILE
          INQUIRE(FILE=OUTFILE,EXIST=EX)
          IF(EX) THEN
            WRITE(*,*) 'FILE ALREADY EXISTS'
            GOTO 5
          ENDIF
          OPEN(1,FILE=OUTFILE,STATUS='NEW',FORM='BINARY')

          WRITE(1) (X(I),I=1,L)

          WRITE(*,*) 'ALL DATA WRITTEN TO FILE '
          WRITE(*,*)'NUMBER OF DATA POINTS IN OUT FILE IS',L
```

```
CLOSE(1)

RETURN
END
```

BLANK

APPENDIX C

PROGRAM BAND

```
C RESEARCH SCIENCES CORPORATION
C MHB 5/5/92

C MAKES 2048 POINT FILE OF ONLY THE INBAND SPECTRAL POINTS
C FOR 8192 POINT EXCEED SPECTRA AND WRITES TO CORRESPONDING FILE.
C GIVEN THAT THE INTERFEROMETER GIVES 0.96423401 CM-1/POINT SAMPLING,
C THEN THE WAVENUMBER OF THE 8192 FILE IS WN(I)= 0.0 + 0.96423401*(I-1) .
C THUS N1=1338 AT 1289.181 CM-1, N2 = 2834 AT 2732.639 CM-1, WHICH ARE
C THE LIMITS OF THE RESPONSE FUNCTION CORRECTION FILE.
C THE START AND END WAVENUMBERS ARE THEN 0.0 CM-1 AND 7898.041 CM-1 .

C THE NEW 2048 FILE START (I=1) AND END WAVENUMBERS ARE NOW CALCULATED
C FROM WN(I)=1289.181+0.96423401*(I-276)= 1024.017+0.96423401*(I-1),
C THEN I=276 GIVES 1289.181 CM-1, I=1772 GIVES 2731.675,WHICH ARE THE
C LIMITS OF THE RESPONSE FUNCTION CORRECTION FILE.
C THEN I=1 GIVES 1024.017 CM-1, AND FINALLY I=2048 GIVES 2997.804

        REAL*4 INBUF(8194),OUTBUF(2048)

        L1=2048

C AQUIRE EXTERNAL FILE AND LOAD INTO INBUF

        WRITE(*,*)'AQUIRE INPUT FILE'
        WRITE(*,*)'ASC OR BINARY INPUT FILE ? (A/B))'
        READ(*,'(A)')Q
        IF((Q.EQ.'A').OR.(Q.EQ.'A'))GOTO 5
        CALL READBN(INBUF,L)
        GOTO 7
5       CALL READAS(INBUF,L)
7       WRITE(*,*)'NUMBER OF POINTS IN FILE =',L

C HARDWIRE N1,N2

        N1=1338
        N2=2834
        N3=2048-(N2-N1+1)
        N4=INT(N3/2.0)
        N5=N3-N4
        N6=N2-N1+1
        WRITE(*,*)'N3,N4,N5,N6=',N3,N4,N5,N6

        DO 3 J=1,2048
        IF(J.LT.N4+1)THEN
        OUTBUF(J)=0.0
        ELSEIF(J.GT.N6+N4)THEN
        OUTBUF(J)=0.0
        ELSE
        I=1338+J-N4-1
        OUTBUF(J)=INBUF(I)
        ENDIF
3       CONTINUE

        WRITE(*,*)'ASC OR BINARY OUTPUT FILE ? (A/B))'
        READ(*,'(A)')Q
        IF((Q.EQ.'A').OR.(Q.EQ.'A'))GOTO 117

        CALL MKBIN(OUTBUF,L1)
```

```fortran
          GOTO 120

117       CALL MKASC(OUTBUF,L1)

120       CONTINUE
          END

C ----------------------------
          SUBROUTINE READAS(X,L)

C         READS AN ASCII 10000 POINT SINGLE COLUMN FILE

          REAL*4 X(10000)
          CHARACTER*30 INFILE

5         WRITE(*,*) ' ENTER ASCII INPUT FILE NAME '
          READ(*,'(A)') INFILE
          OPEN(1,FILE=INFILE,STATUS='OLD',FORM='FORMATTED')

          WRITE(*,*)'ENTER NUMBER OF INITIAL POINTS IN FILE TO BE SKIPPED'
          READ(*,*) NSKIP

C   FIRST NSKIP LINES ARE NOT WRITTEN TO FILE

          I1=1+NSKIP
          DO 20 I=1,10000
          M=I
          READ(1,*,END=200) XVAL
          IF(I.LE.NSKIP)GOTO 20
          IS=I-NSKIP
          X(IS)=XVAL
20        CONTINUE
200       L=M-1-NSKIP

          WRITE(*,*) 'ALL DATA READ '
          CLOSE(1)

          RETURN
          END
C         --------------------
          SUBROUTINE MKASC(INBUF,L)

C OPENS AN ASCII FILE AND WRITES TO IT. L IS NUMBER OF POINTS.

          REAL*4 INBUF(1)
          CHARACTER*30 OUTFILE

          WRITE(*,*) ' ENTER OUTPUT FILE NAME '
          READ(*,'(A)') OUTFILE
          OPEN(1,FILE=OUTFILE,STATUS='NEW',FORM='FORMATTED')

100       FORMAT(E13.6)

9         DO 7 I=1,L
7         WRITE(1,100) INBUF(I)

11        WRITE(*,*) 'ALL DATA WRITTEN TO FILE '

          CLOSE(1)
```

```fortran
      RETURN
      END
C --------------------------------
      SUBROUTINE READBN(INBUF,K)

      CHARACTER*30 INFILE
      REAL*4 INBUF(1)

C READS A REAL*4 (RECORD LENGTH = RECL = 4 BYTES) BINARY INPUT FILE

      WRITE(*,*)'ENTER INPUT FILE NAME'
      READ(*,'(A)') INFILE

      N=10000

      WRITE(*,*)'ENTER NUMBER OF INITIAL POINTS IN FILE TO BE SKIPPED'
      READ(*,*) NSKIP

      OPEN(1,FILE=INFILE ,ACCESS='DIRECT', RECL=4,STATUS='OLD')

C  FIRST NSKIP LINES ARE NOT WRITTEN TO FILE

      I1=1+NSKIP
      DO 5 I=I1,N
      M=I
      READ(1,REC=I, END=6) XVAL
      INBUF(I-NSKIP)=XVAL
5     CONTINUE
6     K=M-1-NSKIP

      CLOSE (1)

      RETURN
      END
C -------------------------
      SUBROUTINE MKBIN(X,L)

C     OPENS A BINARY FILE AND WRITES TO IT .

      REAL*4 X(1)
      CHARACTER*30 OUTFILE
      LOGICAL EX

5     WRITE(*,*) ' ENTER NEW OUTPUT FILE NAME '
      READ(*,'(A)') OUTFILE
      INQUIRE(FILE=OUTFILE,EXIST=EX)
      IF(EX) THEN
        WRITE(*,*) 'FILE ALREADY EXISTS'
        GOTO 5
      ENDIF
      OPEN(1,FILE=OUTFILE,STATUS='NEW',FORM='BINARY')

      WRITE(1) (X(I),I=1,L)

      WRITE(*,*) 'ALL DATA WRITTEN TO FILE '
      WRITE(*,*)'NUMBER OF DATA POINTS IN OUT FILE IS',L
      CLOSE(1)

      RETURN
      END
```

BLANK

```
$DEBUG
$LARGE
        PROGRAM CNOP_OK

c  Research Sciences Corporation,  Marshall H. Bruce , 08/17/93


c 4-th order RUNGE-KUTTA for eight systems,  electrons, N2+, O2+, N+,
c O+, N(4s), N(2d), NO, and NO+, plus 2x16 NO+ vib. levels, involves
c 66 reactions, with  N2+ + O, and N+ + O2 each treated seperately,
c ...gives 40 coupled differential equations.
c        dXi/dt = Fi(Xj's,t), with initial conditions  Xi(to) = Xio


c delare all data types
        INTEGER NLIM
        INTEGER*2 It,Ie,IN2I,IO2I,INI,IOI,INOI,IN4s,IN2d,IEX,KX
        REAL H


c declare the arrays for time t, and the number densities for
c electrons, N2+, O2+, N+, O+, N(4s), N(2d), and total NO+ respectivly
        REAL t(2500),e(2500),N2I(2500),O2I(2500),NI(2500),OI(2500)
        REAL N4s(2500),N2d(2500),NOI(2500),sumion(2500)


c declare arrays for NO+ vibrational levels
c first, the NO+ levels from N2+ + O  --> NO+(v) + N(4S,4D)
        REAL NOP10(2500),NOP11(2500),NOP12(2500),NOP13(2500)
        REAL NOP14(2500),NOP15(2500),NOP16(2500),NOP17(2500)
        REAL NOP18(2500),NOP19(2500),NOP110(2500),NOP111(2500)
        REAL NOP112(2500),NOP113(2500),NOP114(2500),NOP115(2500)
        REAL NOP116(2500)


c second, the NO+ levels from N+ + O2  --> NO+(v) + O
        REAL NOP20(2500),NOP21(2500),NOP22(2500),NOP23(2500)
        REAL NOP24(2500),NOP25(2500),NOP26(2500),NOP27(2500)
        REAL NOP28(2500),NOP29(2500),NOP210(2500),NOP211(2500)
        REAL NOP212(2500),NOP213(2500),NOP214(2500),NOP215(2500)
        REAL NOP216(2500)


c declare chemistry coeffs
        REAL N2IMX,N2IMN,NOIMX,NOIMN
        REAL NIMX,NIMN,N4sMX,N4sMN,N2dMX,N2dMN

        REAL NN,O2,O,Tr,N2Ie,O2Ie,OIe,NIe,NOIe,
     1  N2IO2,N2IO,N2IN4s,O2IN2d,N4sO2I,N2de,NIO2,NIO,N4sPNI,N2dPNI,
     2  N4sPO,N2dPO,NOIA1,NOIA2,NOIA3,NOIN2,NOIP2d,NOIP4s,OIO2,OIN2,
     3  ON2I,O2NI,O2N4s,ON2d,O2N2d,N2N2d,NIPO2,N2O2I,
     4  t0,e0,N2IO,O2IO,OIO,NIO,NOIO,N2DO,N4SO,PI,ASIG,SINTHT,WAIST,
     5  QN2I,QO2I,QOI,Qe,
     6  Vbeam,tdose,
     7  NOIA4,NOIA5,NOIA6,NOIA7,NOIA8,NOIA9,NOIA10,NOIA11,NOIA12,
     8  NOIB2,NOIB3,NOIB4,NOIB5,NOIB6,NOIB7,NOIB8,NOIB9,NOIB10,NOIB11,
     9  NOIA13,NOIA14,NOIA15,NOIA16,
     $  NOIB12,NOIB13,NOIB14,NOIB15,NOIB16

        REAL K1,K2,K3,K4,L1,L2,L3,L4
        REAL M1,M2,M3,M4,N1,N2,N3,N4
        REAL P1,P2,P3,P4,Q1,Q2,Q3,Q4
        REAL R1,R2,R3,R4,S1,S2,S3,S4


c declare intermedeiate scalars for RK, from tN,....NOI116, and
c from tN1,.......NOJ116 .
```

```fortran
      REAL tN,eN,N2IN,O2IN,OIN,NIN,NOIN,N2dN,N4sN
      REAL eN1,N2IN1,O2IN1,OIN1,NIN1,NOIN1,N2dN1,N4sN1

      REAL NOI10,NOI11,NOI12,NOI13
      REAL NOI14,NOI15,NOI16,NOI17
      REAL NOI18,NOI19,NOI110,NOI111
      REAL NOI112,NOI113,NOI114,NOI115,NOI116

      REAL NOI20,NOI21,NOI22,NOI23
      REAL NOI24,NOI25,NOI26,NOI27
      REAL NOI28,NOI29,NOI210,NOI211
      REAL NOI212,NOI213,NOI214,NOI215,NOI216

      REAL NOJ10,NOJ11,NOJ12,NOJ13
      REAL NOJ14,NOJ15,NOJ16,NOJ17
      REAL NOJ18,NOJ19,NOJ110,NOJ111
      REAL NOJ112,NOJ113,NOJ114,NOJ115,NOJ116

      REAL NOJ20,NOJ21,NOJ22,NOJ23
      REAL NOJ24,NOJ25,NOJ26,NOJ27
      REAL NOJ28,NOJ29,NOJ210,NOJ211
      REAL NOJ212,NOJ213,NOJ214,NOJ215,NOJ216
c add NO to the chemistry
      REAL NO(2500)
      REAL NONO,NON,NON1
      REAL N2INO,O2INO,OINO

c make reaction coeffs. available to functions and subs
      COMMON /BLK1/NN,O2,O,Tr,N2Ie,O2Ie,OIe,NIe,NOIe,
     1 N2IO2,N2IO,N2IN4s,O2IN2d,N4sO2I,N2de,NIO2,NIO,N4sPNI,N2dPNI,
     2 N4sPO,N2dPO,NOIA1,NOIA2,NOIA3,NOIN2,NOIP2d,NOIP4s,OIO2,OIN2,
     3 ON2I,O2NI,O2N4s,ON2d,O2N2d,N2N2d,NIPO2,N2O2I,
     4 t0,e0,N2I0,O2I0,OI0,NI0,NOI0,N2D0,N4S0,PI,ASIG,SINTHT,WAIST,
     5 QN2I,QO2I,QOI,Qe,
     6 Vbeam,tdose,
     7 NOIA4,NOIA5,NOIA6,NOIA7,NOIA8,NOIA9,NOIA10,NOIA11,NOIA12,
     8 NOIB2,NOIB3,NOIB4,NOIB5,NOIB6,NOIB7,NOIB8,NOIB9,NOIB10,NOIB11,
     9 NOIA13,NOIA14,NOIA15,NOIA16,
     $ NOIB12,NOIB13,NOIB14,NOIB15,NOIB16

c make reaction coeffs. for added NO available to functions and subs
      COMMON /BLK2/N2INO,O2INO,OINO

C*******************
c       qfactr=1.0
        qfactr=17.0
C*******************

c initialize parameters

c changing H by a factor of two to assure correct integration
c       H=1.0E-04
        H=0.5E-04
c       H=1.0E-5

c number of points currently calculated
      NLIM=2500

c assign O2, N2, O and temperature Tr at altitude:
```

190

```
c let altitude be 115 km

c N2 ambient desity
      NN=7.46E+11

c O2 ambient desity
      O2=1.50E+11

c O ambient desity
      O=1.35E+11

c kinetic temerature at altitude
      Tr=300.0

C Define reaction constants:

c recombination coefficients with electrons

c N2+ + e --> N2                                                      (15)
      N2Ie=1.80E-07*(300./Tr)**(0.39)

c O2+ + e --> O2                                                      (16)
      O2Ie=2.0E-07*(300/Tr)**(0.7)

c O+ + e --> O                                                        (18)
      OIe=3.5E-12*(300/Tr)**(0.7)

c N+ + e --> N                                                        (19)
      NIe=3.5E-12*(300/Tr)**(0.7)

c NO+ + e --> 1/2 N(4S) + 1/2 N(2D) + O                               (17)
      NOIe=4.2E-07*(300/Tr)**(0.85)

c **** test for overall neutrality for ion production and recombination only
c         goto 21

c binary reaction constants

c N2+ + O2 --> N2 + O2+ , charge exchange                             (20)
      N2IO2=5.0E-11*(300/Tr)**(0.8)

c N2IO = NOIP2d + NOIP4s + ON2I, not used as such
c       N2IO=2.66E-11*(300/Tr)**(.44) + .984E-11*(300/Tr)**(.44)

c N2+ + N(4S) --> N2 + N+ , charge exchange                           (23)
      N2IN4s=1.0E-11

c O2+ + N(2D) --> O2 + N+ , charge exchange                           (24)
      O2IN2d=2.5E-10

c O2+ + N(4S) --> NO+(v=0) + O,  NO+(0), O creation                   (6)
      N4sO2I=1.2E-10

c e + N(2D) -->  e + N(4S)                                            (28)
      N2de=3.3E-10*(300/Tr)**(-0.5)

c NIO2 = NIPO2 + N4sPNI + N2dPNI, not used as such
c       NIO2=3.0E-10 + 2.1E-10 + .90E-10

c N+ + O2 -->  NO+(v) + O(1S,1D),  shared amongst vibrational states (13)
```

191

```
            NIPO2=3.0E-10

c O2+ + N2 -->  NO+(0) + NO(0)                                          (7)
        N2O2I=5.0E-16

c N+ + O -->  N(4S) + O+                                                (25)
        NIO=1.00E-12

c N+ + O2  -->  O2+ + N(4S) , charge exchange, excitation              (27)
        N4sPNI=.90E-10

c N+ + O2  -->  O2+ + N(2D)                                             (26)
        N2dPNI=2.1E-10

c never used as such, since = NOIP4s
c       N4sPO=1.4E-11*(300/Tr)**(0.44)

c never used as such, since = NOIP2d
c       N2dPO=1.26E-11*(300/Tr)**(0.44)

c NO+(v) + N2  -->  NO+(v-1) + N2                                       (14)
        NOIN2=7.0E-12

c N2+ + O  -->  NO+(v) + N(2D),  shared amongst vibrational states      (11)
        NOIP2d=1.26E-10*(300/Tr)**(.44)

c N2+ + O  -->  NO+(v) + N(4S),  shared amongst vibrational states      (12)
        NOIP4s=1.4E-10*(300/Tr)**(.44)

c O+ + O2  -->  O2+ + O , charge exchange                               (22)
        OIO2=2.0E-11*(300/Tr)**(0.4)

c O+ + N2  -->  NO+(0) + N(4S)                                          (9)
        OIN2=1.2E-12*(300/Tr)

c N2+ + O --> N2 + O+ , charge exchange                                 (21)
        ON2I=.984E-11*(300/Tr)**(0.44)

c N+ + O2  -->  O2+ + N(2D) , charge exchange, excitation, = N2dPNI
c       O2NI=2.1E-10

c N(4S) + O2  -->  NO(v) + O , currently put in ground state            (4)
        O2N4s=1.0E-12*EXP(-3220/Tr)

c N(2D) + N2  -->  N(4S) + N2,                                          (2)
        ON2d=6.7E-13

c N(2D) + O2  -->  NO(v) + O(1D,3P)                                     (3)
        O2N2d=7.4E-12*(300/Tr)**(-.5)

c N(2D) + N2  -->  N(4S) + N2,                                          (1)
        N2N2d=1.6E-14

c N2+ + NO(0)  -->  NO+(0) + N2 , charge exchange                       (5)
        N2INO=3.3E-10

c O2+ + NO(0)  -->  NO+(0) + O2 , charge exchange                       (8)
        O2INO=4.4E-10

c O+ + NO(0)  -->  NO+(0) + O , charge exchange                         (10)
```

```
        OINO=8.0E-13

c NO+(v) --> NO+(v-1) + hv , fundemental Einstein radiation coeffs.
        NOIA0=0.0
        NOIA1=10.9
        NOIA2=20.2
        NOIA3=28.4
        NOIA4=35.5
        NOIA5=41.5
        NOIA6=46.6
        NOIA7=50.9
        NOIA8=54.3
        NOIA9=57.0
        NOIA10=58.9
        NOIA11=60.2
        NOIA12=60.8
        NOIA13=60.7
        NOIA14=59.9
        NOIA15=0.0
        NOIA16=0.0

c NO+(v) --> NO+(v-2) + hv , ist overtone, Einstein radiation coeffs.
        NOIB0=0.0
        NOIB1=0.0
        NOIB2=0.697
        NOIB3=1.93
        NOIB4=3.55
        NOIB5=5.74
        NOIB6=8.24
        NOIB7=11.1
        NOIB8=14.2
        NOIB9=17.7
        NOIB10=21.3
        NOIB11=25.1
        NOIB12=29.0
        NOIB13=33.2
        NOIB14=37.4
        NOIB15=0.0
        NOIB16=0.0

c21     continue
c ****** end neutrality test


c define the beam ion production rates

        PI=3.1415926
c ASIG is the integrated 3914 A intensity
        ASIG=23.99488E+14
c SINTHT is the sin of the angle the line of sight vector makes
c with the beam axis
        SINTHT=.7047292
c WAISTE is the beam width ( in cm )
        WAIST=226

c QN2I is the beam N2+ volumetric productuion rate
        QN2I=(14.1*ASIG*SINTHT)/(2*PI*WAIST**2)
c put qfactr parameter as QN2I multiplier
        QN2I=qfactr*QN2I
```

```fortran
c Qe is the beam ion pair production rate, which is the electron
c production rate
c hardwire Qe at apogee
c suspend hardwire Qe
c        Qe=2.0E+11
c then QN2I is....
c suspend QN2I
c        QN2I=(0.92*NN)/(1.15*NN+1.5*O2+0.56*O)*Qe

c Use QN2I directly from ASIG (the 3914 A intensity integrated over
c the transverse beam direction) Then Qe is:
        Qe=(1.15*NN+1.5*O2+0.56*O)/(0.92*NN)*QN2I
c O2+ beam production rate
        QO2I=O2/(0.92*NN)*QN2I
c O+ (atomic oxygen ion) beam production rate
        QOI=(0.56*O)/(0.92*NN)*QN2I

c define dose time, Vbeam is transverse beam velocity in cm/sec with
c respect to atmosphere
        Vbeam=24500
c        tdose=3*WAIST/Vbeam

c hardwire dose time
        tdose=.05

c write parameters

        write(*,*)'NN,O2,O,Tr,N2Ie,O2Ie,OIe,NIe,NOIe=',
     1  NN,O2,O,Tr,N2Ie,O2Ie,OIe,NIe,NOIe

        write(*,*)'N2IO2,N2IO,N2IN4s,O2IN2d,N4sO2I=',
     2  N2IO2,N2IO,N2IN4s,O2IN2d,N4sO2I

        write(*,*)'N2de,NIO2,NIPO2,N2O2I,NIO,N4sPNI,N2dPNI=',
     3  N2de,NIO2,NIPO2,N2O2I,NIO,N4sPNI,N2dPNI

        write(*,*)'N4sPO,N2dPO,NOIA1,NOIA2,NOIA3=',
     4  N4sPO,N2dPO,NOIA1,NOIA2,NOIA3

        write(*,*)'NOIN2,NOIP2d,NOIP4s,OIO2,OIN2=',
     5  NOIN2,NOIP2d,NOIP4s,OIO2,OIN2

        write(*,*)'ON2I,O2NI,O2N4s,ON2d,O2N2d,N2N2d=',
     6  ON2I,O2NI,O2N4s,ON2d,O2N2d,N2N2d

        write(*,*)'NIO,NOIO,N2DO,N4SO=',
     8  NIO,NOIO,N2DO,N4SO

        write(*,*)'N2INO,O2INO,OINO,ASIG,SINTHT,WAIST=',
     9  N2INO,O2INO,OINO,ASIG,SINTHT,WAIST

        write(*,*)'QN2I,QO2I,QOI,Qe=',
     1  QN2I,QO2I,QOI,Qe

        write(*,*)'Vbeam,tdose=',
     2  Vbeam,tdose

        write(*,*)
        write(*,*)'hit enter to continue'
        read(*,*)
```

194

```
          write(*,*)' computing chemistry set.....'

C ****************
C **************** FOURTH ORDER RUNGE-KUTTA ---BEGIN---
C ****************

c assign initial values

          t0=-tdose
          e0=0.0
          N2I0=0.0
          O2I0=0.0
          OI0=0.0
          NI0=0.0
          NOI0=0.0
          N2d0=0.0
          N4s0=0.0

          NOI10=0.0
          NOI11=0.0
          NOI12=0.0
          NOI13=0.0
          NOI14=0.0
          NOI15=0.0
          NOI16=0.0
          NOI17=0.0
          NOI18=0.0
          NOI19=0.0
          NOI110=0.0
          NOI111=0.0
          NOI112=0.0
          NOI113=0.0
          NOI114=0.0
          NOI115=0.0
          NOI116=0.0

          NOI20=0.0
          NOI21=0.0
          NOI22=0.0
          NOI23=0.0
          NOI24=0.0
          NOI25=0.0
          NOI26=0.0
          NOI27=0.0
          NOI28=0.0
          NOI29=0.0
          NOI210=0.0
          NOI211=0.0
          NOI212=0.0
          NOI213=0.0
          NOI214=0.0
          NOI215=0.0
          NOI216=0.0

          NON0=0.0
C         NON0=7.0E+7

          tN=t0
          eN=e0
          N2IN=N2I0
```

```
          O2IN=O2IO
          OIN=OIO
          NIN=NIO
          NOIN=NOIO
          NON=NONO
          N2dN=N2dO
          N4sN=N4sO

C USE 4-TH ORDER RUNGE-KUTTA

          DO 10 I = 1,NLIM

          K1 = H*FK(tN,eN,N2IN,O2IN,NIN,OIN,NOIN,N4sN,N2dN)
          L1 = H*FL(tN,eN,N2IN,O2IN,NIN,OIN,NON,N4sN,N2dN)
          M1 = H*FM(tN,eN,N2IN,O2IN,NIN,OIN,NON,N4sN,N2dN)
          N1 = H*FN(tN,eN,N2IN,O2IN,NIN,OIN,NOIN,N4sN,N2dN)
          P1 = H*FP(tN,eN,N2IN,O2IN,NIN,OIN,NON,N4sN,N2dN)

          Q1 = H*FQ(tN,eN,N2IN,O2IN,NIN,OIN,NON,N4sN,N2dN)

          Q110 = H*FQ10(tN,eN,N2IN,O2IN,NIN,OIN,NOI10,NOI11,NOI12,
     $N4sN,N2dN,NON)
          Q111 = H*FQ11(tN,eN,N2IN,O2IN,NIN,OIN,NOI11,NOI12,NOI13,
     $N4sN,N2dN)
          Q112 = H*FQ12(tN,eN,N2IN,O2IN,NIN,OIN,NOI12,NOI13,NOI14,
     $N4sN,N2dN)
          Q113 = H*FQ13(tN,eN,N2IN,O2IN,NIN,OIN,NOI13,NOI14,NOI15,
     $N4sN,N2dN)
          Q114 = H*FQ14(tN,eN,N2IN,O2IN,NIN,OIN,NOI14,NOI15,NOI16,
     $N4sN,N2dN)
          Q115 = H*FQ15(tN,eN,N2IN,O2IN,NIN,OIN,NOI15,NOI16,NOI17,
     $N4sN,N2dN)
          Q116 = H*FQ16(tN,eN,N2IN,O2IN,NIN,OIN,NOI16,NOI17,NOI18,
     $N4sN,N2dN)
          Q117 = H*FQ17(tN,eN,N2IN,O2IN,NIN,OIN,NOI17,NOI18,NOI19,
     $N4sN,N2dN)
          Q118 = H*FQ18(tN,eN,N2IN,O2IN,NIN,OIN,NOI18,NOI19,NOI110,
     $N4sN,N2dN)
          Q119 = H*FQ19(tN,eN,N2IN,O2IN,NIN,OIN,NOI19,NOI110,NOI111,
     $N4sN,N2dN)
          Q1110 = H*FQ110(tN,eN,N2IN,O2IN,NIN,OIN,NOI110,NOI111,NOI112,
     $N4sN,N2dN)

          Q120 = H*FQ20(tN,eN,N2IN,O2IN,NIN,OIN,NOI20,NOI21,NOI22,
     $N4sN,N2dN,NON)
          Q121 = H*FQ21(tN,eN,N2IN,O2IN,NIN,OIN,NOI21,NOI22,NOI23,
     $N4sN,N2dN)
          Q122 = H*FQ22(tN,eN,N2IN,O2IN,NIN,OIN,NOI22,NOI23,NOI24,
     $N4sN,N2dN)
          Q123 = H*FQ23(tN,eN,N2IN,O2IN,NIN,OIN,NOI23,NOI24,NOI25,
     $N4sN,N2dN)
          Q124 = H*FQ24(tN,eN,N2IN,O2IN,NIN,OIN,NOI24,NOI25,NOI26,
     $N4sN,N2dN)
          Q125 = H*FQ25(tN,eN,N2IN,O2IN,NIN,OIN,NOI25,NOI26,NOI27,
     $N4sN,N2dN)
          Q126 = H*FQ26(tN,eN,N2IN,O2IN,NIN,OIN,NOI26,NOI27,NOI28,
     $N4sN,N2dN)
          Q127 = H*FQ27(tN,eN,N2IN,O2IN,NIN,OIN,NOI27,NOI28,NOI29,
     $N4sN,N2dN)
          Q128 = H*FQ28(tN,eN,N2IN,O2IN,NIN,OIN,NOI28,NOI29,NOI210,
```

```
$N4sN,N2dN)
    Q129 = H*FQ29(tN,eN,N2IN,O2IN,NIN,OIN,NOI29,NOI210,NOI211,
$N4sN,N2dN)
    Q1210 = H*FQ210(tN,eN,N2IN,O2IN,NIN,OIN,NOI210,NOI211,NOI212,
$N4sN,N2dN)
    Q1211 = H*FQ211(tN,eN,N2IN,O2IN,NIN,OIN,NOI211,NOI212,NOI213,
$N4sN,N2dN)
    Q1212 = H*FQ212(tN,eN,N2IN,O2IN,NIN,OIN,NOI212,NOI213,NOI214,
$N4sN,N2dN)
    Q1213 = H*FQ213(tN,eN,N2IN,O2IN,NIN,OIN,NOI213,NOI214,NOI215,
$N4sN,N2dN)
    Q1214 = H*FQ214(tN,eN,N2IN,O2IN,NIN,OIN,NOI214,NOI215,NOI216,
$N4sN,N2dN)


    R1 = H*FR(tN,eN,N2IN,O2IN,NIN,OIN,NOIN,N4sN,N2dN)
    S1 = H*FS(tN,eN,N2IN,O2IN,NIN,OIN,NOIN,N4sN,N2dN)

    K2 = H*FK(tN+.5*H,eN+.5*K1,N2IN+.5*L1,O2IN+.5*M1,NIN+.5*N1,OIN+
1    .5*P1,NOIN+.5*Q1,N4sN+.5*R1,N2dN+.5*S1)
    L2 = H*FL(tN+.5*H,eN+.5*K1,N2IN+.5*L1,O2IN+.5*M1,NIN+.5*N1,OIN+
1    .5*P1,NON+.5*Q1,N4sN+.5*R1,N2dN+.5*S1)
    M2 = H*FM(tN+.5*H,eN+.5*K1,N2IN+.5*L1,O2IN+.5*M1,NIN+.5*N1,OIN+
1    .5*P1,NON+.5*Q1,N4sN+.5*R1,N2dN+.5*S1)
    N2 = H*FN(tN+.5*H,eN+.5*K1,N2IN+.5*L1,O2IN+.5*M1,NIN+.5*N1,OIN+
1    .5*P1,NOIN+.5*Q1,N4sN+.5*R1,N2dN+.5*S1)
    P2 = H*FP(tN+.5*H,eN+.5*K1,N2IN+.5*L1,O2IN+.5*M1,NIN+.5*N1,OIN+
1    .5*P1,NON+.5*Q1,N4sN+.5*R1,N2dN+.5*S1)

    Q2 = H*FQ(tN+.5*H,eN+.5*K1,N2IN+.5*L1,O2IN+.5*M1,NIN+.5*N1,OIN+
1    .5*P1,NON+.5*Q1,N4sN+.5*R1,N2dN+.5*S1)

    Q210 = H*FQ10(tN+.5*H,eN+.5*K1,N2IN+.5*L1,O2IN+.5*M1,NIN+.5*N1
$,OIN+.5*P1,NOI10+.5*Q110,NOI11+.5*Q111,NOI12+.5*Q112,N4sN+.5*R1,
$N2dN+.5*S1,NON+.5*Q1)
    Q211 = H*FQ11(tN+.5*H,eN+.5*K1,N2IN+.5*L1,O2IN+.5*M1,NIN+.5*N1
$,OIN+.5*P1,NOI11+.5*Q111,NOI12+.5*Q112,NOI13+.5*Q113,N4sN+.5*R1,
$N2dN+.5*S1)
    Q212 = H*FQ12(tN+.5*H,eN+.5*K1,N2IN+.5*L1,O2IN+.5*M1,NIN+.5*N1
$,OIN+.5*P1,NOI12+.5*Q112,NOI13+.5*Q113,NOI14+.5*Q114,N4sN+.5*R1,
$N2dN+.5*S1)
    Q213 = H*FQ13(tN+.5*H,eN+.5*K1,N2IN+.5*L1,O2IN+.5*M1,NIN+.5*N1
$,OIN+.5*P1,NOI13+.5*Q113,NOI14+.5*Q114,NOI15+.5*Q115,N4sN+.5*R1,
$N2dN+.5*S1)
    Q214 = H*FQ14(tN+.5*H,eN+.5*K1,N2IN+.5*L1,O2IN+.5*M1,NIN+.5*N1
$,OIN+.5*P1,NOI14+.5*Q114,NOI15+.5*Q115,NOI16+.5*Q116,N4sN+.5*R1,
$N2dN+.5*S1)
    Q215 = H*FQ15(tN+.5*H,eN+.5*K1,N2IN+.5*L1,O2IN+.5*M1,NIN+.5*N1
$,OIN+.5*P1,NOI15+.5*Q115,NOI16+.5*Q116,NOI17+.5*Q117,N4sN+.5*R1,
$N2dN+.5*S1)
    Q216 = H*FQ16(tN+.5*H,eN+.5*K1,N2IN+.5*L1,O2IN+.5*M1,NIN+.5*N1
$,OIN+.5*P1,NOI16+.5*Q116,NOI17+.5*Q117,NOI18+.5*Q118,N4sN+.5*R1,
$N2dN+.5*S1)
    Q217 = H*FQ17(tN+.5*H,eN+.5*K1,N2IN+.5*L1,O2IN+.5*M1,NIN+.5*N1
$,OIN+.5*P1,NOI17+.5*Q117,NOI18+.5*Q118,NOI19+.5*Q119,N4sN+.5*R1,
$N2dN+.5*S1)
    Q218 = H*FQ18(tN+.5*H,eN+.5*K1,N2IN+.5*L1,O2IN+.5*M1,NIN+.5*N1
$,OIN+.5*P1,NOI18+.5*Q118,NOI19+.5*Q119,NOI110+.5*Q1110,N4sN+.5*R1,
$N2dN+.5*S1)
    Q219 = H*FQ19(tN+.5*H,eN+.5*K1,N2IN+.5*L1,O2IN+.5*M1,NIN+.5*N1
$,OIN+.5*P1,NOI19+.5*Q119,NOI110+.5*Q1110,NOI111+.5*Q1111,
```

```
$N4sN+.5*R1,N2dN+.5*S1)
      Q2110 = H*FQ110(tN+.5*H,eN+.5*K1,N2IN+.5*L1,O2IN+.5*M1,NIN+.5*N1
$,OIN+.5*P1,NOI110+.5*Q1110,NOI111+.5*Q1111,NOI112+.5*Q1112,
$N4sN+.5*R1,N2dN+.5*S1)


      Q220 = H*FQ20(tN+.5*H,eN+.5*K1,N2IN+.5*L1,O2IN+.5*M1,NIN+.5*N1
$,OIN+.5*P1,NOI20+.5*Q120,NOI21+.5*Q121,NOI22+.5*Q122,N4sN+.5*R1,
$N2dN+.5*S1,NON+.5*Q1)
      Q221 = H*FQ21(tN+.5*H,eN+.5*K1,N2IN+.5*L1,O2IN+.5*M1,NIN+.5*N1
$,OIN+.5*P1,NOI21+.5*Q121,NOI22+.5*Q122,NOI23+.5*Q123,N4sN+.5*R1,
$N2dN+.5*S1)
      Q222 = H*FQ22(tN+.5*H,eN+.5*K1,N2IN+.5*L1,O2IN+.5*M1,NIN+.5*N1
$,OIN+.5*P1,NOI22+.5*Q122,NOI23+.5*Q123,NOI14+.5*Q124,N4sN+.5*R1,
$N2dN+.5*S1)
      Q223 = H*FQ23(tN+.5*H,eN+.5*K1,N2IN+.5*L1,O2IN+.5*M1,NIN+.5*N1
$,OIN+.5*P1,NOI23+.5*Q123,NOI24+.5*Q124,NOI25+.5*Q125,N4sN+.5*R1,
$N2dN+.5*S1)
      Q224 = H*FQ24(tN+.5*H,eN+.5*K1,N2IN+.5*L1,O2IN+.5*M1,NIN+.5*N1
$,OIN+.5*P1,NOI24+.5*Q124,NOI25+.5*Q125,NOI26+.5*Q126,N4sN+.5*R1,
$N2dN+.5*S1)
      Q225 = H*FQ25(tN+.5*H,eN+.5*K1,N2IN+.5*L1,O2IN+.5*M1,NIN+.5*N1
$,OIN+.5*P1,NOI25+.5*Q125,NOI26+.5*Q126,NOI27+.5*Q127,N4sN+.5*R1,
$N2dN+.5*S1)
      Q226 = H*FQ26(tN+.5*H,eN+.5*K1,N2IN+.5*L1,O2IN+.5*M1,NIN+.5*N1
$,OIN+.5*P1,NOI26+.5*Q126,NOI27+.5*Q127,NOI28+.5*Q128,N4sN+.5*R1,
$N2dN+.5*S1)
      Q227 = H*FQ27(tN+.5*H,eN+.5*K1,N2IN+.5*L1,O2IN+.5*M1,NIN+.5*N1
$,OIN+.5*P1,NOI27+.5*Q127,NOI28+.5*Q128,NOI29+.5*Q129,N4sN+.5*R1,
$N2dN+.5*S1)
      Q228 = H*FQ28(tN+.5*H,eN+.5*K1,N2IN+.5*L1,O2IN+.5*M1,NIN+.5*N1
$,OIN+.5*P1,NOI28+.5*Q128,NOI29+.5*Q129,NOI210+.5*Q1210,N4sN+.5*R1,
$N2dN+.5*S1)
      Q229 = H*FQ29(tN+.5*H,eN+.5*K1,N2IN+.5*L1,O2IN+.5*M1,NIN+.5*N1
$,OIN+.5*P1,NOI29+.5*Q129,NOI210+.5*Q1210,NOI211+.5*Q1211,
$N4sN+.5*R1,N2dN+.5*S1)
      Q2210 = H*FQ210(tN+.5*H,eN+.5*K1,N2IN+.5*L1,O2IN+.5*M1,NIN+.5*N1
$,OIN+.5*P1,NOI210+.5*Q1210,NOI211+.5*Q1211,NOI212+.5*Q1212,
$N4sN+.5*R1,N2dN+.5*S1)
      Q2211 = H*FQ211(tN+.5*H,eN+.5*K1,N2IN+.5*L1,O2IN+.5*M1,NIN+.5*N1
$,OIN+.5*P1,NOI211+.5*Q1211,NOI212+.5*Q1212,NOI213+.5*Q1213,
$N4sN+.5*R1,N2dN+.5*S1)
      Q2212 = H*FQ212(tN+.5*H,eN+.5*K1,N2IN+.5*L1,O2IN+.5*M1,NIN+.5*N1
$,OIN+.5*P1,NOI212+.5*Q1212,NOI213+.5*Q1213,NOI214+.5*Q1214,
$N4sN+.5*R1,N2dN+.5*S1)
      Q2213 = H*FQ213(tN+.5*H,eN+.5*K1,N2IN+.5*L1,O2IN+.5*M1,NIN+.5*N1
$,OIN+.5*P1,NOI213+.5*Q1213,NOI214+.5*Q1214,NOI215+.5*Q1215,
$N4sN+.5*R1,N2dN+.5*S1)
      Q2214 = H*FQ214(tN+.5*H,eN+.5*K1,N2IN+.5*L1,O2IN+.5*M1,NIN+.5*N1
$,OIN+.5*P1,NOI214+.5*Q1214,NOI215+.5*Q1215,NOI216+.5*Q1216,
$N4sN+.5*R1,N2dN+.5*S1)


      R2 = H*FR(tN+.5*H,eN+.5*K1,N2IN+.5*L1,O2IN+.5*M1,NIN+.5*N1,OIN+
1    .5*P1,NOIN+.5*Q1,N4sN+.5*R1,N2dN+.5*S1)
      S2 = H*FS(tN+.5*H,eN+.5*K1,N2IN+.5*L1,O2IN+.5*M1,NIN+.5*N1,OIN+
1    .5*P1,NOIN+.5*Q1,N4sN+.5*R1,N2dN+.5*S1)


      K3 = H*FK(tN+.5*H,eN+.5*K2,N2IN+.5*L2,O2IN+.5*M2,NIN+.5*N2,OIN+
1    .5*P2,NOIN+.5*Q2,N4sN+.5*R2,N2dN+.5*S2)
      L3 = H*FL(tN+.5*H,eN+.5*K2,N2IN+.5*L2,O2IN+.5*M2,NIN+.5*N2,OIN+
```

```
1   .5*P2,NON+.5*Q2,N4sN+.5*R2,N2dN+.5*S2)
    M3 = H*FM(tN+.5*H,eN+.5*K2,N2IN+.5*L2,O2IN+.5*M2,NIN+.5*N2,OIN+
1   .5*P2,NON+.5*Q2,N4sN+.5*R2,N2dN+.5*S2)
    N3 = H*FN(tN+.5*H,eN+.5*K2,N2IN+.5*L2,O2IN+.5*M2,NIN+.5*N2,OIN+
1   .5*P2,NOIN+.5*Q2,N4sN+.5*R2,N2dN+.5*S2)
    P3 = H*FP(tN+.5*H,eN+.5*K2,N2IN+.5*L2,O2IN+.5*M2,NIN+.5*N2,OIN+
1   .5*P2,NON+.5*Q2,N4sN+.5*R2,N2dN+.5*S2)


    Q3 = H*FQ(tN+.5*H,eN+.5*K2,N2IN+.5*L2,O2IN+.5*M2,NIN+.5*N2,OIN+
1   .5*P2,NON+.5*Q2,N4sN+.5*R2,N2dN+.5*S2)


    Q310 = H*FQ10(tN+.5*H,eN+.5*K2,N2IN+.5*L2,O2IN+.5*M2,NIN+.5*N2
$,OIN+.5*P2,NOI10+.5*Q210,NOI11+.5*Q211,NOI12+.5*Q212,N4sN+.5*R2,
$N2dN+.5*S2,NON+.5*Q2)
    Q311 = H*FQ11(tN+.5*H,eN+.5*K2,N2IN+.5*L2,O2IN+.5*M2,NIN+.5*N2
$,OIN+.5*P2,NOI11+.5*Q211,NOI12+.5*Q212,NOI13+.5*Q213,N4sN+.5*R2,
$N2dN+.5*S2)
    Q312 = H*FQ12(tN+.5*H,eN+.5*K2,N2IN+.5*L2,O2IN+.5*M2,NIN+.5*N2
$,OIN+.5*P2,NOI12+.5*Q212,NOI13+.5*Q213,NOI14+.5*Q214,N4sN+.5*R2,
$N2dN+.5*S2)
    Q313 = H*FQ13(tN+.5*H,eN+.5*K2,N2IN+.5*L2,O2IN+.5*M2,NIN+.5*N2
$,OIN+.5*P2,NOI13+.5*Q213,NOI14+.5*Q214,NOI15+.5*Q215,N4sN+.5*R2,
$N2dN+.5*S2)
    Q314 = H*FQ14(tN+.5*H,eN+.5*K2,N2IN+.5*L2,O2IN+.5*M2,NIN+.5*N2
$,OIN+.5*P2,NOI14+.5*Q214,NOI15+.5*Q215,NOI16+.5*Q216,N4sN+.5*R2,
$N2dN+.5*S2)
    Q315 = H*FQ15(tN+.5*H,eN+.5*K2,N2IN+.5*L2,O2IN+.5*M2,NIN+.5*N2
$,OIN+.5*P2,NOI15+.5*Q215,NOI16+.5*Q216,NOI17+.5*Q217,N4sN+.5*R2,
$N2dN+.5*S2)
    Q316 = H*FQ16(tN+.5*H,eN+.5*K2,N2IN+.5*L2,O2IN+.5*M2,NIN+.5*N2
$,OIN+.5*P2,NOI16+.5*Q216,NOI17+.5*Q217,NOI18+.5*Q218,N4sN+.5*R2,
$N2dN+.5*S2)
    Q317 = H*FQ17(tN+.5*H,eN+.5*K2,N2IN+.5*L2,O2IN+.5*M2,NIN+.5*N2
$,OIN+.5*P2,NOI17+.5*Q217,NOI18+.5*Q218,NOI19+.5*Q219,N4sN+.5*R2,
$N2dN+.5*S2)
    Q318 = H*FQ18(tN+.5*H,eN+.5*K2,N2IN+.5*L2,O2IN+.5*M2,NIN+.5*N2
$,OIN+.5*P2,NOI18+.5*Q218,NOI19+.5*Q219,NOI110+.5*Q2110,N4sN+.5*R2,
$N2dN+.5*S2)
    Q319 = H*FQ19(tN+.5*H,eN+.5*K2,N2IN+.5*L2,O2IN+.5*M2,NIN+.5*N2
$,OIN+.5*P2,NOI19+.5*Q219,NOI110+.5*Q2110,NOI111+.5*Q2111,
$N4sN+.5*R2,N2dN+.5*S2)
    Q3110 = H*FQ110(tN+.5*H,eN+.5*K2,N2IN+.5*L2,O2IN+.5*M2,NIN+.5*N2
$,OIN+.5*P2,NOI110+.5*Q2110,NOI111+.5*Q2111,NOI112+.5*Q2112,
$N4sN+.5*R2,N2dN+.5*S2)


    Q320 = H*FQ20(tN+.5*H,eN+.5*K2,N2IN+.5*L2,O2IN+.5*M2,NIN+.5*N2
$,OIN+.5*P2,NOI20+.5*Q220,NOI21+.5*Q221,NOI22+.5*Q222,N4sN+.5*R2,
$N2dN+.5*S2,NON+.5*Q2)
    Q321 = H*FQ21(tN+.5*H,eN+.5*K2,N2IN+.5*L2,O2IN+.5*M2,NIN+.5*N2
$,OIN+.5*P2,NOI21+.5*Q221,NOI22+.5*Q222,NOI23+.5*Q223,N4sN+.5*R2,
$N2dN+.5*S2)
    Q322 = H*FQ22(tN+.5*H,eN+.5*K2,N2IN+.5*L2,O2IN+.5*M2,NIN+.5*N2
$,OIN+.5*P2,NOI22+.5*Q222,NOI23+.5*Q223,NOI14+.5*Q224,N4sN+.5*R2,
$N2dN+.5*S2)
    Q323 = H*FQ23(tN+.5*H,eN+.5*K2,N2IN+.5*L2,O2IN+.5*M2,NIN+.5*N2
$,OIN+.5*P2,NOI23+.5*Q223,NOI24+.5*Q224,NOI25+.5*Q225,N4sN+.5*R2,
$N2dN+.5*S2)
    Q324 = H*FQ24(tN+.5*H,eN+.5*K2,N2IN+.5*L2,O2IN+.5*M2,NIN+.5*N2
$,OIN+.5*P2,NOI24+.5*Q224,NOI25+.5*Q225,NOI26+.5*Q226,N4sN+.5*R2,
```

```
$N2dN+.5*S2)
     Q325 = H*FQ25(tN+.5*H,eN+.5*K2,N2IN+.5*L2,O2IN+.5*M2,NIN+.5*N2
$,OIN+.5*P2,NOI25+.5*Q225,NOI26+.5*Q226,NOI27+.5*Q227,N4sN+.5*R2,
$N2dN+.5*S2)
     Q326 = H*FQ26(tN+.5*H,eN+.5*K2,N2IN+.5*L2,O2IN+.5*M2,NIN+.5*N2
$,OIN+.5*P2,NOI26+.5*Q226,NOI27+.5*Q227,NOI28+.5*Q228,N4sN+.5*R2,
$N2dN+.5*S2)
     Q327 = H*FQ27(tN+.5*H,eN+.5*K2,N2IN+.5*L2,O2IN+.5*M2,NIN+.5*N2
$,OIN+.5*P2,NOI27+.5*Q227,NOI28+.5*Q228,NOI29+.5*Q229,N4sN+.5*R2,
$N2dN+.5*S2)
     Q328 = H*FQ28(tN+.5*H,eN+.5*K2,N2IN+.5*L2,O2IN+.5*M2,NIN+.5*N2
$,OIN+.5*P2,NOI28+.5*Q228,NOI29+.5*Q229,NOI210+.5*Q2210,N4sN+.5*R2,
$N2dN+.5*S2)
     Q329 = H*FQ29(tN+.5*H,eN+.5*K2,N2IN+.5*L2,O2IN+.5*M2,NIN+.5*N2
$,OIN+.5*P2,NOI29+.5*Q229,NOI210+.5*Q2210,NOI211+.5*Q2211,
$N4sN+.5*R2,N2dN+.5*S2)
     Q3210 = H*FQ210(tN+.5*H,eN+.5*K2,N2IN+.5*L2,O2IN+.5*M2,NIN+.5*N2
$,OIN+.5*P2,NOI210+.5*Q2210,NOI211+.5*Q2211,NOI212+.5*Q2212,
$N4sN+.5*R2,N2dN+.5*S2)
     Q3211 = H*FQ211(tN+.5*H,eN+.5*K2,N2IN+.5*L2,O2IN+.5*M2,NIN+.5*N2
$,OIN+.5*P2,NOI211+.5*Q2211,NOI212+.5*Q2212,NOI213+.5*Q2213,
$N4sN+.5*R2,N2dN+.5*S2)
     Q3212 = H*FQ212(tN+.5*H,eN+.5*K2,N2IN+.5*L2,O2IN+.5*M2,NIN+.5*N2
$,OIN+.5*P2,NOI212+.5*Q2212,NOI213+.5*Q2213,NOI214+.5*Q2214,
$N4sN+.5*R2,N2dN+.5*S2)
     Q3213 = H*FQ213(tN+.5*H,eN+.5*K2,N2IN+.5*L2,O2IN+.5*M2,NIN+.5*N2
$,OIN+.5*P2,NOI213+.5*Q2213,NOI214+.5*Q2214,NOI215+.5*Q2215,
$N4sN+.5*R2,N2dN+.5*S2)
     Q3214 = H*FQ214(tN+.5*H,eN+.5*K2,N2IN+.5*L2,O2IN+.5*M2,NIN+.5*N2
$,OIN+.5*P2,NOI214+.5*Q2214,NOI215+.5*Q2215,NOI216+.5*Q2216,
$N4sN+.5*R2,N2dN+.5*S2)


     R3 = H*FR(tN+.5*H,eN+.5*K2,N2IN+.5*L2,O2IN+.5*M2,NIN+.5*N2,OIN+
1    .5*P2,NOIN+.5*Q2,N4sN+.5*R2,N2dN+.5*S2)
     S3 = H*FS(tN+.5*H,eN+.5*K2,N2IN+.5*L2,O2IN+.5*M2,NIN+.5*N2,OIN+
1    .5*P2,NOIN+.5*Q2,N4sN+.5*R2,N2dN+.5*S2)


     K4 = H*FK(tN+H,eN+K3,N2IN+L3,O2IN+M3,NIN+N3,OIN+
1    P3,NOIN+Q3,N4sN+R3,N2dN+S3)
     L4 = H*FL(tN+H,eN+K3,N2IN+L3,O2IN+M3,NIN+N3,OIN+
1    P3,NON+Q3,N4sN+R3,N2dN+S3)
     M4 = H*FM(tN+H,eN+K3,N2IN+L3,O2IN+M3,NIN+N3,OIN+
1    P3,NON+Q3,N4sN+R3,N2dN+S3)
     N4 = H*FN(tN+H,eN+K3,N2IN+L3,O2IN+M3,NIN+N3,OIN+
1    P3,NOIN+Q3,N4sN+R3,N2dN+S3)
     P4 = H*FP(tN+H,eN+K3,N2IN+L3,O2IN+M3,NIN+N3,OIN+
1    P3,NON+Q3,N4sN+R3,N2dN+S3)

     Q4 = H*FQ(tN+H,eN+K3,N2IN+L3,O2IN+M3,NIN+N3,OIN+
1    P3,NON+Q3,N4sN+R3,N2dN+S3)

     Q410 = H*FQ10(tN+H,eN+K3,N2IN+L3,O2IN+M3,NIN+N3
$,OIN+P3,NOI10+Q310,NOI11+Q311,NOI12+Q312,N4sN+R3,
$N2dN+S3,NON+Q3)
     Q411 = H*FQ11(tN+H,eN+K3,N2IN+L3,O2IN+M3,NIN+N3
$,OIN+P3,NOI11+Q311,NOI12+Q312,NOI13+Q313,N4sN+R3,
$N2dN+S3)
     Q412 = H*FQ12(tN+H,eN+K3,N2IN+L3,O2IN+M3,NIN+N3
$,OIN+P3,NOI12+Q312,NOI13+Q313,NOI14+Q314,N4sN+R3,
```

```
$N2dN+S3)
     Q413 = H*FQ13(tN+H,eN+K3,N2IN+L3,O2IN+M3,NIN+N3
$,OIN+P3,NOI13+Q313,NOI14+Q314,NOI15+Q315,N4sN+R3,
$N2dN+S3)
     Q414 = H*FQ14(tN+H,eN+K3,N2IN+L3,O2IN+M3,NIN+N3
$,OIN+P3,NOI14+Q314,NOI15+Q315,NOI16+Q316,N4sN+R3,
$N2dN+S3)
     Q415 = H*FQ15(tN+H,eN+K3,N2IN+L3,O2IN+M3,NIN+N3
$,OIN+P3,NOI15+Q315,NOI16+Q316,NOI17+Q317,N4sN+R3,
$N2dN+S3)
     Q416 = H*FQ16(tN+H,eN+K3,N2IN+L3,O2IN+M3,NIN+N3
$,OIN+P3,NOI16+Q316,NOI17+Q317,NOI18+Q318,N4sN+R3,
$N2dN+S3)
     Q417 = H*FQ17(tN+H,eN+K3,N2IN+L3,O2IN+M3,NIN+N3
$,OIN+P3,NOI17+Q317,NOI18+Q318,NOI19+Q319,N4sN+R3,
$N2dN+S3)
     Q418 = H*FQ18(tN+H,eN+K3,N2IN+L3,O2IN+M3,NIN+N3
$,OIN+P3,NOI18+Q318,NOI19+Q319,NOI110+Q3110,N4sN+R3,
$N2dN+S3)
     Q419 = H*FQ19(tN+H,eN+K3,N2IN+L3,O2IN+M3,NIN+N3
$,OIN+P3,NOI19+Q319,NOI110+Q3110,NOI111+Q3111,
$N4sN+R3,N2dN+S3)
     Q4110 = H*FQ110(tN+H,eN+K3,N2IN+L3,O2IN+M3,NIN+N3
$,OIN+P3,NOI110+Q3110,NOI111+Q3111,NOI112+Q3112,
$N4sN+R3,N2dN+S3)


     Q420 = H*FQ20(tN+H,eN+K3,N2IN+L3,O2IN+M3,NIN+N3
$,OIN+P3,NOI20+Q320,NOI21+Q321,NOI22+Q322,N4sN+R3,
$N2dN+S3,NON+Q3)
     Q421 = H*FQ21(tN+H,eN+K3,N2IN+L3,O2IN+M3,NIN+N3
$,OIN+P3,NOI21+Q321,NOI22+Q322,NOI23+Q323,N4sN+R3,
$N2dN+S3)
     Q422 = H*FQ22(tN+H,eN+K3,N2IN+L3,O2IN+M3,NIN+N3
$,OIN+P3,NOI22+Q322,NOI23+Q323,NOI14+Q324,N4sN+R3,
$N2dN+S3)
     Q423 = H*FQ23(tN+H,eN+K3,N2IN+L3,O2IN+M3,NIN+N3
$,OIN+P3,NOI23+Q323,NOI24+Q324,NOI25+Q325,N4sN+R3,
$N2dN+S3)
     Q424 = H*FQ24(tN+H,eN+K3,N2IN+L3,O2IN+M3,NIN+N3
$,OIN+P3,NOI24+Q324,NOI25+Q325,NOI26+Q326,N4sN+R3,
$N2dN+S3)
     Q425 = H*FQ25(tN+H,eN+K3,N2IN+L3,O2IN+M3,NIN+N3
$,OIN+P3,NOI25+Q325,NOI26+Q326,NOI27+Q327,N4sN+R3,
$N2dN+S3)
     Q426 = H*FQ26(tN+H,eN+K3,N2IN+L3,O2IN+M3,NIN+N3
$,OIN+P3,NOI26+Q326,NOI27+Q327,NOI28+Q328,N4sN+R3,
$N2dN+S3)
     Q427 = H*FQ27(tN+H,eN+K3,N2IN+L3,O2IN+M3,NIN+N3
$,OIN+P3,NOI27+Q327,NOI28+Q328,NOI29+Q329,N4sN+R3,
$N2dN+S3)
     Q428 = H*FQ28(tN+H,eN+K3,N2IN+L3,O2IN+M3,NIN+N3
$,OIN+P3,NOI28+Q328,NOI29+Q329,NOI210+Q3210,N4sN+R3,
$N2dN+S3)
     Q429 = H*FQ29(tN+H,eN+K3,N2IN+L3,O2IN+M3,NIN+N3
$,OIN+P3,NOI29+Q329,NOI210+Q3210,NOI211+Q3211,
$N4sN+R3,N2dN+S3)
     Q4210 = H*FQ210(tN+H,eN+K3,N2IN+L3,O2IN+M3,NIN+N3
$,OIN+P3,NOI210+Q3210,NOI211+Q3211,NOI212+Q3212,
$N4sN+R3,N2dN+S3)
     Q4211 = H*FQ211(tN+H,eN+K3,N2IN+L3,O2IN+M3,NIN+N3
```

```
$,OIN+P3,NOI211+Q3211,NOI212+Q3212,NOI213+Q3213,
$N4sN+R3,N2dN+S3) ·
   Q4212 = H*FQ212(tN+H,eN+K3,N2IN+L3,O2IN+M3,NIN+N3
$,OIN+P3,NOI212+Q3212,NOI213+Q3213,NOI214+Q3214,
$N4sN+R3,N2dN+S3)
   Q4213 = H*FQ213(tN+H,eN+K3,N2IN+L3,O2IN+M3,NIN+N3
$,OIN+P3,NOI213+Q3213,NOI214+Q3214,NOI215+Q3215,
$N4sN+R3,N2dN+S3)
   Q4214 = H*FQ214(tN+H,eN+K3,N2IN+L3,O2IN+M3,NIN+N3
$,OIN+P3,NOI214+Q3214,NOI215+Q3215,NOI216+Q3216,
$N4sN+R3,N2dN+S3)

   R4 = H*FR(tN+H,eN+K3,N2IN+L3,O2IN+M3,NIN+N3,OIN+
1  P3,NOIN+Q3,N4sN+R3,N2dN+S3)
   S4 = H*FS(tN+H,eN+K3,N2IN+L3,O2IN+M3,NIN+N3,OIN+
1  P3,NOIN+Q3,N4sN+R3,N2dN+S3)

   tN1 = tN + H
   eN1 = eN + (K1+2.*K2+2.*K3+K4)/6.
   N2IN1 = N2IN +(L1+2.*L2+2.*L3+L4)/6.
   O2IN1 = O2IN + (M1+2.*M2+2.*M3+M4)/6.
   NIN1 = NIN + (N1+2.*N2+2.*N3+N4)/6.
   OIN1 = OIN + (P1+2.*P2+2.*P3+P4)/6.
   NON1 = NON + (Q1+2.*Q2+2.*Q3+Q4)/6.

   NOJ10 = NOI10+(Q110+2.*Q210+2.*Q310+Q410)/6.
   NOJ11 = NOI11+(Q111+2.*Q211+2.*Q311+Q411)/6.
   NOJ12 = NOI12+(Q112+2.*Q212+2.*Q312+Q412)/6.
   NOJ13 = NOI13+(Q113+2.*Q213+2.*Q313+Q413)/6.
   NOJ14 = NOI14+(Q114+2.*Q214+2.*Q314+Q414)/6.
   NOJ15 = NOI15+(Q115+2.*Q215+2.*Q315+Q415)/6.
   NOJ16 = NOI16+(Q116+2.*Q216+2.*Q316+Q416)/6.
   NOJ17 = NOI17+(Q117+2.*Q217+2.*Q317+Q417)/6.
   NOJ18 = NOI18+(Q118+2.*Q218+2.*Q318+Q418)/6.
   NOJ19 = NOI19+(Q119+2.*Q219+2.*Q319+Q419)/6.
   NOJ110 = NOI110+(Q1110+2.*Q2110+2.*Q3110+Q4110)/6.

   NOJ20 = NOI20+(Q120+2.*Q220+2.*Q320+Q420)/6.
   NOJ21 = NOI21+(Q121+2.*Q221+2.*Q321+Q421)/6.
   NOJ22 = NOI22+(Q122+2.*Q222+2.*Q322+Q422)/6.
   NOJ23 = NOI23+(Q123+2.*Q223+2.*Q323+Q423)/6.
   NOJ24 = NOI24+(Q124+2.*Q224+2.*Q324+Q424)/6.
   NOJ25 = NOI25+(Q125+2.*Q225+2.*Q325+Q425)/6.
   NOJ26 = NOI26+(Q126+2.*Q226+2.*Q326+Q426)/6.
   NOJ27 = NOI27+(Q127+2.*Q227+2.*Q327+Q427)/6.
   NOJ28 = NOI28+(Q128+2.*Q228+2.*Q328+Q428)/6.
   NOJ29 = NOI29+(Q129+2.*Q229+2.*Q329+Q429)/6.
   NOJ210 = NOI210+(Q1210+2.*Q2210+2.*Q3210+Q4210)/6.
   NOJ211 = NOI211+(Q1211+2.*Q2211+2.*Q3211+Q4211)/6.
   NOJ212 = NOI212+(Q1212+2.*Q2212+2.*Q3212+Q4212)/6.
   NOJ213 = NOI213+(Q1213+2.*Q2213+2.*Q3213+Q4213)/6.
   NOJ214 = NOI214+(Q1214+2.*Q2214+2.*Q3214+Q4214)/6.

   NOIN1 =
$  NOJ10+NOJ11+NOJ12+NOJ13+NOJ14+NOJ15+NOJ16+NOJ17+
$  NOJ18+NOJ19+NOJ110+NOJ20+NOJ21+NOJ22+NOJ23+
$  NOJ24+NOJ25+NOJ26+NOJ27+NOJ28+NOJ29+NOJ210+
$  NOJ211+NOJ212+NOJ213+NOJ214

   N4sN1 = N4sN + (R1+2.*R2+2.*R3+R4)/6.
```

```fortran
      N2dN1 = N2dN +(S1+2.*S2+2.*S3+S4)/6.

      t(I)   = tN1
      e(I)   = eN1
      N2I(I) = N2IN1
      O2I(I) = O2IN1
      NI(I)  = NIN1
      OI(I)  = OIN1
      NOI(I) = NOIN1
      NO(I)  = NON1

      NOP10(I)=NOJ10
      NOP11(I)=NOJ11
      NOP12(I)=NOJ12
      NOP13(I)=NOJ13
      NOP14(I)=NOJ14
      NOP15(I)=NOJ15
      NOP16(I)=NOJ16
      NOP17(I)=NOJ17
      NOP18(I)=NOJ18
      NOP19(I)=NOJ19
      NOP110(I)=NOJ110

      NOP20(I)=NOJ20
      NOP21(I)=NOJ21
      NOP22(I)=NOJ22
      NOP23(I)=NOJ23
      NOP24(I)=NOJ24
      NOP25(I)=NOJ25
      NOP26(I)=NOJ26
      NOP27(I)=NOJ27
      NOP28(I)=NOJ28
      NOP29(I)=NOJ29
      NOP210(I)=NOJ210
      NOP211(I)=NOJ211
      NOP212(I)=NOJ212
      NOP213(I)=NOJ213
      NOP214(I)=NOJ214

      N4s(I) = N4sN1
      N2d(I) = N2dN1

c writes in order to monitor code
c      write(*,*)'I,tN,t(I),eN,e(I),NOI(I),NOP10(I),NOP11(I),NOP12(I),
c     $ NOP13(I),NOP14(I)=',I,tN,t(I),eN,e(I),NOI(I),NOP10(I),NOP11(I),
c     $ NOP12(I),NOP13(I),NOP14(I)

c      write(*,*)'I,tN,t(I),eN,e(I),NOI(I),NOP20(I),NOP21(I),NOP22(I),
c     $ NOP23(I),NOP24(I)=',I,tN,t(I),eN,e(I),NOI(I),NOP20(I),NOP21(I),
c     $ NOP22(I),NOP23(I),NOP24(I)


c      write(*,*)'I,NO(I),Ft(t(I))=',I,NO(I),Ft(t(I))

c      write(*,*)'I,NON,NON1,Q1,Q2,Q3,Q4=',I,NON,NON1,Q1,Q2,Q3,Q4

c      write(*,*) 'I,O2N2d,O2,N2d=',I,O2N2d,O2,N2d
c      write(*,*) 'I,O2N4s,O2,N4s=',I,O2N4s,O2,N4s
c      write(*,*) 'I,N2INO,N2I,NO=',I,N2INO,N2I,NO
c      write(*,*) 'I,O2INO,O2I,NO=',I,O2INO,O2I,NO
```

203

```fortran
c         write(*,*) 'I,OINO,OI,NO=',I,OINO,OI,NO


          tN   = tN1
          eN  =  eN1
          N2IN  =  N2IN1
          O2IN  =  O2IN1
          NIN  =  NIN1
          OIN  =  OIN1
          NOIN  =  NOIN1
          NON  =  NON1

          NOI10  =  NOJ10
          NOI11  =  NOJ11
          NOI12  =  NOJ12
          NOI13  =  NOJ13
          NOI14  =  NOJ14
          NOI15  =  NOJ15
          NOI16  =  NOJ16
          NOI17  =  NOJ17
          NOI18  =  NOJ18
          NOI19  =  NOJ19
          NOI110  =  NOJ110

          NOI20  =  NOJ20
          NOI21  =  NOJ21
          NOI22  =  NOJ22
          NOI23  =  NOJ23
          NOI24  =  NOJ24
          NOI25  =  NOJ25
          NOI26  =  NOJ26
          NOI27  =  NOJ27
          NOI28  =  NOJ28
          NOI29  =  NOJ29
          NOI210  =  NOJ210
          NOI211  =  NOJ211
          NOI212  =  NOJ212
          NOI213  =  NOJ213
          NOI214  =  NOJ214

          N4sN  =  N4sN1
          N2dN  =  N2dN1

10        CONTINUE

C *****************
C ***************** FOURTH ORDER RUNGE-KUTTA ---END---
C *****************




c find the total ion number density sumion(i)
          do 11 i=1,NLIM
          sumion(i)=N2I(i)+O2I(i)+NI(i)+OI(i)+NOI(i)
11        continue

c sum the NO+ in the field of view, using (14 m / 245 m/s) =.057 sec in window
c         Iwin=INT(.057/H)
c         if(Iwin.gt.NLIM)then
```

204

```
c          write(*,*)'Iwin greater than NLIM'
c          goto 14
c          endif
c          sum=0.0
c          do 12 i=1,Iwin
c          sum=sum+NOI(i)
c12        continue
c multiply by A, = 10.9 for NO+, v = 1 to 0
c          sum=10.9*sum

14         CALL MAXMIN(t,ItMX,tMX,ItMN,tMN,NLIM)
           CALL MAXMIN(e,IeMX,eMX,IeMN,eMN,NLIM)
           CALL MAXMIN(N2I,IN2IMX,N2IMX,IN2IMN,N2IMN,NLIM)
           CALL MAXMIN(O2I,IO2IMX,O2IMX,IO2IMN,O2IMN,NLIM)
           CALL MAXMIN(NI,INIMX,NIMX,INIMN,NIMN,NLIM)
           CALL MAXMIN(OI,IOIMX,OIMX,IOIMN,OIMN,NLIM)
           CALL MAXMIN(NOI,INOIMX,NOIMX,INOIMN,NOIMN,NLIM)
           CALL MAXMIN(N4s,IN4sMX,N4sMX,IN4sMN,N4sMN,NLIM)
           CALL MAXMIN(N2d,IN2dMX,N2dMX,IN2dMN,N2dMN,NLIM)
           CALL MAXMIN(sumion,IsMX,sMX,IsMN,sMN,NLIM)

           write(*,*)'H,qfactr =',H,qfactr
           write(*,*)'Qe =',Qe
           write(*,*)'QN2I =',QN2I
           write(*,*)'tdose =',tdose

           write(*,*)'e(IeMX),sumion(IeMX),NOI(IeMX)=',e(IeMX),sumion(IeMX)
     $     ,NOI(IeMX)

           WRITE(*,*)'ItMN,tMN,ItMX,tMX=',ItMN,tMN,ItMX,tMX
           WRITE(*,*)'IeMX,eMX,IeMN,eMN=',IeMX,eMX,IeMN,eMN
           WRITE(*,*)'IN2IMX,N2IMX,IN2IMN,N2IMN='
     1     ,IN2IMX,N2IMX,IN2IMN,N2IMN
           WRITE(*,*)'IO2IMX,O2IMX,IO2IMN,O2IMN='
     1     ,IO2IMX,O2IMX,IO2IMN,O2IMN
           WRITE(*,*)'INIMX,NIMX,INIMN,NIMN='
     1     ,INIMX,NIMX,INIMN,NIMN
           WRITE(*,*)'IOIMX,OIMX,IOIMN,OIMN='
     1     ,IOIMX,OIMX,IOIMN,OIMN
           WRITE(*,*)'INOIMX,NOIMX,INOIMN,NOIMN='
     1     ,INOIMX,NOIMX,INOIMN,NOIMN
c          WRITE(*,*)'IN4sMX,N4sMX,IN4sMN,N4sMN='
c      1   ,IN4sMX,N4sMX,IN4sMN,N4sMN
c          WRITE(*,*)'IN2dMX,N2dMX,IN2dMN,N2dMN='
c      1   ,IN2dMX,N2dMX,IN2dMN,N2dMN
           WRITE(*,*)'IsMX,sMX,IsMN,sMN='
     1     ,IsMX,sMX,IsMN,sMN


c          write(*,*)'NO+ line integral (photons/cm2/s) in window is',sum
c          write(*,*)
           write(*,*)'hit enter to continue'
           read(*,*)

           write(*,*)'It,Ie,IN2I,INOI =',It,Ie,INI,INOI

           write(*,*)'make FILES, or EXIT?(enter F,or E)'
           read(*,'(A)')Q
           if((Q.EQ.'F').or.(Q.EQ.'f'))goto 17
           goto 900
```

```
17          write(*,*)'enter name for "sumion" file'
            CALL MKASC(sumion,NLIM)
            write(*,*)'enter name for "time" file'
            CALL MKASC(t,NLIM)
            write(*,*)'enter name for "electron" file'
            CALL MKASC(e,NLIM)
            write(*,*)'enter name for "N2+" file'
            CALL MKASC(N2I,NLIM)
            write(*,*)'enter name for "O2"+ file'
            CALL MKASC(O2I,NLIM)
            write(*,*)'enter name for "N+" file'
            CALL MKASC(NI,NLIM)
            write(*,*)'enter name for "O+" file'
            CALL MKASC(OI,NLIM)
            write(*,*)'enter name for "NO+" file'
            CALL MKASC(NOI,NLIM)
            write(*,*)'enter name for "N(4S)" file'
            CALL MKASC(N4s,NLIM)
            write(*,*)'enter name for "N(2D)" file'
            CALL MKASC(N2d,NLIM)
            write(*,*)'enter name for "NO" file'
            CALL MKASC(NO,NLIM)

            write(*,*)'enter name for "NOP10" file'
            CALL MKASC(NOP10,NLIM)
            write(*,*)'enter name for "NOP11" file'
            CALL MKASC(NOP11,NLIM)
            write(*,*)'enter name for "NOP12" file'
            CALL MKASC(NOP12,NLIM)
            write(*,*)'enter name for "NOP13" file'
            CALL MKASC(NOP13,NLIM)
            write(*,*)'enter name for "NOP14" file'
            CALL MKASC(NOP14,NLIM)
            write(*,*)'enter name for "NOP15" file'
            CALL MKASC(NOP15,NLIM)
            write(*,*)'enter name for "NOP16" file'
            CALL MKASC(NOP16,NLIM)
            write(*,*)'enter name for "NOP17" file'
            CALL MKASC(NOP17,NLIM)
            write(*,*)'enter name for "NOP18" file'
            CALL MKASC(NOP18,NLIM)
            write(*,*)'enter name for "NOP19" file'
            CALL MKASC(NOP19,NLIM)
            write(*,*)'enter name for "NOP110" file'
            CALL MKASC(NOP110,NLIM)

            write(*,*)'enter name for "NOP20" file'
            CALL MKASC(NOP20,NLIM)
            write(*,*)'enter name for "NOP21" file'
            CALL MKASC(NOP21,NLIM)
            write(*,*)'enter name for "NOP22" file'
            CALL MKASC(NOP22,NLIM)
            write(*,*)'enter name for "NOP23" file'
            CALL MKASC(NOP23,NLIM)
            write(*,*)'enter name for "NOP24" file'
            CALL MKASC(NOP24,NLIM)
            write(*,*)'enter name for "NOP25" file'
            CALL MKASC(NOP25,NLIM)
            write(*,*)'enter name for "NOP26" file'
```

206

```
            CALL MKASC(NOP26,NLIM)
            write(*,*)'enter name for "NOP27" file'
            CALL MKASC(NOP27,NLIM)
            write(*,*)'enter name for "NOP28" file'
            CALL MKASC(NOP28,NLIM)
            write(*,*)'enter name for "NOP29" file'
            CALL MKASC(NOP29,NLIM)
            write(*,*)'enter name for "NOP210" file'
            CALL MKASC(NOP210,NLIM)
            write(*,*)'enter name for "NOP211" file'
            CALL MKASC(NOP211,NLIM)
            write(*,*)'enter name for "NOP212" file'
            CALL MKASC(NOP212,NLIM)
            write(*,*)'enter name for "NOP213" file'
            CALL MKASC(NOP213,NLIM)
            write(*,*)'enter name for "NOP214" file'
            CALL MKASC(NOP214,NLIM)

900         CONTINUE

            END


C-----------------------
            FUNCTION Ft(t)
c this function is the ABEL inverse transform of the 3914 A beam profile
            REAL F(200)
            REAL t
            REAL NN,O2,O,Tr,N2Ie,O2Ie,OIe,NIe,NOIe,
      1     N2IO2,N2IO,N2IN4s,O2IN2d,N4sO2I,N2de,NIO2,NIO,N4sPNI,N2dPNI,
      2     N4sPO,N2dPO,NOIA1,NOIA2,NOIA3,NOIN2,NOIP2d,NOIP4s,OIO2,OIN2,
      3     ON2I,O2NI,O2N4s,ON2d,O2N2d,N2N2d,NIPO2,N2O2I,
      4     t0,e0,N2IO,O2IO,OIO,NIO,NOIO,N2DO,N4SO,PI,ASIG,SINTHT,WAIST,
      5     QN2I,QO2I,QOI,Qe,
      6     Vbeam,tdose,
      7     NOIA4,NOIA5,NOIA6,NOIA7,NOIA8,NOIA9,NOIA10,NOIA11,NOIA12,
      8     NOIB2,NOIB3,NOIB4,NOIB5,NOIB6,NOIB7,NOIB8,NOIB9,NOIB10,NOIB11,
      9     NOIA13,NOIA14,NOIA15,NOIA16,
      $     NOIB12,NOIB13,NOIB14,NOIB15,NOIB16

            COMMON /BLK1/NN,O2,O,Tr,N2Ie,O2Ie,OIe,NIe,NOIe,
      1     N2IO2,N2IO,N2IN4s,O2IN2d,N4sO2I,N2de,NIO2,NIO,N4sPNI,N2dPNI,
      2     N4sPO,N2dPO,NOIA1,NOIA2,NOIA3,NOIN2,NOIP2d,NOIP4s,OIO2,OIN2,
      3     ON2I,O2NI,O2N4s,ON2d,O2N2d,N2N2d,NIPO2,N2O2I,
      4     t0,e0,N2IO,O2IO,OIO,NIO,NOIO,N2DO,N4SO,PI,ASIG,SINTHT,WAIST,
      5     QN2I,QO2I,QOI,Qe,
      6     Vbeam,tdose,
      7     NOIA4,NOIA5,NOIA6,NOIA7,NOIA8,NOIA9,NOIA10,NOIA11,NOIA12,
      8     NOIB2,NOIB3,NOIB4,NOIB5,NOIB6,NOIB7,NOIB8,NOIB9,NOIB10,NOIB11,
      9     NOIA13,NOIA14,NOIA15,NOIA16,
      $     NOIB12,NOIB13,NOIB14,NOIB15,NOIB16

      DATA (F(I),I=1,151) /
$0.0547970,0.0476440,0.0446150,0.0422104,0.0401156,0.0382139,0.036
$4485,0.0347875,0.0332251,0.0317153,0.0302670,0.0288774,0.0275456,0
$.0262514,0.0250175,0.0238452,0.0227012,0.0215997,0.0205397,0.01951
$99,0.0185393,0.0175972,0.0166924,0.0158242,0.0149917,0.0141940,0.0
$134302,0.0126995,0.0120010,0.0113337,0.0106968,0.0100894,0.0095106
$2,0.00895943,0.00843498,0.00793635,0.00746268,0.00701305,0.0065863
$9,0.00618207,0.00579910,0.00543665,0.00509384,0.00476987,0.0044638
$9,0.00417514,0.00390282,0.00364618,0.00340451,0.00317704,0.0029631
```

207

```
      $2,0.00276207,0.00257324,0.00239601,0.00222976,0.00207394,0.0019279
      $6,0.00179129,0.00166343,0.00154387,0.00143216,0.00132783,0.0012304
      $7,0.00113966,0.00105501,0.000976145,0.000903682,0.000835292,0.0007
      $71687,0.000712574,0.000657664,0.000606676,0.000559369,0.000515508,
      $0.000474845,0.000437186,0.000402320,0.000370058,0.000340217,0.0003
      $12637,0.000287158,0.000263630,0.000241918,0.000221893,0.000203429,
      $0.000186418,0.000170754,0.000156331,0.000143063,0.000130863,0.0001
      $19649,0.000109347,0.0000998881,0.0000912075,0.0000832445,0.0000759
      $416,0.0000692520,0.0000631233,0.0000575120,0.0000523779,0.00004767
      $95,0.0000433858,0.0000394625,0.0000358776,0.0000326035,0.000029618
      $2,0.0000268947,0.0000244104,0.0000221469,0.0000200855,0.0000182079
      $,0.0000164994,0.0000149452,0.0000135316,0.0000122469,0.0000110798,
      $0.0000100195,0.00000905756,0.00000818471,0.00000739278,0.000006674
      $85,0.00000602427,0.00000543516,0.00000490160,0.00000441877,0.00000
      $398196,0.00000358687,0.00000322977,0.00000290717,0.00000261576,0.0
      $0000235265,0.00000211521,0.00000190103,0.00000170791,0.00000153379
      $,0.00000137691,0.00000123562,0.00000110842,0.000000993985,0.000000
      $890965,0.000000798383,0.000000715139,0.000000640349,0.000000573175
      $,0.000000512873,0.000000458716,0.000000410144,0.000000366581,0.000
      $000327545,0.000000292543,0.000000261190 /


c       Ft=1.0
c       IF((t.LT.-tdose).OR.(t.GT.0))THEN
c       Ft=0.0
c       ENDIF

This is the initial 3914 A beam profile, here not used directly.
c define the normalized beam profile with parameters
c where   tdose=3*WAIST/Vbeam,
c all terms suspended
c       Ft= p**(1-1/p)/(2*WAIST*GAMMA(1/p))*EXP(-(1/p)*
c     1  EXP(-(1/p)*ABS((Vbeam*t-CENTROID)/WAIST)**p)
c hardwire f(t)
c       Ft=0.187373*EXP(-2.08538E-04*ABS(2.45E+04*t+211)**1.49)

c this function is the ABEL inverse transform of the 3914 A beam profile
c (done elsewhere) using the above data F(I) set as input
c tdose = .05 sec
c time inteval is   H = .1 meter / 245 meters/sec = 0.000408163 sec
c start at -tdose = -.05 sec,
c tdose time is .05 sec / .000408163 sec = 122.5 time intevals

      IF((t.GE.-tdose).AND.(t.LT.0.0))THEN
      I=INT(122.5-2450*(t+tdose)+1)
      Ft=F(I)
      ENDIF
      IF((t.GE.0.0).AND.(t.LE.tdose))THEN
      I=INT(2450*t+1)
      Ft=F(I)
      ENDIF
      IF((t.LT.-tdose).OR.(t.GT.tdose))THEN
      Ft=0.0
      ENDIF

      RETURN
      END

C ------------------------
c e , the electron production and loss function
```

```
      FUNCTION FK(t,e,N2I,O2I,NI,OI,NOI,N4s,N2d)

      REAL t,e,N2I,O2I,NI,OI,NOI,N4s,N2d
      REAL NN,O2,O,Tr,N2Ie,O2Ie,OIe,NIe,NOIe,
     1 N2IO2,N2IO,N2IN4s,O2IN2d,N4sO2I,N2de,NIO2,NIO,N4sPNI,N2dPNI,
     2 N4sPO,N2dPO,NOIA1,NOIA2,NOIA3,NOIN2,NOIP2d,NOIP4s,OIO2,OIN2,
     3 ON2I,O2NI,O2N4s,ON2d,O2N2d,N2N2d,NIPO2,N2O2I,
     4 t0,e0,N2IO,O2IO,OIO,NIO,NOIO,N2DO,N4SO,PI,ASIG,SINTHT,WAIST,
     5 QN2I,QO2I,QOI,Qe,
     6 Vbeam,tdose,
     7 NOIA4,NOIA5,NOIA6,NOIA7,NOIA8,NOIA9,NOIA10,NOIA11,NOIA12,
     8 NOIB2,NOIB3,NOIB4,NOIB5,NOIB6,NOIB7,NOIB8,NOIB9,NOIB10,NOIB11,
     9 NOIA13,NOIA14,NOIA15,NOIA16,           ..  ...
     $ NOIB12,NOIB13,NOIB14,NOIB15,NOIB16

      COMMON /BLK1/NN,O2,O,Tr,N2Ie,O2Ie,OIe,NIe,NOIe,
     1 N2IO2,N2IO,N2IN4s,O2IN2d,N4sO2I,N2de,NIO2,NIO,N4sPNI,N2dPNI,
     2 N4sPO,N2dPO,NOIA1,NOIA2,NOIA3,NOIN2,NOIP2d,NOIP4s,OIO2,OIN2,
     3 ON2I,O2NI,O2N4s,ON2d,O2N2d,N2N2d,NIPO2,N2O2I,
     4 t0,e0,N2IO,O2IO,OIO,NIO,NOIO,N2DO,N4SO,PI,ASIG,SINTHT,WAIST,
     5 QN2I,QO2I,QOI,Qe,
     6 Vbeam,tdose,
     7 NOIA4,NOIA5,NOIA6,NOIA7,NOIA8,NOIA9,NOIA10,NOIA11,NOIA12,
     8 NOIB2,NOIB3,NOIB4,NOIB5,NOIB6,NOIB7,NOIB8,NOIB9,NOIB10,NOIB11,
     9 NOIA13,NOIA14,NOIA15,NOIA16,
     $ NOIB12,NOIB13,NOIB14,NOIB15,NOIB16
c e
      FK=Qe*Ft(t)-(N2Ie*N2I+O2Ie*O2I+NIe*NI+OIe*OI+
     1 NOIe*NOI)*e
      RETURN
      END
C-------------------------
c N2I , the N2+ production and loss function
      FUNCTION FL(t,e,N2I,O2I,NI,OI,NO,N4s,N2d)

      REAL t,e,N2I,O2I,NI,OI,NO,N4s,N2d
      REAL NN,O2,O,Tr,N2Ie,O2Ie,OIe,NIe,NOIe,
     1 N2IO2,N2IO,N2IN4s,O2IN2d,N4sO2I,N2de,NIO2,NIO,N4sPNI,N2dPNI,
     2 N4sPO,N2dPO,NOIA1,NOIA2,NOIA3,NOIN2,NOIP2d,NOIP4s,OIO2,OIN2,
     3 ON2I,O2NI,O2N4s,ON2d,O2N2d,N2N2d,NIPO2,N2O2I,
     4 t0,e0,N2IO,O2IO,OIO,NIO,NOIO,N2DO,N4SO,PI,ASIG,SINTHT,WAIST,
     5 QN2I,QO2I,QOI,Qe,
     6 Vbeam,tdose,
     7 NOIA4,NOIA5,NOIA6,NOIA7,NOIA8,NOIA9,NOIA10,NOIA11,NOIA12,
     8 NOIB2,NOIB3,NOIB4,NOIB5,NOIB6,NOIB7,NOIB8,NOIB9,NOIB10,NOIB11,
     9 NOIA13,NOIA14,NOIA15,NOIA16,
     $ NOIB12,NOIB13,NOIB14,NOIB15,NOIB16

      REAL N2INO,O2INO,OINO

      COMMON /BLK1/NN,O2,O,Tr,N2Ie,O2Ie,OIe,NIe,NOIe,
     1 N2IO2,N2IO,N2IN4s,O2IN2d,N4sO2I,N2de,NIO2,NIO,N4sPNI,N2dPNI,
     2 N4sPO,N2dPO,NOIA1,NOIA2,NOIA3,NOIN2,NOIP2d,NOIP4s,OIO2,OIN2,
     3 ON2I,O2NI,O2N4s,ON2d,O2N2d,N2N2d,NIPO2,N2O2I,
     4 t0,e0,N2IO,O2IO,OIO,NIO,NOIO,N2DO,N4SO,PI,ASIG,SINTHT,WAIST,
     5 QN2I,QO2I,QOI,Qe,
     6 Vbeam,tdose,
     7 NOIA4,NOIA5,NOIA6,NOIA7,NOIA8,NOIA9,NOIA10,NOIA11,NOIA12,
     8 NOIB2,NOIB3,NOIB4,NOIB5,NOIB6,NOIB7,NOIB8,NOIB9,NOIB10,NOIB11,
     9 NOIA13,NOIA14,NOIA15,NOIA16, .
```

```fortran
     $    NOIB12,NOIB13,NOIB14,NOIB15,NOIB16

          COMMON /BLK2/N2INO,O2INO,OINO
c N2+
          FL=QN2I*Ft(t)-(N2Ie*e+ON2I*O+NOIP2d*O+NOIP4s*O+N2IN4s*N4s
     1    +N2IO2*O2)*N2I - N2INO*N2I*NO

          RETURN
          END
C------------------------
c O2I, the O2+ production and loss function
          FUNCTION FM(t,e,N2I,O2I,NI,OI,NO,N4s,N2d)

          REAL t,e,N2I,O2I,NI,OI,NO,N4s,N2d
          REAL NN,O2,O,Tr,N2Ie,O2Ie,OIe,NIe,NOIe,
     1    N2IO2,N2IO,N2IN4s,O2IN2d,N4sO2I,N2de,NIO2,NIO,N4sPNI,N2dPNI,
     2    N4sPO,N2dPO,NOIA1,NOIA2,NOIA3,NOIN2,NOIP2d,NOIP4s,OIO2,OIN2,
     3    ON2I,O2NI,O2N4s,ON2d,O2N2d,N2N2d,NIPO2,N2O2I,
     4    t0,e0,N2I0,O2I0,OIO,NIO,NOIO,N2D0,N4S0,PI,ASIG,SINTHT,WAIST,
     5    QN2I,QO2I,QOI,Qe,
     6    Vbeam,tdose,
     7    NOIA4,NOIA5,NOIA6,NOIA7,NOIA8,NOIA9,NOIA10,NOIA11,NOIA12,
     8    NOIB2,NOIB3,NOIB4,NOIB5,NOIB6,NOIB7,NOIB8,NOIB9,NOIB10,NOIB11,
     9    NOIA13,NOIA14,NOIA15,NOIA16,
     $    NOIB12,NOIB13,NOIB14,NOIB15,NOIB16

          REAL N2INO,O2INO,OINO

          COMMON /BLK1/NN,O2,O,Tr,N2Ie,O2Ie,OIe,NIe,NOIe,
     1    N2IO2,N2IO,N2IN4s,O2IN2d,N4sO2I,N2de,NIO2,NIO,N4sPNI,N2dPNI,
     2    N4sPO,N2dPO,NOIA1,NOIA2,NOIA3,NOIN2,NOIP2d,NOIP4s,OIO2,OIN2,
     3    ON2I,O2NI,O2N4s,ON2d,O2N2d,N2N2d,NIPO2,N2O2I,
     4    t0,e0,N2I0,O2I0,OIO,NIO,NOIO,N2D0,N4S0,PI,ASIG,SINTHT,WAIST,
     5    QN2I,QO2I,QOI,Qe,
     6    Vbeam,tdose,
     7    NOIA4,NOIA5,NOIA6,NOIA7,NOIA8,NOIA9,NOIA10,NOIA11,NOIA12,
     8    NOIB2,NOIB3,NOIB4,NOIB5,NOIB6,NOIB7,NOIB8,NOIB9,NOIB10,NOIB11,
     9    NOIA13,NOIA14,NOIA15,NOIA16,
     $    NOIB12,NOIB13,NOIB14,NOIB15,NOIB16

          COMMON /BLK2/N2INO,O2INO,OINO
c O2+
          FM=QO2I*Ft(t)+(N4sPNI*O2*NI+N2dPNI*O2*NI+N2IO2*O2*N2I+
     1    OIO2*O2*OI)-(O2Ie*e+O2IN2d*N2d+N4sO2I*N4s+N2O2I*NN)*O2I
     2    -O2INO*O2I*NO

          RETURN
          END
C------------------------
c NI , the N+ production and loss function
          FUNCTION FN(t,e,N2I,O2I,NI,OI,NOI,N4s,N2d)

          REAL t,e,N2I,O2I,NI,OI,NOI,N4s,N2d
          REAL NN,O2,O,Tr,N2Ie,O2Ie,OIe,NIe,NOIe,
     1    N2IO2,N2IO,N2IN4s,O2IN2d,N4sO2I,N2de,NIO2,NIO,N4sPNI,N2dPNI,
     2    N4sPO,N2dPO,NOIA1,NOIA2,NOIA3,NOIN2,NOIP2d,NOIP4s,OIO2,OIN2,
     3    ON2I,O2NI,O2N4s,ON2d,O2N2d,N2N2d,NIPO2,N2O2I,
     4    t0,e0,N2I0,O2I0,OIO,NIO,NOIO,N2D0,N4S0,PI,ASIG,SINTHT,WAIST,
     5    QN2I,QO2I,QOI,Qe,
     6    Vbeam,tdose,
```

```
      7   NOIA4,NOIA5,NOIA6,NOIA7,NOIA8,NOIA9,NOIA10,NOIA11,NOIA12,
      8   NOIB2,NOIB3,NOIB4,NOIB5,NOIB6,NOIB7,NOIB8,NOIB9,NOIB10,NOIB11,
      9   NOIA13,NOIA14,NOIA15,NOIA16,
      $   NOIB12,NOIB13,NOIB14,NOIB15,NOIB16

          COMMON /BLK1/NN,O2,O,Tr,N2Ie,O2Ie,OIe,NIe,NOIe,
      1   N2IO2,N2IO,N2IN4s,O2IN2d,N4sO2I,N2de,NIO2,NIO,N4sPNI,N2dPNI,
      2   N4sPO,N2dPO,NOIA1,NOIA2,NOIA3,NOIN2,NOIP2d,NOIP4s,OIO2,OIN2,
      3   ON2I,O2NI,O2N4s,ON2d,O2N2d,N2N2d,NIPO2,N2O2I,
      4   t0,e0,N2IO,O2IO,OIO,NIO,NOIO,N2DO,N4SO,PI,ASIG,SINTHT,WAIST,
      5   QN2I,QO2I,QOI,Qe,
      6   Vbeam,tdose,
      7   NOIA4,NOIA5,NOIA6,NOIA7,NOIA8,NOIA9,NOIA10,NOIA11,NOIA12,
      8   NOIB2,NOIB3,NOIB4,NOIB5,NOIB6,NOIB7,NOIB8,NOIB9,NOIB10,NOIB11,
      9   NOIA13,NOIA14,NOIA15,NOIA16,
      $   NOIB12,NOIB13,NOIB14,NOIB15,NOIB16
c N+
          FN=0.25*QN2I*Ft(t)+(N2IN4s*N4s*N2I+O2IN2d*N2d*O2I)
      1   -(NIe*e+NIO*O+NIPO2*O2+N4sPNI*O2+N2dPNI*O2)*NI
          RETURN
          END
C-------------------------
c OI , the O+ production and loss function
          FUNCTION FP(t,e,N2I,O2I,NI,OI,NO,N4s,N2d)

          REAL t,e,N2I,O2I,NI,OI,NO,N4s,N2d
          REAL NN,O2,O,Tr,N2Ie,O2Ie,OIe,NIe,NOIe,
      1   N2IO2,N2IO,N2IN4s,O2IN2d,N4sO2I,N2de,NIO2,NIO,N4sPNI,N2dPNI,
      2   N4sPO,N2dPO,NOIA1,NOIA2,NOIA3,NOIN2,NOIP2d,NOIP4s,OIO2,OIN2,
      3   ON2I,O2NI,O2N4s,ON2d,O2N2d,N2N2d,NIPO2,N2O2I,
      4   t0,e0,N2IO,O2IO,OIO,NIO,NOIO,N2DO,N4SO,PI,ASIG,SINTHT,WAIST,
      5   QN2I,QO2I,QOI,Qe,
      6   Vbeam,tdose,
      7   NOIA4,NOIA5,NOIA6,NOIA7,NOIA8,NOIA9,NOIA10,NOIA11,NOIA12,
      8   NOIB2,NOIB3,NOIB4,NOIB5,NOIB6,NOIB7,NOIB8,NOIB9,NOIB10,NOIB11,
      9   NOIA13,NOIA14,NOIA15,NOIA16,
      $   NOIB12,NOIB13,NOIB14,NOIB15,NOIB16

          REAL N2INO,O2INO,OINO

          COMMON /BLK1/NN,O2,O,Tr,N2Ie,O2Ie,OIe,NIe,NOIe,
      1   N2IO2,N2IO,N2IN4s,O2IN2d,N4sO2I,N2de,NIO2,NIO,N4sPNI,N2dPNI,
      2   N4sPO,N2dPO,NOIA1,NOIA2,NOIA3,NOIN2,NOIP2d,NOIP4s,OIO2,OIN2,
      3   ON2I,O2NI,O2N4s,ON2d,O2N2d,N2N2d,NIPO2,N2O2I,
      4   t0,e0,N2IO,O2IO,OIO,NIO,NOIO,N2DO,N4SO,PI,ASIG,SINTHT,WAIST,
      5   QN2I,QO2I,QOI,Qe,
      6   Vbeam,tdose,
      7   NOIA4,NOIA5,NOIA6,NOIA7,NOIA8,NOIA9,NOIA10,NOIA11,NOIA12,
      8   NOIB2,NOIB3,NOIB4,NOIB5,NOIB6,NOIB7,NOIB8,NOIB9,NOIB10,NOIB11,
      9   NOIA13,NOIA14,NOIA15,NOIA16,
      $   NOIB12,NOIB13,NOIB14,NOIB15,NOIB16

          COMMON /BLK2/N2INO,O2INO,OINO
c O+
          FP=(0.5*QO2I+QOI)*Ft(t)+(NIO*O*NI+ON2I*O*N2I)
      1   -(OIe*e+OIO2*O2+OIN2*NN)*OI
      2   -OINO*OI*NO

          RETURN
          END
```

211

```
C------------------------
c NO , the NO production and loss function
c ( total NO, all vibrational levels lumped together)
      FUNCTION FQ(t,e,N2I,O2I,NI,OI,NO,N4s,N2d)

      REAL t,e,N2I,O2I,NI,OI,NO,N4s,N2d
      REAL NN,O2,O,Tr,N2Ie,O2Ie,OIe,NIe,NOIe,
     1 N2IO2,N2IO,N2IN4s,O2IN2d,N4sO2I,N2de,NIO2,NIO,N4sPNI,N2dPNI,
     2 N4sPO,N2dPO,NOIA1,NOIA2,NOIA3,NOIN2,NOIP2d,NOIP4s,OIO2,OIN2,
     3 ON2I,O2NI,O2N4s,ON2d,O2N2d,N2N2d,NIPO2,N2O2I,
     4 t0,e0,N2IO,O2IO,OIO,NIO,NOIO,N2D0,N4S0,PI,ASIG,SINTHT,WAIST,
     5 QN2I,QO2I,QOI,Qe,
     6 Vbeam,tdose,
     7 NOIA4,NOIA5,NOIA6,NOIA7,NOIA8,NOIA9,NOIA10,NOIA11,NOIA12,
     8 NOIB2,NOIB3,NOIB4,NOIB5,NOIB6,NOIB7,NOIB8,NOIB9,NOIB10,NOIB11,
     9 NOIA13,NOIA14,NOIA15,NOIA16,
     $ NOIB12,NOIB13,NOIB14,NOIB15,NOIB16

      REAL N2INO,O2INO,OINO

      COMMON /BLK1/NN,O2,O,Tr,N2Ie,O2Ie,OIe,NIe,NOIe,
     1 N2IO2,N2IO,N2IN4s,O2IN2d,N4sO2I,N2de,NIO2,NIO,N4sPNI,N2dPNI,
     2 N4sPO,N2dPO,NOIA1,NOIA2,NOIA3,NOIN2,NOIP2d,NOIP4s,OIO2,OIN2,
     3 ON2I,O2NI,O2N4s,ON2d,O2N2d,N2N2d,NIPO2,N2O2I,
     4 t0,e0,N2IO,O2IO,OIO,NIO,NOIO,N2D0,N4S0,PI,ASIG,SINTHT,WAIST,
     5 QN2I,QO2I,QOI,Qe,
     6 Vbeam,tdose,
     7 NOIA4,NOIA5,NOIA6,NOIA7,NOIA8,NOIA9,NOIA10,NOIA11,NOIA12,
     8 NOIB2,NOIB3,NOIB4,NOIB5,NOIB6,NOIB7,NOIB8,NOIB9,NOIB10,NOIB11,
     9 NOIA13,NOIA14,NOIA15,NOIA16,
     $ NOIB12,NOIB13,NOIB14,NOIB15,NOIB16

      COMMON /BLK2/N2INO,O2INO,OINO
c NO
      FQ=
     1   O2N2d*O2*N2d
     2  +O2N4s*O2*N4s
     3  -N2INO*N2I*NO
     4  -O2INO*O2I*NO
     5  -OINO*OI*NO

      RETURN
      END
C------------------------
c N4s , the N(4S) production and loss function

      FUNCTION FR(t,e,N2I,O2I,NI,OI,NOI,N4s,N2d)

      REAL t,e,N2I,O2I,NI,OI,NOI,N4s,N2d
      REAL NN,O2,O,Tr,N2Ie,O2Ie,OIe,NIe,NOIe,
     1 N2IO2,N2IO,N2IN4s,O2IN2d,N4sO2I,N2de,NIO2,NIO,N4sPNI,N2dPNI,
     2 N4sPO,N2dPO,NOIA1,NOIA2,NOIA3,NOIN2,NOIP2d,NOIP4s,OIO2,OIN2,
     3 ON2I,O2NI,O2N4s,ON2d,O2N2d,N2N2d,NIPO2,N2O2I,
     4 t0,e0,N2IO,O2IO,OIO,NIO,NOIO,N2D0,N4S0,PI,ASIG,SINTHT,WAIST,
     5 QN2I,QO2I,QOI,Qe,
     6 Vbeam,tdose,
     7 NOIA4,NOIA5,NOIA6,NOIA7,NOIA8,NOIA9,NOIA10,NOIA11,NOIA12,
     8 NOIB2,NOIB3,NOIB4,NOIB5,NOIB6,NOIB7,NOIB8,NOIB9,NOIB10,NOIB11,
     9 NOIA13,NOIA14,NOIA15,NOIA16,  ·
     $ NOIB12,NOIB13,NOIB14,NOIB15,NOIB16
```

```fortran
        COMMON /BLK1/NN,O2,O,Tr,N2Ie,O2Ie,OIe,NIe,NOIe,
     1  N2IO2,N2IO,N2IN4s,O2IN2d,N4sO2I,N2de,NIO2,NIO,N4sPNI,N2dPNI,
     2  N4sPO,N2dPO,NOIA1,NOIA2,NOIA3,NOIN2,NOIP2d,NOIP4s,OIO2,OIN2,
     3  ON2I,O2NI,O2N4s,ON2d,O2N2d,N2N2d,NIPO2,N2O2I,
     4  t0,e0,N2IO,O2IO,OIO,NIO,NOIO,N2DO,N4SO,PI,ASIG,SINTHT,WAIST,
     5  QN2I,QO2I,QOI,Qe,
     6  Vbeam,tdose,
     7  NOIA4,NOIA5,NOIA6,NOIA7,NOIA8,NOIA9,NOIA10,NOIA11,NOIA12,
     8  NOIB2,NOIB3,NOIB4,NOIB5,NOIB6,NOIB7,NOIB8,NOIB9,NOIB10,NOIB11,
     9  NOIA13,NOIA14,NOIA15,NOIA16,
     $  NOIB12,NOIB13,NOIB14,NOIB15,NOIB16
c N(4S)

        FR=0.625*QN2I*Ft(t)+(N2de*e*N2d+N4sPNI*O2*NI+ON2d*O*N2d
     1  +NOIP4s*O*N2I+OIN2*NN*OI+0.07*N2Ie*e*N2I+N2N2d*NN*N2d+
     2  0.24*NOIe*e*NOI+NIO*O*NI)-(N4sO2I*O2I+N2IN4s*N2I+
     3  O2N4s*O2)*N4s

        RETURN
        END
C-------------------------
c N2d , the N(2D) production and loss function
        FUNCTION FS(t,e,N2I,O2I,NI,OI,NOI,N4s,N2d)

        REAL t,e,N2I,O2I,NI,OI,NOI,N4s,N2d
        REAL NN,O2,O,Tr,N2Ie,O2Ie,OIe,NIe,NOIe,
     1  N2IO2,N2IO,N2IN4s,O2IN2d,N4sO2I,N2de,NIO2,NIO,N4sPNI,N2dPNI,
     2  N4sPO,N2dPO,NOIA1,NOIA2,NOIA3,NOIN2,NOIP2d,NOIP4s,OIO2,OIN2,
     3  ON2I,O2NI,O2N4s,ON2d,O2N2d,N2N2d,NIPO2,N2O2I,
     4  t0,e0,N2IO,O2IO,OIO,NIO,NOIO,N2DO,N4SO,PI,ASIG,SINTHT,WAIST,
     5  QN2I,QO2I,QOI,Qe,
     6  Vbeam,tdose,
     7  NOIA4,NOIA5,NOIA6,NOIA7,NOIA8,NOIA9,NOIA10,NOIA11,NOIA12,
     8  NOIB2,NOIB3,NOIB4,NOIB5,NOIB6,NOIB7,NOIB8,NOIB9,NOIB10,NOIB11,
     9  NOIA13,NOIA14,NOIA15,NOIA16,
     $  NOIB12,NOIB13,NOIB14,NOIB15,NOIB16

        COMMON /BLK1/NN,O2,O,Tr,N2Ie,O2Ie,OIe,NIe,NOIe,
     1  N2IO2,N2IO,N2IN4s,O2IN2d,N4sO2I,N2de,NIO2,NIO,N4sPNI,N2dPNI,
     2  N4sPO,N2dPO,NOIA1,NOIA2,NOIA3,NOIN2,NOIP2d,NOIP4s,OIO2,OIN2,
     3  ON2I,O2NI,O2N4s,ON2d,O2N2d,N2N2d,NIPO2,N2O2I,
     4  t0,e0,N2IO,O2IO,OIO,NIO,NOIO,N2DO,N4SO,PI,ASIG,SINTHT,WAIST,
     5  QN2I,QO2I,QOI,Qe,
     6  Vbeam,tdose,
     7  NOIA4,NOIA5,NOIA6,NOIA7,NOIA8,NOIA9,NOIA10,NOIA11,NOIA12,
     8  NOIB2,NOIB3,NOIB4,NOIB5,NOIB6,NOIB7,NOIB8,NOIB9,NOIB10,NOIB11,
     9  NOIA13,NOIA14,NOIA15,NOIA16,
     $  NOIB12,NOIB13,NOIB14,NOIB15,NOIB16
c N(2D)
        FS=.625*QN2I*Ft(t)+(N2dPNI*O2*NI+NOIP2d*O*N2I+
     1  0.93*N2Ie*e*N2I+0.76*NOIe*e*NOI)-(O2IN2d*O2I+N2de*e+ON2d*O+
     2  N2N2d*NN+O2N2d*O2)*N2d

        RETURN
        END
C-------------------------
c NOI10(t), ( NO+, from N2+ + O,in vibrational level 0 )
        FUNCTION FQ10(t,e,N2I,O2I,NI,OI,NOI10,NOI11,NOI12,N4s,N2d,NO)

        REAL t,e,N2I,O2I,NI,OI,NO,N4s,N2d
```

213

```
      REAL NOI10,NOI11,NOI12,NOI13
      REAL NOI14,NOI15,NOI16,NOI17
      REAL NOI18,NOI19,NOI110,NOI111
      REAL NOI112,NOI113,NOI114,NOI115,NOI116
      REAL NOI20,NOI21,NOI22,NOI23
      REAL NOI24,NOI25,NOI26,NOI27
      REAL NOI28,NOI29,NOI210,NOI211
      REAL NOI212,NOI213,NOI214,NOI215,NOI216

      REAL NN,O2,O,Tr,N2Ie,O2Ie,OIe,NIe,NOIe,
     1 N2IO2,N2IO,N2IN4s,O2IN2d,N4sO2I,N2de,NIO2,NIO,N4sPNI,N2dPNI,
     2 N4sPO,N2dPO,NOIA1,NOIA2,NOIA3,NOIN2,NOIP2d,NOIP4s,OIO2,OIN2,
     3 ON2I,O2NI,O2N4s,ON2d,O2N2d,N2N2d,NIPO2,N2O2I,
     4 t0,e0,N2IO,O2IO,OIO,NIO,NOIO,N2DO,N4SO,PI,ASIG,SINTHT,WAIST,
     5 QN2I,QO2I,QOI,Qe,
     6 Vbeam,tdose,
     7 NOIA4,NOIA5,NOIA6,NOIA7,NOIA8,NOIA9,NOIA10,NOIA11,NOIA12,
     8 NOIB2,NOIB3,NOIB4,NOIB5,NOIB6,NOIB7,NOIB8,NOIB9,NOIB10,NOIB11,
     9 NOIA13,NOIA14,NOIA15,NOIA16,
     $ NOIB12,NOIB13,NOIB14,NOIB15,NOIB16

      REAL N2INO,O2INO,OINO

      COMMON /BLK1/NN,O2,O,Tr,N2Ie,O2Ie,OIe,NIe,NOIe,
     1 N2IO2,N2IO,N2IN4s,O2IN2d,N4sO2I,N2de,NIO2,NIO,N4sPNI,N2dPNI,
     2 N4sPO,N2dPO,NOIA1,NOIA2,NOIA3,NOIN2,NOIP2d,NOIP4s,OIO2,OIN2,
     3 ON2I,O2NI,O2N4s,ON2d,O2N2d,N2N2d,NIPO2,N2O2I,
     4 t0,e0,N2IO,O2IO,OIO,NIO,NOIO,N2DO,N4SO,PI,ASIG,SINTHT,WAIST,
     5 QN2I,QO2I,QOI,Qe,
     6 Vbeam,tdose,
     7 NOIA4,NOIA5,NOIA6,NOIA7,NOIA8,NOIA9,NOIA10,NOIA11,NOIA12,
     8 NOIB2,NOIB3,NOIB4,NOIB5,NOIB6,NOIB7,NOIB8,NOIB9,NOIB10,NOIB11,
     9 NOIA13,NOIA14,NOIA15,NOIA16,
     $ NOIB12,NOIB13,NOIB14,NOIB15,NOIB16

      COMMON /BLK2/N2INO,O2INO,OINO
c the first line is set to zero, assumes no ground state contribution
c from N2+ + O
c for non NO+ source we share the ground state production 50/50
c here for FQ10 and also for FQ20

      FQ10 = (0.0*NOIP2d*O*N2I + 0.0*NOIP4s*O*N2I)
     1 +( N2INO*N2I*NO + O2INO*O2I*NO + OINO*OI*NO)/2
     2 -NOIe*e*NOI10
     3 -(NOIA0*NOI10-NOIA1*NOI11)
     4 -(NOIB0*NOI10-NOIB2*NOI12)
     5 -(-NOIN2*NN*NOI11)

      RETURN
      END
C-------------------------
c NOI11(t), (   NO+, from N2+ + O,in vibrational level 1 )
      FUNCTION FQ11(t,e,N2I,O2I,NI,OI,NOI11,NOI12,NOI13,N4s,N2d)

      REAL t,e,N2I,O2I,NI,OI,NOI,N4s,N2d

      REAL NOI10,NOI11,NOI12,NOI13
      REAL NOI14,NOI15,NOI16,NOI17
      REAL NOI18,NOI19,NOI110,NOI111
```

214

```
          REAL NOI112,NOI113,NOI114,NOI115,NOI116
          REAL NOI20,NOI21,NOI22,NOI23
          REAL NOI24,NOI25,NOI26,NOI27
          REAL NOI28,NOI29,NOI210,NOI211
          REAL NOI212,NOI213,NOI214,NOI215,NOI216

          REAL NN,O2,O,Tr,N2Ie,O2Ie,OIe,NIe,NOIe,
     1    N2IO2,N2IO,N2IN4s,O2IN2d,N4sO2I,N2de,NIO2,NIO,N4sPNI,N2dPNI,
     2    N4sPO,N2dPO,NOIA1,NOIA2,NOIA3,NOIN2,NOIP2d,NOIP4s,OIO2,OIN2,
     3    ON2I,O2NI,O2N4s,ON2d,O2N2d,N2N2d,NIPO2,N2O2I,
     4    t0,e0,N2IO,O2IO,OIO,NIO,NOIO,N2D0,N4S0,PI,ASIG,SINTHT,WAIST,
     5    QN2I,QO2I,QOI,Qe,
     6    Vbeam,tdose,
     7    NOIA4,NOIA5,NOIA6,NOIA7,NOIA8,NOIA9,NOIA10,NOIA11,NOIA12,
     8    NOIB2,NOIB3,NOIB4,NOIB5,NOIB6,NOIB7,NOIB8,NOIB9,NOIB10,NOIB11,
     9    NOIA13,NOIA14,NOIA15,NOIA16,
     $    NOIB12,NOIB13,NOIB14,NOIB15,NOIB16

          COMMON /BLK1/NN,O2,O,Tr,N2Ie,O2Ie,OIe,NIe,NOIe,
     1    N2IO2,N2IO,N2IN4s,O2IN2d,N4sO2I,N2de,NIO2,NIO,N4sPNI,N2dPNI,
     2    N4sPO,N2dPO,NOIA1,NOIA2,NOIA3,NOIN2,NOIP2d,NOIP4s,OIO2,OIN2,
     3    ON2I,O2NI,O2N4s,ON2d,O2N2d,N2N2d,NIPO2,N2O2I,
     4    t0,e0,N2IO,O2IO,OIO,NIO,NOIO,N2D0,N4S0,PI,ASIG,SINTHT,WAIST,
     5    QN2I,QO2I,QOI,Qe,
     6    Vbeam,tdose,
     7    NOIA4,NOIA5,NOIA6,NOIA7,NOIA8,NOIA9,NOIA10,NOIA11,NOIA12,
     8    NOIB2,NOIB3,NOIB4,NOIB5,NOIB6,NOIB7,NOIB8,NOIB9,NOIB10,NOIB11,
     9    NOIA13,NOIA14,NOIA15,NOIA16,
     $    NOIB12,NOIB13,NOIB14,NOIB15,NOIB16


          FQ11 = .5838*NOIP2d*O*N2I
     1    + .0600*NOIP4s*O*N2I
     2    +(N4sO2I*O2I*N4s+N2O2I*NN*O2I+OIN2*NN*OI)*0.0
     3    -NOIe*e*NOI11
     4    -(NOIA1*NOI11-NOIA2*NOI12)
     5    -(NOIB1*NOI11-NOIB3*NOI13)
     6    -(NOIN2*NN*NOI11-NOIN2*NN*NOI12)
          RETURN
          END
C-------------------------
c NOI12(t), ( NO+, from N2+ + O,in vibrational level 2 )
          FUNCTION FQ12(t,e,N2I,O2I,NI,OI,NOI12,NOI13,NOI14,N4s,N2d)

          REAL t,e,N2I,O2I,NI,OI,NOI,N4s,N2d

          REAL NOI10,NOI11,NOI12,NOI13
          REAL NOI14,NOI15,NOI16,NOI17
          REAL NOI18,NOI19,NOI110,NOI111
          REAL NOI112,NOI113,NOI114,NOI115,NOI116
          REAL NOI20,NOI21,NOI22,NOI23
          REAL NOI24,NOI25,NOI26,NOI27
          REAL NOI28,NOI29,NOI210,NOI211
          REAL NOI212,NOI213,NOI214,NOI215,NOI216

          REAL NN,O2,O,Tr,N2Ie,O2Ie,OIe,NIe,NOIe,
     1    N2IO2,N2IO,N2IN4s,O2IN2d,N4sO2I,N2de,NIO2,NIO,N4sPNI,N2dPNI,
     2    N4sPO,N2dPO,NOIA1,NOIA2,NOIA3,NOIN2,NOIP2d,NOIP4s,OIO2,OIN2,
     3    ON2I,O2NI,O2N4s,ON2d,O2N2d,N2N2d,NIPO2,N2O2I,
     4    t0,e0,N2IO,O2IO,OIO,NIO,NOIO,N2D0,N4S0,PI,ASIG,SINTHT,WAIST,
```

215

```
     5   QN2I,QO2I,QOI,Qe,
     6   Vbeam,tdose,
     7   NOIA4,NOIA5,NOIA6,NOIA7,NOIA8,NOIA9,NOIA10,NOIA11,NOIA12,
     8   NOIB2,NOIB3,NOIB4,NOIB5,NOIB6,NOIB7,NOIB8,NOIB9,NOIB10,NOIB11,
     9   NOIA13,NOIA14,NOIA15,NOIA16,
     $   NOIB12,NOIB13,NOIB14,NOIB15,NOIB16

         COMMON /BLK1/NN,O2,O,Tr,N2Ie,O2Ie,OIe,NIe,NOIe,
     1   N2IO2,N2IO,N2IN4s,O2IN2d,N4sO2I,N2de,NIO2,NIO,N4sPNI,N2dPNI,
     2   N4sPO,N2dPO,NOIA1,NOIA2,NOIA3,NOIN2,NOIP2d,NOIP4s,OIO2,OIN2,
     3   ON2I,O2NI,O2N4s,ON2d,O2N2d,N2N2d,NIPO2,N2O2I,
     4   t0,e0,N2I0,O2I0,OI0,NI0,NOI0,N2D0,N4S0,PI,ASIG,SINTHT,WAIST,
     5   QN2I,QO2I,QOI,Qe,
     6   Vbeam,tdose,
     7   NOIA4,NOIA5,NOIA6,NOIA7,NOIA8,NOIA9,NOIA10,NOIA11,NOIA12,
     8   NOIB2,NOIB3,NOIB4,NOIB5,NOIB6,NOIB7,NOIB8,NOIB9,NOIB10,NOIB11,
     9   NOIA13,NOIA14,NOIA15,NOIA16,
     $   NOIB12,NOIB13,NOIB14,NOIB15,NOIB16


         FQ12 = .1731*NOIP2d*O*N2I
     1   + .0500*NOIP4s*O*N2I
     2   +(N4sO2I*O2I*N4s+N2O2I*NN*O2I+OIN2*NN*OI)*0.0
     3   -NOIe*e*NOI12
     4   -(NOIA2*NOI12-NOIA3*NOI13)
     5   -(NOIB2*NOI12-NOIB4*NOI14)
     6   -(NOIN2*NN*NOI12-NOIN2*NN*NOI13)
         RETURN
         END
C------------------------
c NOI13(t), (   NO+, from N2+ + O,in vibrational level 3 )
         FUNCTION FQ13(t,e,N2I,O2I,NI,OI,NOI13,NOI14,NOI15,N4s,N2d)

         REAL t,e,N2I,O2I,NI,OI,NOI,N4s,N2d

         REAL NOI10,NOI11,NOI12,NOI13
         REAL NOI14,NOI15,NOI16,NOI17
         REAL NOI18,NOI19,NOI110,NOI111
         REAL NOI112,NOI113,NOI114,NOI115,NOI116
         REAL NOI20,NOI21,NOI22,NOI23
         REAL NOI24,NOI25,NOI26,NOI27
         REAL NOI28,NOI29,NOI210,NOI211
         REAL NOI212,NOI213,NOI214,NOI215,NOI216


         REAL NN,O2,O,Tr,N2Ie,O2Ie,OIe,NIe,NOIe,
     1   N2IO2,N2IO,N2IN4s,O2IN2d,N4sO2I,N2de,NIO2,NIO,N4sPNI,N2dPNI,
     2   N4sPO,N2dPO,NOIA1,NOIA2,NOIA3,NOIN2,NOIP2d,NOIP4s,OIO2,OIN2,
     3   ON2I,O2NI,O2N4s,ON2d,O2N2d,N2N2d,NIPO2,N2O2I,
     4   t0,e0,N2I0,O2I0,OI0,NI0,NOI0,N2D0,N4S0,PI,ASIG,SINTHT,WAIST,
     5   QN2I,QO2I,QOI,Qe,
     6   Vbeam,tdose,
     7   NOIA4,NOIA5,NOIA6,NOIA7,NOIA8,NOIA9,NOIA10,NOIA11,NOIA12,
     8   NOIB2,NOIB3,NOIB4,NOIB5,NOIB6,NOIB7,NOIB8,NOIB9,NOIB10,NOIB11,
     9   NOIA13,NOIA14,NOIA15,NOIA16,
     $   NOIB12,NOIB13,NOIB14,NOIB15,NOIB16

         COMMON /BLK1/NN,O2,O,Tr,N2Ie,O2Ie,OIe,NIe,NOIe,
     1   N2IO2,N2IO,N2IN4s,O2IN2d,N4sO2I,N2de,NIO2,NIO,N4sPNI,N2dPNI,
     2   N4sPO,N2dPO,NOIA1,NOIA2,NOIA3,NOIN2,NOIP2d,NOIP4s,OIO2,OIN2,
     3   ON2I,O2NI,O2N4s,ON2d,O2N2d,N2N2d,NIPO2,N2O2I,
```

```
      4 t0,e0,N2I0,O2I0,OI0,NI0,NOI0,N2D0,N4S0,PI,ASIG,SINTHT,WAIST,
      5 QN2I,QO2I,QOI,Qe,
      6 Vbeam,tdose,
      7 NOIA4,NOIA5,NOIA6,NOIA7,NOIA8,NOIA9,NOIA10,NOIA11,NOIA12,
      8 NOIB2,NOIB3,NOIB4,NOIB5,NOIB6,NOIB7,NOIB8,NOIB9,NOIB10,NOIB11,
      9 NOIA13,NOIA14,NOIA15,NOIA16,
      $ NOIB12,NOIB13,NOIB14,NOIB15,NOIB16


        FQ13 = 0.0*NOIP2d*O*N2I
      1 + .0394*NOIP4s*O*N2I
      2 +(N4sO2I*O2I*N4s+N2O2I*NN*O2I+OIN2*NN*OI)*0.0
      3 -NOIe*e*NOI13
      4 -(NOIA3*NOI13-NOIA4*NOI14)
      5 -(NOIB3*NOI13-NOIB5*NOI15)
      6 -(NOIN2*NN*NOI13-NOIN2*NN*NOI14)
        RETURN
        END
C-------------------------
c NOI14(t), (  NO+, from N2+ + O,in vibrational level 4 )
        FUNCTION FQ14(t,e,N2I,O2I,NI,OI,NOI14,NOI15,NOI16,N4s,N2d)

        REAL t,e,N2I,O2I,NI,OI,NOI,N4s,N2d

        REAL NOI10,NOI11,NOI12,NOI13
        REAL NOI14,NOI15,NOI16,NOI17
        REAL NOI18,NOI19,NOI110,NOI111
        REAL NOI112,NOI113,NOI114,NOI115,NOI116
        REAL NOI20,NOI21,NOI22,NOI23
        REAL NOI24,NOI25,NOI26,NOI27
        REAL NOI28,NOI29,NOI210,NOI211
        REAL NOI212,NOI213,NOI214,NOI215,NOI216


        REAL NN,O2,O,Tr,N2Ie,O2Ie,OIe,NIe,NOIe,
      1 N2IO2,N2IO,N2IN4s,O2IN2d,N4sO2I,N2de,NIO2,NIO,N4sPNI,N2dPNI,
      2 N4sPO,N2dPO,NOIA1,NOIA2,NOIA3,NOIN2,NOIP2d,NOIP4s,OIO2,OIN2,
      3 ON2I,O2NI,O2N4s,ON2d,O2N2d,N2N2d,NIPO2,N2O2I,
      4 t0,e0,N2I0,O2I0,OI0,NI0,NOI0,N2D0,N4S0,PI,ASIG,SINTHT,WAIST,
      5 QN2I,QO2I,QOI,Qe,
      6 Vbeam,tdose,
      7 NOIA4,NOIA5,NOIA6,NOIA7,NOIA8,NOIA9,NOIA10,NOIA11,NOIA12,
      8 NOIB2,NOIB3,NOIB4,NOIB5,NOIB6,NOIB7,NOIB8,NOIB9,NOIB10,NOIB11,
      9 NOIA13,NOIA14,NOIA15,NOIA16,
      $ NOIB12,NOIB13,NOIB14,NOIB15,NOIB16


        COMMON /BLK1/NN,O2,O,Tr,N2Ie,O2Ie,OIe,NIe,NOIe,
      1 N2IO2,N2IO,N2IN4s,O2IN2d,N4sO2I,N2de,NIO2,NIO,N4sPNI,N2dPNI,
      2 N4sPO,N2dPO,NOIA1,NOIA2,NOIA3,NOIN2,NOIP2d,NOIP4s,OIO2,OIN2,
      3 ON2I,O2NI,O2N4s,ON2d,O2N2d,N2N2d,NIPO2,N2O2I,
      4 t0,e0,N2I0,O2I0,OI0,NI0,NOI0,N2D0,N4S0,PI,ASIG,SINTHT,WAIST,
      5 QN2I,QO2I,QOI,Qe,
      6 Vbeam,tdose,
      7 NOIA4,NOIA5,NOIA6,NOIA7,NOIA8,NOIA9,NOIA10,NOIA11,NOIA12,
      8 NOIB2,NOIB3,NOIB4,NOIB5,NOIB6,NOIB7,NOIB8,NOIB9,NOIB10,NOIB11,
      9 NOIA13,NOIA14,NOIA15,NOIA16,
      $ NOIB12,NOIB13,NOIB14,NOIB15,NOIB16


        FQ14 = 0.0*NOIP2d*O*N2I
      1 + .0239*NOIP4s*O*N2I
```

217

```
      2   +(N4sO2I*O2I*N4s+N2O2I*NN*O2I+OIN2*NN*OI)*0.0
      3   -NOIe*e*NOI14
      4   -(NOIA4*NOI14-NOIA5*NOI15)
      5   -(NOIB4*NOI14-NOIB6*NOI16)
      6   -(NOIN2*NN*NOI14-NOIN2*NN*NOI15)
          RETURN
          END
C------------------------
c NOI15(t), (  NO+, from N2+ + O,in vibrational level 5 )
          FUNCTION FQ15(t,e,N2I,O2I,NI,OI,NOI15,NOI16,NOI17,N4s,N2d)

          REAL t,e,N2I,O2I,NI,OI,NOI,N4s,N2d

          REAL NOI10,NOI11,NOI12,NOI13
          REAL NOI14,NOI15,NOI16,NOI17
          REAL NOI18,NOI19,NOI110,NOI111
          REAL NOI112,NOI113,NOI114,NOI115,NOI116
          REAL NOI20,NOI21,NOI22,NOI23
          REAL NOI24,NOI25,NOI26,NOI27
          REAL NOI28,NOI29,NOI210,NOI211
          REAL NOI212,NOI213,NOI214,NOI215,NOI216

          REAL NN,O2,O,Tr,N2Ie,O2Ie,OIe,NIe,NOIe,
      1   N2IO2,N2IO,N2IN4s,O2IN2d,N4sO2I,N2de,NIO2,NIO,N4sPNI,N2dPNI,
      2   N4sPO,N2dPO,NOIA1,NOIA2,NOIA3,NOIN2,NOIP2d,NOIP4s,OIO2,OIN2,
      3   ON2I,O2NI,O2N4s,ON2d,O2N2d,N2N2d,NIPO2,N2O2I,
      4   t0,e0,N2I0,O2I0,OI0,NI0,NOI0,N2D0,N4S0,PI,ASIG,SINTHT,WAIST,
      5   QN2I,QO2I,QOI,Qe,
      6   Vbeam,tdose,
      7   NOIA4,NOIA5,NOIA6,NOIA7,NOIA8,NOIA9,NOIA10,NOIA11,NOIA12,
      8   NOIB2,NOIB3,NOIB4,NOIB5,NOIB6,NOIB7,NOIB8,NOIB9,NOIB10,NOIB11,
      9   NOIA13,NOIA14,NOIA15,NOIA16,
      $   NOIB12,NOIB13,NOIB14,NOIB15,NOIB16

          COMMON /BLK1/NN,O2,O,Tr,N2Ie,O2Ie,OIe,NIe,NOIe,
      1   N2IO2,N2IO,N2IN4s,O2IN2d,N4sO2I,N2de,NIO2,NIO,N4sPNI,N2dPNI,
      2   N4sPO,N2dPO,NOIA1,NOIA2,NOIA3,NOIN2,NOIP2d,NOIP4s,OIO2,OIN2,
      3   ON2I,O2NI,O2N4s,ON2d,O2N2d,N2N2d,NIPO2,N2O2I,
      4   t0,e0,N2I0,O2I0,OI0,NI0,NOI0,N2D0,N4S0,PI,ASIG,SINTHT,WAIST,
      5   QN2I,QO2I,QOI,Qe,
      6   Vbeam,tdose,
      7   NOIA4,NOIA5,NOIA6,NOIA7,NOIA8,NOIA9,NOIA10,NOIA11,NOIA12,
      8   NOIB2,NOIB3,NOIB4,NOIB5,NOIB6,NOIB7,NOIB8,NOIB9,NOIB10,NOIB11,
      9   NOIA13,NOIA14,NOIA15,NOIA16,
      $   NOIB12,NOIB13,NOIB14,NOIB15,NOIB16


          FQ15 = 0.0*NOIP2d*O*N2I
      1   + .0227*NOIP4s*O*N2I
      2   +(N4sO2I*O2I*N4s+N2O2I*NN*O2I+OIN2*NN*OI)*0.0
      3   -NOIe*e*NOI15
      4   -(NOIA5*NOI15-NOIA6*NOI16)
      5   -(NOIB5*NOI15-NOIB7*NOI17)
      6   -(NOIN2*NN*NOI15-NOIN2*NN*NOI16)
          RETURN
          END
C------------------------
c NOI16(t), (  NO+, from N2+ + O,in vibrational level 6 )
          FUNCTION FQ16(t,e,N2I,O2I,NI,OI,NOI16,NOI17,NOI18,N4s,N2d)
```

218

```
          REAL t,e,N2I,O2I,NI,OI,NOI,N4s,N2d

          REAL NOI10,NOI11,NOI12,NOI13
          REAL NOI14,NOI15,NOI16,NOI17
          REAL NOI18,NOI19,NOI110,NOI111
          REAL NOI112,NOI113,NOI114,NOI115,NOI116
          REAL NOI20,NOI21,NOI22,NOI23
          REAL NOI24,NOI25,NOI26,NOI27
          REAL NOI28,NOI29,NOI210,NOI211
          REAL NOI212,NOI213,NOI214,NOI215,NOI216

          REAL NN,O2,O,Tr,N2Ie,O2Ie,OIe,NIe,NOIe,
     1    N2IO2,N2IO,N2IN4s,O2IN2d,N4sO2I,N2de,NIO2,NIO,N4sPNI,N2dPNI,
     2    N4sPO,N2dPO,NOIA1,NOIA2,NOIA3,NOIN2,NOIP2d,NOIP4s,OIO2,OIN2,
     3    ON2I,O2NI,O2N4s,ON2d,O2N2d,N2N2d,NIPO2,N2O2I,
     4    t0,e0,N2IO,O2IO,OIO,NIO,NOIO,N2DO,N4SO,PI,ASIG,SINTHT,WAIST,
     5    QN2I,QO2I,QOI,Qe,
     6    Vbeam,tdose,
     7    NOIA4,NOIA5,NOIA6,NOIA7,NOIA8,NOIA9,NOIA10,NOIA11,NOIA12,
     8    NOIB2,NOIB3,NOIB4,NOIB5,NOIB6,NOIB7,NOIB8,NOIB9,NOIB10,NOIB11,
     9    NOIA13,NOIA14,NOIA15,NOIA16,
     $    NOIB12,NOIB13,NOIB14,NOIB15,NOIB16

          COMMON /BLK1/NN,O2,O,Tr,N2Ie,O2Ie,OIe,NIe,NOIe,
     1    N2IO2,N2IO,N2IN4s,O2IN2d,N4sO2I,N2de,NIO2,NIO,N4sPNI,N2dPNI,
     2    N4sPO,N2dPO,NOIA1,NOIA2,NOIA3,NOIN2,NOIP2d,NOIP4s,OIO2,OIN2,
     3    ON2I,O2NI,O2N4s,ON2d,O2N2d,N2N2d,NIPO2,N2O2I,
     4    t0,e0,N2IO,O2IO,OIO,NIO,NOIO,N2DO,N4SO,PI,ASIG,SINTHT,WAIST,
     5    QN2I,QO2I,QOI,Qe,
     6    Vbeam,tdose,
     7    NOIA4,NOIA5,NOIA6,NOIA7,NOIA8,NOIA9,NOIA10,NOIA11,NOIA12,
     8    NOIB2,NOIB3,NOIB4,NOIB5,NOIB6,NOIB7,NOIB8,NOIB9,NOIB10,NOIB11,
     9    NOIA13,NOIA14,NOIA15,NOIA16,
     $    NOIB12,NOIB13,NOIB14,NOIB15,NOIB16


          FQ16 = 0.0*NOIP2d*O*N2I
     1    + .0165*NOIP4s*O*N2I
     2    +(N4sO2I*O2I*N4s+N2O2I*NN*O2I+OIN2*NN*OI)*0.0
     3    -NOIe*e*NOI16
     4    -(NOIA6*NOI16-NOIA7*NOI17)
     5    -(NOIB6*NOI16-NOIB8*NOI18)
     6    -(NOIN2*NN*NOI16-NOIN2*NN*NOI17)
          RETURN
          END
C------------------------
c NOI17(t), (  NO+, from N2+ + O,in vibrational level 7 )
          FUNCTION FQ17(t,e,N2I,O2I,NI,OI,NOI17,NOI18,NOI19,N4s,N2d)

          REAL t,e,N2I,O2I,NI,OI,NOI,N4s,N2d

          REAL NOI10,NOI11,NOI12,NOI13
          REAL NOI14,NOI15,NOI16,NOI17
          REAL NOI18,NOI19,NOI110,NOI111
          REAL NOI112,NOI113,NOI114,NOI115,NOI116
          REAL NOI20,NOI21,NOI22,NOI23
          REAL NOI24,NOI25,NOI26,NOI27
          REAL NOI28,NOI29,NOI210,NOI211
          REAL NOI212,NOI213,NOI214,NOI215,NOI216
```

```fortran
      REAL NN,O2,O,Tr,N2Ie,O2Ie,OIe,NIe,NOIe,
     1 N2IO2,N2IO,N2IN4s,O2IN2d,N4sO2I,N2de,NIO2,NIO,N4sPNI,N2dPNI,
     2 N4sPO,N2dPO,NOIA1,NOIA2,NOIA3,NOIN2,NOIP2d,NOIP4s,OIO2,OIN2,
     3 ON2I,O2NI,O2N4s,ON2d,O2N2d,N2N2d,NIPO2,N2O2I,
     4 t0,e0,N2IO,O2IO,OIO,NIO,NOIO,N2DO,N4SO,PI,ASIG,SINTHT,WAIST,
     5 QN2I,QO2I,QOI,Qe,
     6 Vbeam,tdose,
     7 NOIA4,NOIA5,NOIA6,NOIA7,NOIA8,NOIA9,NOIA10,NOIA11,NOIA12,
     8 NOIB2,NOIB3,NOIB4,NOIB5,NOIB6,NOIB7,NOIB8,NOIB9,NOIB10,NOIB11,
     9 NOIA13,NOIA14,NOIA15,NOIA16,
     $ NOIB12,NOIB13,NOIB14,NOIB15,NOIB16

      COMMON /BLK1/NN,O2,O,Tr,N2Ie,O2Ie,OIe,NIe,NOIe,
     1 N2IO2,N2IO,N2IN4s,O2IN2d,N4sO2I,N2de,NIO2,NIO,N4sPNI,N2dPNI,
     2 N4sPO,N2dPO,NOIA1,NOIA2,NOIA3,NOIN2,NOIP2d,NOIP4s,OIO2,OIN2,
     3 ON2I,O2NI,O2N4s,ON2d,O2N2d,N2N2d,NIPO2,N2O2I,
     4 t0,e0,N2IO,O2IO,OIO,NIO,NOIO,N2DO,N4SO,PI,ASIG,SINTHT,WAIST,
     5 QN2I,QO2I,QOI,Qe,
     6 Vbeam,tdose,
     7 NOIA4,NOIA5,NOIA6,NOIA7,NOIA8,NOIA9,NOIA10,NOIA11,NOIA12,
     8 NOIB2,NOIB3,NOIB4,NOIB5,NOIB6,NOIB7,NOIB8,NOIB9,NOIB10,NOIB11,
     9 NOIA13,NOIA14,NOIA15,NOIA16,
     $ NOIB12,NOIB13,NOIB14,NOIB15,NOIB16


      FQ17 = 0.0*NOIP2d*O*N2I
     1 + .0232*NOIP4s*O*N2I
     2 +(N4sO2I*O2I*N4s+N2O2I*NN*O2I+OIN2*NN*OI)*0.0
     3 -NOIe*e*NOI17
     4 -(NOIA7*NOI17-NOIA8*NOI18)
     5 -(NOIB7*NOI17-NOIB9*NOI19)
     6 -(NOIN2*NN*NOI17-NOIN2*NN*NOI18)
      RETURN
      END
C-------------------------
c NOI18(t), (  NO+, from N2+ + O,in vibrational level 8 )
      FUNCTION FQ18(t,e,N2I,O2I,NI,OI,NOI18,NOI19,NOI110,N4s,N2d)

      REAL t,e,N2I,O2I,NI,OI,NOI,N4s,N2d

      REAL NOI10,NOI11,NOI12,NOI13
      REAL NOI14,NOI15,NOI16,NOI17
      REAL NOI18,NOI19,NOI110,NOI111
      REAL NOI112,NOI113,NOI114,NOI115,NOI116
      REAL NOI20,NOI21,NOI22,NOI23
      REAL NOI24,NOI25,NOI26,NOI27
      REAL NOI28,NOI29,NOI210,NOI211
      REAL NOI212,NOI213,NOI214,NOI215,NOI216

      REAL NN,O2,O,Tr,N2Ie,O2Ie,OIe,NIe,NOIe,
     1 N2IO2,N2IO,N2IN4s,O2IN2d,N4sO2I,N2de,NIO2,NIO,N4sPNI,N2dPNI,
     2 N4sPO,N2dPO,NOIA1,NOIA2,NOIA3,NOIN2,NOIP2d,NOIP4s,OIO2,OIN2,
     3 ON2I,O2NI,O2N4s,ON2d,O2N2d,N2N2d,NIPO2,N2O2I,
     4 t0,e0,N2IO,O2IO,OIO,NIO,NOIO,N2DO,N4SO,PI,ASIG,SINTHT,WAIST,
     5 QN2I,QO2I,QOI,Qe,
     6 Vbeam,tdose,
     7 NOIA4,NOIA5,NOIA6,NOIA7,NOIA8,NOIA9,NOIA10,NOIA11,NOIA12,
     8 NOIB2,NOIB3,NOIB4,NOIB5,NOIB6,NOIB7,NOIB8,NOIB9,NOIB10,NOIB11,
     9 NOIA13,NOIA14,NOIA15,NOIA16,
     $ NOIB12,NOIB13,NOIB14,NOIB15,NOIB16
```

220

```
        COMMON /BLK1/NN,O2,O,Tr,N2Ie,O2Ie,OIe,NIe,NOIe,
     1  N2IO2,N2IO,N2IN4s,O2IN2d,N4sO2I,N2de,NIO2,NIO,N4sPNI,N2dPNI,
     2  N4sPO,N2dPO,NOIA1,NOIA2,NOIA3,NOIN2,NOIP2d,NOIP4s,OIO2,OIN2,
     3  ON2I,O2NI,O2N4s,ON2d,O2N2d,N2N2d,NIPO2,N2O2I,
     4  t0,e0,N2IO,O2IO,OIO,NIO,NOIO,N2DO,N4SO,PI,ASIG,SINTHT,WAIST,
     5  QN2I,QO2I,QOI,Qe,
     6  Vbeam,tdose,
     7  NOIA4,NOIA5,NOIA6,NOIA7,NOIA8,NOIA9,NOIA10,NOIA11,NOIA12,
     8  NOIB2,NOIB3,NOIB4,NOIB5,NOIB6,NOIB7,NOIB8,NOIB9,NOIB10,NOIB11,
     9  NOIA13,NOIA14,NOIA15,NOIA16,
     $  NOIB12,NOIB13,NOIB14,NOIB15,NOIB16


        FQ18 = 0.0*NOIP2d*O*N2I
     1  + .0075*NOIP4s*O*N2I
     2  +(N4sO2I*O2I*N4s+N2O2I*NN*O2I+OIN2*NN*OI)*0.0
     3  -NOIe*e*NOI18
     4  -(NOIA8*NOI18-NOIA9*NOI19)
     5  -(NOIB8*NOI18-NOIB10*NOI110)
     6  -(NOIN2*NN*NOI18-NOIN2*NN*NOI19)
        RETURN
        END
C------------------------
c NOI19(t), (  NO+, from N2+ + O,in vibrational level 9 )
        FUNCTION FQ19(t,e,N2I,O2I,NI,OI,NOI19,NOI110,NOI111,N4s,N2d)

        REAL t,e,N2I,O2I,NI,OI,NOI,N4s,N2d

        REAL NOI10,NOI11,NOI12,NOI13
        REAL NOI14,NOI15,NOI16,NOI17
        REAL NOI18,NOI19,NOI110,NOI111
        REAL NOI112,NOI113,NOI114,NOI115,NOI116
        REAL NOI20,NOI21,NOI22,NOI23
        REAL NOI24,NOI25,NOI26,NOI27
        REAL NOI28,NOI29,NOI210,NOI211
        REAL NOI212,NOI213,NOI214,NOI215,NOI216

        REAL NN,O2,O,Tr,N2Ie,O2Ie,OIe,NIe,NOIe,
     1  N2IO2,N2IO,N2IN4s,O2IN2d,N4sO2I,N2de,NIO2,NIO,N4sPNI,N2dPNI,
     2  N4sPO,N2dPO,NOIA1,NOIA2,NOIA3,NOIN2,NOIP2d,NOIP4s,OIO2,OIN2,
     3  ON2I,O2NI,O2N4s,ON2d,O2N2d,N2N2d,NIPO2,N2O2I,
     4  t0,e0,N2IO,O2IO,OIO,NIO,NOIO,N2DO,N4SO,PI,ASIG,SINTHT,WAIST,
     5  QN2I,QO2I,QOI,Qe,
     6  Vbeam,tdose,
     7  NOIA4,NOIA5,NOIA6,NOIA7,NOIA8,NOIA9,NOIA10,NOIA11,NOIA12,
     8  NOIB2,NOIB3,NOIB4,NOIB5,NOIB6,NOIB7,NOIB8,NOIB9,NOIB10,NOIB11,
     9  NOIA13,NOIA14,NOIA15,NOIA16,
     $  NOIB12,NOIB13,NOIB14,NOIB15,NOIB16

        COMMON /BLK1/NN,O2,O,Tr,N2Ie,O2Ie,OIe,NIe,NOIe,
     1  N2IO2,N2IO,N2IN4s,O2IN2d,N4sO2I,N2de,NIO2,NIO,N4sPNI,N2dPNI,
     2  N4sPO,N2dPO,NOIA1,NOIA2,NOIA3,NOIN2,NOIP2d,NOIP4s,OIO2,OIN2,
     3  ON2I,O2NI,O2N4s,ON2d,O2N2d,N2N2d,NIPO2,N2O2I,
     4  t0,e0,N2IO,O2IO,OIO,NIO,NOIO,N2DO,N4SO,PI,ASIG,SINTHT,WAIST,
     5  QN2I,QO2I,QOI,Qe,
     6  Vbeam,tdose,
     7  NOIA4,NOIA5,NOIA6,NOIA7,NOIA8,NOIA9,NOIA10,NOIA11,NOIA12,
     8  NOIB2,NOIB3,NOIB4,NOIB5,NOIB6,NOIB7,NOIB8,NOIB9,NOIB10,NOIB11,
     9  NOIA13,NOIA14,NOIA15,NOIA16,
```

```
     $   NOIB12,NOIB13,NOIB14,NOIB15,NOIB16


         FQ19 = 0.0*NOIP2d*O*N2I
     1   + .0000*NOIP4s*O*N2I
     2   +(N4sO2I*O2I*N4s+N2O2I*NN*O2I+OIN2*NN*OI)*0.0
     3   -NOIe*e*NOI19
     4   -(NOIA9*NOI19-NOIA10*NOI110)
     5   -(NOIB9*NOI19-NOIB11*NOI111)
     6   -(NOIN2*NN*NOI19-NOIN2*NN*NOI110)
         RETURN
         END
C-------------------------
c NOI110(t), (  NO+, from N2+ + O,in vibrational level 10 )
         FUNCTION FQ110(t,e,N2I,O2I,NI,OI,NOI10,NOI11,NOI12,N4s,N2d)

         REAL t,e,N2I,O2I,NI,OI,NOI,N4s,N2d

         REAL NOI10,NOI11,NOI12,NOI13
         REAL NOI14,NOI15,NOI16,NOI17
         REAL NOI18,NOI19,NOI110,NOI111
         REAL NOI112,NOI113,NOI114,NOI115,NOI116
         REAL NOI20,NOI21,NOI22,NOI23
         REAL NOI24,NOI25,NOI26,NOI27
         REAL NOI28,NOI29,NOI210,NOI211
         REAL NOI212,NOI213,NOI214,NOI215,NOI216


         REAL NN,O2,O,Tr,N2Ie,O2Ie,OIe,NIe,NOIe,
     1   N2IO2,N2IO,N2IN4s,O2IN2d,N4sO2I,N2de,NIO2,NIO,N4sPNI,N2dPNI,
     2   N4sPO,N2dPO,NOIA1,NOIA2,NOIA3,NOIN2,NOIP2d,NOIP4s,OIO2,OIN2,
     3   ON2I,O2NI,O2N4s,ON2d,O2N2d,N2N2d,NIPO2,N2O2I,
     4   t0,e0,N2IO,O2IO,OIO,NIO,NOIO,N2DO,N4SO,PI,ASIG,SINTHT,WAIST,
     5   QN2I,QO2I,QOI,Qe,
     6   Vbeam,tdose,
     7   NOIA4,NOIA5,NOIA6,NOIA7,NOIA8,NOIA9,NOIA10,NOIA11,NOIA12,
     8   NOIB2,NOIB3,NOIB4,NOIB5,NOIB6,NOIB7,NOIB8,NOIB9,NOIB10,NOIB11,
     9   NOIA13,NOIA14,NOIA15,NOIA16,
     $   NOIB12,NOIB13,NOIB14,NOIB15,NOIB16


         COMMON /BLK1/NN,O2,O,Tr,N2Ie,O2Ie,OIe,NIe,NOIe,
     1   N2IO2,N2IO,N2IN4s,O2IN2d,N4sO2I,N2de,NIO2,NIO,N4sPNI,N2dPNI,
     2   N4sPO,N2dPO,NOIA1,NOIA2,NOIA3,NOIN2,NOIP2d,NOIP4s,OIO2,OIN2,
     3   ON2I,O2NI,O2N4s,ON2d,O2N2d,N2N2d,NIPO2,N2O2I,
     4   t0,e0,N2IO,O2IO,OIO,NIO,NOIO,N2DO,N4SO,PI,ASIG,SINTHT,WAIST,
     5   QN2I,QO2I,QOI,Qe,
     6   Vbeam,tdose,
     7   NOIA4,NOIA5,NOIA6,NOIA7,NOIA8,NOIA9,NOIA10,NOIA11,NOIA12,
     8   NOIB2,NOIB3,NOIB4,NOIB5,NOIB6,NOIB7,NOIB8,NOIB9,NOIB10,NOIB11,
     9   NOIA13,NOIA14,NOIA15,NOIA16,
     $   NOIB12,NOIB13,NOIB14,NOIB15,NOIB16


         FQ110 = 0.0*NOIP2d*O*N2I
     1   + 0.0*NOIP4s*O*N2I
     2   +(N4sO2I*O2I*N4s+N2O2I*NN*O2I+OIN2*NN*OI)*0.0
     3   -NOIe*e*NOI110
     4   -(NOIA10*NOI110-NOIA11*NOI111)
     5   -(NOIB10*NOI110-NOIB12*NOI112)
     6   -(NOIN2*NN*NOI110-NOIN2*NN*NOI111)
         RETURN
```

```
      END
C------------------------
c NOI111(t),  ( NO+, from N2+ + O,in vibrational level 11 )
      FUNCTION FQ111(t,e,N2I,O2I,NI,OI,NOI111,NOI112,NOI113,N4s,N2d)

      REAL t,e,N2I,O2I,NI,OI,NOI,N4s,N2d

      REAL NOI10,NOI11,NOI12,NOI13
      REAL NOI14,NOI15,NOI16,NOI17
      REAL NOI18,NOI19,NOI110,NOI111
      REAL NOI112,NOI113,NOI114,NOI115,NOI116
      REAL NOI20,NOI21,NOI22,NOI23
      REAL NOI24,NOI25,NOI26,NOI27
      REAL NOI28,NOI29,NOI210,NOI211
      REAL NOI212,NOI213,NOI214,NOI215,NOI216

      REAL NN,O2,O,Tr,N2Ie,O2Ie,OIe,NIe,NOIe,
     1 N2IO2,N2IO,N2IN4s,O2IN2d,N4sO2I,N2de,NIO2,NIO,N4sPNI,N2dPNI,
     2 N4sPO,N2dPO,NOIA1,NOIA2,NOIA3,NOIN2,NOIP2d,NOIP4s,OIO2,OIN2,
     3 ON2I,O2NI,O2N4s,ON2d,O2N2d,N2N2d,NIPO2,N2O2I,
     4 t0,e0,N2IO,O2IO,OIO,NIO,NOIO,N2DO,N4SO,PI,ASIG,SINTHT,WAIST,
     5 QN2I,QO2I,QOI,Qe,
     6 Vbeam,tdose,
     7 NOIA4,NOIA5,NOIA6,NOIA7,NOIA8,NOIA9,NOIA10,NOIA11,NOIA12,
     8 NOIB2,NOIB3,NOIB4,NOIB5,NOIB6,NOIB7,NOIB8,NOIB9,NOIB10,NOIB11,
     9 NOIA13,NOIA14,NOIA15,NOIA16,
     $ NOIB12,NOIB13,NOIB14,NOIB15,NOIB16

      COMMON /BLK1/NN,O2,O,Tr,N2Ie,O2Ie,OIe,NIe,NOIe,
     1 N2IO2,N2IO,N2IN4s,O2IN2d,N4sO2I,N2de,NIO2,NIO,N4sPNI,N2dPNI,
     2 N4sPO,N2dPO,NOIA1,NOIA2,NOIA3,NOIN2,NOIP2d,NOIP4s,OIO2,OIN2,
     3 ON2I,O2NI,O2N4s,ON2d,O2N2d,N2N2d,NIPO2,N2O2I,
     4 t0,e0,N2IO,O2IO,OIO,NIO,NOIO,N2DO,N4SO,PI,ASIG,SINTHT,WAIST,
     5 QN2I,QO2I,QOI,Qe,
     6 Vbeam,tdose,
     7 NOIA4,NOIA5,NOIA6,NOIA7,NOIA8,NOIA9,NOIA10,NOIA11,NOIA12,
     8 NOIB2,NOIB3,NOIB4,NOIB5,NOIB6,NOIB7,NOIB8,NOIB9,NOIB10,NOIB11,
     9 NOIA13,NOIA14,NOIA15,NOIA16,
     $ NOIB12,NOIB13,NOIB14,NOIB15,NOIB16


      FQ111 = 0.0*NOIP2d*O*N2I
     1 + 0.0*NOIP4s*O*N2I
     2 +(N4sO2I*O2I*N4s+N2O2I*NN*O2I+OIN2*NN*OI)*0.0
     3 -NOIe*e*NOI111
     4 -(NOIA11*NOI111-NOIA12*NOI112)
     5 -(NOIB11*NOI111-NOIB13*NOI113)
     6 -(NOIN2*NN*NOI111-NOIN2*NN*NOI112)
      RETURN
      END
C--------------------------
c NOI112(t),  ( NO+, from N2+ + O,in vibrational level 12 )
      FUNCTION FQ112(t,e,N2I,O2I,NI,OI,NOI112,NOI113,NOI114,N4s,N2d)

      REAL t,e,N2I,O2I,NI,OI,NOI,N4s,N2d

      REAL NOI10,NOI11,NOI12,NOI13
      REAL NOI14,NOI15,NOI16,NOI17
      REAL NOI18,NOI19,NOI110,NOI111
      REAL NOI112,NOI113,NOI114,NOI115,NOI116
```

```
          REAL NOI20,NOI21,NOI22,NOI23
          REAL NOI24,NOI25,NOI26,NOI27
          REAL NOI28,NOI29,NOI210,NOI211
          REAL NOI212,NOI213,NOI214,NOI215,NOI216

          REAL NN,O2,O,Tr,N2Ie,O2Ie,OIe,NIe,NOIe,
     1    N2IO2,N2IO,N2IN4s,O2IN2d,N4sO2I,N2de,NIO2,NIO,N4sPNI,N2dPNI,
     2    N4sPO,N2dPO,NOIA1,NOIA2,NOIA3,NOIN2,NOIP2d,NOIP4s,OIO2,OIN2,
     3    ON2I,O2NI,O2N4s,ON2d,O2N2d,N2N2d,NIPO2,N2O2I,
     4    t0,e0,N2IO,O2IO,OIO,NIO,NOIO,N2D0,N4S0,PI,ASIG,SINTHT,WAIST,
     5    QN2I,QO2I,QOI,Qe,
     6    Vbeam,tdose,
     7    NOIA4,NOIA5,NOIA6,NOIA7,NOIA8,NOIA9.,NOIA10,NOIA11,NOIA12,
     8    NOIB2,NOIB3,NOIB4,NOIB5,NOIB6,NOIB7,NOIB8,NOIB9,NOIB10,NOIB11,
     9    NOIA13,NOIA14,NOIA15,NOIA16,
     $    NOIB12,NOIB13,NOIB14,NOIB15,NOIB16

          COMMON /BLK1/NN,O2,O,Tr,N2Ie,O2Ie,OIe,NIe,NOIe,
     1    N2IO2,N2IO,N2IN4s,O2IN2d,N4sO2I,N2de,NIO2,NIO,N4sPNI,N2dPNI,
     2    N4sPO,N2dPO,NOIA1,NOIA2,NOIA3,NOIN2,NOIP2d,NOIP4s,OIO2,OIN2,
     3    ON2I,O2NI,O2N4s,ON2d,O2N2d,N2N2d,NIPO2,N2O2I,
     4    t0,e0,N2IO,O2IO,OIO,NIO,NOIO,N2D0,N4S0,PI,ASIG,SINTHT,WAIST,
     5    QN2I,QO2I,QOI,Qe,
     6    Vbeam,tdose,
     7    NOIA4,NOIA5,NOIA6,NOIA7,NOIA8,NOIA9,NOIA10,NOIA11,NOIA12,
     8    NOIB2,NOIB3,NOIB4,NOIB5,NOIB6,NOIB7,NOIB8,NOIB9,NOIB10,NOIB11,
     9    NOIA13,NOIA14,NOIA15,NOIA16,
     $    NOIB12,NOIB13,NOIB14,NOIB15,NOIB16


          FQ112 = 0.0*NOIP2d*O*N2I
     1    + 0.0*NOIP4s*O*N2I
     2    +(N4sO2I*O2I*N4s+N2O2I*NN*O2I+OIN2*NN*OI)*0.0
     3    -NOIe*e*NOI112
     4    -(NOIA12*NOI112-NOIA13*NOI113)
     5    -(NOIB12*NOI112-NOIB14*NOI114)
     6    -(NOIN2*NN*NOI112-NOIN2*NN*NOI113)
          RETURN
          END
C------------------------
c NOI113(t), (  NO+, from N2+ + O,in vibrational level 13 )
          FUNCTION FQ113(t,e,N2I,O2I,NI,OI,NOI113,NOI114,NOI115,N4s,N2d)

          REAL t,e,N2I,O2I,NI,OI,NOI,N4s,N2d

          REAL NOI10,NOI11,NOI12,NOI13
          REAL NOI14,NOI15,NOI16,NOI17
          REAL NOI18,NOI19,NOI110,NOI111
          REAL NOI112,NOI113,NOI114,NOI115,NOI116
          REAL NOI20,NOI21,NOI22,NOI23
          REAL NOI24,NOI25,NOI26,NOI27
          REAL NOI28,NOI29,NOI210,NOI211
          REAL NOI212,NOI213,NOI214,NOI215,NOI216

          REAL NN,O2,O,Tr,N2Ie,O2Ie,OIe,NIe,NOIe,
     1    N2IO2,N2IO,N2IN4s,O2IN2d,N4sO2I,N2de,NIO2,NIO,N4sPNI,N2dPNI,
     2    N4sPO,N2dPO,NOIA1,NOIA2,NOIA3,NOIN2,NOIP2d,NOIP4s,OIO2,OIN2,
     3    ON2I,O2NI,O2N4s,ON2d,O2N2d,N2N2d,NIPO2,N2O2I,
     4    t0,e0,N2IO,O2IO,OIO,NIO,NOIO,N2D0,N4S0,PI,ASIG,SINTHT,WAIST,
     5    QN2I,QO2I,QOI,Qe,.
```

```
      6    Vbeam,tdose,
      7    NOIA4,NOIA5,NOIA6,NOIA7,NOIA8,NOIA9,NOIA10,NOIA11,NOIA12,
      8    NOIB2,NOIB3,NOIB4,NOIB5,NOIB6,NOIB7,NOIB8,NOIB9,NOIB10,NOIB11,
      9    NOIA13,NOIA14,NOIA15,NOIA16,
      $    NOIB12,NOIB13,NOIB14,NOIB15,NOIB16

           COMMON /BLK1/NN,O2,O,Tr,N2Ie,O2Ie,OIe,NIe,NOIe,
      1    N2IO2,N2IO,N2IN4s,O2IN2d,N4sO2I,N2de,NIO2,NIO,N4sPNI,N2dPNI,
      2    N4sPO,N2dPO,NOIA1,NOIA2,NOIA3,NOIN2,NOIP2d,NOIP4s,OIO2,OIN2,
      3    ON2I,O2NI,O2N4s,ON2d,O2N2d,N2N2d,NIPO2,N2O2I,
      4    t0,e0,N2IO,O2IO,OIO,NIO,NOIO,N2D0,N4S0,PI,ASIG,SINTHT,WAIST,
      5    QN2I,QO2I,QOI,Qe,
      6    Vbeam,tdose,
      7    NOIA4,NOIA5,NOIA6,NOIA7,NOIA8,NOIA9,NOIA10,NOIA11,NOIA12,
      8    NOIB2,NOIB3,NOIB4,NOIB5,NOIB6,NOIB7,NOIB8,NOIB9,NOIB10,NOIB11,
      9    NOIA13,NOIA14,NOIA15,NOIA16,
      $    NOIB12,NOIB13,NOIB14,NOIB15,NOIB16


           FQ113 = 0.0*NOIP2d*O*N2I
      1    + 0.0*NOIP4s*O*N2I
      2    +(N4sO2I*O2I*N4s+N2O2I*NN*O2I+OIN2*NN*OI)*0.0
      3    -NOIe*e*NOI113
      4    -(NOIA13*NOI113-NOIA14*NOI114)
      5    -(NOIB13*NOI113-NOIB15*NOI115)
      6    -(NOIN2*NN*NOI113-NOIN2*NN*NOI114)
           RETURN
           END
C-------------------------
c NOI114(t), (  NO+, from N2+ + O,in vibrational level 14 )
           FUNCTION FQ114(t,e,N2I,O2I,NI,OI,NOI114,NOI115,NOI116,N4s,N2d)

           REAL t,e,N2I,O2I,NI,OI,NOI,N4s,N2d

           REAL NOI10,NOI11,NOI12,NOI13
           REAL NOI14,NOI15,NOI16,NOI17
           REAL NOI18,NOI19,NOI110,NOI111
           REAL NOI112,NOI113,NOI114,NOI115,NOI116
           REAL NOI20,NOI21,NOI22,NOI23
           REAL NOI24,NOI25,NOI26,NOI27
           REAL NOI28,NOI29,NOI210,NOI211
           REAL NOI212,NOI213,NOI214,NOI215,NOI216

           REAL NN,O2,O,Tr,N2Ie,O2Ie,OIe,NIe,NOIe,
      1    N2IO2,N2IO,N2IN4s,O2IN2d,N4sO2I,N2de,NIO2,NIO,N4sPNI,N2dPNI,
      2    N4sPO,N2dPO,NOIA1,NOIA2,NOIA3,NOIN2,NOIP2d,NOIP4s,OIO2,OIN2,
      3    ON2I,O2NI,O2N4s,ON2d,O2N2d,N2N2d,NIPO2,N2O2I,
      4    t0,e0,N2IO,O2IO,OIO,NIO,NOIO,N2D0,N4S0,PI,ASIG,SINTHT,WAIST,
      5    QN2I,QO2I,QOI,Qe,
      6    Vbeam,tdose,
      7    NOIA4,NOIA5,NOIA6,NOIA7,NOIA8,NOIA9,NOIA10,NOIA11,NOIA12,
      8    NOIB2,NOIB3,NOIB4,NOIB5,NOIB6,NOIB7,NOIB8,NOIB9,NOIB10,NOIB11,
      9    NOIA13,NOIA14,NOIA15,NOIA16,
      $    NOIB12,NOIB13,NOIB14,NOIB15,NOIB16


           COMMON /BLK1/NN,O2,O,Tr,N2Ie,O2Ie,OIe,NIe,NOIe,
      1    N2IO2,N2IO,N2IN4s,O2IN2d,N4sO2I,N2de,NIO2,NIO,N4sPNI,N2dPNI,
      2    N4sPO,N2dPO,NOIA1,NOIA2,NOIA3,NOIN2,NOIP2d,NOIP4s,OIO2,OIN2,
      3    ON2I,O2NI,O2N4s,ON2d,O2N2d,N2N2d,NIPO2,N2O2I,
      4    t0,e0,N2IO,O2IO,OIO,NIO,NOIO,N2D0,N4S0,PI,ASIG,SINTHT,WAIST,
```

```
      5  QN2I,QO2I,QOI,Qe,
      6  Vbeam,tdose,
      7  NOIA4,NOIA5,NOIA6,NOIA7,NOIA8,NOIA9,NOIA10,NOIA11,NOIA12,
      8  NOIB2,NOIB3,NOIB4,NOIB5,NOIB6,NOIB7,NOIB8,NOIB9,NOIB10,NOIB11,
      9  NOIA13,NOIA14,NOIA15,NOIA16,
      $  NOIB12,NOIB13,NOIB14,NOIB15,NOIB16


         FQ114= 0.0*NOIP2d*O*N2I
      1  + 0.0*NOIP4s*O*N2I
      2  +(N4sO2I*O2I*N4s+N2O2I*NN*O2I+OIN2*NN*OI)*0.0
      3  -NOIe*e*NOI114
      4  -(NOIA14*NOI114-NOIA15*NOI115)
      5  -(NOIB14*NOI114-NOIB16*NOI116)
      6  -(NOIN2*NN*NOI114-NOIN2*NN*NOI115)
         RETURN
         END

C------------------------
c NOI20(t), (  NO+, from N+ + O2,in vibrational level 0 )
         FUNCTION FQ20(t,e,N2I,O2I,NI,OI,NOI20,NOI21,NOI22,N4s,N2d,NO)

         REAL t,e,N2I,O2I,NI,OI,NO,N4s,N2d

         REAL NOI10,NOI11,NOI12,NOI13
         REAL NOI14,NOI15,NOI16,NOI17
         REAL NOI18,NOI19,NOI110,NOI111
         REAL NOI112,NOI113,NOI114,NOI115,NOI116
         REAL NOI20,NOI21,NOI22,NOI23
         REAL NOI24,NOI25,NOI26,NOI27
         REAL NOI28,NOI29,NOI210,NOI211
         REAL NOI212,NOI213,NOI214,NOI215,NOI216

         REAL NN,O2,O,Tr,N2Ie,O2Ie,OIe,NIe,NOIe,
      1  N2IO2,N2IO,N2IN4s,O2IN2d,N4sO2I,N2de,NIO2,NIO,N4sPNI,N2dPNI,
      2  N4sPO,N2dPO,NOIA1,NOIA2,NOIA3,NOIN2,NOIP2d,NOIP4s,OIO2,OIN2,
      3  ON2I,O2NI,O2N4s,ON2d,O2N2d,N2N2d,NIPO2,N2O2I,
      4  t0,e0,N2IO,O2IO,OIO,NIO,NOIO,N2DO,N4SO,PI,ASIG,SINTHT,WAIST,
      5  QN2I,QO2I,QOI,Qe,
      6  Vbeam,tdose,
      7  NOIA4,NOIA5,NOIA6,NOIA7,NOIA8,NOIA9,NOIA10,NOIA11,NOIA12,
      8  NOIB2,NOIB3,NOIB4,NOIB5,NOIB6,NOIB7,NOIB8,NOIB9,NOIB10,NOIB11,
      9  NOIA13,NOIA14,NOIA15,NOIA16,
      $  NOIB12,NOIB13,NOIB14,NOIB15,NOIB16

         REAL N2INO,O2INO,OINO

         COMMON /BLK1/NN,O2,O,Tr,N2Ie,O2Ie,OIe,NIe,NOIe,
      1  N2IO2,N2IO,N2IN4s,O2IN2d,N4sO2I,N2de,NIO2,NIO,N4sPNI,N2dPNI,
      2  N4sPO,N2dPO,NOIA1,NOIA2,NOIA3,NOIN2,NOIP2d,NOIP4s,OIO2,OIN2,
      3  ON2I,O2NI,O2N4s,ON2d,O2N2d,N2N2d,NIPO2,N2O2I,
      4  t0,e0,N2IO,O2IO,OIO,NIO,NOIO,N2DO,N4SO,PI,ASIG,SINTHT,WAIST,
      5  QN2I,QO2I,QOI,Qe,
      6  Vbeam,tdose,
      7  NOIA4,NOIA5,NOIA6,NOIA7,NOIA8,NOIA9,NOIA10,NOIA11,NOIA12,
      8  NOIB2,NOIB3,NOIB4,NOIB5,NOIB6,NOIB7,NOIB8,NOIB9,NOIB10,NOIB11,
      9  NOIA13,NOIA14,NOIA15,NOIA16,
      $  NOIB12,NOIB13,NOIB14,NOIB15,NOIB16

         COMMON /BLK2/N2INO,O2INO,OINO .
```

226

```
c note that we hardwire SMITH,BIERBAUM,and LEONE population as the nascent
c for all FQ2v's .
c the first line is set to zero, assumes no ground state contribution
c from N+ + O2+
c for non NO+ sources we share the ground state production 50/50
c here for FQ20 and also for FQ10

        FQ20 = 0.0*NIPO2*O2*NI
    1   +( N2INO*N2I*NO + O2INO*O2I*NO + OINO*OI*NO)/2
    2   -NOIe*e*NOI20
    3   -(NOIA0*NOI20-NOIA1*NOI21)
    4   -(NOIB0*NOI20-NOIB2*NOI22)
    5   -(-NOIN2*NN*NOI21)

        RETURN
        END
C-----------------------
c NOI21(t), ( NO+, from N+ + O2,in vibrational level 1 )
        FUNCTION FQ21(t,e,N2I,O2I,NI,OI,NOI21,NOI22,NOI23,N4s,N2d)

        REAL t,e,N2I,O2I,NI,OI,NOI,N4s,N2d

        REAL NOI10,NOI11,NOI12,NOI13
        REAL NOI14,NOI15,NOI16,NOI17
        REAL NOI18,NOI19,NOI110,NOI111
        REAL NOI112,NOI113,NOI114,NOI115,NOI116
        REAL NOI20,NOI21,NOI22,NOI23
        REAL NOI24,NOI25,NOI26,NOI27
        REAL NOI28,NOI29,NOI210,NOI211
        REAL NOI212,NOI213,NOI214,NOI215,NOI216

        REAL NN,O2,O,Tr,N2Ie,O2Ie,OIe,NIe,NOIe,
    1   N2IO2,N2IO,N2IN4s,O2IN2d,N4sO2I,N2de,NIO2,NIO,N4sPNI,N2dPNI,
    2   N4sPO,N2dPO,NOIA1,NOIA2,NOIA3,NOIN2,NOIP2d,NOIP4s,OIO2,OIN2,
    3   ON2I,O2NI,O2N4s,ON2d,O2N2d,N2N2d,NIPO2,N2O2I,
    4   t0,e0,N2IO,O2IO,OIO,NIO,NOIO,N2DO,N4SO,PI,ASIG,SINTHT,WAIST,
    5   QN2I,QO2I,QOI,Qe,
    6   Vbeam,tdose,
    7   NOIA4,NOIA5,NOIA6,NOIA7,NOIA8,NOIA9,NOIA10,NOIA11,NOIA12,
    8   NOIB2,NOIB3,NOIB4,NOIB5,NOIB6,NOIB7,NOIB8,NOIB9,NOIB10,NOIB11,
    9   NOIA13,NOIA14,NOIA15,NOIA16,
    $   NOIB12,NOIB13,NOIB14,NOIB15,NOIB16

        COMMON /BLK1/NN,O2,O,Tr,N2Ie,O2Ie,OIe,NIe,NOIe,
    1   N2IO2,N2IO,N2IN4s,O2IN2d,N4sO2I,N2de,NIO2,NIO,N4sPNI,N2dPNI,
    2   N4sPO,N2dPO,NOIA1,NOIA2,NOIA3,NOIN2,NOIP2d,NOIP4s,OIO2,OIN2,
    3   ON2I,O2NI,O2N4s,ON2d,O2N2d,N2N2d,NIPO2,N2O2I,
    4   t0,e0,N2IO,O2IO,OIO,NIO,NOIO,N2DO,N4SO,PI,ASIG,SINTHT,WAIST,
    5   QN2I,QO2I,QOI,Qe,
    6   Vbeam,tdose,
    7   NOIA4,NOIA5,NOIA6,NOIA7,NOIA8,NOIA9,NOIA10,NOIA11,NOIA12,
    8   NOIB2,NOIB3,NOIB4,NOIB5,NOIB6,NOIB7,NOIB8,NOIB9,NOIB10,NOIB11,
    9   NOIA13,NOIA14,NOIA15,NOIA16,
    $   NOIB12,NOIB13,NOIB14,NOIB15,NOIB16


        FQ21 =
    1   .055*NIPO2*O2*NI
    2   +(N4sO2I*O2I*N4s+N2O2I*NN*O2I+OIN2*NN*OI)*0.0
```

227

```
      3    -NOIe*e*NOI21
      4    -(NOIA1*NOI21-NOIA2*NOI22)
      5    -(NOIB1*NOI21-NOIB3*NOI23)
      6    -(NOIN2*NN*NOI21-NOIN2*NN*NOI22)
           RETURN
           END
C-----------------------
c NOI22(t), (  NO+, from N+ + O2,in vibrational level 2 )
           FUNCTION FQ22(t,e,N2I,O2I,NI,OI,NOI22,NOI23,NOI24,N4s,N2d)

           REAL t,e,N2I,O2I,NI,OI,NOI,N4s,N2d

           REAL NOI10,NOI11,NOI12,NOI13
           REAL NOI14,NOI15,NOI16,NOI17
           REAL NOI18,NOI19,NOI110,NOI111
           REAL NOI112,NOI113,NOI114,NOI115,NOI116
           REAL NOI20,NOI21,NOI22,NOI23
           REAL NOI24,NOI25,NOI26,NOI27
           REAL NOI28,NOI29,NOI210,NOI211
           REAL NOI212,NOI213,NOI214,NOI215,NOI216

           REAL NN,O2,O,Tr,N2Ie,O2Ie,OIe,NIe,NOIe,
      1    N2IO2,N2IO,N2IN4s,O2IN2d,N4sO2I,N2de,NIO2,NIO,N4sPNI,N2dPNI,
      2    N4sPO,N2dPO,NOIA1,NOIA2,NOIA3,NOIN2,NOIP2d,NOIP4s,OIO2,OIN2,
      3    ON2I,O2NI,O2N4s,ON2d,O2N2d,N2N2d,NIPO2,N2O2I,
      4    t0,e0,N2IO,O2IO,OIO,NIO,NOIO,N2DO,N4SO,PI,ASIG,SINTHT,WAIST,
      5    QN2I,QO2I,QOI,Qe,
      6    Vbeam,tdose,
      7    NOIA4,NOIA5,NOIA6,NOIA7,NOIA8,NOIA9,NOIA10,NOIA11,NOIA12,
      8    NOIB2,NOIB3,NOIB4,NOIB5,NOIB6,NOIB7,NOIB8,NOIB9,NOIB10,NOIB11,
      9    NOIA13,NOIA14,NOIA15,NOIA16,
      $    NOIB12,NOIB13,NOIB14,NOIB15,NOIB16

           COMMON /BLK1/NN,O2,O,Tr,N2Ie,O2Ie,OIe,NIe,NOIe,
      1    N2IO2,N2IO,N2IN4s,O2IN2d,N4sO2I,N2de,NIO2,NIO,N4sPNI,N2dPNI,
      2    N4sPO,N2dPO,NOIA1,NOIA2,NOIA3,NOIN2,NOIP2d,NOIP4s,OIO2,OIN2,
      3    ON2I,O2NI,O2N4s,ON2d,O2N2d,N2N2d,NIPO2,N2O2I,
      4    t0,e0,N2IO,O2IO,OIO,NIO,NOIO,N2DO,N4SO,PI,ASIG,SINTHT,WAIST,
      5    QN2I,QO2I,QOI,Qe,
      6    Vbeam,tdose,
      7    NOIA4,NOIA5,NOIA6,NOIA7,NOIA8,NOIA9,NOIA10,NOIA11,NOIA12,
      8    NOIB2,NOIB3,NOIB4,NOIB5,NOIB6,NOIB7,NOIB8,NOIB9,NOIB10,NOIB11,
      9    NOIA13,NOIA14,NOIA15,NOIA16,
      $    NOIB12,NOIB13,NOIB14,NOIB15,NOIB16


           FQ22 =
      1    .069*NIPO2*O2*NI
      2    +(N4sO2I*O2I*N4s+N2O2I*NN*O2I+OIN2*NN*OI)*0.0
      3    -NOIe*e*NOI22
      4    -(NOIA2*NOI22-NOIA3*NOI23)
      5    -(NOIB2*NOI22-NOIB4*NOI24)
      6    -(NOIN2*NN*NOI22-NOIN2*NN*NOI23)
           RETURN
           END
C-----------------------
c NOI23(t), (  NO+, from N+ + O2,in vibrational level 3 )
           FUNCTION FQ23(t,e,N2I,O2I,NI,OI,NOI23,NOI24,NOI25,N4s,N2d)

           REAL t,e,N2I,O2I,NI,OI,NOI,N4s,N2d
```

```fortran
        REAL NOI10,NOI11,NOI12,NOI13
        REAL NOI14,NOI15,NOI16,NOI17
        REAL NOI18,NOI19,NOI110,NOI111
        REAL NOI112,NOI113,NOI114,NOI115,NOI116
        REAL NOI20,NOI21,NOI22,NOI23
        REAL NOI24,NOI25,NOI26,NOI27
        REAL NOI28,NOI29,NOI210,NOI211
        REAL NOI212,NOI213,NOI214,NOI215,NOI216

        REAL NN,O2,O,Tr,N2Ie,O2Ie,OIe,NIe,NOIe,
     1  N2IO2,N2IO,N2IN4s,O2IN2d,N4sO2I,N2de,NIO2,NIO,N4sPNI,N2dPNI,
     2  N4sPO,N2dPO,NOIA1,NOIA2,NOIA3,NOIN2,NOIP2d,NOIP4s,OIO2,OIN2,
     3  ON2I,O2NI,O2N4s,ON2d,O2N2d,N2N2d,NIPO2,N2O2I,
     4  t0,e0,N2IO,O2IO,OIO,NIO,NOIO,N2DO,N4SO,PI,ASIG,SINTHT,WAIST,
     5  QN2I,QO2I,QOI,Qe,
     6  Vbeam,tdose,
     7  NOIA4,NOIA5,NOIA6,NOIA7,NOIA8,NOIA9,NOIA10,NOIA11,NOIA12,
     8  NOIB2,NOIB3,NOIB4,NOIB5,NOIB6,NOIB7,NOIB8,NOIB9,NOIB10,NOIB11,
     9  NOIA13,NOIA14,NOIA15,NOIA16,
     $  NOIB12,NOIB13,NOIB14,NOIB15,NOIB16

        COMMON /BLK1/NN,O2,O,Tr,N2Ie,O2Ie,OIe,NIe,NOIe,
     1  N2IO2,N2IO,N2IN4s,O2IN2d,N4sO2I,N2de,NIO2,NIO,N4sPNI,N2dPNI,
     2  N4sPO,N2dPO,NOIA1,NOIA2,NOIA3,NOIN2,NOIP2d,NOIP4s,OIO2,OIN2,
     3  ON2I,O2NI,O2N4s,ON2d,O2N2d,N2N2d,NIPO2,N2O2I,
     4  t0,e0,N2IO,O2IO,OIO,NIO,NOIO,N2DO,N4SO,PI,ASIG,SINTHT,WAIST,
     5  QN2I,QO2I,QOI,Qe,
     6  Vbeam,tdose,
     7  NOIA4,NOIA5,NOIA6,NOIA7,NOIA8,NOIA9,NOIA10,NOIA11,NOIA12,
     8  NOIB2,NOIB3,NOIB4,NOIB5,NOIB6,NOIB7,NOIB8,NOIB9,NOIB10,NOIB11,
     9  NOIA13,NOIA14,NOIA15,NOIA16,
     $  NOIB12,NOIB13,NOIB14,NOIB15,NOIB16


        FQ23 =
     1  .092*NIPO2*O2*NI
     2  +(N4sO2I*O2I*N4s+N2O2I*NN*O2I+OIN2*NN*OI)*0.0
     3  -NOIe*e*NOI23
     4  -(NOIA3*NOI23-NOIA4*NOI24)
     5  -(NOIB3*NOI23-NOIB5*NOI25)
     6  -(NOIN2*NN*NOI23-NOIN2*NN*NOI24)
        RETURN
        END
C-------------------------
c NOI24(t), (  NO+, from N+ + O2,in vibrational level 4 )
        FUNCTION FQ24(t,e,N2I,O2I,NI,OI,NOI24,NOI25,NOI26,N4s,N2d)

        REAL t,e,N2I,O2I,NI,OI,NOI,N4s,N2d

        REAL NOI10,NOI11,NOI12,NOI13
        REAL NOI14,NOI15,NOI16,NOI17
        REAL NOI18,NOI19,NOI110,NOI111
        REAL NOI112,NOI113,NOI114,NOI115,NOI116
        REAL NOI20,NOI21,NOI22,NOI23
        REAL NOI24,NOI25,NOI26,NOI27
        REAL NOI28,NOI29,NOI210,NOI211
        REAL NOI212,NOI213,NOI214,NOI215,NOI216

        REAL NN,O2,O,Tr,N2Ie,O2Ie,OIe,NIe,NOIe,
```

229

```fortran
     1    N2IO2,N2IO,N2IN4s,O2IN2d,N4sO2I,N2de,NIO2,NIO,N4sPNI,N2dPNI,
     2    N4sPO,N2dPO,NOIA1,NOIA2,NOIA3,NOIN2,NOIP2d,NOIP4s,OIO2,OIN2,
     3    ON2I,O2NI,O2N4s,ON2d,O2N2d,N2N2d,NIPO2,N2O2I,
     4    t0,e0,N2IO,O2IO,OIO,NIO,NOIO,N2DO,N4SO,PI,ASIG,SINTHT,WAIST,
     5    QN2I,QO2I,QOI,Qe,
     6    Vbeam,tdose,
     7    NOIA4,NOIA5,NOIA6,NOIA7,NOIA8,NOIA9,NOIA10,NOIA11,NOIA12,
     8    NOIB2,NOIB3,NOIB4,NOIB5,NOIB6,NOIB7,NOIB8,NOIB9,NOIB10,NOIB11,
     9    NOIA13,NOIA14,NOIA15,NOIA16,
     $    NOIB12,NOIB13,NOIB14,NOIB15,NOIB16

          COMMON /BLK1/NN,O2,O,Tr,N2Ie,O2Ie,OIe,NIe,NOIe,
     1    N2IO2,N2IO,N2IN4s,O2IN2d,N4sO2I,N2de,NIO2,NIO,N4sPNI,N2dPNI,
     2    N4sPO,N2dPO,NOIA1,NOIA2,NOIA3,NOIN2,NOIP2d,NOIP4s,OIO2,OIN2,
     3    ON2I,O2NI,O2N4s,ON2d,O2N2d,N2N2d,NIPO2,N2O2I,
     4    t0,e0,N2IO,O2IO,OIO,NIO,NOIO,N2DO,N4SO,PI,ASIG,SINTHT,WAIST,
     5    QN2I,QO2I,QOI,Qe,
     6    Vbeam,tdose,
     7    NOIA4,NOIA5,NOIA6,NOIA7,NOIA8,NOIA9,NOIA10,NOIA11,NOIA12,
     8    NOIB2,NOIB3,NOIB4,NOIB5,NOIB6,NOIB7,NOIB8,NOIB9,NOIB10,NOIB11,
     9    NOIA13,NOIA14,NOIA15,NOIA16,
     $    NOIB12,NOIB13,NOIB14,NOIB15,NOIB16


          FQ24 =
     1    .112*NIPO2*O2*NI
     2    +(N4sO2I*O2I*N4s+N2O2I*NN*O2I+OIN2*NN*OI)*0.0
     3    -NOIe*e*NOI24
     4    -(NOIA4*NOI24-NOIA5*NOI25)
     5    -(NOIB4*NOI24-NOIB6*NOI26)
     6    -(NOIN2*NN*NOI24-NOIN2*NN*NOI25)
          RETURN
          END
C-------------------------
c NOI25(t), (  NO+, from N+ + O2,in vibrational level 5 )
          FUNCTION FQ25(t,e,N2I,O2I,NI,OI,NOI25,NOI26,NOI27,N4s,N2d)

          REAL t,e,N2I,O2I,NI,OI,NOI,N4s,N2d

          REAL NOI10,NOI11,NOI12,NOI13
          REAL NOI14,NOI15,NOI16,NOI17
          REAL NOI18,NOI19,NOI110,NOI111
          REAL NOI112,NOI113,NOI114,NOI115,NOI116
          REAL NOI20,NOI21,NOI22,NOI23
          REAL NOI24,NOI25,NOI26,NOI27
          REAL NOI28,NOI29,NOI210,NOI211
          REAL NOI212,NOI213,NOI214,NOI215,NOI216

          REAL NN,O2,O,Tr,N2Ie,O2Ie,OIe,NIe,NOIe,
     1    N2IO2,N2IO,N2IN4s,O2IN2d,N4sO2I,N2de,NIO2,NIO,N4sPNI,N2dPNI,
     2    N4sPO,N2dPO,NOIA1,NOIA2,NOIA3,NOIN2,NOIP2d,NOIP4s,OIO2,OIN2,
     3    ON2I,O2NI,O2N4s,ON2d,O2N2d,N2N2d,NIPO2,N2O2I,
     4    t0,e0,N2IO,O2IO,OIO,NIO,NOIO,N2DO,N4SO,PI,ASIG,SINTHT,WAIST,
     5    QN2I,QO2I,QOI,Qe,
     6    Vbeam,tdose,
     7    NOIA4,NOIA5,NOIA6,NOIA7,NOIA8,NOIA9,NOIA10,NOIA11,NOIA12,
     8    NOIB2,NOIB3,NOIB4,NOIB5,NOIB6,NOIB7,NOIB8,NOIB9,NOIB10,NOIB11,
     9    NOIA13,NOIA14,NOIA15,NOIA16,
     $    NOIB12,NOIB13,NOIB14,NOIB15,NOIB16
```

```
      COMMON /BLK1/NN,O2,O,Tr,N2Ie,O2Ie,OIe,NIe,NOIe,
     1 N2IO2,N2IO,N2IN4s,O2IN2d,N4sO2I,N2de,NIO2,NIO,N4sPNI,N2dPNI,
     2 N4sPO,N2dPO,NOIA1,NOIA2,NOIA3,NOIN2,NOIP2d,NOIP4s,OIO2,OIN2,
     3 ON2I,O2NI,O2N4s,ON2d,O2N2d,N2N2d,NIPO2,N2O2I,
     4 t0,e0,N2IO,O2IO,OIO,NIO,NOIO,N2DO,N4SO,PI,ASIG,SINTHT,WAIST,
     5 QN2I,QO2I,QOI,Qe,
     6 Vbeam,tdose,
     7 NOIA4,NOIA5,NOIA6,NOIA7,NOIA8,NOIA9,NOIA10,NOIA11,NOIA12,
     8 NOIB2,NOIB3,NOIB4,NOIB5,NOIB6,NOIB7,NOIB8,NOIB9,NOIB10,NOIB11,
     9 NOIA13,NOIA14,NOIA15,NOIA16,
     $ NOIB12,NOIB13,NOIB14,NOIB15,NOIB16


      FQ25 =
     1 .127*NIPO2*O2*NI
     2 +(N4sO2I*O2I*N4s+N2O2I*NN*O2I+OIN2*NN*OI)*0.0
     3 -NOIe*e*NOI25
     4 -(NOIA5*NOI25-NOIA6*NOI26)
     5 -(NOIB5*NOI25-NOIB7*NOI27)
     6 -(NOIN2*NN*NOI25-NOIN2*NN*NOI26)
      RETURN
      END
C-------------------------
c NOI26(t), (  NO+, from N+ + O2,in vibrational level 6 )
      FUNCTION FQ26(t,e,N2I,O2I,NI,OI,NOI26,NOI27,NOI28,N4s,N2d)

      REAL t,e,N2I,O2I,NI,OI,NOI,N4s,N2d

      REAL NOI10,NOI11,NOI12,NOI13
      REAL NOI14,NOI15,NOI16,NOI17
      REAL NOI18,NOI19,NOI110,NOI111
      REAL NOI112,NOI113,NOI114,NOI115,NOI116
      REAL NOI20,NOI21,NOI22,NOI23
      REAL NOI24,NOI25,NOI26,NOI27
      REAL NOI28,NOI29,NOI210,NOI211
      REAL NOI212,NOI213,NOI214,NOI215,NOI216

      REAL NN,O2,O,Tr,N2Ie,O2Ie,OIe,NIe,NOIe,
     1 N2IO2,N2IO,N2IN4s,O2IN2d,N4sO2I,N2de,NIO2,NIO,N4sPNI,N2dPNI,
     2 N4sPO,N2dPO,NOIA1,NOIA2,NOIA3,NOIN2,NOIP2d,NOIP4s,OIO2,OIN2,
     3 ON2I,O2NI,O2N4s,ON2d,O2N2d,N2N2d,NIPO2,N2O2I,
     4 t0,e0,N2IO,O2IO,OIO,NIO,NOIO,N2DO,N4SO,PI,ASIG,SINTHT,WAIST,
     5 QN2I,QO2I,QOI,Qe,
     6 Vbeam,tdose,
     7 NOIA4,NOIA5,NOIA6,NOIA7,NOIA8,NOIA9,NOIA10,NOIA11,NOIA12,
     8 NOIB2,NOIB3,NOIB4,NOIB5,NOIB6,NOIB7,NOIB8,NOIB9,NOIB10,NOIB11,
     9 NOIA13,NOIA14,NOIA15,NOIA16,
     $ NOIB12,NOIB13,NOIB14,NOIB15,NOIB16

      COMMON /BLK1/NN,O2,O,Tr,N2Ie,O2Ie,OIe,NIe,NOIe,
     1 N2IO2,N2IO,N2IN4s,O2IN2d,N4sO2I,N2de,NIO2,NIO,N4sPNI,N2dPNI,
     2 N4sPO,N2dPO,NOIA1,NOIA2,NOIA3,NOIN2,NOIP2d,NOIP4s,OIO2,OIN2,
     3 ON2I,O2NI,O2N4s,ON2d,O2N2d,N2N2d,NIPO2,N2O2I,
     4 t0,e0,N2IO,O2IO,OIO,NIO,NOIO,N2DO,N4SO,PI,ASIG,SINTHT,WAIST,
     5 QN2I,QO2I,QOI,Qe,
     6 Vbeam,tdose,
     7 NOIA4,NOIA5,NOIA6,NOIA7,NOIA8,NOIA9,NOIA10,NOIA11,NOIA12,
     8 NOIB2,NOIB3,NOIB4,NOIB5,NOIB6,NOIB7,NOIB8,NOIB9,NOIB10,NOIB11,
     9 NOIA13,NOIA14,NOIA15,NOIA16,
     $ NOIB12,NOIB13,NOIB14,NOIB15,NOIB16
```

231

```
      FQ26 =
    1 .147*NIPO2*O2*NI
    2 +(N4sO2I*O2I*N4s+N2O2I*NN*O2I+OIN2*NN*OI)*0.0
    3 -NOIe*e*NOI26
    4 -(NOIA6*NOI26-NOIA7*NOI27)
    5 -(NOIB6*NOI26-NOIB8*NOI28)
    6 -(NOIN2*NN*NOI26-NOIN2*NN*NOI27)
      RETURN
      END
C-------------------------
c NOI27(t), (  NO+, from N+ + O2,in vibrational level 7 )
      FUNCTION FQ27(t,e,N2I,O2I,NI,OI,NOI27,NOI28,NOI29,N4s,N2d)

      REAL t,e,N2I,O2I,NI,OI,NOI,N4s,N2d

      REAL NOI10,NOI11,NOI12,NOI13
      REAL NOI14,NOI15,NOI16,NOI17
      REAL NOI18,NOI19,NOI110,NOI111
      REAL NOI112,NOI113,NOI114,NOI115,NOI116
      REAL NOI20,NOI21,NOI22,NOI23
      REAL NOI24,NOI25,NOI26,NOI27
      REAL NOI28,NOI29,NOI210,NOI211
      REAL NOI212,NOI213,NOI214,NOI215,NOI216

      REAL NN,O2,O,Tr,N2Ie,O2Ie,OIe,NIe,NOIe,
    1 N2IO2,N2IO,N2IN4s,O2IN2d,N4sO2I,N2de,NIO2,NIO,N4sPNI,N2dPNI,
    2 N4sPO,N2dPO,NOIA1,NOIA2,NOIA3,NOIN2,NOIP2d,NOIP4s,OIO2,OIN2,
    3 ON2I,O2NI,O2N4s,ON2d,O2N2d,N2N2d,NIPO2,N2O2I,
    4 t0,e0,N2I0,O2I0,OI0,NI0,NOI0,N2D0,N4S0,PI,ASIG,SINTHT,WAIST,
    5 QN2I,QO2I,QOI,Qe,
    6 Vbeam,tdose,
    7 NOIA4,NOIA5,NOIA6,NOIA7,NOIA8,NOIA9,NOIA10,NOIA11,NOIA12,
    8 NOIB2,NOIB3,NOIB4,NOIB5,NOIB6,NOIB7,NOIB8,NOIB9,NOIB10,NOIB11,
    9 NOIA13,NOIA14,NOIA15,NOIA16,
    $ NOIB12,NOIB13,NOIB14,NOIB15,NOIB16

      COMMON /BLK1/NN,O2,O,Tr,N2Ie,O2Ie,OIe,NIe,NOIe,
    1 N2IO2,N2IO,N2IN4s,O2IN2d,N4sO2I,N2de,NIO2,NIO,N4sPNI,N2dPNI,
    2 N4sPO,N2dPO,NOIA1,NOIA2,NOIA3,NOIN2,NOIP2d,NOIP4s,OIO2,OIN2,
    3 ON2I,O2NI,O2N4s,ON2d,O2N2d,N2N2d,NIPO2,N2O2I,
    4 t0,e0,N2I0,O2I0,OI0,NI0,NOI0,N2D0,N4S0,PI,ASIG,SINTHT,WAIST,
    5 QN2I,QO2I,QOI,Qe,
    6 Vbeam,tdose,
    7 NOIA4,NOIA5,NOIA6,NOIA7,NOIA8,NOIA9,NOIA10,NOIA11,NOIA12,
    8 NOIB2,NOIB3,NOIB4,NOIB5,NOIB6,NOIB7,NOIB8,NOIB9,NOIB10,NOIB11,
    9 NOIA13,NOIA14,NOIA15,NOIA16,
    $ NOIB12,NOIB13,NOIB14,NOIB15,NOIB16


      FQ27 =
    1 .171*NIPO2*O2*NI
    2 +(N4sO2I*O2I*N4s+N2O2I*NN*O2I+OIN2*NN*OI)*0.0
    3 -NOIe*e*NOI27
    4 -(NOIA7*NOI27-NOIA8*NOI28)
    5 -(NOIB7*NOI27-NOIB9*NOI29)
    6 -(NOIN2*NN*NOI27-NOIN2*NN*NOI28)
      RETURN
      END
```

232

```
C------------------------
c NOI28(t), (  NO+, from N+ + O2,in vibrational level 8 )
        FUNCTION FQ28(t,e,N2I,O2I,NI,OI,NOI28,NOI29,NOI210,N4s,N2d)

        REAL t,e,N2I,O2I,NI,OI,NOI,N4s,N2d

        REAL NOI10,NOI11,NOI12,NOI13
        REAL NOI14,NOI15,NOI16,NOI17
        REAL NOI18,NOI19,NOI110,NOI111
        REAL NOI112,NOI113,NOI114,NOI115,NOI116
        REAL NOI20,NOI21,NOI22,NOI23
        REAL NOI24,NOI25,NOI26,NOI27
        REAL NOI28,NOI29,NOI210,NOI211
        REAL.NOI212,NOI213,NOI214,NOI215,NOI216

        REAL NN,O2,O,Tr,N2Ie,O2Ie,OIe,NIe,NOIe,
     1  N2IO2,N2IO,N2IN4s,O2IN2d,N4sO2I,N2de,NIO2,NIO,N4sPNI,N2dPNI,
     2  N4sPO,N2dPO,NOIA1,NOIA2,NOIA3,NOIN2,NOIP2d,NOIP4s,OIO2,OIN2,
     3  ON2I,O2NI,O2N4s,ON2d,O2N2d,N2N2d,NIPO2,N2O2I,
     4  t0,e0,N2IO,O2IO,OIO,NIO,NOIO,N2DO,N4SO,PI,ASIG,SINTHT,WAIST,
     5  QN2I,QO2I,QOI,Qe,
     6  Vbeam,tdose,
     7  NOIA4,NOIA5,NOIA6,NOIA7,NOIA8,NOIA9,NOIA10,NOIA11,NOIA12,
     8  NOIB2,NOIB3,NOIB4,NOIB5,NOIB6,NOIB7,NOIB8,NOIB9,NOIB10,NOIB11,
     9  NOIA13,NOIA14,NOIA15,NOIA16,
     $  NOIB12,NOIB13,NOIB14,NOIB15,NOIB16

        COMMON /BLK1/NN,O2,O,Tr,N2Ie,O2Ie,OIe,NIe,NOIe,
     1  N2IO2,N2IO,N2IN4s,O2IN2d,N4sO2I,N2de,NIO2,NIO,N4sPNI,N2dPNI,
     2  N4sPO,N2dPO,NOIA1,NOIA2,NOIA3,NOIN2,NOIP2d,NOIP4s,OIO2,OIN2,
     3  ON2I,O2NI,O2N4s,ON2d,O2N2d,N2N2d,NIPO2,N2O2I,
     4  t0,e0,N2IO,O2IO,OIO,NIO,NOIO,N2DO,N4SO,PI,ASIG,SINTHT,WAIST,
     5  QN2I,QO2I,QOI,Qe,
     6  Vbeam,tdose,
     7  NOIA4,NOIA5,NOIA6,NOIA7,NOIA8,NOIA9,NOIA10,NOIA11,NOIA12,
     8  NOIB2,NOIB3,NOIB4,NOIB5,NOIB6,NOIB7,NOIB8,NOIB9,NOIB10,NOIB11,
     9  NOIA13,NOIA14,NOIA15,NOIA16,
     $  NOIB12,NOIB13,NOIB14,NOIB15,NOIB16


        FQ28 =
     1  .073*NIPO2*O2*NI
     2  +(N4sO2I*O2I*N4s+N2O2I*NN*O2I+OIN2*NN*OI)*0.0
     3  -NOIe*e*NOI28
     4  -(NOIA8*NOI28-NOIA9*NOI29)
     5  -(NOIB8*NOI28-NOIB10*NOI210)
     6  -(NOIN2*NN*NOI28-NOIN2*NN*NOI29)
        RETURN
        END
C------------------------
c NOI29(t), (  NO+, from N+ + O2,in vibrational level 9 )
        FUNCTION FQ29(t,e,N2I,O2I,NI,OI,NOI29,NOI210,NOI211,N4s,N2d)

        REAL t,e,N2I,O2I,NI,OI,NOI,N4s,N2d

        REAL NOI10,NOI11,NOI12,NOI13
        REAL NOI14,NOI15,NOI16,NOI17
        REAL NOI18,NOI19,NOI110,NOI111
        REAL NOI112,NOI113,NOI114,NOI115,NOI116
        REAL NOI20,NOI21,NOI22,NOI23
```

233

```
           REAL NOI24,NOI25,NOI26,NOI27
           REAL NOI28,NOI29,NOI210,NOI211
           REAL NOI212,NOI213,NOI214,NOI215,NOI216

           REAL NN,O2,O,Tr,N2Ie,O2Ie,OIe,NIe,NOIe,
      1    N2IO2,N2IO,N2IN4s,O2IN2d,N4sO2I,N2de,NIO2,NIO,N4sPNI,N2dPNI,
      2    N4sPO,N2dPO,NOIA1,NOIA2,NOIA3,NOIN2,NOIP2d,NOIP4s,OIO2,OIN2,
      3    ON2I,O2NI,O2N4s,ON2d,O2N2d,N2N2d,NIPO2,N2O2I,
      4    t0,e0,N2IO,O2IO,OIO,NIO,NOIO,N2DO,N4SO,PI,ASIG,SINTHT,WAIST,
      5    QN2I,QO2I,QOI,Qe,
      6    Vbeam,tdose,
      7    NOIA4,NOIA5,NOIA6,NOIA7,NOIA8,NOIA9,NOIA10,NOIA11,NOIA12,
      8    NOIB2,NOIB3,NOIB4,NOIB5,NOIB6,NOIB7,NOIB8,NOIB9,NOIB10,NOIB11,
      9    NOIA13,NOIA14,NOIA15,NOIA16,
      $    NOIB12,NOIB13,NOIB14,NOIB15,NOIB16

           COMMON /BLK1/NN,O2,O,Tr,N2Ie,O2Ie,OIe,NIe,NOIe,
      1    N2IO2,N2IO,N2IN4s,O2IN2d,N4sO2I,N2de,NIO2,NIO,N4sPNI,N2dPNI,
      2    N4sPO,N2dPO,NOIA1,NOIA2,NOIA3,NOIN2,NOIP2d,NOIP4s,OIO2,OIN2,
      3    ON2I,O2NI,O2N4s,ON2d,O2N2d,N2N2d,NIPO2,N2O2I,
      4    t0,e0,N2IO,O2IO,OIO,NIO,NOIO,N2DO,N4SO,PI,ASIG,SINTHT,WAIST,
      5    QN2I,QO2I,QOI,Qe,
      6    Vbeam,tdose,
      7    NOIA4,NOIA5,NOIA6,NOIA7,NOIA8,NOIA9,NOIA10,NOIA11,NOIA12,
      8    NOIB2,NOIB3,NOIB4,NOIB5,NOIB6,NOIB7,NOIB8,NOIB9,NOIB10,NOIB11,
      9    NOIA13,NOIA14,NOIA15,NOIA16,
      $    NOIB12,NOIB13,NOIB14,NOIB15,NOIB16


           FQ29 =
      1    .006*NIPO2*O2*NI
      2    +(N4sO2I*O2I*N4s+N2O2I*NN*O2I+OIN2*NN*OI)*0.0
      3    -NOIe*e*NOI29
      4    -(NOIA9*NOI29-NOIA10*NOI210)
      5    -(NOIB9*NOI29-NOIB11*NOI211)
      6    -(NOIN2*NN*NOI29-NOIN2*NN*NOI210)
           RETURN
           END
C--------------------------
c NOI210(t), (  NO+, from N+ + O2,in vibrational level 10 )
           FUNCTION FQ210(t,e,N2I,O2I,NI,OI,NOI20,NOI21,NOI22,N4s,N2d)

           REAL t,e,N2I,O2I,NI,OI,NOI,N4s,N2d

           REAL NOI10,NOI11,NOI12,NOI13
           REAL NOI14,NOI15,NOI16,NOI17
           REAL NOI18,NOI19,NOI110,NOI111
           REAL NOI112,NOI113,NOI114,NOI115,NOI116
           REAL NOI20,NOI21,NOI22,NOI23
           REAL NOI24,NOI25,NOI26,NOI27
           REAL NOI28,NOI29,NOI210,NOI211
           REAL NOI212,NOI213,NOI214,NOI215,NOI216

           REAL NN,O2,O,Tr,N2Ie,O2Ie,OIe,NIe,NOIe,
      1    N2IO2,N2IO,N2IN4s,O2IN2d,N4sO2I,N2de,NIO2,NIO,N4sPNI,N2dPNI,
      2    N4sPO,N2dPO,NOIA1,NOIA2,NOIA3,NOIN2,NOIP2d,NOIP4s,OIO2,OIN2,
      3    ON2I,O2NI,O2N4s,ON2d,O2N2d,N2N2d,NIPO2,N2O2I,
      4    t0,e0,N2IO,O2IO,OIO,NIO,NOIO,N2DO,N4SO,PI,ASIG,SINTHT,WAIST,
      5    QN2I,QO2I,QOI,Qe,
      6    Vbeam,tdose,
```

234

```fortran
      7 NOIA4,NOIA5,NOIA6,NOIA7,NOIA8,NOIA9,NOIA10,NOIA11,NOIA12,
      8 NOIB2,NOIB3,NOIB4,NOIB5,NOIB6,NOIB7,NOIB8,NOIB9,NOIB10,NOIB11,
      9 NOIA13,NOIA14,NOIA15,NOIA16,
      $ NOIB12,NOIB13,NOIB14,NOIB15,NOIB16

        COMMON /BLK1/NN,O2,O,Tr,N2Ie,O2Ie,OIe,NIe,NOIe,
      1 N2IO2,N2IO,N2IN4s,O2IN2d,N4sO2I,N2de,NIO2,NIO,N4sPNI,N2dPNI,
      2 N4sPO,N2dPO,NOIA1,NOIA2,NOIA3,NOIN2,NOIP2d,NOIP4s,OIO2,OIN2,
      3 ON2I,O2NI,O2N4s,ON2d,O2N2d,N2N2d,NIPO2,N2O2I,
      4 t0,e0,N2IO,O2IO,OIO,NIO,NOIO,N2DO,N4SO,PI,ASIG,SINTHT,WAIST,
      5 QN2I,QO2I,QOI,Qe,
      6 Vbeam,tdose,
      7 NOIA4,NOIA5,NOIA6,NOIA7,NOIA8,NOIA9,NOIA10,NOIA11,NOIA12,
      8 NOIB2,NOIB3,NOIB4,NOIB5,NOIB6,NOIB7,NOIB8,NOIB9,NOIB10,NOIB11,
      9 NOIA13,NOIA14,NOIA15,NOIA16,
      $ NOIB12,NOIB13,NOIB14,NOIB15,NOIB16


        FQ210 =
      1 .012*NIPO2*O2*NI
      2 +(N4sO2I*O2I*N4s+N2O2I*NN*O2I+OIN2*NN*OI)*0.0
      3 -NOIe*e*NOI210
      4 -(NOIA10*NOI210-NOIA11*NOI211)
      5 -(NOIB10*NOI210-NOIB12*NOI212)
      6 -(NOIN2*NN*NOI210-NOIN2*NN*NOI211)
        RETURN
        END
C------------------------
c NOI211(t), (  NO+, from N+ + O2,in vibrational level 11 )
        FUNCTION FQ211(t,e,N2I,O2I,NI,OI,NOI211,NOI212,NOI213,N4s,N2d)

        REAL t,e,N2I,O2I,NI,OI,NOI,N4s,N2d

        REAL NOI10,NOI11,NOI12,NOI13
        REAL NOI14,NOI15,NOI16,NOI17
        REAL NOI18,NOI19,NOI110,NOI111
        REAL NOI112,NOI113,NOI114,NOI115,NOI116
        REAL NOI20,NOI21,NOI22,NOI23
        REAL NOI24,NOI25,NOI26,NOI27
        REAL NOI28,NOI29,NOI210,NOI211
        REAL NOI212,NOI213,NOI214,NOI215,NOI216

        REAL NN,O2,O,Tr,N2Ie,O2Ie,OIe,NIe,NOIe,
      1 N2IO2,N2IO,N2IN4s,O2IN2d,N4sO2I,N2de,NIO2,NIO,N4sPNI,N2dPNI,
      2 N4sPO,N2dPO,NOIA1,NOIA2,NOIA3,NOIN2,NOIP2d,NOIP4s,OIO2,OIN2,
      3 ON2I,O2NI,O2N4s,ON2d,O2N2d,N2N2d,NIPO2,N2O2I,
      4 t0,e0,N2IO,O2IO,OIO,NIO,NOIO,N2DO,N4SO,PI,ASIG,SINTHT,WAIST,
      5 QN2I,QO2I,QOI,Qe,
      6 Vbeam,tdose,
      7 NOIA4,NOIA5,NOIA6,NOIA7,NOIA8,NOIA9,NOIA10,NOIA11,NOIA12,
      8 NOIB2,NOIB3,NOIB4,NOIB5,NOIB6,NOIB7,NOIB8,NOIB9,NOIB10,NOIB11,
      9 NOIA13,NOIA14,NOIA15,NOIA16,
      $ NOIB12,NOIB13,NOIB14,NOIB15,NOIB16

        COMMON /BLK1/NN,O2,O,Tr,N2Ie,O2Ie,OIe,NIe,NOIe,
      1 N2IO2,N2IO,N2IN4s,O2IN2d,N4sO2I,N2de,NIO2,NIO,N4sPNI,N2dPNI,
      2 N4sPO,N2dPO,NOIA1,NOIA2,NOIA3,NOIN2,NOIP2d,NOIP4s,OIO2,OIN2,
      3 ON2I,O2NI,O2N4s,ON2d,O2N2d,N2N2d,NIPO2,N2O2I,
      4 t0,e0,N2IO,O2IO,OIO,NIO,NOIO,N2DO,N4SO,PI,ASIG,SINTHT,WAIST,
      5 QN2I,QO2I,QOI,Qe,
```

```
      6   Vbeam,tdose,
      7   NOIA4,NOIA5,NOIA6,NOIA7,NOIA8,NOIA9,NOIA10,NOIA11,NOIA12,
      8   NOIB2,NOIB3,NOIB4,NOIB5,NOIB6,NOIB7,NOIB8,NOIB9,NOIB10,NOIB11,
      9   NOIA13,NOIA14,NOIA15,NOIA16,
      $   NOIB12,NOIB13,NOIB14,NOIB15,NOIB16


          FQ211 =
      1   .063*NIPO2*O2*NI
      2   +(N4sO2I*O2I*N4s+N2O2I*NN*O2I+OIN2*NN*OI)*0.0
      3   -NOIe*e*NOI211
      4   -(NOIA11*NOI211-NOIA12*NOI212)
      5   -(NOIB11*NOI211-NOIB13*NOI213)
      6   -(NOIN2*NN*NOI211-NOIN2*NN*NOI212)
          RETURN
          END
C------------------------
c NOI212(t), (  NO+, from N+ + O2,in vibrational level 12 )
          FUNCTION FQ212(t,e,N2I,O2I,NI,OI,NOI212,NOI213,NOI214,N4s,N2d)

          REAL t,e,N2I,O2I,NI,OI,NOI,N4s,N2d

          REAL NOI10,NOI11,NOI12,NOI13
          REAL NOI14,NOI15,NOI16,NOI17
          REAL NOI18,NOI19,NOI110,NOI111
          REAL NOI112,NOI113,NOI114,NOI115,NOI116
          REAL NOI20,NOI21,NOI22,NOI23
          REAL NOI24,NOI25,NOI26,NOI27
          REAL NOI28,NOI29,NOI210,NOI211
          REAL NOI212,NOI213,NOI214,NOI215,NOI216


          REAL NN,O2,O,Tr,N2Ie,O2Ie,OIe,NIe,NOIe,
      1   N2IO2,N2IO,N2IN4s,O2IN2d,N4sO2I,N2de,NIO2,NIO,N4sPNI,N2dPNI,
      2   N4sPO,N2dPO,NOIA1,NOIA2,NOIA3,NOIN2,NOIP2d,NOIP4s,OIO2,OIN2,
      3   ON2I,O2NI,O2N4s,ON2d,O2N2d,N2N2d,NIPO2,N2O2I,
      4   t0,e0,N2I0,O2I0,OI0,NI0,NOI0,N2D0,N4S0,PI,ASIG,SINTHT,WAIST,
      5   QN2I,QO2I,QOI,Qe,
      6   Vbeam,tdose,
      7   NOIA4,NOIA5,NOIA6,NOIA7,NOIA8,NOIA9,NOIA10,NOIA11,NOIA12,
      8   NOIB2,NOIB3,NOIB4,NOIB5,NOIB6,NOIB7,NOIB8,NOIB9,NOIB10,NOIB11,
      9   NOIA13,NOIA14,NOIA15,NOIA16,
      $   NOIB12,NOIB13,NOIB14,NOIB15,NOIB16


          COMMON /BLK1/NN,O2,O,Tr,N2Ie,O2Ie,OIe,NIe,NOIe,
      1   N2IO2,N2IO,N2IN4s,O2IN2d,N4sO2I,N2de,NIO2,NIO,N4sPNI,N2dPNI,
      2   N4sPO,N2dPO,NOIA1,NOIA2,NOIA3,NOIN2,NOIP2d,NOIP4s,OIO2,OIN2,
      3   ON2I,O2NI,O2N4s,ON2d,O2N2d,N2N2d,NIPO2,N2O2I,
      4   t0,e0,N2I0,O2I0,OI0,NI0,NOI0,N2D0,N4S0,PI,ASIG,SINTHT,WAIST,
      5   QN2I,QO2I,QOI,Qe,
      6   Vbeam,tdose,
      7   NOIA4,NOIA5,NOIA6,NOIA7,NOIA8,NOIA9,NOIA10,NOIA11,NOIA12,
      8   NOIB2,NOIB3,NOIB4,NOIB5,NOIB6,NOIB7,NOIB8,NOIB9,NOIB10,NOIB11,
      9   NOIA13,NOIA14,NOIA15,NOIA16,
      $   NOIB12,NOIB13,NOIB14,NOIB15,NOIB16


          FQ212 =
      1   .071*NIPO2*O2*NI
      2   +(N4sO2I*O2I*N4s+N2O2I*NN*O2I+OIN2*NN*OI)*0.0
      3   -NOIe*e*NOI212
```

236

```
      4   -(NOIA12*NOI212-NOIA13*NOI213)
      5   -(NOIB12*NOI212-NOIB14*NOI214)
      6   -(NOIN2*NN*NOI212-NOIN2*NN*NOI213)
          RETURN
          END
C------------------------
c NOI213(t), (  NO+, from N+ + O2,in vibrational level 13 )
          FUNCTION FQ213(t,e,N2I,O2I,NI,OI,NOI213,NOI214,NOI215,N4s,N2d)

          REAL t,e,N2I,O2I,NI,OI,NOI,N4s,N2d

          REAL NOI10,NOI11,NOI12,NOI13
          REAL NOI14,NOI15,NOI16,NOI17
          REAL NOI18,NOI19,NOI110,NOI111
          REAL NOI112,NOI113,NOI114,NOI115,NOI116
          REAL NOI20,NOI21,NOI22,NOI23
          REAL NOI24,NOI25,NOI26,NOI27
          REAL NOI28,NOI29,NOI210,NOI211
          REAL NOI212,NOI213,NOI214,NOI215,NOI216

          REAL NN,O2,O,Tr,N2Ie,O2Ie,OIe,NIe,NOIe,
      1   N2IO2,N2IO,N2IN4s,O2IN2d,N4sO2I,N2de,NIO2,NIO,N4sPNI,N2dPNI,
      2   N4sPO,N2dPO,NOIA1,NOIA2,NOIA3,NOIN2,NOIP2d,NOIP4s,OIO2,OIN2,
      3   ON2I,O2NI,O2N4s,ON2d,O2N2d,N2N2d,NIPO2,N2O2I,
      4   t0,e0,N2IO,O2IO,OIO,NIO,NOIO,N2DO,N4SO,PI,ASIG,SINTHT,WAIST,
      5   QN2I,QO2I,QOI,Qe,
      6   Vbeam,tdose,
      7   NOIA4,NOIA5,NOIA6,NOIA7,NOIA8,NOIA9,NOIA10,NOIA11,NOIA12,
      8   NOIB2,NOIB3,NOIB4,NOIB5,NOIB6,NOIB7,NOIB8,NOIB9,NOIB10,NOIB11,
      9   NOIA13,NOIA14,NOIA15,NOIA16,
      $   NOIB12,NOIB13,NOIB14,NOIB15,NOIB16

          COMMON /BLK1/NN,O2,O,Tr,N2Ie,O2Ie,OIe,NIe,NOIe,
      1   N2IO2,N2IO,N2IN4s,O2IN2d,N4sO2I,N2de,NIO2,NIO,N4sPNI,N2dPNI,
      2   N4sPO,N2dPO,NOIA1,NOIA2,NOIA3,NOIN2,NOIP2d,NOIP4s,OIO2,OIN2,
      3   ON2I,O2NI,O2N4s,ON2d,O2N2d,N2N2d,NIPO2,N2O2I,
      4   t0,e0,N2IO,O2IO,OIO,NIO,NOIO,N2DO,N4SO,PI,ASIG,SINTHT,WAIST,
      5   QN2I,QO2I,QOI,Qe,
      6   Vbeam,tdose,
      7   NOIA4,NOIA5,NOIA6,NOIA7,NOIA8,NOIA9,NOIA10,NOIA11,NOIA12,
      8   NOIB2,NOIB3,NOIB4,NOIB5,NOIB6,NOIB7,NOIB8,NOIB9,NOIB10,NOIB11,
      9   NOIA13,NOIA14,NOIA15,NOIA16,
      $   NOIB12,NOIB13,NOIB14,NOIB15,NOIB16


          FQ213 =
      1   .012*NIPO2*O2*NI
      2   +(N4sO2I*O2I*N4s+N2O2I*NN*O2I+OIN2*NN*OI)*0.0
      3   -NOIe*e*NOI213
      4   -(NOIA13*NOI213-NOIA14*NOI214)
      5   -(NOIB13*NOI213-NOIB15*NOI215)
      6   -(NOIN2*NN*NOI213-NOIN2*NN*NOI214)
          RETURN
          END
C------------------------
c NOI214(t), (  NO+, from N+ + O2,in vibrational level 14 )
          FUNCTION FQ214(t,e,N2I,O2I,NI,OI,NOI214,NOI215,NOI216,N4s,N2d)

          REAL t,e,N2I,O2I,NI,OI,NOI,N4s,N2d
```

```fortran
      REAL NOI10,NOI11,NOI12,NOI13
      REAL NOI14,NOI15,NOI16,NOI17
      REAL NOI18,NOI19,NOI110,NOI111
      REAL NOI112,NOI113,NOI114,NOI115,NOI116
      REAL NOI20,NOI21,NOI22,NOI23
      REAL NOI24,NOI25,NOI26,NOI27
      REAL NOI28,NOI29,NOI210,NOI211
      REAL NOI212,NOI213,NOI214,NOI215,NOI216

      REAL NN,O2,O,Tr,N2Ie,O2Ie,OIe,NIe,NOIe,
     1 N2IO2,N2IO,N2IN4s,O2IN2d,N4sO2I,N2de,NIO2,NIO,N4sPNI,N2dPNI,
     2 N4sPO,N2dPO,NOIA1,NOIA2,NOIA3,NOIN2,NOIP2d,NOIP4s,OIO2,OIN2,
     3 ON2I,O2NI,O2N4s,ON2d,O2N2d,N2N2d,NIPO2,N2O2I,
     4 t0,e0,N2IO,O2IO,OIO,NIO,NOIO,N2DO,N4SO,PI,ASIG,SINTHT,WAIST,
     5 QN2I,QO2I,QOI,Qe,
     6 Vbeam,tdose,
     7 NOIA4,NOIA5,NOIA6,NOIA7,NOIA8,NOIA9,NOIA10,NOIA11,NOIA12,
     8 NOIB2,NOIB3,NOIB4,NOIB5,NOIB6,NOIB7,NOIB8,NOIB9,NOIB10,NOIB11,
     9 NOIA13,NOIA14,NOIA15,NOIA16,
     $ NOIB12,NOIB13,NOIB14,NOIB15,NOIB16

      COMMON /BLK1/NN,O2,O,Tr,N2Ie,O2Ie,OIe,NIe,NOIe,
     1 N2IO2,N2IO,N2IN4s,O2IN2d,N4sO2I,N2de,NIO2,NIO,N4sPNI,N2dPNI,
     2 N4sPO,N2dPO,NOIA1,NOIA2,NOIA3,NOIN2,NOIP2d,NOIP4s,OIO2,OIN2,
     3 ON2I,O2NI,O2N4s,ON2d,O2N2d,N2N2d,NIPO2,N2O2I,
     4 t0,e0,N2IO,O2IO,OIO,NIO,NOIO,N2DO,N4SO,PI,ASIG,SINTHT,WAIST,
     5 QN2I,QO2I,QOI,Qe,
     6 Vbeam,tdose,
     7 NOIA4,NOIA5,NOIA6,NOIA7,NOIA8,NOIA9,NOIA10,NOIA11,NOIA12,
     8 NOIB2,NOIB3,NOIB4,NOIB5,NOIB6,NOIB7,NOIB8,NOIB9,NOIB10,NOIB11,
     9 NOIA13,NOIA14,NOIA15,NOIA16,
     $ NOIB12,NOIB13,NOIB14,NOIB15,NOIB16


      FQ214=
     1 .002*NIPO2*O2*NI
     2 +(N4sO2I*O2I*N4s+N2O2I*NN*O2I+OIN2*NN*OI)*0.0
     3 -NOIe*e*NOI214
     4 -(NOIA14*NOI214-NOIA15*NOI215)
     5 -(NOIB14*NOI214-NOIB16*NOI216)
     6 -(NOIN2*NN*NOI214-NOIN2*NN*NOI215)
      RETURN
      END

C----------------------
      SUBROUTINE MAXMIN(X,IMAX,XMAX,IMIN,XMIN,NLIM)
      REAL X(1),XMAX,XMIN
      INTEGER IMAX,IMIN,NLIM
      IMAX=1
      IMIN=1
      DO 10 I=1,NLIM
      IF(X(IMAX).LT.X(I))IMAX=I
      IF(X(IMIN).GT.X(I))IMIN=I
10    CONTINUE
      XMAX=X(IMAX)
      XMIN=X(IMIN)
      RETURN
      END
C     ----------------------
      SUBROUTINE MKASC(INBUF,L)
```

```fortran
C         OPENS AN ASCII FILE AND WRITES TO IT. L IS NUMBER OF POINTS.

          REAL*4 INBUF(1)
          CHARACTER*30 OUTFILE

          WRITE(*,*) ' ENTER OUTPUT FILE NAME '
          READ(*,'(A)') OUTFILE
          OPEN(1,FILE=OUTFILE,STATUS='NEW',FORM='FORMATTED')

          DO 5 I=1,L
5         WRITE(1,100) INBUF(I)
100       format(E13.6)

          WRITE(*,*) 'ALL DATA WRITTEN TO FILE '

          CLOSE(1)
          RETURN
          END
```